LEABHARLANN CHOLÁISTE NA TRÍONÓIDE, BAILE ÁTHA CLIATH | TRINITY COLLEGE LIBRARY DUBLIN
Ollscoil Átha Cliath | The University of Dublin

Terms and Conditions of Use of Digitised Theses from Trinity College Library Dublin

Copyright statement

All material supplied by Trinity College Library is protected by copyright (under the Copyright and Related Rights Act, 2000 as amended) and other relevant Intellectual Property Rights. By accessing and using a Digitised Thesis from Trinity College Library you acknowledge that all Intellectual Property Rights in any Works supplied are the sole and exclusive property of the copyright and/or other IPR holder. Specific copyright holders may not be explicitly identified. Use of materials from other sources within a thesis should not be construed as a claim over them.

A non-exclusive, non-transferable licence is hereby granted to those using or reproducing, in whole or in part, the material for valid purposes, providing the copyright owners are acknowledged using the normal conventions. Where specific permission to use material is required, this is identified and such permission must be sought from the copyright holder or agency cited.

Liability statement

By using a Digitised Thesis, I accept that Trinity College Dublin bears no legal responsibility for the accuracy, legality or comprehensiveness of materials contained within the thesis, and that Trinity College Dublin accepts no liability for indirect, consequential, or incidental, damages or losses arising from use of the thesis for whatever reason. Information located in a thesis may be subject to specific use constraints, details of which may not be explicitly described. It is the responsibility of potential and actual users to be aware of such constraints and to abide by them. By making use of material from a digitised thesis, you accept these copyright and disclaimer provisions. Where it is brought to the attention of Trinity College Library that there may be a breach of copyright or other restraint, it is the policy to withdraw or take down access to a thesis while the issue is being resolved.

Access Agreement

By using a Digitised Thesis from Trinity College Library you are bound by the following Terms & Conditions. Please read them carefully.

I have read and I understand the following statement: All material supplied via a Digitised Thesis from Trinity College Library is protected by copyright and other intellectual property rights, and duplication or sale of all or part of any of a thesis is not permitted, except that material may be duplicated by you for your research use or for educational purposes in electronic or print form providing the copyright owners are acknowledged using the normal conventions. You must obtain permission for any other use. Electronic or print copies may not be offered, whether for sale or otherwise to anyone. This copy has been supplied on the understanding that it is copyright material and that no quotation from the thesis may be published without proper acknowledgement.

Coordination and Hydrogen Bonded Networks Featuring 4,4'-dicarboxy-2,2'-bipyridine.

Eithne Tynan Pascual

B.A. (*Mod.*), P. Grad. Dip. (Stat.)

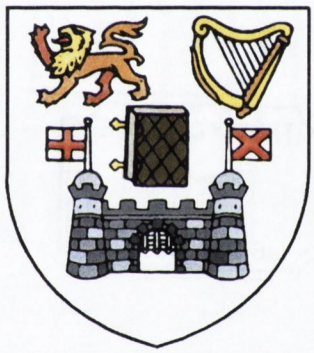

A thesis submitted to the University of Dublin for the degree of

Doctor of Philosophy

Department of Chemistry

University of Dublin

2004

TRINITY COLLEGE
14 OCT 2004
LIBRARY DUBLIN
THOS S
7420

Declaration

This thesis has not been submitted as an exercise for a degree at any other University. Except where otherwise indicated, the work described herein has been carried out by the author alone. I, the undersigned, do also give permission to the Libraries of Trinity College, Dublin, to copy this thesis in whole or in part without further reference to me.

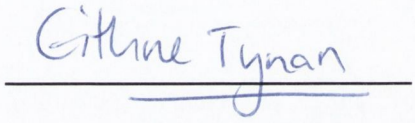

Eithne Tynan

DECLARATION

This thesis has not been submitted as an exercise for a degree at any other university.
Except where stated, the work described therein was carried out by me alone.

I give permission for the Library to lend or copy this thesis upon request.

Signed: Gthne Tynan

Acknowledgements

First and foremost I would like to thank my supervisors, Dr. Paul. E. Kruger and Dr. Anthea C. Lees, for giving me the opportunity to do my postgraduate studies in this lab. Also thank them for their constant encouragement and support.

A special thank you must go to Dr. Paul Jensen for teaching me all I know about crystallography and for all the assistance provided in this matter. Thank you also to Dr. Mark Nieuwenhuyzen, 'Woody', at QUB for the structures solved before the CCD at Trinity was up and running.

I'd like to thank all the academic staff that have helped me along the way. I also need to thank the technical staff in the department for helping with all the different instrumentation: Martin, Patsy, John O'Brien, Fred, Teresa, Ed, Seamus, Peggy, Brendan and Mark. And the secretarial staff: Tess, Helen and Corinne.

A big, big thank you to all the members of the Kruger group, past and present, for it really wouldn't be the same without you: Brian, Murray, Sylvie, Michelle W., Sandrine, Niamh, Paul, Karen, Rob, Michelle H. and Phil Mackey. Thanks for a great time. Thanks also to all the other students in the department.

A great big thanks to my 'Dublin' friends over the past years, which have made my experience here so much more enjoyable. I must mention the 'girlies': Caoimhe, Deirdre, Jenny and Siobhan. Thanks for everything over the past seven years.

I would like to thank Vince for all the constant support during this long period, and for putting up with all my temper tantrums in the final stages of this endeavour. Thanks, babe. Finally I want to thank my family: my dad, my brother and sisters, Niall, Rónait and Eilin, for helping me so much during this period and with everything I have decided to do in my life. Thanks for all the love and support during the rough patches. Unfortunately my mother won't see this, but I'm sure she'd be proud, and I'd like to thank her for everything she did for me throughout her life.

Table of Contents

Declaration.....ii

Acknowledgements.....iii

Table of Contents.....iv

Summary.....viii

Abbreviations.....x

Chapter One – Introduction.....1

1.1 Supramolecular chemistry.....2

1.1.1 Hydrogen bonding.....2

1.2 Self assembly and molecular recognition.....5

1.3 Crystal engineering.....7

1.4 Organic crystal engineering.....9

1.5 Inorganic crystal engineering.....13

1.5.1 Coordination polymers.....15

1.5.2 Networks.....18

1.5.3 Metal-Organic Frameworks (MOFs).....21

1.5.4 Hydrogen bonded networks of coordination complexes.....24

1.6 Hydrothermal synthesis.....29

1.7 Present study.....30

Chapter Two - Coordination polymers incorporating 4,4'-dicarboxy-2,2'-bipyridine.....33

2.1 Introduction.....34

2.2 Reaction of Cu(II) with 4,4'-dicarboxy-2,2'-bipyridine.....34

2.2.1 Reaction of $Cu(NO_3)_2$ with 4,4'-Na_2dcbp.....34

2.2.2 Crystal structure of $\{[Cu(4,4'\text{-dcbp})(H_2O)_2]\cdot 2H_2O\}_n$ (**1**).....34

2.2.3 Thermal analysis and magnetic properties of **1**.....40

2.3 Reaction of Co(II) with 4,4'-dicarboxy-2,2'-bipyridine.....42

2.3.1 Reaction of $CoSO_4$ and 4,4'-H_2dcbp.....42

2.3.2 Crystal structure of β-$[Co(4,4'\text{-dcbp})(H_2O)_2]_n$ (***2***).....42

2.3.3 Comparison of α- and β-polymorphs of $[Co(4,4'\text{-dcbp})(H_2O)_2]_n$.....48
2.3.4 Thermal analysis and magnetic properties of α-$[Co(4,4'\text{-dcbp})(H_2O)_2]_n$ and **2**.....50
2.4 Reaction of Mn(II) with 4,4'-dicarboxy-2,2'-bipyridine.....52
2.4.1 Reaction of $MnCl_2$ with 4,4'-H_2dcbp.....52
2.4.2 Crystal structure of $\{[Mn(4,4'\text{-dcbp})]\cdot ½DMF\}_n$ (**3**).....54
2.4.3 Crystal structure of $\{[Mn(4,4'\text{-dcbp})]\cdot ½(DEF)\}_n$ (**4**).....60
2.4.4 Structural comparison of $\{[Mn(4,4'\text{-dcbp})]\cdot ½DMF\}_n$ (**3**) and $\{[Mn(4,4'\text{-dcbp})]\cdot 2H_2O\}_n$ (**5**).....62
2.4.5 Thermal analysis and magnetic properties of **3** and **5**.....69
2.5 Conclusions.....72
Chapter Three – First row transition metal complexes incorporating 4,4'-dicarboxy-2,2'-bipyridine and other pyridine based ligands or coordinating inorganic anions.....75
3.1. Complexes incorporating 4,4'-dicarboxy-2,2'-bipyridine and other pyridine based ligands.....76
Preamble.....76
3.1.1 Reaction of Co(II) with 4,4'-dicarboxy-2,2'-bipyridine and 4,4'-bipyridine.....76
3.1.2 Crystal structure of $\{[Co(4,4'\text{-dcbp})(py)(H_2O)_2]\cdot(½\ 4,4'\text{-bipy})\cdot 2H_2O\}_n$.(**6**).....76
3.1.3 Reaction of Cu(II) with 4,4'-dicarboxy-2,2'-bipyridine and 4,4'-bipyridine.....83
3.1.4 Crystal structure of $\{[Cu(4,4'\text{-dcbp})(4,4'\text{-bipy})(H_2O)]\cdot 4½H_2O\}_n$ (**7**).....83
3.1.5 Crystal structure of $[Cu_4(OH)_4(2,2'\text{-bipy})_4)(\mu\text{-}4,4'\text{-bipy})_2][Cu_4(OH)_4(2,2\text{-bipy})_4(4,4'\text{-bipy})_2(\mu\text{-}4,4'\text{-bipy})]\cdot(NO_3)_8\cdot xH_2O$ (**8**).....88
3.1.6 Conclusions.....99
3.2 Complexes incorporating 4,4'-dicarboxy-2,2'-bipyridine and coordinating inorganic anions.....100
Preamble.....100
3.2.1 Reaction of Cu(II) and 4,4'-H_2dcbp under acidic conditions.....100
3.2.2 Crystal structure of $[Cu(4,4'\text{-}H_2dcbp)Cl_2]_2\cdot 2H_2O$ (**9**).....101
3.2.3 Crystal structure of $\{[Cu(4,4'\text{-}H_2dcbp)(SO_4)]\cdot ⅓H_2O\}_n$ (**10**).....108
3.2.4 Thermal analysis and magnetic properties of **10**.....112
3.2.5 Crystal structure of $[Cu(4,4'\text{-}H_2dcbp)(NO_3)_2(H_2O)]$ (***11***).....114
3.2.6 Conclusions.....118

Chapter Four -Hydrogen bonded complexes of 4,4'-dicarboxy-2,2'-bipyridine with first row transition metals.....120

Preamble.....121

4.1 Reaction of Co(II) with 4,4'-dicarboxy-2,2'-bipyridine.....121

4.1.1 Reaction of Co(II) with 4,4'-H_2dcbp.....121

4.1.2 Crystal structure of $[Co(4,4'\text{-dcbp})(H_2O)_4]\cdot 4H_2O$ (**12**).....121

4.1.3 Crystal structure of $[Me_2NH_2]_{1.5}[Co(4,4'\text{-}H_{5/6}dcbp)_3]\cdot 10½H_2O$ (**13**).....125

4.2 Reaction of Cu(II) with 4,4'-dicarboxy-2,2'-bipyridine.....129

4.2.1 Reaction of Cu(II) with 4,4'-H_2dcbp.....129

4.2.2 Crystal structure of $[Me_2NH_2]_2[Cu(4,4'\text{-dcbp})_2(H_2O)]\cdot 4H_2O$ (**14**).....130

4.2.3 Crystal structure of $[Na_2][Cu(4,4'\text{-dcbp})_2(H_2O)].10H_2O$ (**15**).....135

4.3 Conclusions.....140

Chapter Five - Synthesis and structural characterization of 4,4'-substituted-2,2'-bipyridines and some of their derivatives.....142

5.1 Synthesis, crystallization and characterization of 4,4'-dicarboxy-2,2'-bipyridine and some of its salts.....143

Preamble.....143

5.1.1 Synthesis and crystallization of 4,4'-H_2dcbp.....143

5.1.2 Crystal structure of 4,4'-H_2dcbp (**16**).....143

5.1.3 Synthesis and crystallization of (4,4'-H_3dcbp)(Cl).....147

5.1.4 Crystal structure of (4,4'-H_3dcbp)(Cl) (**17**).....148

5.1.5 Synthesis of $[(TBA)(4,4'\text{-Hdcbp})]\cdot 4H_2O$.....151

5.1.6 Crystal structure of $[(TBA)(4,4'\text{-Hdcbp}]\cdot 4H_2O$ (**18**).....151

5.1.7 Synthesis of $(DEA)_2$(4,4'-dcbp).....155

5.1.8 Crystal structure of $(DEA)_2$(4,4'-dcbp) (**19**).....155

5.2 Synthesis and structural characterization of ester derivatives of 4,4'-H_2dcbp....160

5.2.1 Synthesis and crystallization of 4,4'-dimethylcarboxy-2,2'-bipyridine (4,4'-dmcbp), 4,4'-diethylcarboxy-2,2'-bipyridine (4,4'-decbp), 4,4'-diisopropylcarboxy-2,2'-bipyridine (4,4'-dpcbp), and 4,4'-dibutylcarboxy-2,2'-bipyridine (4,4'-dbcb).....160

5.2.2 Crystal structure of 4,4'-dmcbp (**20**).....160

5.2.3 Crystal structure of 4,4'-decbp (**21**).....163

5.2.4 Crystal structure of 4,4'-dpcbp (**22**).....165

5.2.5 Crystal structure of 4,4'-dbcbp (**23**).....167

5.3 Conclusions....169

Chapter Six- Materials & Methods. Experimental....172

6.1 Materials and methods....173

6.1.1 Reagents....173

6.1.2 Elemental analysis....173

6.1.3 Nuclear magnetic resonance spectroscopy....173

6.1.4 Infrared spectroscopy....173

6.1.5 Thermogravimetric analysis (TGA)....173

6.1.6 X-Ray crystal diffraction....173

6.1.7 Solvo(hydro)thermal synthesis....174

6.1.8 Magnetic measurements....175

6.2 Experimental....176

6.2.1 Chapter 2....176

6.2.2 Chapter 3....177

6.2.3 Chapter 4....179

6.2.4 Chapter 5....180

Appendix....183

Chapter 1....184

Chapter 3....186

Chapter 5....188

Attached CD-ROM....189

References....190

Publications....205

Summary

The research presented in this thesis lies within the general area of supramolecular and coordination chemistry. More specifically, this project involves the study of 4,4'-dicarboxy-2,2'-bipyridine (4,4'-H_2dcbp) as a linker for the formation of extended networks, either *via* hydrogen bonding or coordination. Due to the insolubility of 4,4,'-H_2dcbp all the reactions within this thesis were carried out under solvothermal conditions, or using a base to deprotonate the ligand under ambient conditions. Paramagnetic metal ions were employed throughout in order to study the 4,4'-dcbp ligand as a propagator of magnetic exchange.

Chapter 2 describes the formation of first row transition metal containing coordination polymers incorporating 4,4'-dcbp. The reaction of Cu(II) with 4,4'-dcbp yielded a 2D coordination polymer, $\{[Cu(4,4'\text{-dcbp})(H_2O)_2]\cdot 2H_2O\}_n$ (**1**). The individual 2D layers in **1** form a (4,4) net, in the 'windows' of which lie the lattice water molecules, however, offset stacking of the layers prevents the formation of channels in **1**. Hydrothermal reaction of Co(II) with 4,4'-H_2dcbp produced two polymorphs: α-$[Co(4,4'\text{-dcbp})(H_2O)_2]$ and β-$[Co(4,4'\text{-dcbp})(H_2O)_2]$ (**2**). These exhibit very different packing modes: the α-polymorph displays channels in its structure, while **2** is more effectively packed and does not display channels. The different connectivity of the 4,4'-dcbp ligands and the Co(II) ions, give rise to a (12,3) net in the α-polymorph and a (10,3)-a net in **2**. Hydrothermal reaction of Mn(II) with 4,4'-H_2dcbp produced three different pseudo-polymorphs depending on the solvent employed. When DMF was used $\{[Mn(4,4'\text{-dcbp})]\cdot ½DMF\}_n$ (**3**) was formed, while when DEF was used $\{[Mn(4,4'\text{-dcbp})]\cdot ½DEF\}_n$ (**4**) was formed. The use of water as the main solvent produced $\{[Mn(4,4'\text{-dcbp})]\cdot 2H_2O\}_n$ (**5**). All three display channels in their structures, in which lie the solvent molecules. **3** and **4** have identical 3D networks and only differ in the solvent within the channels, while **5** differs in both the connectivity of the 3D network and the solvent molecules in the channels. Thermal analysis of **3** and **5**, shows that **3** irreversibly 'enclathrates' DMF, while **5** reversibly binds water. Furthermore the crystal structure of the empty network in **5**, **5a**, was determined.

Chapter 3 consist of two sections. The first describes the synthesis of first row transition metal coordination polymers incorporating 4,4'-dcbp as well as other nitrogen-based ligands. Thus, 4,4'-bipy was used in addition to 4,4'-dcbp. Hydrothermal reaction of Co(II) with 4,4'-H_2dcbp, 4,4'-bipy and pyridine yielded $[Co(4,4'\text{-dcbp})(H_2O)_2(py)]$ $(½4,4'\text{-bipy})\cdot 2H_2O\}_n$ (**6**), while hydrothermal reaction of Cu(II) with 4,4'-H_2dcbp, 4,4'-bipy and pyridine yielded {[Cu(4,4'-dcbp)

$(4,4'\text{-bipy})(H_2O)_2]\cdot 4\frac{1}{2}H_2O\}_n$ (**7**). Both form similar 1D coordination polymers which pack into 3D networks through hydrogen bonding. In **6**, 4,4'-bipy is not coordinating and sits in the lattice, while it coordinates in a monodentate fashion in **7**. As a by-product of the second reaction another complex was formed: $[Cu_4(OH)_4(2,2'\text{-bipy})_4(\mu\text{-}4,4'\text{-bipy})_2][Cu_4(OH)_4(2,2'\text{-bipy})_4(4,4'\text{-bipy})_2(\mu\text{-}4,4'\text{-bipy})]\cdot(NO3)_8\cdot 10H_2O$ (**8**).

In the second section of Chapter 3, the synthesis of metal complexes incorporating 4,4'-H_2dcbp as well as coordinating inorganic anions is reported. Hydrothermal reaction of Cu(II) and 4,4'-H_2dcbp under acidic conditions produced $[Cu(4,4'\text{-}H_2dcbp)Cl_2]_2\cdot 2H_2O$ (**9**), $\{[Cu(4,4'\text{-}H_2dcbp)(SO_4)]\cdot\frac{1}{2}H_2O\}_n$ (**10**) and $[Cu(4,4'\text{-}H_2dcbp)(NO_3)_2(H_2O)]$ (**11**) when hydrochloric, sulfuric and nitric acids were used, respectively. In all three cases, the ligand is protonated and thus, coordinates the metal ions through the bipyridine site only, while the carboxylic acids participate in hydrogen bonding. **9** and **11** are discrete metal complexes, which are hydrogen bonded into a 3D network. Bridging of the copper atoms in **10** by the sulfate anions results in a 1D polymer. As a result of the hydrogen bonding interactions between the 1D polymer, channels, occupied by the lattice water molecules, are formed in **10**.

Chapter 4 describes the synthesis of first row transition metal complexes of 4,4'-dcbp. The mono-4,4'-dcbp complex of Co(II), $[Co(4,4'\text{-dcbp})(H_2O)_4]\cdot 4H_2O$ (**12**), was obtained by reaction of Co(II) with 4,4'-dcbp, using triethylamine to deprotonate the ligand, while the tris-chelated Co(II) complex, $[Me_2NH_2][Co(4,4'\text{-}H_{5/6}dcbp)_3]\cdot 10\frac{1}{2}H_2O$ (**13**), was obtained by hydrothermal reaction of Co(II) and 4,4'-H_2dcbp. Hydrothermal reaction of Cu(II) and 4,4'-H_2dcbp yielded $[Me_2NH_2]_2[Cu(4,4'\text{-dcbp})_2(H_2O)]\cdot 4H_2O$ (**14**), while reaction at ambient conditions employing NaOH to deprotonate the ligand yielded $[Na_2][Cu(4,4'\text{-dcbp})_2(H_2O)_2]\cdot 10\frac{1}{2}H_2O$ (**15**). In all cases, the metal complexes π-stack to form 2D layers which are then hydrogen bonding with the lattice water molecules and cations to form a 3D network.

Chapter 5 describes and compares the crystal structures of 4,4'-H_2dcbp (**16**) and various of its salts: $(4,4'\text{-}H_3dcbp)(Cl)$ (**17**), $[(TBA)(4,4'\text{-Hdcbp})]\cdot 4H_2O$ (**18**) and $(DEA)_2(4,4'\text{-dcbp})$ (**19**). These were obtained as by-products of some of the above reactions. The different hydrogen bonding capabilities in each salt result in dramatically different networks being formed. For comparison the structures of a series of ester derivatives of 4,4'-H_2dcbp are reported: 4,4'-dimethylcarboxy-2,2'-bipyridine, 4,4'-diethylcarboxy-2,2'-bipyridine, 4,4'-diisopropylcarboxy-2,2'-bipyridine and 4,4'-dibutylcarboxy-2,2'-bipyridine.

Abbreviations

0D	Zero-dimensional
1D	One-dimensional
^{1}H-NMR	Proton nuclear magnetic resonance spectroscopy
2,2'-bipy	2,2'-bipyridine
2D	Two-dimensional
3D	Three-dimensional
4,4'-bipy	4,4'-bipyridine
4,4'-dbcbp	4,4'-dibutylcarboxy-2,2'-bipyridine
4,4'-dcbp	4,4'-dicarboxylate-2,2'-bipyridine
4,4'-decbp	4,4'-diethylcarboxy-2,2'-bipyridine
4,4'-dmcbp	4,4'-dimethylcarboxy-2,2'-bipyridine
4,4'-dpcbp	4,4'-diisopropylcarboxy-2,2'-bipyridine
4,4'-H_2dcbp	4,4'-dicarboxy-2,2'-bipyridine
4,4'-Hdcbp	4-carboxylic-4'-carboxylate-2,2'-bipyridine
4,4'-Na_2dcbp	Sodium salt of 4,4'-dicarboxy-2,2'-bipyridine
$CDCl_3$	Deuterated chloroform
Cl	Chloride anion
CSD	Cambridge Structural Database
DEA	Diethylammonium
DEF	Diethyl formamide
DMA	Dimethylammonium
DMF	Dimethyl formamide
DMSO	Dimethyl sulfoxide
DNA	Deoxyribonucleic acid
ES-MS	Electrospray mass spectrometry
EtOH	Ethanol
g	Lande factor
H	Magnetic field
H_3TMA	Trimesic acid
HINA	Isonicotinic acid
Hrs	Hours
INA	Isonicotinate anion
IR	Infrared
J	Exchange coupling constant

Mg	Milligrams
MOF	Metal-organic framework
NO_3	Nitrate anion
Py	Pyridine
s	Spin quantum number
SBU	Secondary building unit
SO_4	Sulfate anion
TGA	Thermal gravimetric analysis
TMA	Trimesate anion
α-Po	α-polonium
δ	Chemical shift
μ	Magnetic moment (in BM)
μ-	Bridging

Chapter One

Introduction.

1.1 Supramolecular chemistry

Supramolecular chemistry has become one of the most popular areas of experimental chemistry, rapidly developing over recent years. Lehn[1] has defined the field as "the chemistry of molecular assemblies and of the intermolecular bond", concerning interactions *between* rather than *within* molecules. The very word itself means "beyond the molecule". In this, it distinguishes itself from the classical fields of chemistry in which the behaviour and properties of individual molecules are studied. Essentially, we can describe the field as the study of covalently bonded molecular building blocks held together by non-covalent intermolecular forces.[2] These non-covalent interactions are secondary and their rupture does not affect the covalent skeleton. Some of these include: electrostatic and ion-pairing interactions between oppositely charged ionic species, hydrogen-bonding between complementary substituents, π-stacking between aromatic rings, hydrophobic and solvatophobic effects through association of appropriate functional groups, steric repulsion and other donor-acceptor interactions between Lewis bases and Lewis acids. These are the same forces that Nature uses to bind its molecular assemblies, and indeed the inspiration for designing supramolecular systems is drawn from studying the molecular interactions of larger biological species. This is reflected in the terminology used to describe supramolecular systems, where, frequently, the partners of a supramolecular species are described as host-guest or receptor-substrate. However, chemistry is not limited to systems similar to those found in biology, but is free to create unknown species and to invent novel processes.

With the development of supramolecular chemistry there has been a change in focus from single molecules, often constructed step by step via the formation of direct covalent linkages, towards molecular assemblies, where the molecular components are held together with 'supramolecular glue', in the form of non-covalent intermolecular contacts. Intermolecular forces are, however, in general weaker than covalent bonds, so that supramolecular species are thermodynamically less stable, kinetically more labile and dynamically more flexible than molecules.

1.1.1 Hydrogen bonding.

The hydrogen bond is the most important and prevalent of all directional non-covalent interactions. Although it was discovered almost a hundred years ago,[§3, 4] it is still a topic of vital scientific research. The reason for this is the fundamental role

---

[§] The concept of the hydrogen bond is attributed to W. M. Latimer and W. H. Rodebush, and independently to M. L. Huggins, however the terms *near valence* and *weak union* were used by Werner, Hantzch and Pfeiffer, and Moore and Winmill, respectively, in the early 20th century.

hydrogen bonds play in the structure, function, and dynamics of vast number of chemical systems, ranging from inorganic to biological chemistry.[5-7] However, what constitutes a hydrogen bond? Despite the numerous studies which have tried to address this question, currently a definitive answer does not exist. Ideas of what constitutes a hydrogen-bond are in a constant state of flux.[8, 9] Pauling was one of the first to give a definition of a hydrogen bond in the 1940s:[10] "Under certain conditions an atom of hydrogen is attracted by rather strong forces to two atoms, instead of only one, so that it may be considered to be acting as a bond between them. This is called the *hydrogen bond*. [...] The hydrogen bond is largely ionic in character, and is formed only between the most electronegative atoms [...]. Although the hydrogen bond is not a strong bond (its bond energy [...] being only about 5 kcal/mol[†]) it has great significance in determining the properties of substances." In the first book devoted entirely to hydrogen bonding Pimental and McClellan gave the first modern and more general definition of the phenomenon: "A hydrogen bond exists between the functional group A-H, and an atom or a group of atoms B in the same or different molecules when a) there is evidence of bond formation (association or chelation), b) there is evidence that this new bond linking A-H and B specifically involves a hydrogen atom already bonded to A".[11] This definition leaves the chemical nature of the participants, including their polarities and net charges, unspecified, and thus enables an evaluation of the hydrogen bonding potential of groups like C-H and P-H, amongst others, and of π-acceptors. Yet another, simpler, textbook-type definition of the hydrogen bond was provided by Atkins as "a link formed by a hydrogen atom lying between two strongly electronegative atoms".[12] The great disparity between all the above definitions is obvious and reflects the problems in coming up with a single hydrogen bond definition that encompasses all of the above. According to Pimentel and McClellan, a C-H··O interaction would be considered a hydrogen bond, whereas it wouldn't by Pauling's definition. Most current definitions tend to refer to Pauling, a definition that was insightful and visionary when proposed, but it should be borne in mind that in the intervening sixty years of chemical progress there are many examples (as the C-H···O bond above) of what are widely considered to be hydrogen bonds that are precluded from Pauling's definition.

For the purposes of this thesis a hydrogen bond is represented as D-H···A (D for *proton donor*, A for *proton acceptor*), and usually occurs when D is sufficiently electronegative to enhance the acidic nature of the proton, and where the acceptor A has a region of high electron density which can interact strongly with the acidic hydrogen. As the hydrogen atom has no inner core of electrons, the side facing away from the D-H bond presents a virtually naked nucleus. This positive charge is attracted

---

[†] 5 kcal/mol ~ 21 kJ/mol

to the high electron density of an atom in a nearby molecule and so this side of the hydrogen atom can get quite close to the neighbouring electron-rich atom and interact strongly with it (the closer it gets, the stronger the electrostatic interaction). In the context of this thesis most hydrogen bonds involve water and carboxylic acids, or carboxylates, with the rest involving nitrogen containing ligands such as 4,4'-bipyridine. Figure 1.1 shows an example of hydrogen bonds between water molecules with ideal bond lengths and angles.

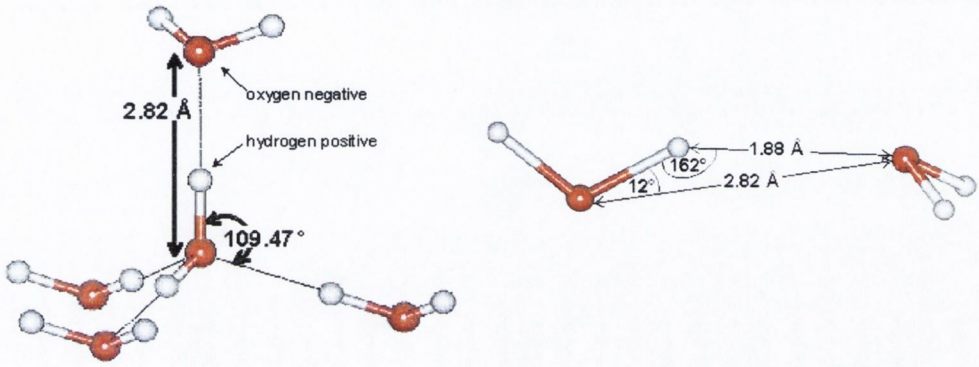

Figure 1.1– Schematic representation of hydrogen bonds between molecules, showing ideal bond lengths and angles.[13]

Hydrogen bonds can exist with a continuum of strengths. However, it can be useful, for practical reasons, to classify them in some way according to strength. Jeffrey[7] classified hydrogen bonds into three different types: 'strong', 'moderate' and 'weak'. Strong hydrogen bonds are formed between ions and molecules when there is a deficiency of electron density in the donor group (eg. $-O^{+}-H$), or an excess of electron density in the acceptor group (eg. Cl^{-}, COO^{-}). This is to be expected since a deficiency of electrons of the donor group further deshields the proton leaving it with a significant positive charge, while an excess of electrons on the acceptor group increases its negative charge and the interaction with the deshielded proton. For this reason, these are sometimes referred to as *ionic hydrogen bonds*. Moderate hydrogen bonds are generally formed between neutral donor (eg. O-H, N-H) and acceptor (eg. C=O) groups. The donor atoms are highly electronegative relative to hydrogen while the acceptor atoms have lone-pair unshared electrons. These are the most common hydrogen bonds in both chemistry and Nature and thus are sometimes referred to as 'normal' hydrogen bonds. Weak hydrogen bonds are formed when the hydrogen atom is covalently bonded to a slightly more electroneutral atom, as in C-H, or when the acceptor group has no lone pairs but has π-electrons, such as an aromatic ring. These type of hydrogen bonds are often referred to as 'non-conventional' hydrogen bonds. The strength of a hydrogen bond is not determined just by the type of atoms involved in it, but also by

other properties. Table 1.1 shows some of the geometrical, energetic and functional properties for the three different types of hydrogen bonds. This classification is to be used as a guide only and does not attempt to divide hydrogen bonds into strict compartments, since all the mentioned properties lie in a continuous range with no 'natural' borderline between these categories.[14]

Table 1.1- Strong, moderate and weak hydrogen bonds following the classification of Jeffrey.[7]

	STRONG	***MODERATE***	***WEAK***
Interaction type	Quasi-covalent	Mainly electrostatic	Electrostatic/ dispersion
Bond lengths	D-H $\approx$ H···A	D-H < H···A	D-H << H···A
H···A (Å)	~1.2-1.5	~1.5-2.2	2.2-3.2
D···A (Å)	2.2-2.5	2.5-3.2	3.2-4.0
Bond angles (°)	175-180	130-180	90-150
Directionality	Strong	Moderate	Weak
Bond energy (kcal.mol^{-1})	14-40	4-15	<4

1.2 Self assembly and molecular recognition

Supramolecular self-assembly may be defined as the process by which a supramolecular species forms spontaneously from its components. The concept of self-assembly was first introduced by Lehn and co-workers after their work in the spontaneous generation of inorganic helicates,[15] but it is very far from a unique feature of supramolecular systems - it is ubiquitous in biological systems, from which the inspiration behind this concept was taken. An illustrative example of the phenomenon of self-assembly is the well-known formation of the DNA double helix. Each strand of DNA consists of a phosphorylated sugar backbone, to which a series of purine and pyrimidine bases are connected. Two strands self-assemble into a double helix through the recognition and spontaneous association of complementary nucleotide base pairs (Figure 1.2). This is an all-or-nothing process, where a certain number of base pairs are required to form before the final assembly of the double-helix will occur, but once this nucleation point is reached, a cascade propagation sequence completes the process. The entire process is driven by nothing stronger than hydrogen bonding, π-π stacking and other very weak interactions. These interactions are readily reversible so that the final product is in thermodynamic equilibrium with its components. This allows for the facile assembly or disassembly of the overall structure and means that the process is highly amenable to error-checking and if necessary, self-correction. The formation of the DNA double helix illustrates the concept of complementarity that is required for the formation of all non-covalent interactions between molecules.

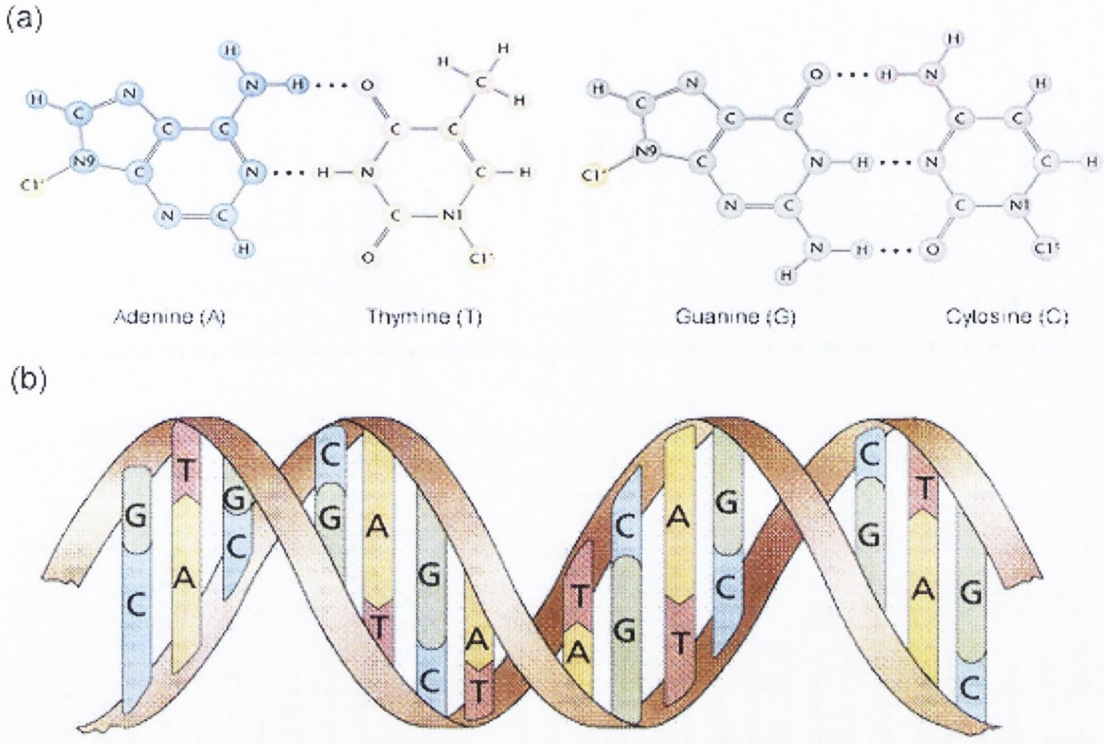

Figure 1.2 – (a) Hydrogen bonding between complementary base pairs in DNA.[16] (b) Schematic representation of the DNA double helix, assembled from the molecular recognition and self-assembly of the nucleotide base pairs.

The above example demonstrates the ability of biological systems to employ the process of self-assembly to generate large ordered supramolecular arrays. It is from these kinds of examples that synthetic supramolecular chemists can draw inspiration. From the analysis of biological systems we can learn several things. Firstly, self-assembly processes are economical by virtue of the fact that they are highly convergent. Secondly, the supramolecular assemblies can be rapidly, accurately and efficiently synthesized from relatively simple subunits. Thirdly, the use of identical subunits in the assembling process means keeping the diversity of interactions to a minimum, thus only requiring a relatively small amount of information for the formation of a large structure. Finally, molecular recognition *via* many, weak, non-covalent interactions leads to a reversible 'intelligent' synthetic pathway, which is self-checking and able to correct itself as and when required, and thus afford a product representing a thermodynamic minimum.[17]

Through the use of non-covalent interactions, and taking from the lessons learned from Nature, chemists have produced some quite beautiful self-assembled synthetic systems, though despite this, there is still a long way to go before individual systems match the biological ones in both subtlety and function.

1.3 Crystal engineering

The term 'crystal engineering' is usually attributed to Schmidt in relation to his studies in the field of topochemistry.[18] However, as pointed out by Braga recently,[19] an earlier reference to crystal engineering exists in the proceedings of the American Physical Society Meeting held in Mexico City in 1955, with an abstract entitled "Crystal Engineering: a new concept in crystallography". In it, R. Pepinsky goes on to say: "Crystallization of organic ions with metal-containing complex ions of suitable sizes, charges and solubilities results in structures with cells and symmetries determined chiefly by packing of complex ions. These cells and symmetries are to a good extent controllable: hence crystals with advantageous properties can be 'engineered' [...]". While the idea of *making crystals by design* was there fifty years ago, it was the article by Schmidt in 1971 that marked the birth of the field. It became clear that crystals were the result of a series of molecular recognition events and self-assembly, rather than the result of the need of Nature to 'avoid a vacuum'. Subsequently, it has become clear that crystal engineering is closely linked to the concepts developed in supramolecular chemistry. Indeed, as referred to by Dunitz, the crystal is "a supermolecule *par excellence*: a lump of matter, of macroscopic dimensions, millions of molecules long, held together in a periodic arrangement by just the same kind of noncovalent bonding interactions as are responsible for molecular recognition and complexation [...]"(Figure 1.3).[20]

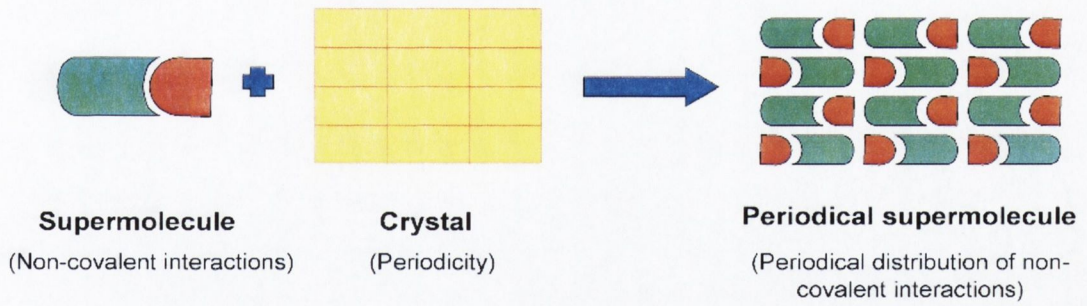

Figure 1.3 – Schematic representation of the crystal as a supermolecule.

The field of crystal engineering only began to flourish in the early 1990s due, presumably, to a number of factors. Small molecule crystallography was becoming more accessible to the non-crystallographer. With the advent of CCD diffractometers, data collection could be performed in hours, rather than days. Reflection analysis and processing and visualization software became simpler and the more-accessible Cambridge Structural Database was regarded as a library of intermolecular interactions. This, coupled with the supramolecular perception of crystals, heightened the interest in

crystal engineering within the chemical community and brought the field of crystal engineering forward.

Crystal engineering can be simply defined as 'making crystals by design'. This implies a knowledge and understanding of the capability of the constituent building blocks to engage in intermolecular interactions. Thus, it requires two steps: analysis followed by synthesis - not very different to classical chemistry experiments. The crystal can therefore be identified as a retrosynthetic target. By analysing crystal structures in terms of intermolecular interactions, repetitive patterns may be recognised, which can then be exploited by the chemist in the construction of the building blocks.

The properties of a crystalline material are tightly linked with its structure. Therefore, by predicting and controlling the crystal structure of a molecule, the properties of the resulting solid can also be controlled. Thus crystal engineering is shifting from devising structures to designing properties.[21, 22] While the engineering of functional materials at the molecular and supramolecular levels is still in its infancy,[23-26] applications in areas such as catalysis, storage, non-linear optics, sieves and sensors should be expected in the future.

Although crystal engineering has its roots in the study of 'organic' solids it has grown to include materials that also contain inorganic moieties, so much that organometallic[27-29] and coordination networks[30, 31] now represent the largest class of engineered crystal structures. The incorporation of transition-metal ions provides magnetic, electronic, photochemical and catalytic properties for the formation of functional materials.[32, 33]

Amongst all the intermolecular interactions available to the 'crystal maker', strong hydrogen bonds and coordination bonds are the interactions of choice, due to their strength and directionality.[34] Nonetheless, weaker interactions have been well exploited in crystal engineering studies and should not be disregarded.[14, 35-39] For the purposes of this thesis only strong interactions will be considered, except in Chapter 5.

We cannot, as of yet, predict crystal structures.[40, 41] This requires analysis of the recognition features of the molecular building blocks and prediction of how they will optimize close packing in the solid state. This implies determining the space group the molecule will crystallize in and this still remains a significant challenge. However, crystal engineering is only concerned with predicting stoichiometry and architecture and consequently is less precise and allows for 'easier' prediction of the networks formed. While we are able to design networks that will invariably self-assemble, there is still the issue of obtaining good quality single crystals suitable for X-Ray diffraction analysis. Indeed crystallization still remains a 'black art', as put by Ball,[42] and a clearer understanding of crystal growth is much needed.[43]

Although a vast number of crystal structures have been 'engineered' successfully, the majority have been discovered by accident rather than by design and thus 'serendipity' still plays an important role in this field. Nevertheless, as the field continues to expand, and with it our understanding of intermolecular interactions, the engineering of solids should become more predictable.

The following is an account of crystal engineering strategies: from hydrogen bonded networks to coordination polymers. The main focus will be on structures that are most relevant to the contents of this thesis.

1.4 Organic crystal engineering

The hydrogen bond has been described as the 'master-key interaction in supramolecular chemistry' and this is directly reflected in crystal engineering.[9] Organic solids packed through hydrogen bonds were the first structures to be studied in the field of crystal engineering.[44] Extensive studies of organic hydrogen-bonded solid-state structures carried out by Etter and co-workers identified the clear pattern preference of certain functional groups such as amides and diaryl ureas. This led to a method for describing these hydrogen-bond patterns, as well as a set of empirical rules with some predictive ability regarding hydrogen bonded organic compounds, known as Etter's rules.[45] There are three rules with broad, but not universal, generality that apply to neutral organic molecules: 1) all good proton donors and acceptors are used in hydrogen bonding; 2) six-membered-ring intramolecular hydrogen bonds form in preference to intermolecular hydrogen bonds; 3) the best proton donors and acceptors remaining after intramolecular hydrogen bond formation form intermolecular hydrogen bonds to one another.

The need to relate and correlate hydrogen bonding in some systematic way led to the proposal by Etter of a graph-set approach.[45] This method was further extended by Bernstein and Davis.[46] Using graph-set analysis all hydrogen bond patterns can be described in terms of chains (C), rings (R), intramolecular hydrogen bonds (S, for 'self') and other finite patterns (D, for 'discrete'). These are the pattern designators (G). The number of hydrogen bond donors (d) and acceptors (a) can be identified and added to the pattern designators as a subscript and a superscript respectively, which are dropped when both values are 1. To complete the notation the total number of atoms (n), including H, in the pattern (also known as the *degree* of the pattern) is given in brackets after the pattern designator. This gives a total graph set descriptor $G_d^a(n)$. Some examples of hydrogen bonds showing the four fundamental motifs are illustrated in Figure 1.4. Graph-set notation can be initially assigned to motifs and then to higher-level networks. Graph-set analysis can be employed in crystal engineering to identify

isographic relationships (i.e. chemically different functional groups having the same graph-set) and prevailing hydrogen bond patterns, and is indeed a very valuable tool.

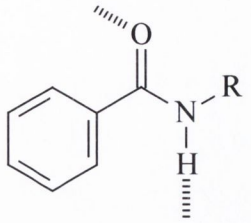

$C(4) \equiv C_1^1(4)$

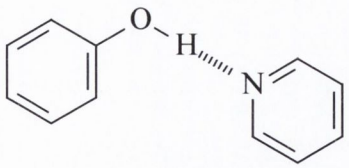

$D \equiv D_1^1(2)$

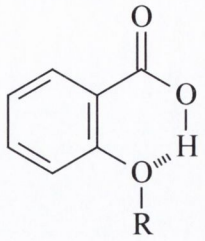

S(6)

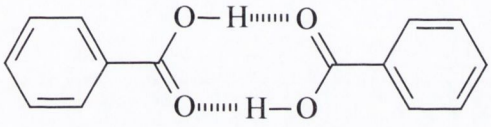

$R_2^2(8)$

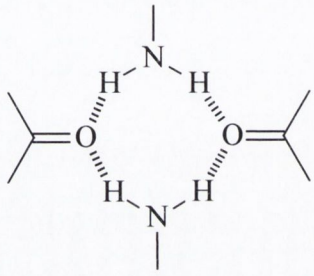

$R_4^2(8)$

Figure 1.4 – Examples of different motifs of hydrogen bonds with their graph sets.

In conjunction with Etter's studies, work in solid-state organic chemistry by Desiraju afforded the concept of supramolecular synthons[47] as an analogy to molecular synthons in organic synthesis.[48] Desiraju has defined supramolecular synthons as "structural units within supermolecules which can be formed and/or assemble by known or conceivable synthetic operations involving intermolecular interactions". Thus, supramolecular synthons are substructrural motifs, which incorporate the chemical and geometrical characteristics of intermolecular interactions, and are a key tool in crystal engineering. Figure 1.5 shows some representative examples of supramolecular synthons. It must be noted that in the definition of supramolecular synthons are included interactions other than the hydrogen bond, such as aryl-aryl interactions and short contacts between halides, but it is mainly synthons based on hydrogen bonding interactions that have found the most use in crystal engineering. This is because the goal of crystal engineering is to recognize and design synthons that are robust enough to be exchanged from one network structure to another, and these are best provided by hydrogen bonds. Strong hydrogen bonds, such as N-H···O and O-H··O, have been the prime interaction of choice. However, one must be careful and also consider weaker interactions, as in several instances it is these that have dictated the strong hydrogen bonded synthons.[37]

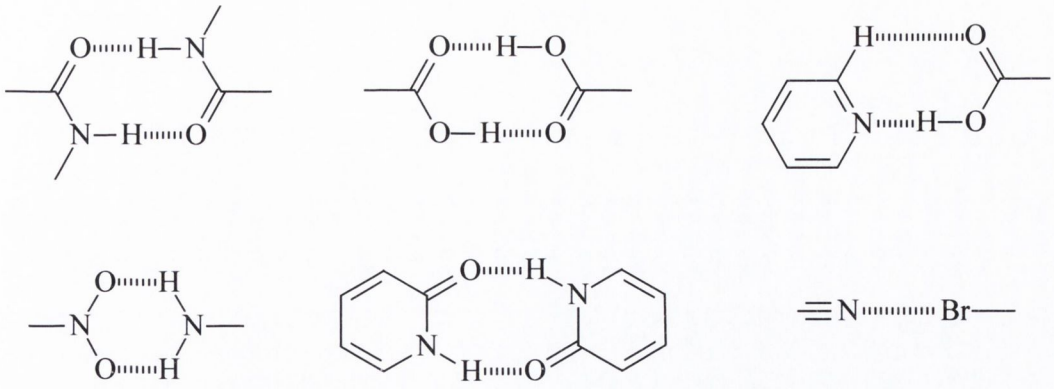

Figure 1.5 – Some examples of supramolecular synthons.

Carboxylic acids are perhaps the most commonly used functional groups in crystal engineering studies. They have been widely studied crystallographically[49] with two common motifs being observed in the solid state: dimers and catemers, as shown in Figure 1.6.

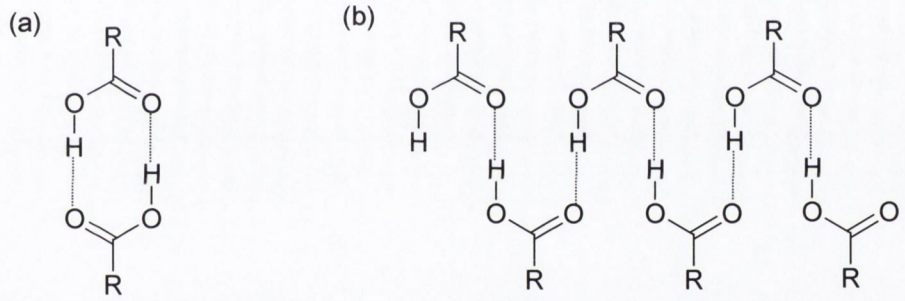

Figure 1.6 – Hydrogen bonded motifs formed by carboxylic acids: (a) dimer, (b) catemer.

While the catemer motif has been observed, it is nonetheless rare and it is the carboxylic dimer ($R_2^2(8)$) that is more commonly formed. This supramolecular synthon may be used to assemble a variety of supermolecules, as illustrated in Figure 1.7. Benzoic acid forms zero-dimensional dimers. By incorporating another carboxylic acid functionality in the benzene ring, as in terephthalic acid, with a linear predisposition, a one-dimensional chain is formed. The incorporation of a third carboxylic acid group, as in trimesic acid (H_3TMA), with its threefold symmetry, then produces a two-dimensional sheet. The logical progression from this is to use adamantane-1,3,5,7-tetracarboxylic acid with its tetrahedrally disposed carboxy functionality which forms a three-dimensional diamondoid network.

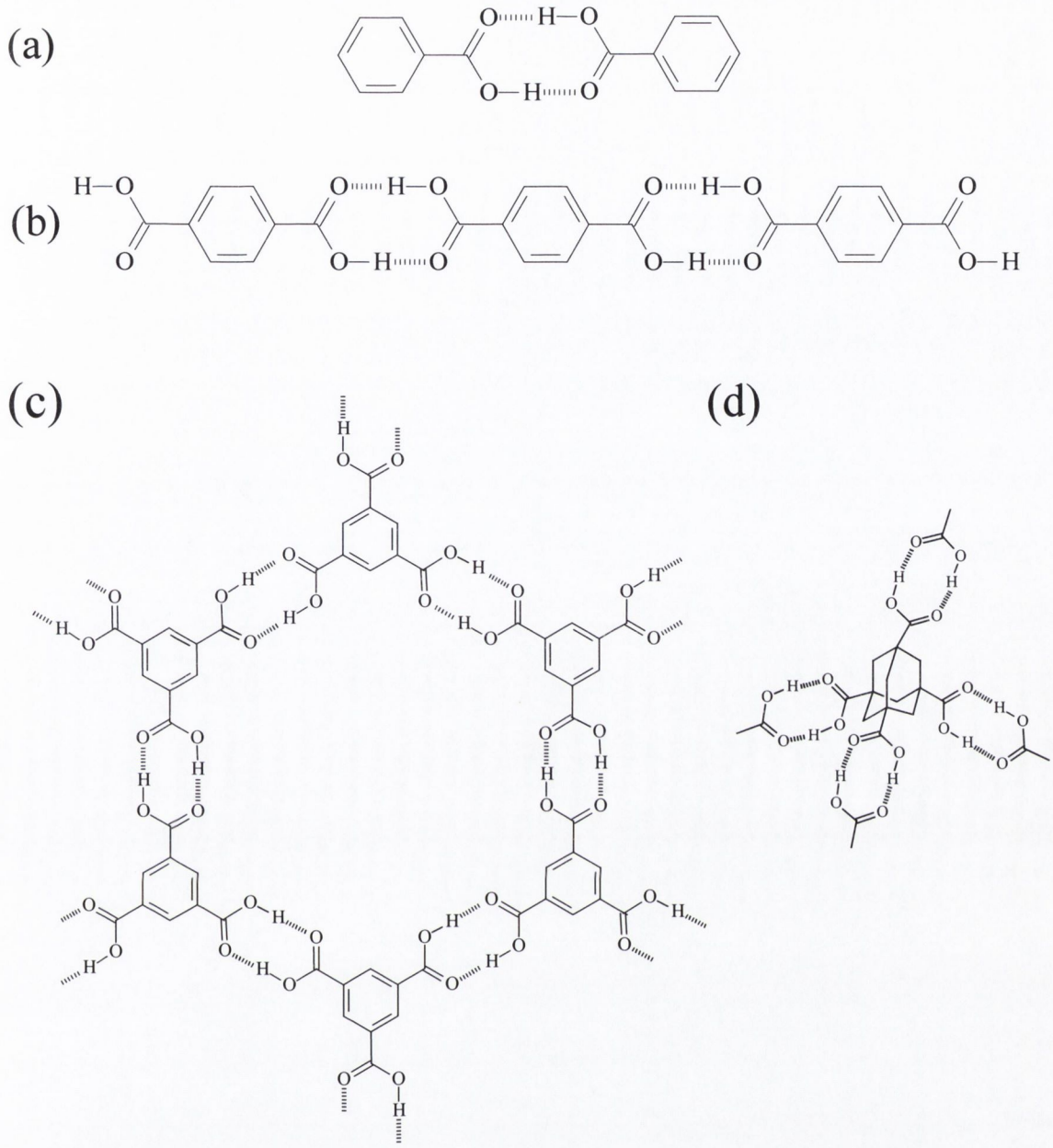

Figure 1.7 – Construction of zero-, one-, two- and three-dimensional networks using the carboxylic acid dimer synthon.

In addition to structures based on the homomeric carboxy dimer, a range of binary co-crystals, have been assembled through robust heteromeric interactions.[50, 51] Using the carboxylic acid-pyridine interaction, co-crystals of 4,4'-bipy with various carboxylic acids have been formed.[52] As 4,4'-bipy has two linearly disposed hydrogen bonding sites, the majority of the structures formed are expanded versions of the networks formed solely by the carboxylic acids. The chicken-wire grid formed by $[H_3TMA][4,4'\text{-bipy}]_{1.5}$ resembles that of H_3TMA but contains larger holes in the structure due to the inclusion of 4,4'-bipy in the network.[53]

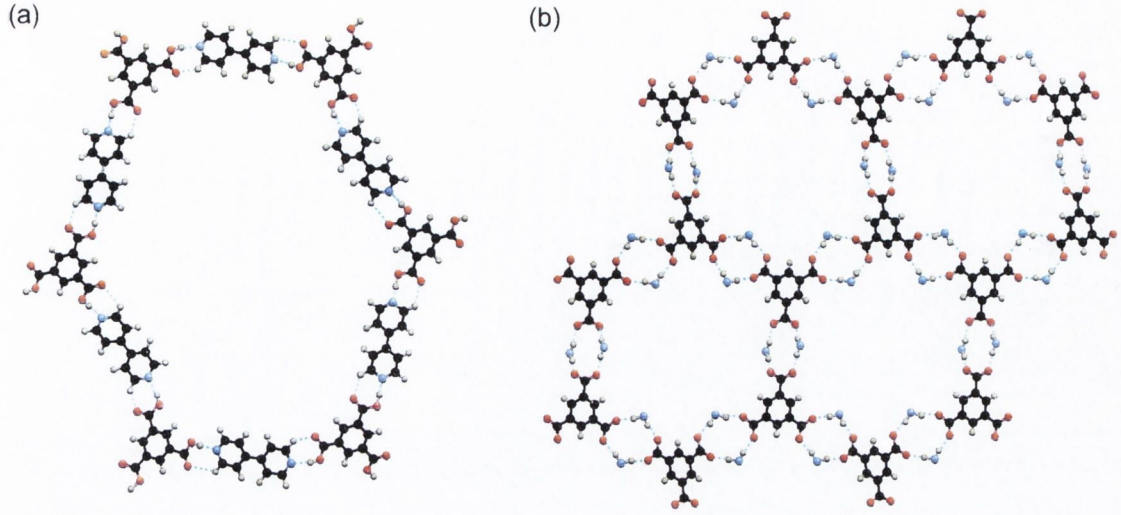

Figure 1.8 – (a) Detail of one of the cavities formed by $[H_3TMA][4,4'\text{-bipy}]_{1.5}$. (b) Network formed by $[NH_2(Bu^t)_2]_3[TMA]$. Note both are expanded versions of the honeycomb network of H_3TMA.

Hydrogen bonded networks of deprotonated carboxylic acids with various substituted ammonium cations have also been assembled.[54-57] These tend to produce lamellar structures which by mimicking the structure and properties of naturally occurring clays may find applications in storage and separation. The carboxylate and dialkylammonium moieties can self-assemble in two different motifs shown in Figure 1.9. The assembly of TMA with dicyclohexylammonium generates the anticipated honeycomb array through the $R_4^2(8)$ or $R_4^4(12)$ motif depending on the solvent employed.[56, 57]

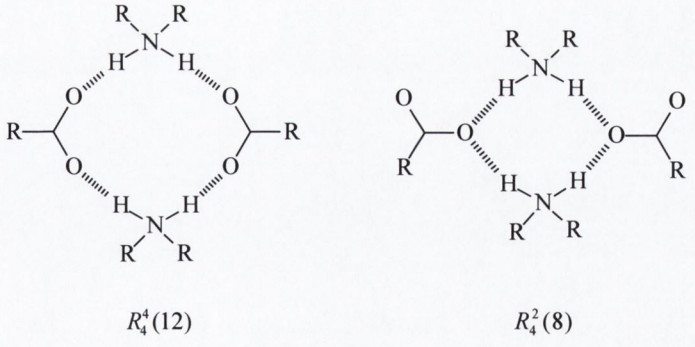

Figure 1.9 – Two different motifs that can occur through self-assembly of dialkylammonium and carboxylate moieties.

1.5 Inorganic crystal engineering

The field of crystal engineering was fuelled by the advent of supramolecular chemistry, and while originally concerned with organic molecules recently the metallosupramolecular field has started to receive more attention[58]. The essential idea behind the inclusion of metals into organic supramolecular structures is to incorporate

the photochemical, photophysical and electrochemical properties offered by transition metals. The geometric requirements of transition metal ions allow metals to be used as building blocks responsible for connecting subunits in a controlled fashion. The emphasis lies in the choice of ligand and the choice of metal ions in order to control the outcome, where the metal acts as both 'cement' holding the ligands together and as a centre orienting them in a given direction. Metal ions have several properties that make them especially useful for applications in supramolecular assemblies:

a) a set of coordination geometries,
b) a range of binding strengths from very weak to very strong (from 2 kJ/mol to 250 kJ/mol), and a range of formation and dissociation kinetics, from labile to inert,
c) a variety of photochemical, electronic and magnetic properties.

There is a plethora of examples of the use of metal ions in the formation of supramolecular systems, some of which are shown in Figure 1.10. Some of these include discrete molecular species such as molecular triangles, squares and other polyhedra,[59-62] helicates[63-65] and catenanes[66, 67] as well as infinite supramolecular structures such as chains,[68-70] ladders,[71-73] and adamantoid networks.[30] Quite often innovative design features have been required to achieve the desired structures. The field remains an exciting and fast moving one that continues to produce a range of new materials, and it is the promise of useful molecular devices that drives the continuing widespread interest in the field.[74, 75]

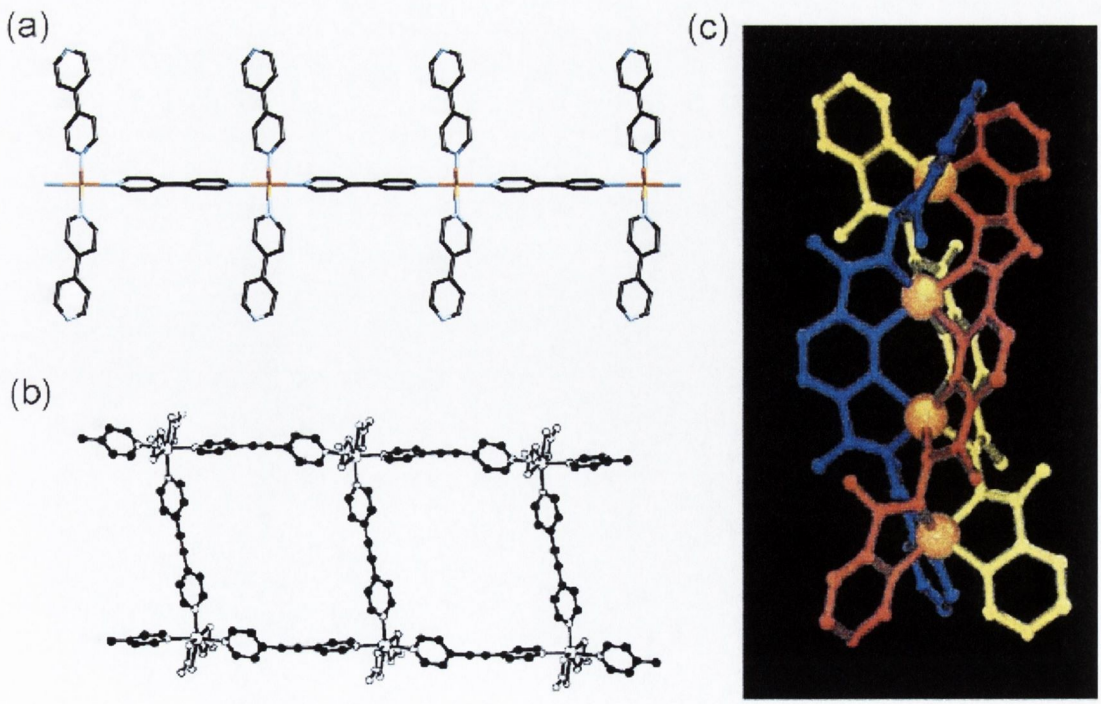

Figure 1.10 – Some examples of metallosupramolecular architectures: (a) an infinite chain;[76] (b) an infinite ladder;[73] (c) a discrete molecular helicate.[77]

1.5.1 Coordination polymers

The synthesis and study of coordination polymers has grown enormously in the last decade to become the biggest area of study within crystal engineering, and still continues to expand exponentially. Coordination polymers are 'infinite' metal-organic assemblies that extend into one, two or three dimensions *via* metal-ligand bonding. Metal-ligand bonds are stronger and more directional than other weak interactions, such as hydrogen bonding and π-π stacking, and thus allow for a more reliable prediction of the resulting structure. However, while the metal-ligand bonds play a key role in dictating the structure, weaker interactions also play a part in the packing of these coordination polymers and must not be neglected. In addition metal ions provide a set of geometries, such as octahedral, not available with organic molecules, for the construction of unprecedented architectures.

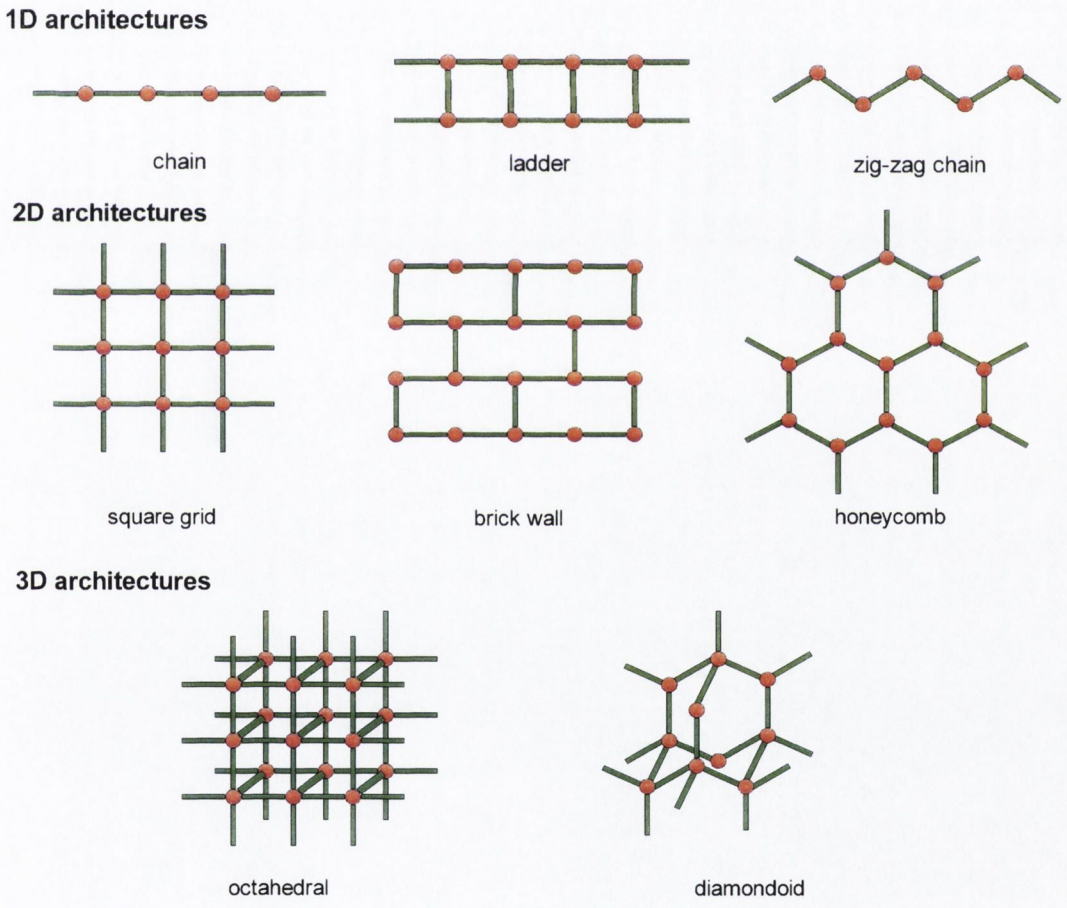

Figure 1.11 – Schematic representation of some 1D, 2D and 3D networks available for the construction of coordination polymers with the metal ion (red circle) as the node and a linear bifunctional ligand (green line) as a spacer. The metal geometry, metal-to-ligand ratio, solvent and reaction conditions will ultimately determine the type of network formed.

Robson may be considered the pioneer in the field of coordination polymer 'engineering' and it was his initial studies that facilitated the rapid development of the field.[78-83] The approach adopted by Robson is an extrapolation of the seminal work by Wells in structural inorganic chemistry[84, 85] and describes the rational synthesis of new coordination polymers based on simple network prototypes. A particular network (net) is selected as a specific topological model on which the structure is 'engineered'. Thus the construction and further spontaneous assembly of molecular building blocks with an appropriate stereochemistry and functionality to a particular net may lead to the intended network. One example of this approach is the structure of diamond, which consists of tetrahedral carbon atoms connected together to give a simple 3D network. If the carbon atoms are replaced with tetrahedral metal centres (e.g. Cd(II)) and the C-C bonds with linear bridging ligands (e.g. cyanide), a new structure is formed ($[Cd(CN)_2]$), shown in Figure 1.12, which has the same topology as diamond.[79] In this case the C-C bonds of 1.54 Å are replaced with much longer Cd-CN-Cd bridges of 5.46 Å resulting in a very porous network which actually consists of two identical interpenetrating networks.

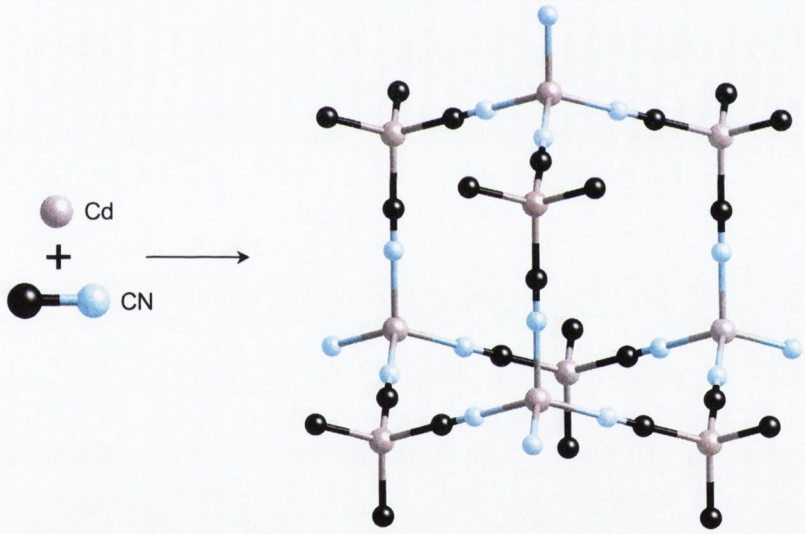

Figure 1.12 – Network formed by $Cd(CN)_2$, which has the same topology as diamond.

In principle, to make a coordination polymer all that is necessary is to allow to react a metal ion with a potentially bridging ligand. Thus, the ligands must possess multiple, divergent coordination sites. Currently, the majority of bridging ligands are nitrogen- and oxygen-donor ligands, however phosphine-based ligands have also been successfully employed.[86, 87] Some examples of ligands used in the formation of coordination polymers are shown in Figure 1.13. The use of rigid ligands is also of great importance. By reducing the conformational freedom of the ligand, the degrees of freedom in the system are reduced and therefore network structure predicition is more reliable. Thus aromatic ligands feature significantly in the construction of coordination polymers. One of the most prominent ligands is 4,4'-bipyridine.[80, 88-96] It has two linearly

disposed coordination sites, and although it can rotate about the C-C bond this does not affect the orientation of the lone pairs. Thus, when combined with the different metal geometries available, diverse architectures such as chains, ladders, grids and octahedral networks are effectively formed.

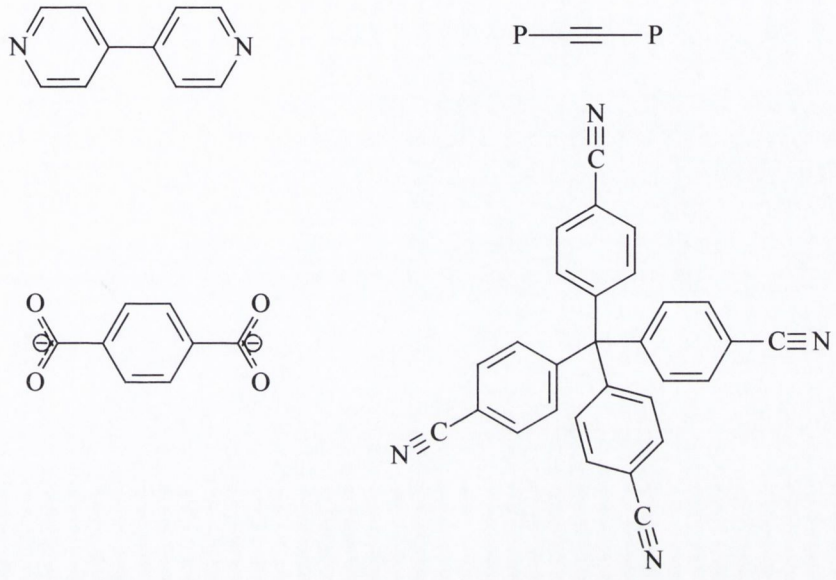

Figure 1.13 – Representative examples of ligands used in the construction of coordination polymers.

The 'node and spacer' approach has been very successful at producing predictable network architectures. However a particular metal and ligand combination may be linked in a number of ways even with the same stoichiometry. This is termed polymorphism or supramolecular isomerism, which are in themselves interesting phenomenons.[50, 97] Weaker interactions involving the ligand, counterions and solvent molecules may also produce a different structure to that formed if only the metal-ligand interactions are taken into consideration. In addition, the same nodal geometry may produce different topologies. For example tetrahedral nodes may give rise to diamond, lonsdaleite and quartz networks. Thus, it is quite common to obtain unexpected results, which, sometimes, are more interesting than the original target structures.

As with organic polymeric systems, coordination polymers are most often not soluble as such. Thus routine characterization techniques (NMR, MS, UV, *etc.*) are of little use to the coordination polymer chemist and instead structural analysis is heavily reliant on X-ray crystallography and other solid state techniques (DSC, TGA, microanalysis, *etc.*). Indeed, without knowing the crystal structure, the interpretation of any subsequent properties would be very hard. Thus, the production of single crystals is essential for the characterization of coordination polymers.

The design of coordination polymers has moved from a topological and aesthetic goal to a more 'practical' purpose where structure design leads to desirable

properties. The modularity of an organic ligand (steric-electronic properties, chirality, size, functionalisation, *etc.*) may be fused with the inherent physico-chemical properties of transition metals (colour, magnetism, catalysis, chemical and photo-reactivity) to yield 'smart' compounds. Some of the applications of these compounds may include catalysis, electrical conductivity, luminescence, magnetism, non-linear optics or zeolitic behaviour.[32]

1.5.2 Networks

Over twenty-five years ago, Wells provided a survey of the simpler nets,[85] however he noted that his compilation is not exhaustive, and that there does not exist an all-inclusive method of deriving nets. This has provided a useful catalogue of nets relevant to chemistry.

One way to represent the topology or connectivity of a given net is in terms of the general symbol (n,p), where p is the number of connections to neighbouring nodes that radiate from any centre or node, and n is the number of nodes in the smallest closed circuits in the net. Thus, the number 6 in the symbol (6,3) indicates that the smallest complete circuits in the net are hexagons, and the number 3 indicates that each node is connected to three other nodes. Figure 1.14(b) shows two versions of the (6,3) net, which are geometrically different but topologically identical. This also illustrates the point that although nets may be geometrically deformed, provided no connections are broken, the topology is considered to remain unchanged.[98]

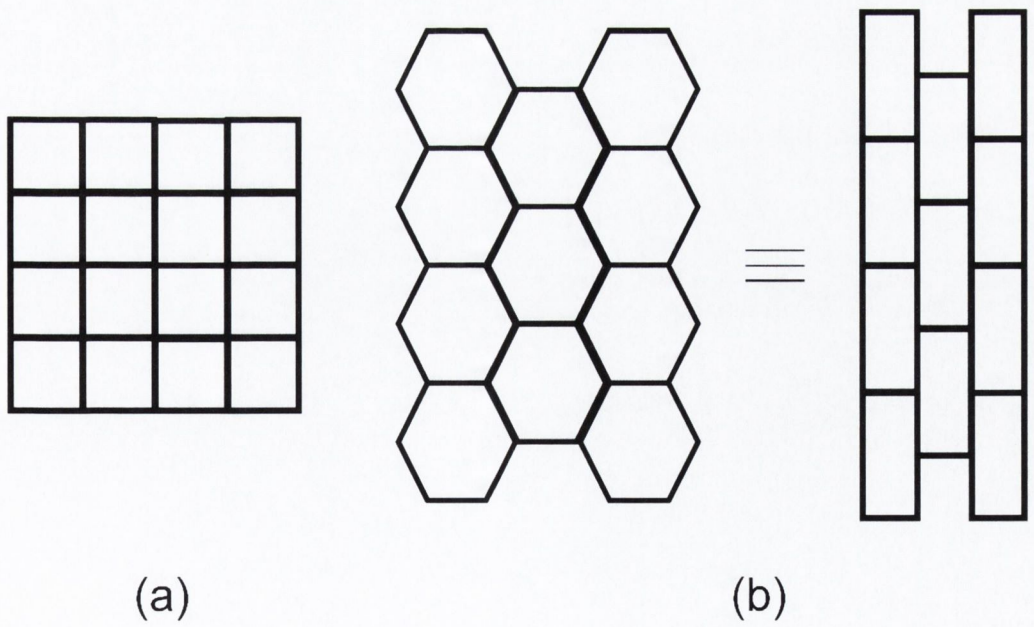

Figure 1.14 – (a) Schematic representation of the so-called (4,4) net. (b) Schematic representation of two geometrically different forms of the topologically equivalent (6,3) net.

A 'shortest circuit' is defined as the shortest circuit possible, which includes a given pair of links from a node. Thus, each pair of links from a node has a 'shortest circuit' associated with it. For each link emanating from a *p*-connected node there are (*p*-1) other links *via* which to return to the original node. Hence for any node there are *p*(*p*-1)/2 'shortest circuits'. The factor of *p*(*p*-1) must be halved so that each 'shortest circuit' is not counted twice, since it does not matter from which direction the circuit is completed. As paradoxical as it may sound, the 'shortest circuits' for a given node are not necessarily all the same size. The (*n*,*p*) network notation strictly applies only when all the 'shortest circuits' originating from any node in the net are all *n*-gons (as is observed for the (6,3) network in Figure 1.14(b)).

When this is not the case the more complete Schläfli notation $n^{p(p-1)/2}$ should be used. In the network shown in Figure 1.14(a), four of the six 'shortest circuits' for each node involve four nodes (*cis* links[†]), while the other two involve six nodes (*trans* links) In this case the complete Schläfli notation of $[4^4.6^2]$ should be used.[98] Wells simplified this to 4^4 or (4,4) by arbitrarily excluding circuits involving co-linear connections.

A number of 3D nets are often described by the names of materials displaying the relevant topology. Diamond, lonsdalite, and quartz have already been mentioned as examples of 3D nets with tetrahedral nodes. Another example is that of α-polonium (α-Po or NaCl), which contains six-connected octahedral nodes linked to form a cubic network (Figure 1.15). Some networks contain more than one type of node connectivity. The rutile (TiO_2) network is one example that contains both octahedral six-connecting nodes and trigonal three-connecting nodes in the ratio 1:2 (Figure 1.15). When applying the Schläfli notation to these networks the same principles apply (with regard to 'shortest circuits') but the two different nodes are dealt with separately.

[†] A *cis* link can be defined as a connector lying in a *cis* orientation to the connector traversed upon exiting the node. Similarly a *trans* link is a connector lying in a *trans* orientation to the exiting connector.

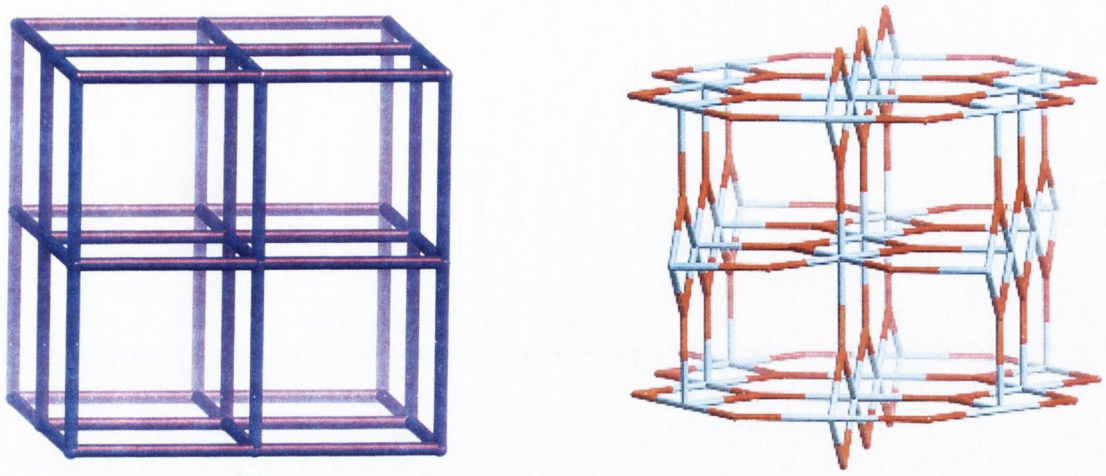

(a) (b)

Figure 1.15 - (a) α-Po (NaCl) type network consisting of six-connected nodes. (b) Rutile (TiO_2) type network consisting of six- and three-connected nodes in a 1:2 ratio.

Various 3-connected nets have been catalogued by Wells.[85] In the *uniform* (*n*,3) nets every node is 3-connecting and the shortest circuits involving all three different pairs of connections radiating from each node are *n*-gons. The (6,3) net has already been mentioned and is the only (*n*,3) plane net. The 3D 3-connected nets include the (12,3) and the (10,3) net. The (12,3) net is the one with the largest *n* value considered by Wells. The (12,3) net, as shown in Figure 1.16(a), where all nodes are planar, can be described in terms of 'double' sixfold helices, where all helices are parallel and of the same handedness, thus the net is intrinsically chiral. This net occupies a unique position amongst all the uniform nets in showing self-entanglement such that some of its shortest circuits have other shortest circuits passing through them. Seven (10,3) connected nets are known and are catalogued alphabetically from (10,3)-a to (10,3)-g according to symmetry. The (10,3)-a net, sometimes referred to as the $SrSi_2$-related net, is the simplest and most symmetrical of the 3D 3-connected nets. It is shown in its most symmetrical form (cubic), with links of equal length and exactly 120° interbond angles, in Figure 1.16(b). Parallel to each of the crystallographic cubic axes are four-fold helices which are all of the same hand, and therefore, like (12,3), this net is also enantiomorphic. Wells referred to the (10,3)-a net as the three-connected analogue of diamond, and in the same way diamond is presently the dominant structure for four-connected coordination polymers, the (10,3)-a net may be expected to dominate three-connected networks in years to come. Indeed, as the field of coordination polymers grows more examples of structures with the (10,3)-a topology have been discovered.[99-108] The many well-known simple 3D nets provide realistic targets for crystal engineers to model future materials upon.

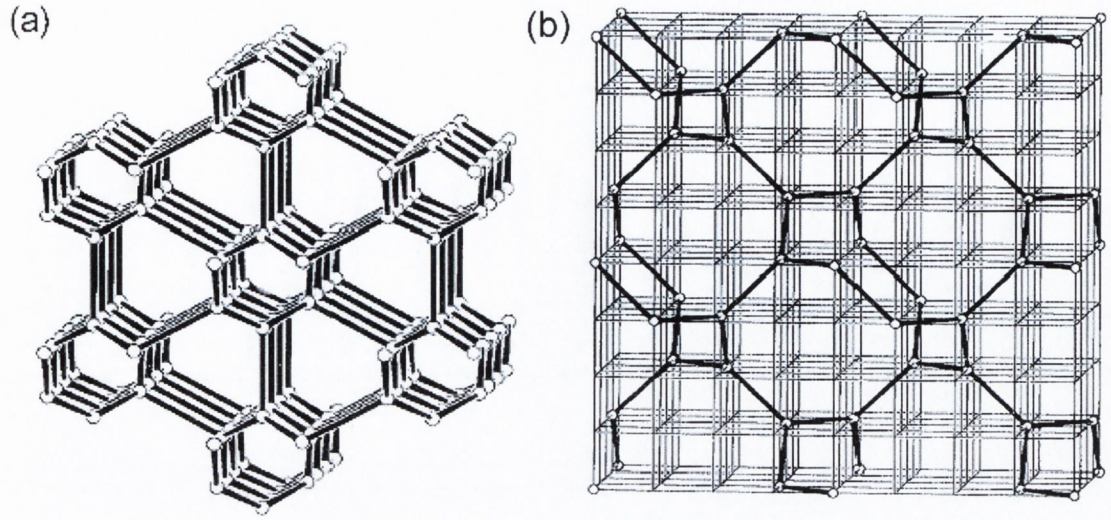

Figure 1.16 – (a) Representation of the chiral (12,3) net in which all nodes are planar and equivalent.[109] (b) Representation of the chiral (10,3)-a net.[99]

1.5.3 Metal-organic frameworks (MOFs)

From a survey of the possible networks structures available for the synthesis of coordination polymers, the presence of voids or cavities in the architectures is evident. A direct consequence of this is the generation of open framework coordination polymers with high levels of porosity. Thus, one of the most promising applications of coordination polymer design is in the production of nano- or microporous materials.[110-114] The term 'metal-organic framework' implies a combination of a metal ion and an organic ligand, and so all coordination polymers fall in this class. However the term has become synonymous with coordination polymers that exhibit porosity, and is normally, though not exclusively, used to describe such structures. The formation of accessible channels within a structure makes these promising materials for applications in catalysis, separation, gas storage and molecular recognition. Zeolites, which are typically aluminosilicate based, are the prime example of porous materials.[115] The uniform nature and high degree of porosity within the crystalline forms allows the passage of smaller molecule or ions throughout their network structures. Thus, they have found many diverse applications, from petrol cracking in the oil industry to the home market as water softeners in detergents. However, metal-organic frameworks offer various benefits over their inorganic rivals such as greater control over pore size and shape, as well as more gentle synthetic techniques. In addition, porous metal-organic frameworks may offer properties, such as chiral recognition and redox activity, unavailable in traditional inorganic zeolites.

In the same way that supramolecular synthons have been identified and exploited in the design of hydrogen bonded networks, recurring structural motifs which arise from a number of metal ions and ligands have been identified from polymeric

structures or discrete metal complexes. These are referred to as secondary building units (SBUs).[116] The connection of these SBUs with an organic linker should produce an extended network. This approach was first adopted by Yaghi and co-workers in their use of carboxylate based ligands for the construction of MOFs.[117-120] Carboxylates tend to chelate metal ions into stable metal-oxygen-carbon 'clusters'.[121] Figure 1.17(a) shows the 'paddle-wheel' type of dinuclear carboxylate cluster, which contains four acetate groups coordinated to two metal centres. Figure 1.17(b) shows a trinuclear cluster where six acetate groups coordinate to three metal centres. Functionalisation of the acetate groups to include a second carboxylate coordination site allows for these clusters to be linked together.

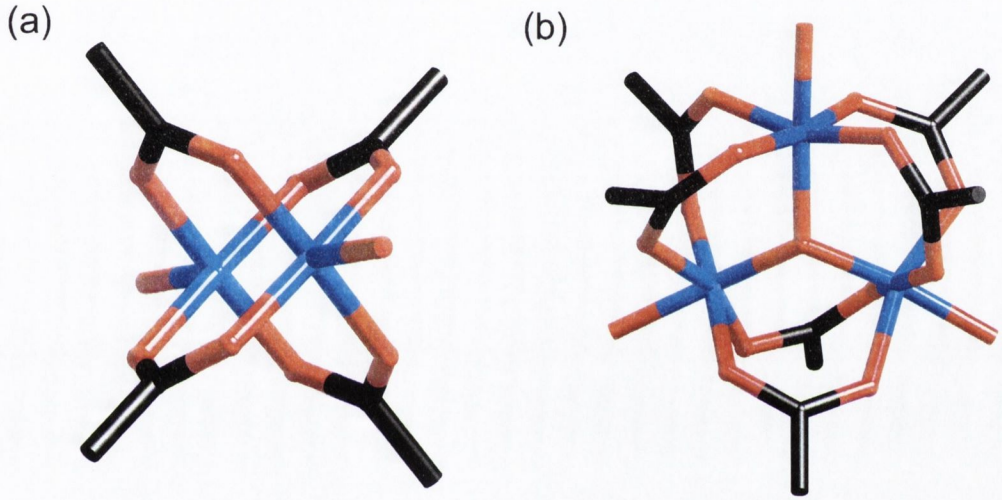

Figure 1.17 – (a) 'Paddle-wheel' dinuclear carboxylate cluster. (b) Trinuclear carboxylate cluster.

By aggregating metal ions into these metal-carboxylate clusters, the networks formed using multitopic carboxylate ligands are inherently more rigid than those formed using N-donor ligands. Furthermore, interpenetrated structures are less likely to form due to the bulk associated with metal-carboxylate clusters. Anionic carboxylate ligands provide the charge balance, and since the resulting framework is neutral the need for counterions in the network, which may obstruct any channels formed, is avoided. Thus, the construction of MOFs is dominated by multitopic carboxylate ligands, which have led to the formation of robust porous frameworks. Some of these ligands are shown in Figure 1.18. The increasing distance between the carboxylate moieties allows a measure of control over the size of the cavities bound by the networks.[122]

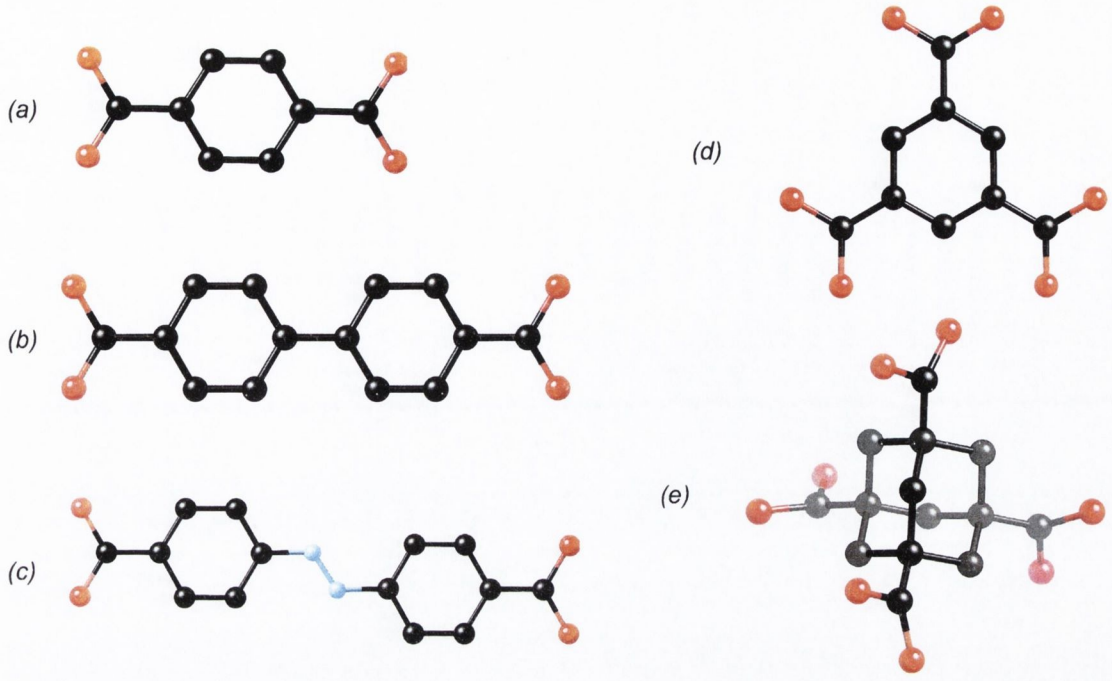

Figure 1.18 – Carboxylate-containing ligands used in the formation of metal-organic-frameworks.

Figure 1.19 shows the structures of a selection of porous coordination polymers prepared by Yaghi and co-workers,[123] with the cativies highlighted in yellow. These MOFs consist of Zn-O-C clusters held together with different bridging groups. The length of the bridging unit determines the dimensions of the cavity and thus the porosity of the polymer. Additionally, the pores can be chemically modified without changing the resulting network by functionalization of the carboxylate ligands. Despite the large amount of free volume (up to 90%) in these polymeric systems, remarkably, the networks do not interpenetrate. Interpenetration is largely undesirable in these systems as it generally leads to small pore size. However, in one instance interpenetration of the networks has led to added structural rigidity whilst still maintaining high porosity (67%).[119]

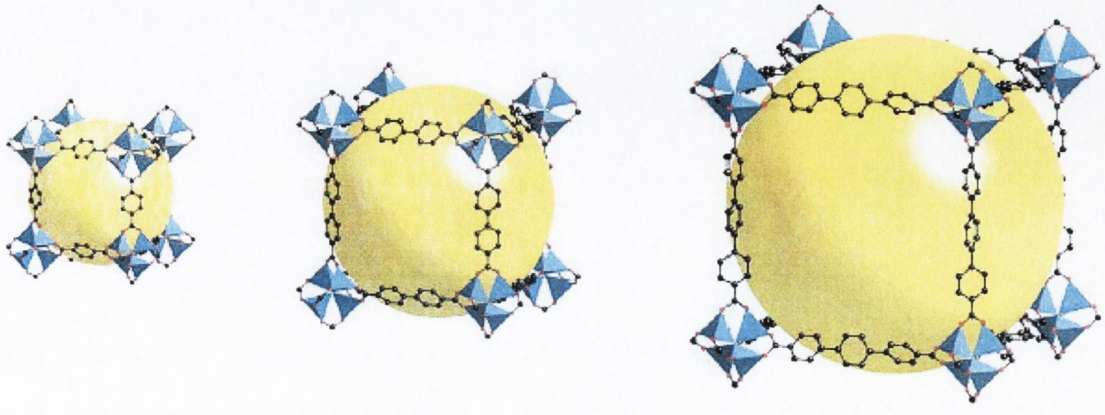

Figure 1.19 – A selection of zinc-containing metal-organic-frameworks of differing porosity. Note the different bridging units used to expand the dimensions of the network.[123]

Applications of these porous frameworks are currently being explored. Research into the use of fuel cells as an alternative to combustion engines is a growing area of current study. One of the problems associated with fuel cells is the storage of hydrogen, which is used as a fuel source. The fact that the MOF complexes form porous networks means that they may have a potential use in the storage of hydrogen for use in fuel cells.[124, 125] These MOFs have shown remarkable internal surface area properties, because unlike zeolites, they do not have internal 'walls'. Indeed the current "world record" is held by a zinc-MOF, which has a specific surface area of approximately 3000 m^2g^{-1} compared to carbon nanotubes (200 m^2g^{-1}) and zeolites (700 m^2g^{-1}).[124, 126]

In addition to Yaghi's studies of carboxylate-based MOFs, recent work by Kitagawa,[127-129] Kim,[130] and Murray,[131] amongst others,[132-135] have established the potential applications of these materials in gas sorption, storage, catalysis, enantioselective separation and as optical switches. Kitagawa described the synthesis, structural characterization and gas sorption properties of a series of coordination polymers. Secondly, Kim demonstrated that a porous homochiral metal-organic material is capable of both enantioselective separation and catalysis. Finally, Murray demonstrated that a nanoporous framework displayed reversible absorption of guest molecules which induced a spin transition in Fe(II) that was sensitive to the nature of the sorbed guests, thus signalling their presence.

1.5.4 Hydrogen bonded networks of coordination complexes.

Organic solids assemble through hydrogen bond interactions, while inorganic coordination polymers involve mainly strong metal-ligand interactions. However an alternative approach has emerged recently whereby coordination complexes are first generated and then assembled *via* intermolecular interactions.[136-139] This approach offers higher solubility than coordination polymers, a more predictable and controllable outcome and higher flexibility of the network (at the expense of strength). The intermolecular interactions discussed earlier for organic solids can also be applied to coordination complexes. A particular functional group will essentially form the same interactions whether as part of an organic molecule or a metal bound-ligand. Thus, the supramolecular synthons previously described can also be exploited here. However, there is a catch, the very atoms which can participate in hydrogen bonding may also provide a coordination site to the metal ions. This is best exemplified by the carboxylic acid functional group which can form the robust carboxy dimer through hydrogen bonding, but is also known to coordinate to metal ions in the deprotonated form. This may be overcome by the employment of ligands that offer an efficient metal coordination site as well as hydrogen bonding functionalities. Thus the peripheral groups are not affected by metal coordination and retain their capacity to participate in

intermolecular bonding. The inherent geometry of the metal ion may then be propagated through hydrogen-bonding of the ligand peripheral sites into a specific supramolecular architecture, as shown in Figure 1.20.

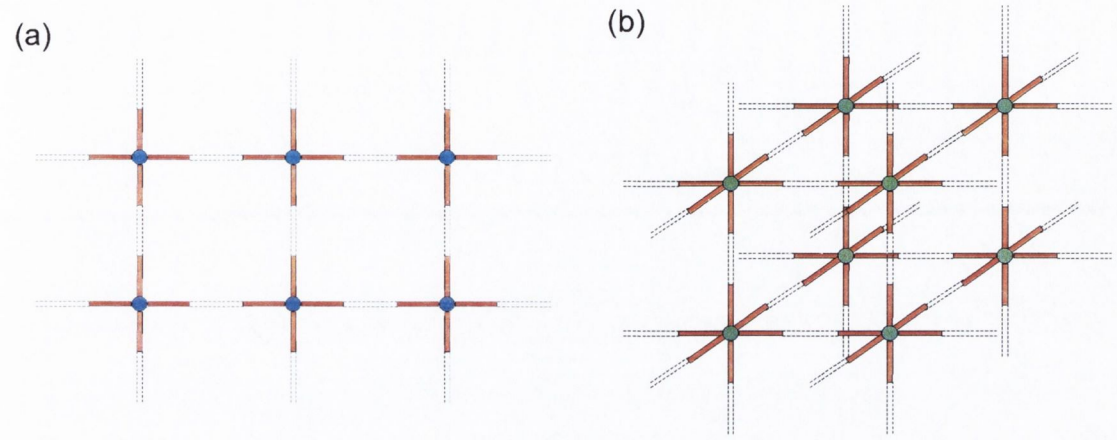

Figure 1.20 – Schematic representation of two type of architectures that may be formed from hydrogen bonded complexes. (a) A square planar metal ion, such as Pt^{2+}, may form a 2D sheet; (b) An octahedral metal ion, such as Fe^{2+}, may form a 3D network.

The first hydrogen-bonded coordination complexes, built with this strategy in mind, were assembled by Mingos and co-workers, where they employed metal-bound ligands with a DNA base-pair like hydrogen bond functionality to produce infinite architectures through co-crystallisation with organic molecules.[140] Many other hydrogen-bonded complexes have been assembled using isonicotinic acid and isonicotinamides, and related derivatives, since they possess a metal-coordinating pyridine site on one end and a carboxylic or carboxamide group capable of forming robust self-complementary hydrogen bonds at the other end (Figure 1.21).

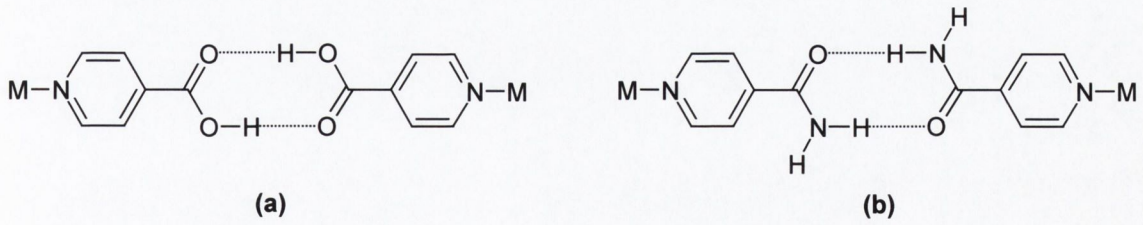

Figure 1.21 – Hydrogen bonding interactions of metal-bound isonicotinic acid (a) and isonicotinamide (b).

One-dimensional chains of Ag(I) with isonicotinamide have been obtained through self-complementary amide-amide dimer interactions[141] while ladders have been obtained from a combination of dimer and catemer amide-amide interactions.[142] The use of isonicotinic acid (HINA), and its derivatives in similar systems was found to yield different structures.[143] When the ligand is protonated and the complex formed is

cationic, hydrogen bonding occurs through carboxylic acid-counterion interactions, rather than the self-complementary acid dimers. When the ligand is deprotonated it may provide the balance charge for the metal ion and thus produce a neutral complex and a structure void of counterions. These type of complexes associate through the robust, charge assisted $COOH\text{-}COO^-$ synthon (Figure 1.22(a)). One advantage of using these neutral complexes is that, due to the absence of counterions in the structure, more space is available for possible guest molecules and the hydrogen bonding interactions become more predictable and controllable as no ligand-counterion interactions are possible. In this manner, a 2D square grid network of $Pt(INA)_2(HINA)_2$ has been assembled through $COOH\text{-}COO^-$ interactions (Figure 1.22(b)).[144] Though interpenetration of the nets occurs, channels occupied by water molecules are still present.

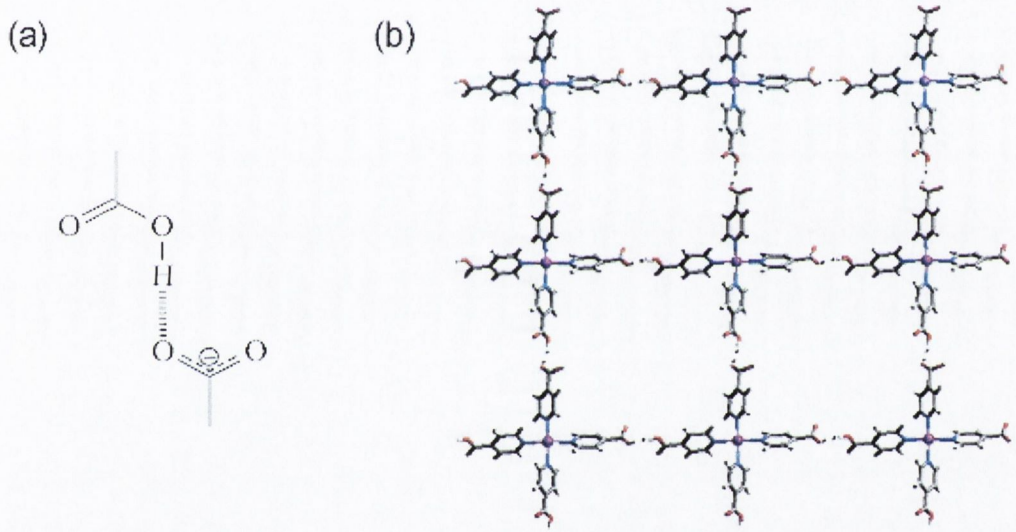

Figure 1.22 – (a) Carboxylic acid-carboxylate synthon. (b) 2D hydrogen bonded square grid assembled through charge assisted carboxylic acid-carboxylate hydrogen bonds.[144]

While the majority of hydrogen bonded assemblies of metal complexes result in 1D and 2D networks, a few examples of 3D networks exist.[145] Unusual trigonal planar Ag(I)-isonicotinamide complexes self-assemble to generate a 3D structure with $ThSi_2$-like topology.[146] As is common in these networks, interpenetration prevents the formation of channels. Initially, it would seem that the arrangement of six pyridine-based ligands, such as isonicotinic acid, around an octahedral metal centre would provide the ideal building block for the assembly of 3D hydrogen-bonded networks, but steric constraints usually prevent the formation of hexapyridyl complexes. In contrast, tris-chelated octahedral complexes are some of the best known transition metal complexes and are easily accessible. However, these tend to form propeller-like complexes that assemble in two-dimensions. Anionic metal complexes of 2,2'-biimidazolate self-

assemble via complementary NH···N bonds to create a 2D 'honeycomb' motif.[147] Self-assembly of cationic Fe(II) tris-complexes of 2,2'-bipyridines with urea-like substituents at the periphery have yielded 2D sheets with channels present in the structure (Figure 1.23).[148] In all these complexes Δ or Λ centres alternate, which invariably leads to the formation of a 2D network, whereas building blocks of the same chiral configuration should assemble into 3D networks.[149]

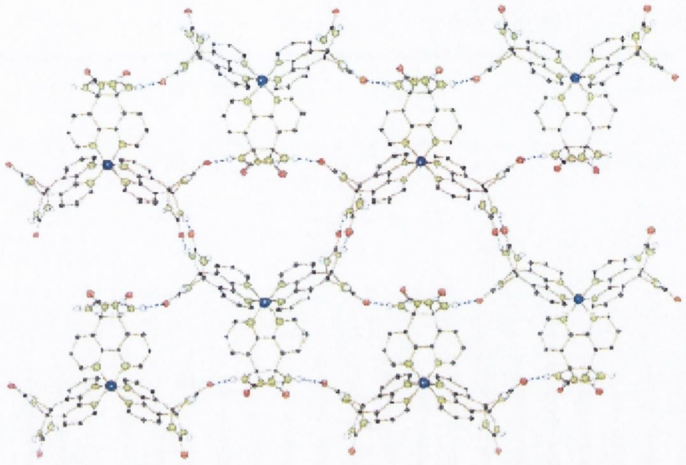

Figure 1.23 – 2D layer formed *via* hydrogen bonding of tris-chelated metal complexes. Note adjacent complexes are of opposite chirality.[148]

While all the examples above are of hydrogen bonded coordination complexes which assemble through direct ligand-ligand interactions, there are other examples where the coordination complexes are hydrogen bonded through counterions or neutral organic molecules. One widely used approach is the assembly of halometallates, such as $[MX_4]$, with protonated dications such as 4,4'-bipyridinium.[150-152] The metal-bound halides participate in hydrogen bonding with the 4,4'-bipyridinium to yield 1D assemblies, as shown in Figure 1.24. Similarly, neutral 4,4'-bipyridine molecules have been used as spacers in the assembly of encapsulated lanthanide species. The lanthanide building blocks are assembled through NH···4,4'-bipy···HN hydrogen bond interactions to produced 2D and 3D networks.[153] 4,7-phenanthroline has also been used as a neutral spacer between first-row transition metal aquo ions to yield three-dimensional networks *via* M-OH···N hydrogen bonds.[154]

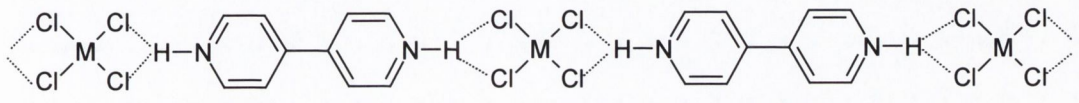

Figure 1.24 – Linear assembly of halometallates and 4,4'-bipyridinium *via* N-H···Cl hydrogen bonds.

From all the examples just discussed it is evident that hydrogen bonds are capable of assembling metal complexes into desirable motifs, even in the presence of competing solvent-metal and solvent-solvent interactions.

An extension of the hydrogen bonding of discrete metal complexes is the combination of low dimensionality coordination polymers (1D or 2D) with hydrogen bonds (Figure 1.25).[155-157] This approach has the advantage that it combines the strength of the coordination polymers with the flexibility of the soft hydrogen bonding interactions.

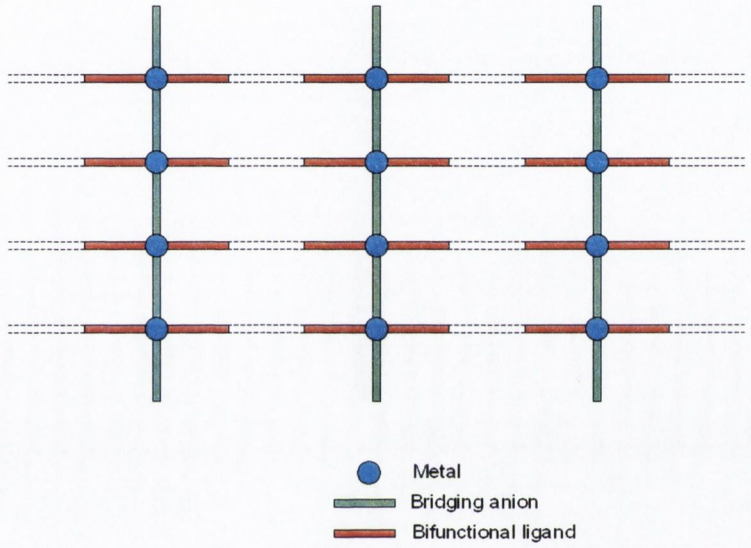

Figure 1.25 – Schematic representation of the strategy for the connection of coordination polymers through hydrogen bonds. A 1D polymeric chain is assembled into a 2D hydrogen bonded network.

For example, copper(I) halides can form neutral, one-dimensional stair or step chains[158] on which bifunctional ligands may be attached. Ligands may include substituted pyridine based ligands which can participate in self-complementary hydrogen-bonding and thus bridge the coordination polymers into a higher dimension. Therefore ligands such as isonicotinic acid, isonicotinamide and related derivatives are ideal for the construction of such networks, much like in the assembly of metal complexes. Aakeröy and co-workers have successfully employed this strategy and have synthesized various 2D sheets of Cu(I) halides coordination polymers bridged *via* self-complementary hydrogen bonding of carboxylic acid, carboxamide and oxime functionalities.[159] Similar systems have been isolated by Xu and co-workers by employing isonicotinic acid to bridge CuBr chains through hydrogen bonding.[160] In contrast to the complexes obtained by Aakeröy et al., where no interactions are observed between the 2D sheets, weak C-H···Br interactions exist between the sheets, thus linking them into a 3D supramolecular network.

Similarly, Nishikiori and co-workers have synthesized inclusion compounds for large, planar aromatic guest molecules.[161] Thiocyanato bridged Ni(II) chains are linked *via* self-complementary carboxylic acid hydrogen bonding of isonicotinic acid molecules bound to the chains. The 2D networks display channel-like cavities where biphenyl guests reside. The size of the cavities was enlarged by employing fumaric acid as a linear spacer which can also participate in self-complementary hydrogen bonding with the isonicotinic acid molecules.

1.6 Hydrothermal synthesis

Solvothermal processes can be defined as chemical reactions or transformations in a solvent under supercritical conditions or near such a pressure-temperature domain.[162] These processes have been mainly developed in the following scientific areas:

(a) The synthesis of new materials,

(b) the development of new processes for preparing functional materials, and

(c) the shaping of materials (crystal growth).

The elevated temperature and (autogenous) pressure created under solvothermal conditions allow for the isolation of metastable phases which would normally be impossible to produce using conventional reflux temperatures. Another important benefit of the solvothermal method is that differential solubilites of the reactants are less often a problem. Materials which are only sparingly soluble in a particular solvent at ambient conditions are generally sufficiently soluble under hydrothermal conditions to allow isolation of a solid product containing those precursors. Solvothermal processes are therefore a powerful route for the preparation of novel materials.[163]

The development of this approach for materials synthesis has developed rapidly since the first international conference on solvothermal reactions was held in 1994. While various solvents have been studied, water is the real driving force, and a whole sub-area, hydrothermal synthesis, has been developed. Hydrothermal synthesis has been widely used in the preparation of new materials such as zeolites and aluminophosphates.[164] The process has even found use in the production of artificial diamonds. Hydrothermal reactions have also been extensively applied to the synthesis of coordination complexes and clusters for the preparation of chemical sensors, microporous and magnetic materials. Much effort has been focused on the preparation of inorganic-organic hybrid materials.

Finally, in addition to new materials it is an interesting aside to say that hydrothermal chemistry is currently attracting studies on the origin of life and/or environmental issues. It is hypothesised, for example, that rich hydrothermal reactions

occurred in the sea and that all microorganisms have high-temperature ancestors. More and more evidence supports the idea of a hydrothermal origin to life, with micro-organisms found in hydrothermal vents (Figure 1.26).

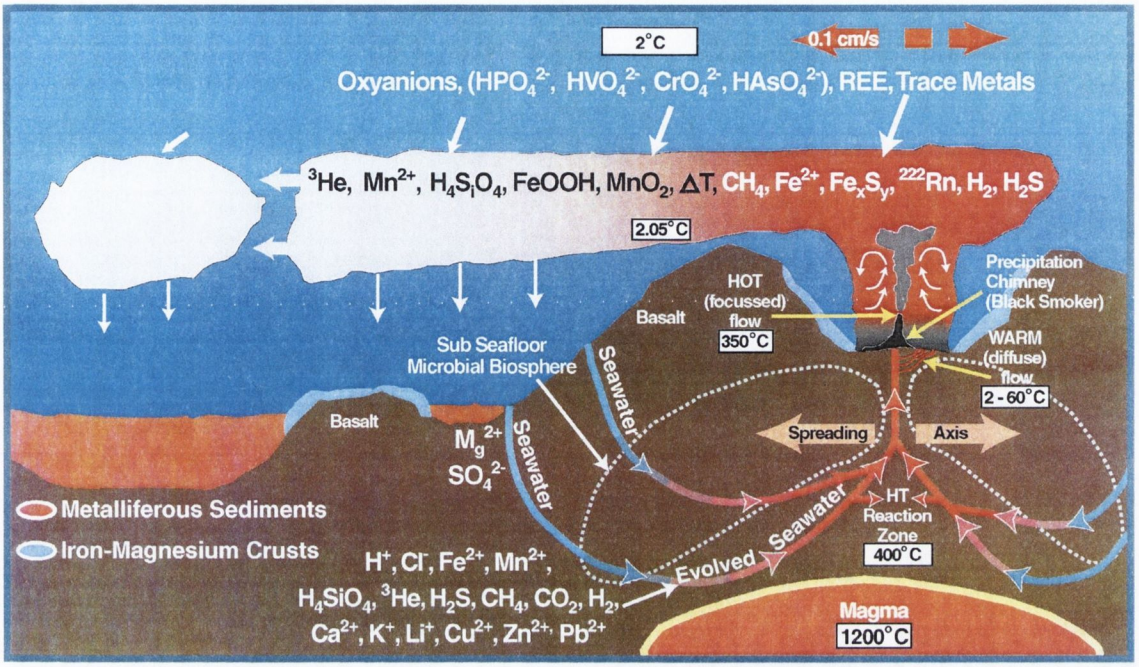

Figure 1.26 – Schematic of hydrothermal vent chemistry and a vent itself.[165]

A large number of novel materials have been synthesised from hydrothermal reactions. The increasing interest in hydrothermal synthesis derives from its advantages in terms of high reactivity of reactants and formation of metastable or unique condensed phases. The new materials it has returned have provoked significant interest in many fields such as photochemistry, catalysis and biology.

1.7 Present study

The main aim of this body of work is the study of 4,4'-dicarboxy-2,2'-bipyridine (4,4'-H_2dcbp) as a ligand for the formation of extended networks (Scheme 1). Most of the ligands used in the construction of extended solids are either nitrogen or oxygen-based, nevertheless pyridine-carboxylic acids, which combine both nitrogen and oxygen-donor sites, have also been used successfully.[166-170] However the use of bipyridyl-dicarboxylates remains relatively unexplored. While 4,4'-H_2dcbp complexes have been extensively studied in photochemistry and electron transfer reactions,[171-174] the use of 4,4'-H_2dcbp as a ligand in the construction of extended networks was unknown at the onset of this study. Since then various reports have emerged where 4,4'-H_2dcbp has been employed specifically for this purpose. Three reports include first-row transition metal ions,[175-177] while a fourth involves the use of lanthanide ions.[178] Various coordination polymers with the related 5,5'-H_2dcbp have also been produced by

Zubieta[179] and Lee.[180] Zubieta has also employed this ligand for the synthesis of organic/inorganic hybrid materials.[181]

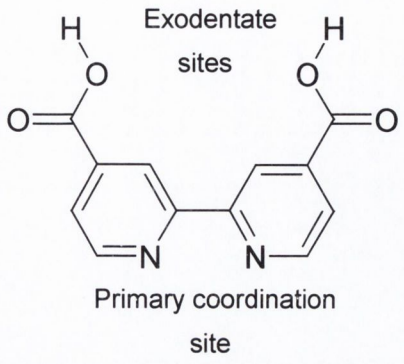

Scheme 1

The incorporation of functionalised poly-pyridines in the formation of extended networks, is particularly attractive, as the coordination chemistry of these ligands is especially rich and the physicochemical properties of the compounds extremely diverse.[182] In addition to chelating capacity at the primary bipyridyl coordination site, 4,4'-H_2dcbp has the potential to enter into self-complementary hydrogen bonding through the peripheral carboxylic acids, forming dimers or catemers or charge-assisted carboxylate-carboxylic acid hydrogen bonds. When deprotonated, 4,4'-H_2dcbp possesses dual coordination capabilities, with additional exo-dentate binding sites which, as shown in Figure 1.27, can coordinate to metal ions in diverse modes and provide the potential for the formation of metal-carboxylate clusters or bridging units. Additionally, the carboxylate moiety provides the charge balance thus obviating the need for counterions.

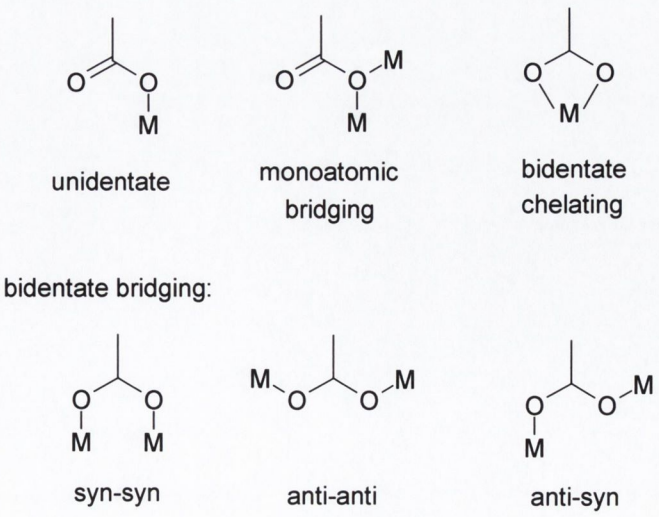

Figure 1.27 – Some of the coordination modes of carboxylates.

One of the implications in using bidentate chelating ligands is the formation of $[M(bidentate)_3]^{n+}$ units which may exist in two chiral conformations (Δ or Λ), and thus the incorporation of these into a supramolecular structure presents an opportunity to fine tune the stereochemistry of these supramolecules. The presence of a chelating nitrogen site can give rise to chiral complexes (Δ or Λ), and the controlled incorporation of these into a supramolecular architecture gives access to the formation of chiral networks through the use of achiral ligands.

In terms of topology 4,4'-H_2dcbp can act as a 3-connector (Figure 1.28) and as a result its incorporation into extended networks may give rise to the formation of the little known (*n*,3) connected nets.

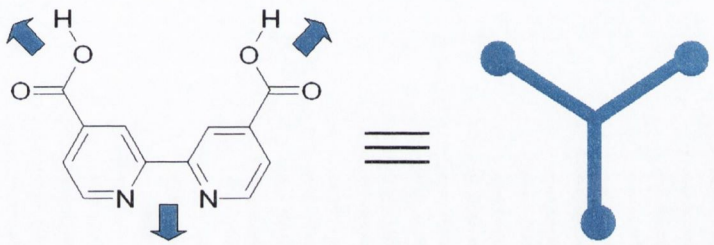

Figure 1.28 – Schematic representation of 4,4'-H_2dcbp as a 3-connector.

To illustrate the approach used in the formation of extended networks using 4,4'-H_2dcbp, an octahedral ion, such as Co^{2+}, with three 4,4'-H_2dcbp ligands around it is taken as an example of a building block. There are two approaches to the formation of extended networks: the coordination polymer approach and the hydrogen bonding approach. In the former the exodentate sites are deprotonated and used to bind the metal ions into carboxylate clusters, as described previously for carboxylic acids. Using the latter approach the ligand is protonated and can then participate in hydrogen bonding through the peripheral sites, thus propagating the octahedral geometry of the metal ion and form a pseudooctahedral network (deviation from ideal cubic geometry arises from the bite angle of the bipyridine moiety)(Figure 1.29).

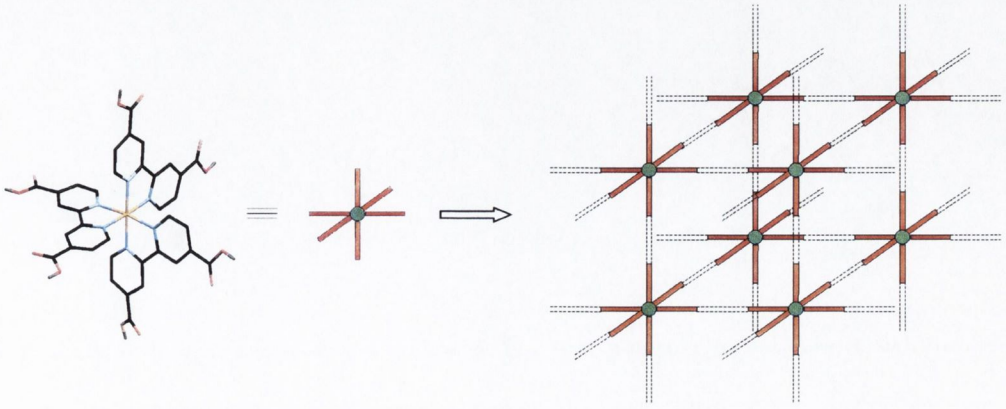

Figure 1.29 – Employment of an octahedral node with a 4,4'-H_2dcbp connector generates a pseudo-octahedral network.

Chapter Two

Coordination Polymers Incorporating 4,4'-dicarboxy-2,2'-bipyridine.

2.1 Introduction

As mentioned in Chapter 1, the interest in the synthesis of coordination polymers has grown considerably in the last few years. The use of carboxylate ligands as metal-centre linkers for the formation of coordination polymers has been exploited to great success by many chemists. There are two main advantages to the use of aromatic carboxylate ligands: firstly, as anionic ligands they provide the charge balance required for the networks, which means that voids in any resultant polymeric network are not occupied by counterions; secondly, they introduce rigidity into the network, making it robust towards dissociation. By employing 4,4'-dicarboxy-2,2'-bipyridine as a ligand we combine the primary 2,2'-bipyridyl chelating site, for which a myriad of coordination complexes are known, with the carboxylate functionality which incorporates the advantages mentioned above.

2.2 Reaction of Cu(II) with 4,4'-dicarboxy-2,2'-bipyridine.

2.2.1 Reaction of $Cu(NO_3)_2$ with 4,4'-Na_2dcbp.

An aqueous solution of $Cu(NO_3)_2$ was allowed to react with the sodium salt of 4,4'-dcbp in a 1:1 molar ratio, in the presence of $(NH_4)_2HPO_4$,and brought to pH~10 by addition of dilute NaOH, producing a blue solution from which small, blue crystals grew on evaporation. An infrared spectrum showed the presence of deprotonated 4,4'-dcbp ($\nu_{as}(CO_2^-)$ 1617 cm^{-1}, $\nu_s(CO_2^-)$ 1379 cm^{-1}) as well as water (3400 cm^{-1}). An X-Ray diffraction study, performed by Dr. Mark Nieuwenhuyzen of the Queen's University Belfast, showed these crystals to be a polymeric complex of formula $\{[Cu(4,4'\text{-dcbp})(H_2O)_2]\cdot 2H_2O\}_n$ (**1**)

Reaction of an aqueous solution of $Cu(NO_3)_2$ with 4,4'-Na_2dcbp in a 1:2 molar ratio at pH~7 also produced a blue solution from which blue crystals grew on evaporation. A crystal suitable for an X-Ray diffraction study was selected and from this the structure was determined to be a different, discrete complex of formula $[Na_2][Cu(4,4'\text{-dcbp})_2(H_2O)]\cdot 10\frac{1}{2}H_2O$, which will be described in Chapter 4.

*2.2.2 Crystal structure of $\{[Cu(4,4'\text{-dcbp})(H_2O)_2]\cdot 2H_2O\}_n$ (**1**).*

The structure of **1** was refined in the orthorhombic *Pnna* space group and crystallographic details are shown in Table 2.1. Atomic numbering scheme and atom connectivity for **1** are shown in Figure 2.1. The Cu atoms reside on 4*d* Wyckoff positions of the *Pnna* unit cell, hence, one half of each Cu(II) environment is related to the other by 2-fold rotation. Three different 4,4'-dcbp ligands occupy the equatorial positions of each Cu(II) atom. Two 4,4'-dcbp ligands coordinate *via* a single carboxylate oxygen (O2) *trans* to the nitrogens of the other chelating 4,4'-dcbp. Water

molecules (O1) occupy the axial positions on each Cu(II). The pseudo-octahedral centres display typical Jahn-Teller distortion with equatorial bond lengths of 1.960(3) Å (Cu1-O2) and 2.002(4) Å (Cu1-N1) and axial bond lengths of 2.443(5) Å (Cu1-O1) (See Table 2.2). Further distortion from octahedral symmetry can be seen in the *cis* coordination bond angles which range from 80.8(2)° (N1-Cu1-N1A) to 95.0(2)° (N1-Cu1-O1). The pyridyl rings of the 4,4'-dcbp ligand are slightly twisted with a torsion angle of 8° about the C1-C1A bond. The carboxylate groups are also twisted at 24° with respect to the aromatic rings. The C–O bond lengths differ for the coordinated (C6-O2 1.270(6) Å) and uncoordinated (C6-O3 1.241(6) Å) oxygens.

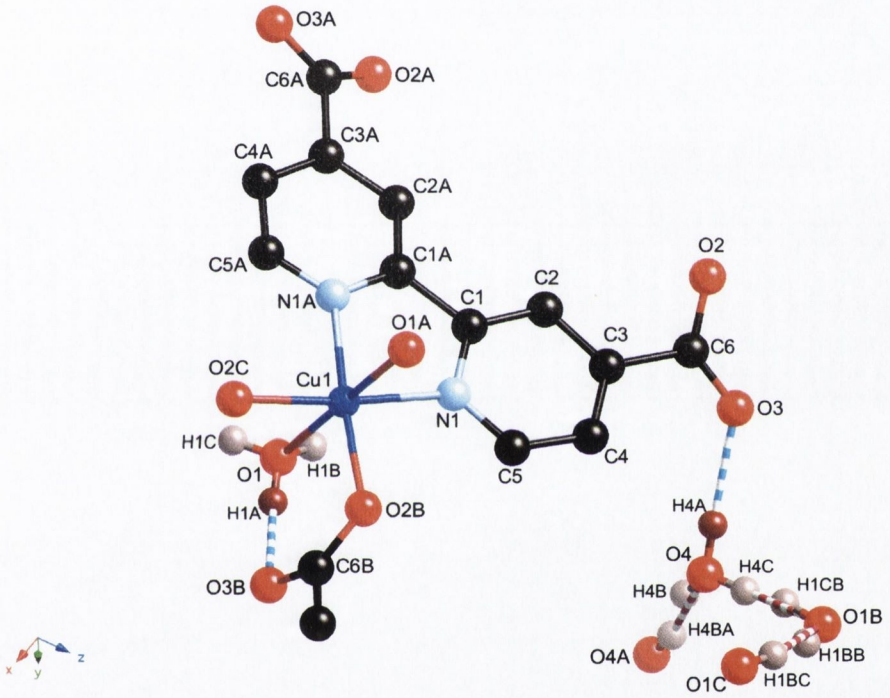

Figure 2.1- Atomic numbering scheme in **1**. The dashed bonds depict the unique hydrogen bonds. Dark brown hydrogen atoms are at full occupancy, whereas paler ones are at half-occupancy. Blue and white dashed bonds represent full occupancy hydrogen bonds and red and white dashed bonds represent hydrogen bonds which alternate between two disorderd protons. (Bipyridyl hydrogen atoms omitted for clarity).

The crystal structure shows that **1** contains two unique water molecules, O1 (coordinated) and O4 (lattice). One hydrogen atom position of each is fully occupied and is donated to an uncoordinated carboxylate oxygen. O1 donates H1A to O3 (O1···O3 2.790(5) Å) and O4 donates H4A to O3 (O4···O3 2.806(5) Å). The remaining hydrogen atom on each water molecule is disordered over two positions, alternating between donating a hydrogen bond to a lattice water molecule (O4) or to a coordinated water molecule (O1) (Figure 2.1). Full details of hydrogen bonding are given in Table 2.3.

Table 2.1 – Crystallographic data for **1**.

Compound		**1**
Chemical Formula		$CuC_{12}H_{14}N_2O_8$
Formula weight		377.79
Crystal system		Orthorhombic
Space group		*Pnna*
μ (MoK_α)/ mm^{-1}		1.560
a/Å		14.7685(9)
b/Å		10.8176(7)
c/Å		9.0272(5)
α/°		90
β/°		90
γ/°		90
V/$Å^3$		1442.2(2)
Z		4
D_{calc}/gcm^{-3}		1.740
T/K		173(2)
Crystal size	max /mm	0.20
	mid /mm	0.15
	min /mm	0.10
$2\theta_{max}$/°		50.0
Min/Max trans. Factor		0.787/1.000
R_{int}		0.0555
R_1, $wR_2[I>2\sigma(I)]$[a]		0.0532, 0.1059
R_1, wR_2 (all data)		0.0585, 0.1076
Reflections–	collected:	10531
	unique:	1276
	observed:	1158

[a] $R_1 = \Sigma||F_o| - |F_c||/\Sigma|F_o|$, $wR_2 = [\Sigma w(F_o^2 - F_c^2)^2/\Sigma w(F_o^2)^2]^{1/2}$

Table 2.2 – Selected bond lengths (Å) and angles (°) for **1**.

Cu1-N1	2.002(4)	N1-Cu1-N1^{i}	80.8(2)
Cu1-O1	2.443(5)	N1-Cu1-O1	95.0(2)
Cu1-O2	1.960(3)	N1^{i}-Cu1-O1	86.0(2)
		N1-Cu1-O2^{ii}	174.6(2)
		O1-Cu1-O1^{i}	178.7(2)
		O1-Cu1-O2^{iii}	93.8(1)
		O1-Cu1-O2^{ii}	85.3(1)

Symmetry codes: i = x, 0.5-y, 1.5-z; ii = 0.5+x, 0.5-y, 0.5+z; iii = 0.5+x, y, 1-z.

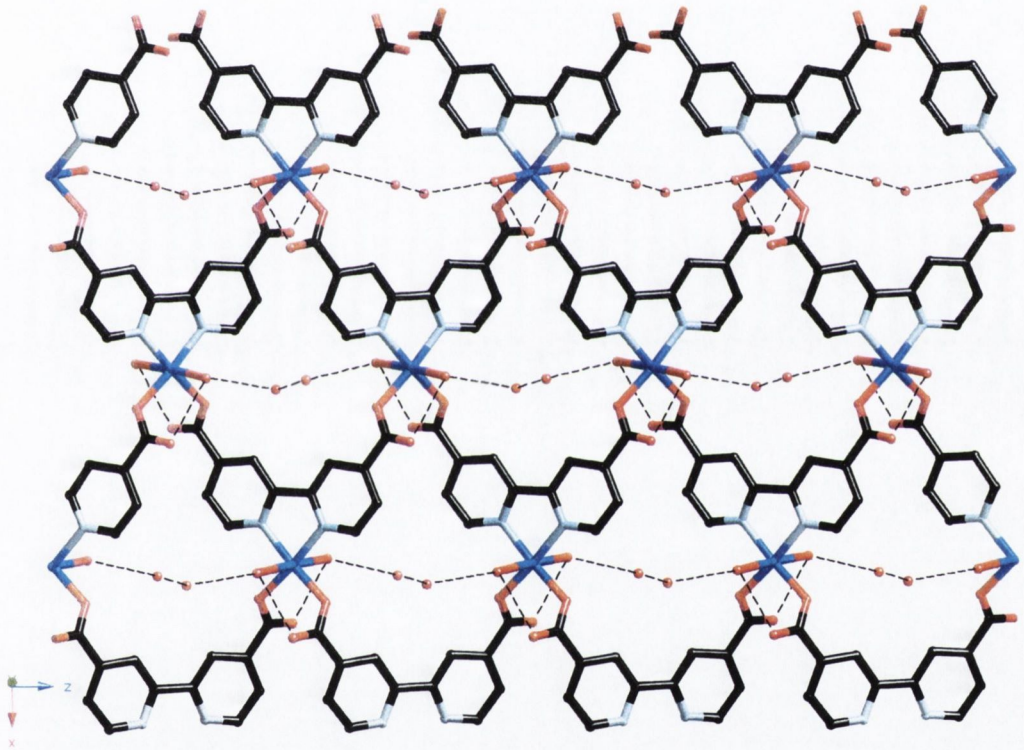

Figure 2.2- A single 2D layer in the structure of **1**, viewed approximately perpendicular to the sheet. The dotted lines depict the hydrogen bonding within the layer. The lattice water molecules lie in the windows of the (4,4) net. (Hydrogen atoms omitted for clarity)

The 2D polymer formed by coordination of 4,4'-dcbp to Cu(II) is of (4,4) topology. This assignment considers the metal atoms only as nodes with each node connected to four others through 4,4'-dcbp bridges. It should be noted that if both the metal ion and the 4,4'-dcbp ligand are considered as separate nodes then each would be 3-connecting giving a (6,3) topology for the 2D polymeric sheets in **1**.

Table 2.3 – Parameters of hydrogen bonding for **1**. (D-H distances fixed at 0.84(1) Å)

D–H···A	*d(H···A)/Å*	*d(D···A)/Å*	*<(D–H···A)/°*
O1-H1A···O3^{i}	2.00	2.790(5)	160
O1-H1B···O1^{ii}	1.98	2.795(8)	163
O1-H1C···O4^{iii}	2.00	2.807(6)	164
O4-H4A···O3	1.98	2.806(5)	178
O4-H4B···O4^{iv}	2.01	2.839(9)	171
O4-H4C···O1^{v}	2.00	2.807(6)	164

Symmetry codes: i = 0.5+x, y, 1-z; ii = 0.5-x, -y, z; iii = 0.5-x, -y, 1+z; iv = x, -0.5-y, 0.5-z; v = 0.5-x, -y, z-1.

Figure 2.2 shows the hydrogen bonding interactions contained within a single 2D layer of **1**. Hydrogen bonding occurs within each Cu(II) coordination sphere between coordinated water and uncoordinated carboxylate oxygen. The two lattice water molecules exist as hydrogen bonded pairs in the 'windows' of the 2D network with one on each side of the mean plane of the sheet, on which all Cu(II) centres reside. These pairs of lattice waters link the Cu(II) centres across the short diagonals of the (4,4) network by hydrogen bonding between coordinated water molecules on opposite sides of the sheet.

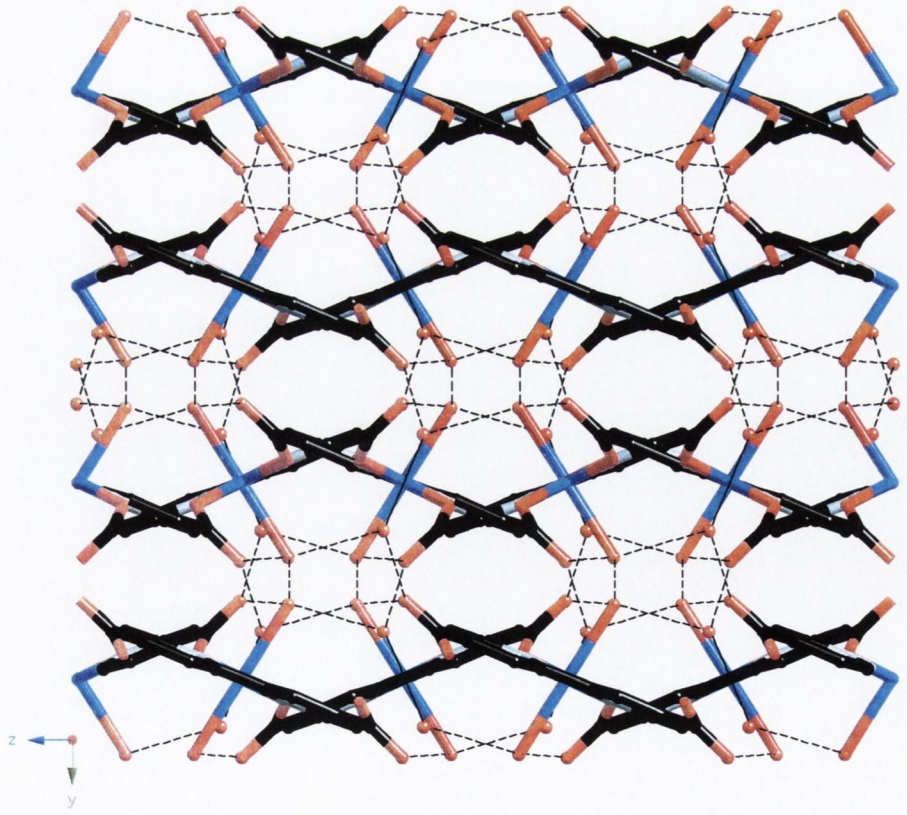

Figure 2.3 - The packing of the 2D layers of **1** showing both intra- and inter-layer hydrogen bonding connections as dashed lines. Note the corrugated nature of the 2D sheets. (Hydrogen atoms omitted for clarity. View along (100))

Figure 2.3 shows the packing of these 2D layers viewed edge on to the sheets and highlights the corrugated nature of the 2D Cu(4,4'-dcbp) network. There are two types of inter-layer hydrogen bond connections. One is between the coordinated water molecules on adjacent sheets and the other is between the lattice water molecules contained within each sheet and the uncoordinated carboxylate oxygen atoms on adjacent sheets. Examination of the hydrogen bond network formed by only the disordered protons reveals 1D infinite helical chains spiralling about two-fold screw axes down the *b* axis. This requires all protons within a single infinite helical hydrogen bonded chain to be ordered since all water molecules must be either donating or accepting protons in the same direction along the chain. Since the structure is centrosymmetric, both left and right-handed helical chains are present with those of opposite handedness related by inversion and glide plane symmetry. The positions of the protons in any one helical chain, however, are unable to affect those in adjacent helical chains. Therefore, although order of these protons exists in the *b* direction, none exists with respect to the *a* and *c* directions resulting in the overall disordered average for the crystal structure.

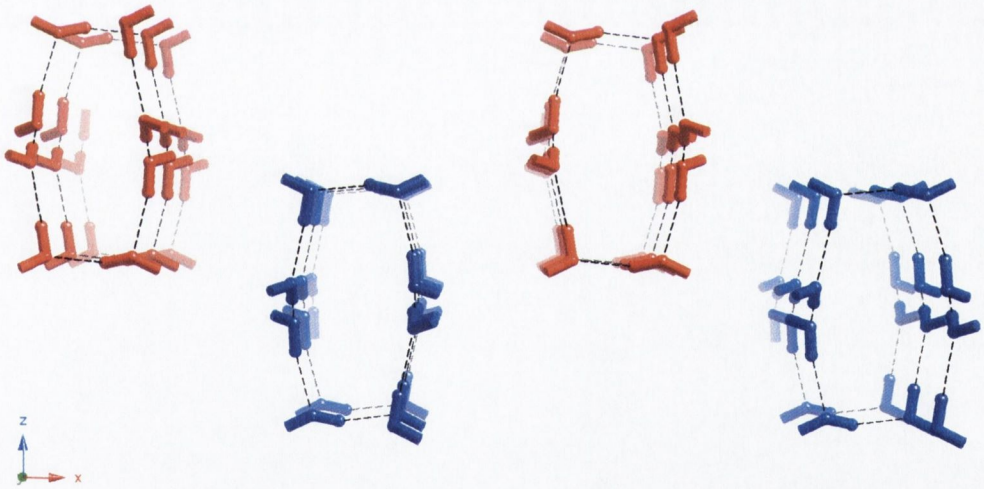

Figure 2.4 – Hydrogen bond network formed by the disordered protons in **1,** giving rise to 1D helical chains spiralling down the *b* direction. All protons within a chain are ordered (as shown), but not in the overall structure. Right-handed helices are shown in red and left-handed helices in blue.

The overall network resulting from both coordination and hydrogen bonding interactions is represented by the schematic diagram in Figure 2.5. The blue nodes represent the Cu atom positions, while the red nodes represent the midpoint of each pair of lattice water molecules. Hydrogen bonds to the coordinated water molecules and carboxylate oxygen atoms are represented by connection to the relevant Cu atom

position. The network consists of an equivalent number of 10-connecting and 4-connecting nodes. Each 10-connecting node is linked to six other 10-connectors and four 4-connectors while each 4-connector is linked to four 10-connectors. The six 'shortest circuits' for the 4-connectors all include four nodes. Analysis of the forty-five 'shortest circuits' for the 10-connectors gives thirty-one circuits involving four nodes and fourteen that include six nodes. Therefore the Schläfli notation for the network is $(4^6)(4^{31}.6^{14})$.

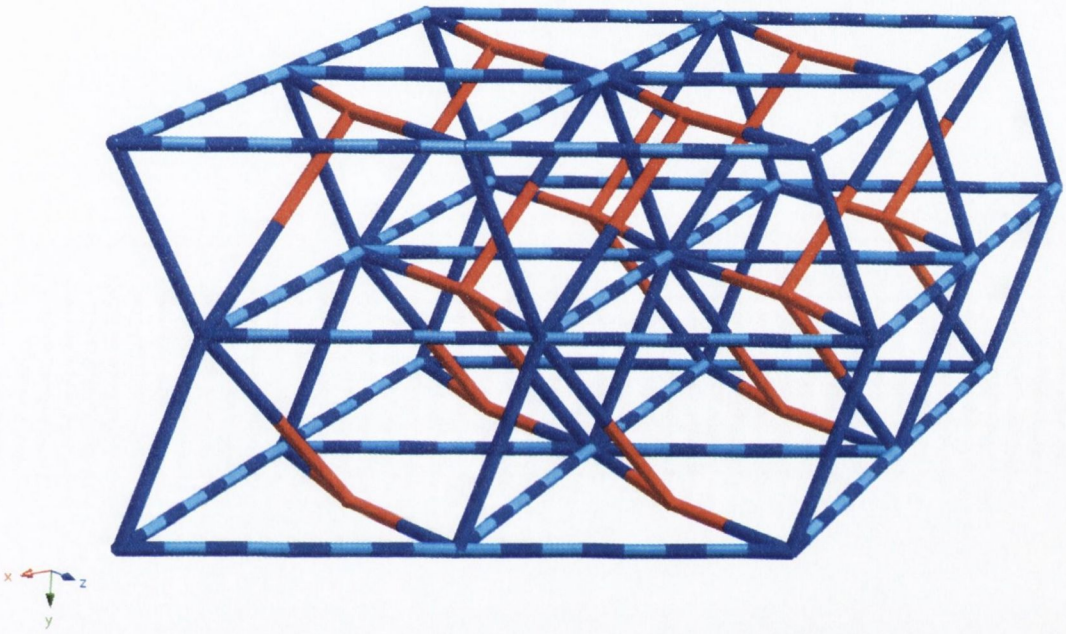

Figure 2.5- Schematic diagram for the overall 3D network of **1**. The 10-connecting nodes (blue centres) are the positions of the Cu atoms. The 4-connecting nodes (red centres) represent the midpoint of each pair of lattice water molecules. Blue-banded bonds represent bridging via coordinated 4,4'-dcbp (i.e. (4,4) sheets). Other bonds represent hydrogen bonding pathways as follows: blue only -between coordinated water molecules, blue/red (in plane of (4,4) sheets) - between coordinated and lattice water molecules, and other blue/red -between lattice water molecules and uncoordinated carboxylate oxygen atoms.

*2.2.3 Thermal analysis and magnetic properties of **1**.*

Thermogravimetric analysis of **1** reveals a weight loss of 17% between 50 and 82°C, consistent with the loss of all water molecules, lattice and coordinated (calcd. 19%). No further weight loss is observed until decomposition begins at 320°C. Crystallinity is lost with the loss of the water molecules, producing a dark blue amorphous solid. Reimmersion of this solid in water does not reproduce the crystal product.

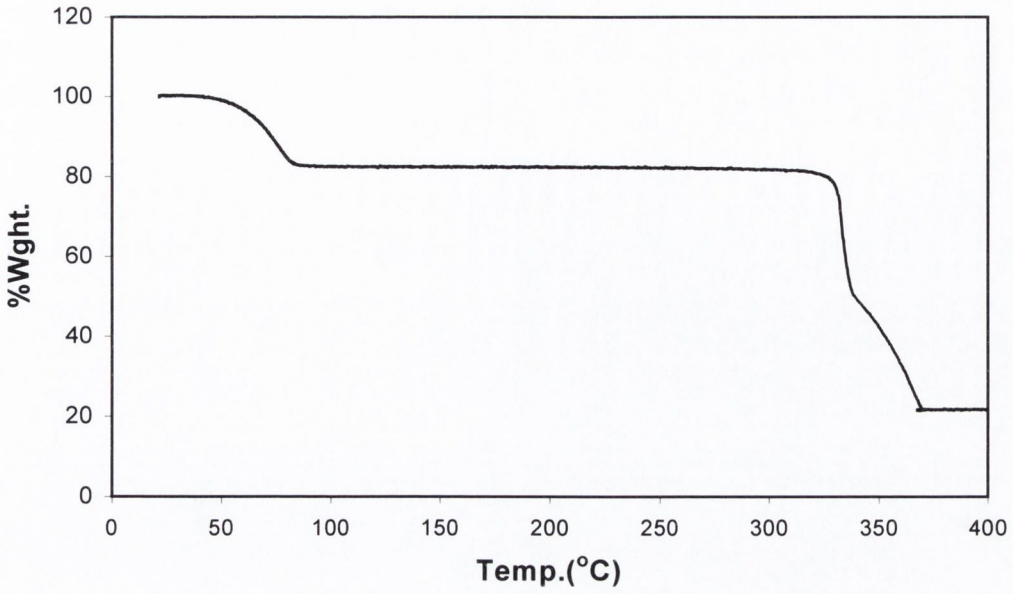

Figure 2.6 – Thermogravimetric analysis curve for **1**. The curve shows 17% weight loss in between 50 and 80°C, corresponding to the loss of all water molecules (lattice and coordinated).

A variable temperature magnetic susceptibility study on a powdered sample of **1** was perfomed over the temperature range 300-4.2 K in order to elucidate the nature of any interaction across the 4,4'-dcbp bridge. The magnetic data are shown in Figure 2.7. The data were adequately described through a simple Bleaney-Bowers[183] expression for a Cu(II) square lattice. Least-squares fitting leads to the following to a coupling constant, J, of -0.29(1)cm^{-1}, g = 2.08(1). This is indicative of extremely weak antiferromagnetic coupling.

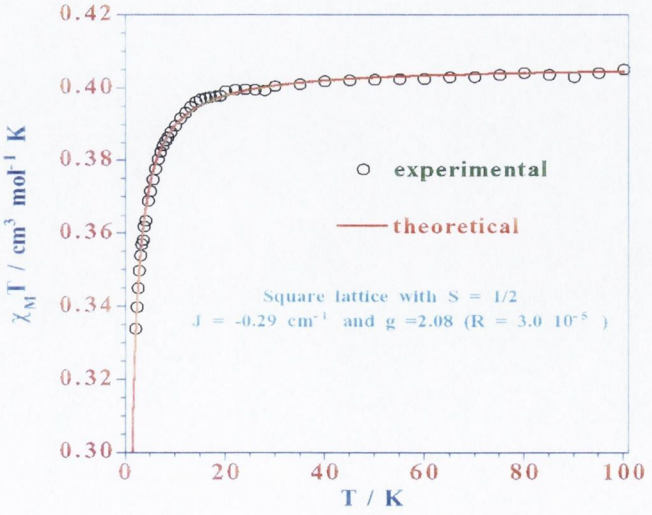

Figure 2.7 - $\chi_m T$ *versus* T plot for **1**. The red line indicates the theoretical fit. Curve is characteristic of very weak antiferromagnetism.

2.3 Reaction of Co(II) with 4,4'-dicarboxy-2,2'-bipyridine.

2.3.1 Reaction of $CoSO_4$ and 4,4'-H_2dcbp.

$CoSO_4$ and 4,4'-H_2dcbp (1:1) were reacted hydrothermally, with excess pyridine, at 185 °C for 3 days, which, following slow cooling, directly produced orange crystals. On close inspection of the crystalline sample, two different types of crystals were identified: orange prisms and pale salmon coloured needles. A cell check of the orange prisms revealed these to be the previously reported $[Co(4,4'\text{-dcbp})(H_2O)_2]_n$ (hereafter referred to as the α-polymorph).[175] A preliminary X-ray diffraction analysis of the paler needles, as expected, revealed different cell parameters to those of the orange prisms. After a full X-ray diffraction study, the structure was determined to be a polymorph of α-$[Co(4,4'\text{-dcbp})(H_2O)_2]_n$. The structure of α-$[Co(4,4'\text{-dcbp})(H_2O)_2]_n$ has been discussed by Kempe and co-workers[175] and so only the structure of the new β-$[Co(4,4'\text{-dcbp})(H_2O)_2]_n$ (**2**) will be discussed in detail here. Comparisons of the two networks and their physical properties follow.

2.3.2 *Crystal structure of β-$[Co(4,4'\text{-dcbp})(H_2O)_2]_n$* (**2**).

The structure of **2** was refined in the chiral $P2_12_12_1$ orthorhombic space group. The crystals were found to be racemic twins with approximately 67% of the crystal being the left hand and 33% the right hand. Crystallographic details are shown in Table 2.5. The complex formed is a neutral, 3D coordination polymer of 1:1 metal-ligand stoichiometry. The atomic numbering scheme and atom connectivity for the asymmetric unit are shown in Figure 2.8. The geometry around the cobalt ion is distorted octahedral, with the equatorial positions occupied by the chelating nitrogen atoms of a 4,4'-dcbp ligand, a carboxylate oxygen atom of an adjacent 4,4'-dcbp ligand and a coordinated water molecule. The axial positions are occupied by a second coordinated water molecule and a carboxylate oxygen atom of a third 4,4'-dcbp ligand. Distortion from ideal geometry arises due to the bite angle of the nitrogen atoms in the 4,4'-dcbp ligand (N1-Co1-N2 77.97(7) Å). Further distortion is observed in the coordination bond angles which range from 83.17(7) Å (O2-Co1-O6) to 103.68(7) Å (O6-Co1-N2) for the *cis* angles, and from 167.17(6) Å (N2-Co1-O1) to 177.86(7) Å (O2-Co1-O5) for the *trans* angles (See Table 2.4). The 4,4'-dcbp ligand is fully deprotonated and is coordinating to three different metals. One of the carboxylate groups is coordinating in a bridging bidentate (*anti-syn*) fashion to two different cobalt atoms, while the other carboxylate group participates only in hydrogen bonding with the coordinated water molecules and is not directly bound to the Co(II) centre. This is the first 4,4'-dcbp complex to display this type of coordination mode, with one of the carboxylates bidentate and the other non-coordinating, in addition to chelation through

the bipyridine nitrogen atoms. The carboxylate group about C11 is twisted at 32° with respect to the aromatic ring to which it is attached, while the corresponding angle about C12 is 23°. A torsion angle of 9° also exists between the pyridyl groups of the ligand. The C-O bond lengths differ for the coordinating oxygen atoms about C11 (C11-O1 1.270(3) Å, C11-O2 1.243(3) Å), while those for the noncoordinating oxygen atoms about C12 are equivalent (C12-O3 1.246(3) Å, C12-O4 1.252(3) Å).

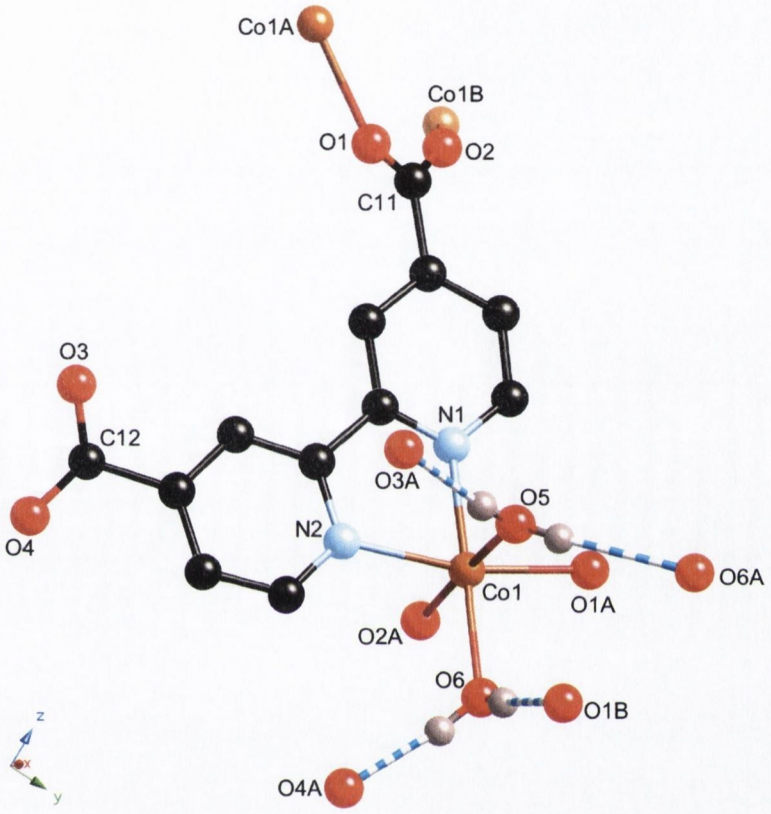

Figure 2.8 – Atom connectivity and labelling scheme for **2**. The blue and white dashed lines depict the unique hydrogen bonds. (Bipyridyl hydrogens omitted for clarity)

Table 2.4 – Selected bond lengths (Å), distances (Å) and angles (°) for **2**.

Co1-N1	2.120(2)	N1-Co1-N2	77.97(7)
Co1-N2	2.124(2)	N2-Co1-O6	103.68(7)
Co1-O1^{i}	2.085(2)	N1-Co1-O1^{i}	89.27(6)
Co1-O2^{ii}	2.106(2)	O6-Co1-O2^{ii}	83.17(7)
Co1-O5	2.090(2)	N2-Co1-O1^{i}	167.17(6)
Co1-O6	2.103(2)	N1-Co1-O6	175.03(8)
Co1···Co1^{iii}	4.8163(5)	O5-Co1-O2^{ii}	177.86(7)

Symmetry codes: i = -x, y-0.5, 0.5-z; ii = 0.5-x, -y, z-0.5; iii = 0.5+x, -0.5-y, -z;

Table 2.5 - Crystallographic data for α- and β-$[Co(4,4'\text{-dcbp})(H_2O)_2]_n$ (**2**).

Compound	**α-$[Co(4,4'\text{-dcbp})(H_2O)_2]_n$‡**	**2**
Chemical Formula	$CoC_{12}H_{10}N_2O_6$	$CoC_{12}H_{10}N_2O_6$
Formula weight	337.15	337.15
Crystal system	Trigonal	Orthorhombic
Space group	$P3_121$	$P2_12_12_1$
μ (MoK_α)/ mm^{-1}	1.297	1.520
a/Å	11.8551(3)	6.7145(5)
b/Å	11.8551(3)	13.0147(9)
c/Å	8.3410(5)	13.2121(9)
α/°	90	90
β/°	90	90
γ/°	120	90
V/$Å^3$	1015.22(7)	1154.6(1)
Z	3	4
D_{calc}/gcm^{-3}	1.654	1.940
T/K	153(2)	153(2)
Crystal size max /mm	0.18	0.20
mid /mm	0.13	0.05
min /mm	0.10	0.04
$2\theta_{max}$/°	56.60	59.98
Min/Max trans. Factor	0.848/1.000	0.846/1.000
R_{int}	0.0248	0.0306
R_1, $wR_2[I>2\sigma(I)]$[a]	0.0340, 0.0795	0.0345, 0.0739
R_1, wR_2 (all data)	0.0344, 0.0797	0.0382, 0.0752
Flack parameter	0.06(2)	0.328(14)
Reflections – collected:	9345	9015
unique:	1605	3282
observed:	1595	3067

[a] $R_1 = \Sigma||F_o| - |F_c||/\Sigma|F_o|$, $wR_2 = [\Sigma w(F_o^2 - F_c^2)^2/\Sigma w(F_o^2)^2]^{1/2}$

‡ Crystallographic details for this structure refer to data collected at Trinity College Dublin, and not that reported in the literature.

Table 2.6 – Parameters of hydrogen bonding for **2**. (D-H distances fixed at 0.84(1) Å)

D–H···A	d(H···A)/Å	d(D···A)/Å	<(D–H···A)/°
O5-H5A···O3^{i}	1.82	2.645(3)	1.67
O5-H5B···O6^{ii}	2.32	3.144(3)	165
O6-H6A···O4^{iii}	1.77	2.603(2)	173
O6-H6B···O1^{iv}	1.97	2.810(3)	174

Symmetry codes: i = x-0.5, 0.5-y, -z; ii = x-0.5, 0.5-y, -z; iv = -x, y-0.5, -0.5-z; iv = -0.5-x, -y, z-0.5.

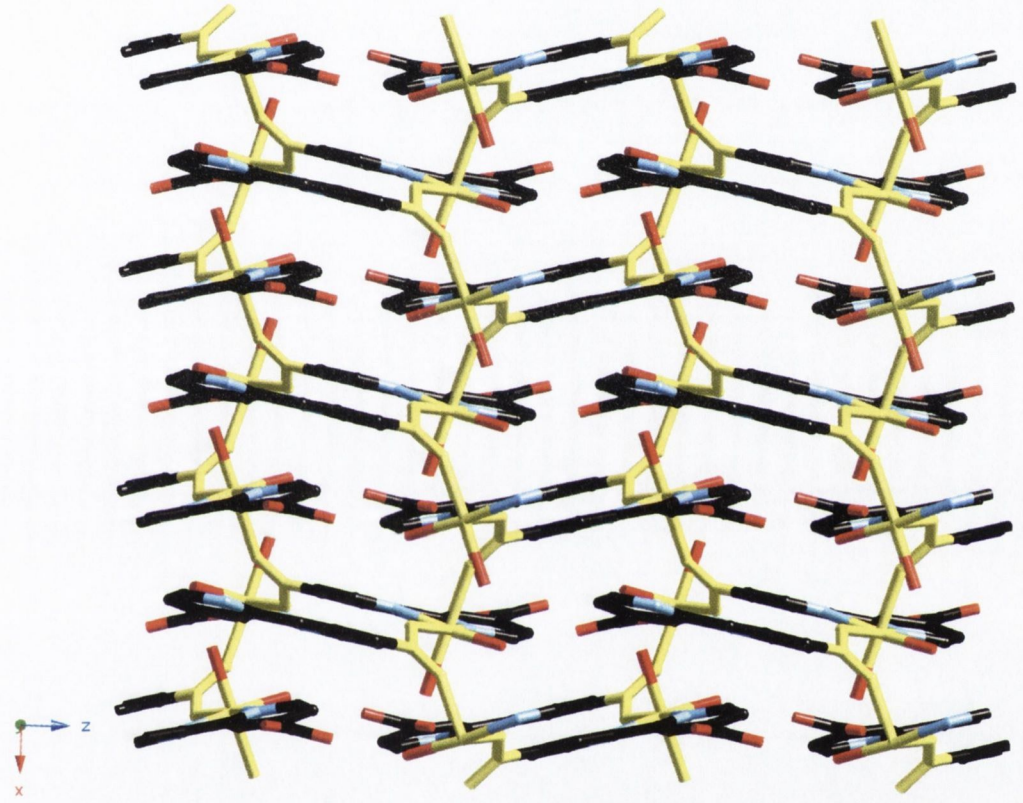

Figure 2.9 – Overall packing diagram of **2** viewed down the (010) direction. Carboxylato bridged cobalt chains are spiralling down the *a* direction and have been highlighted in yellow. All helical chains in the network are of the same handedness, in this case left. (Hydrogen atoms omitted for clarity)

The overall packing of **2** results in a three dimensional coordination polymer as shown in Figure 2.9. Bridging of the cobalt atoms by the bidentate carboxylate of the 4,4'-dcbp ligand gives rise to infinite Co-OCO-Co chains spiralling down the *a* direction. All helical chains in the structure are left handed rendering the overall structure of **2** chiral. The *anti-syn* coordination mode of the carboxylate gives a metal-to-metal distance across the carboxylate bridge of 4.8163(5) Å. The chains are linked in the *b* and *c* directions by the 4,4'-dcbp ligand, through coordination at the bipyridyl chelating site. Weaker hydrogen bonded links also occur through the interaction of the non-coordinating oxygen atoms of the 4,4'-dcbp ligand with the coordinated water

molecules (O6···O4 2.604 Å, O5···O3 2.645 Å). Further hydrogen bonding occurs between the water molecules (O5···O6 3.144 Å) and between the coordinating carboxylate group and one of the water molecules (O6···O1 2.810 Å). These act as intramolecular hydrogen bonds within the chains, i.e. they further link the chains down the *a* direction. A schematic representation of the links between the chains is shown in Figure 2.10. Slight overlap of the 4,4'-dcbp ligands gives rise to offset face-to-face π-π interactions (separation at closest contact is 3.292(3) Å), which further reinforce the 3D network.

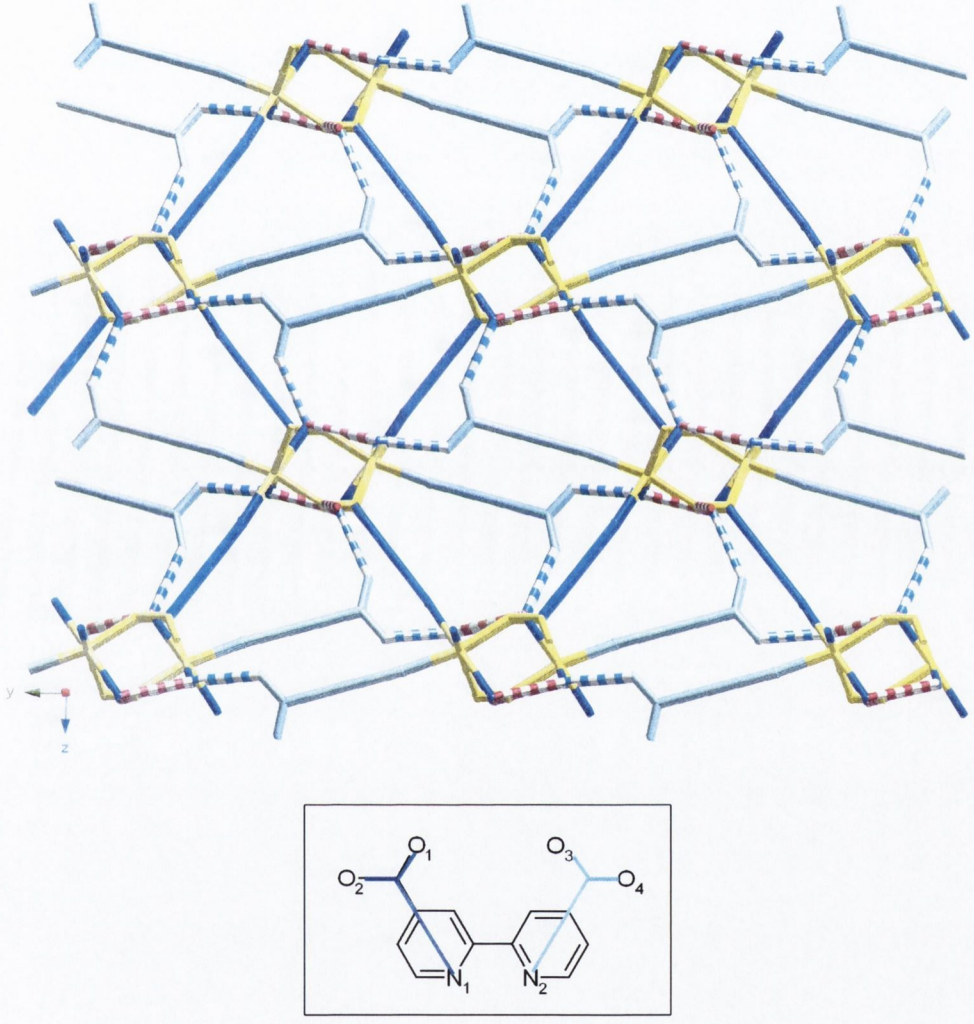

Figure 2.10 – Schematic representation of the overall packing of **2**. The cobalt-carboxylate chains are shown in yellow. The 4,4'-dcbp ligand is divided into two isonicotinate subunits, with a single link from the coordinating nitrogen atom to the carboxylate carbon atom *para* to it (as shown in insert). The 'tridentate' isonicotinate subunit links the chains in the *b* and *c* directions through coordination (dark blue bonds), while the other subunit (pale blue bonds) links the chains in a weaker fashion through hydrogen bonding of the non-coordinating carboxylate oxygen atoms with the coordinated water molecules (blue and white dashed bonds). Additional hydrogen bonding between the coordinated water molecules and the carboxylate groups further links the cobalt chains down the *a* direction (red and white dashed bonds).

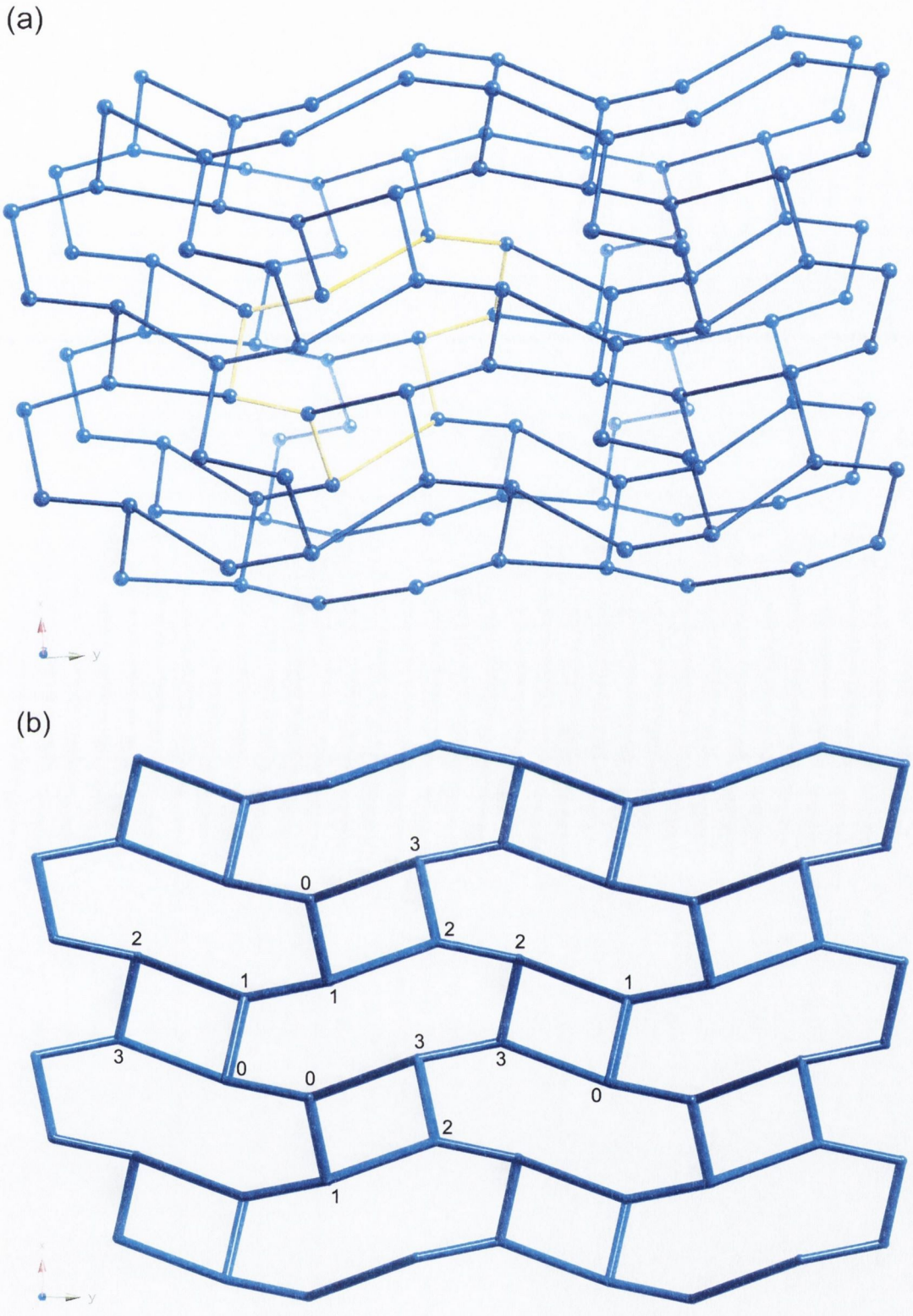

Figure 2.11 – (a) Schematic diagram for the coordination network in **2**. Both the 4,4'-dcbp ligand and the cobalt atoms serve as 3-connecting nodes. There are ten nodes in the shortest circuit, giving rise to a net of (10, 3) topology. (A single circuit has been highlighted in yellow. One half of the nodes represent Co atoms, the other represents the midpoint between the bidentate carboxylate of the 4,4'-dcbp ligand and the nitrogen opposite to it.); (b) projection of the net along 4-fold screw axis as a plane 4.8^2 net. Note all helices are of the same handedness, in this case left-handed.

The overall connectivity of the 3D network resulting from coordination is represented by the schematic diagram in Figure 2.11. Both the cobalt atoms and the 4,4'-dcbp ligands act as 3-connecting nodes and therefore the net belongs to the uniform 3-connected nets. The shortest circuit to arrive back at the same point involves ten nodes and thus the net is of (10,3) topology. A single circuit has been highlighted in Figure 2.11. There are seven uniform (10,3) connected nets, as described by Wells.[85] The topology of **2** is that of the (10,3)-a net, the most symmetrical of all the possible three-connected nets. This net is chiral and has 4-fold helices parallel to each of the crystallographic axes, all of the same hand. Projection of the net down the 4-fold screw axis produces a plane 4.8^2 net (Figure 2.11b).

2.3.3 Comparison of α- and β-polymorphs of [Co(4,4'-dcbp)(H$_2$O)$_2$]$_n$.

The structure of α-[Co(4,4'-dcbp)(H$_2$O)$_2$]$_n$ is shown in Figure 2.12 and was previously reported by Kempe and co-workers.[175] The data collection by Kempe was performed at –73 °C. A data collection at –120 °C was performed at Trinity College, Dublin. Solving and refinement of the structure at lower temperature naturally yielded slightly different parameters. The parameters from the latter collection will be used in the present discussion, since collection of the data for the β-polymorph (**2**) was also performed at this lower temperature. The two polymorphs of [Co(4,4'-dcbp)(H$_2$O)$_2$]$_n$ crystallise in different space groups. The α-polymorph has higher symmetry, with adjacent units related by 3_1 screw axes. Additionally one half of the [Co (4,4'-dcbp)(H$_2$O)$_2$]$_n$ unit is related to the other by a two-fold rotation axis, and thus, the structure was refined in the chiral $P3_121$ trigonal space group. Crystallographic details for both α- and β-[Co(4,4'-dcbp)(H$_2$O)$_2$]$_n$ are shown in Table 2.5.

The two polymorphs arise due to the different connectivity around the cobalt atom. The geometry around the cobalt atoms is octahedral for both, but in the α-polymorph the two coordinated water molecules occupy *cis* positions which are *trans* to the chelating nitrogen atoms, leaving the carboxylate oxygen atoms in *trans* positions. In the β-polymorph all like donors occupy *cis* positions. This results in a different orientation for the 4,4'-dcbp ligand in the networks relative to each metal centre. Furthermore, the 4,4'-dcbp ligands differ in the way they coordinate through the carboxylate groups in the two polymorphs. As explained above, for **2** the 4,4'-dcbp ligand coordinates to a cobalt atom through the chelating nitrogen atoms and to two further cobalt atoms through a single carboxylate which coordinates in a bridging bidentate fashion. For the α-polymorph the ligand also coordinates to a cobalt atom through the chelating nitrogen atoms, but then uses *both* carboxylates to coordinate in a monodentate fashion to two cobalt atoms. This overall more symmetrical mode of coordination for the ligand, combined with the more symmetrical coordination sphere

around the cobalt atom, gives rise to a higher symmetry structure for the α-polymorph, as mentioned above.

In both structures, the coordinated water molecules participate in hydrogen bonding with the noncoordinated carboxylate oxygen atoms. This hydrogen bonding interaction gives rise to infinite chiral water chains (double helices) in the α-polymorph as shown in Figure 2.12b. In the β-polymorph carboxylato-bridged cobalt helical chains are present, as explained earlier (Figure 2.9). The packing of the α-polymorph gives rise to channels along the *c* direction (Figure 2.12), whereas the packing of the β-polymorph is more efficient, with a considerably higher density of 1.940 g/cm^{-3} (*c.f.* 1.654 g/cm^{-3}), and therefore no accessible channels are formed.

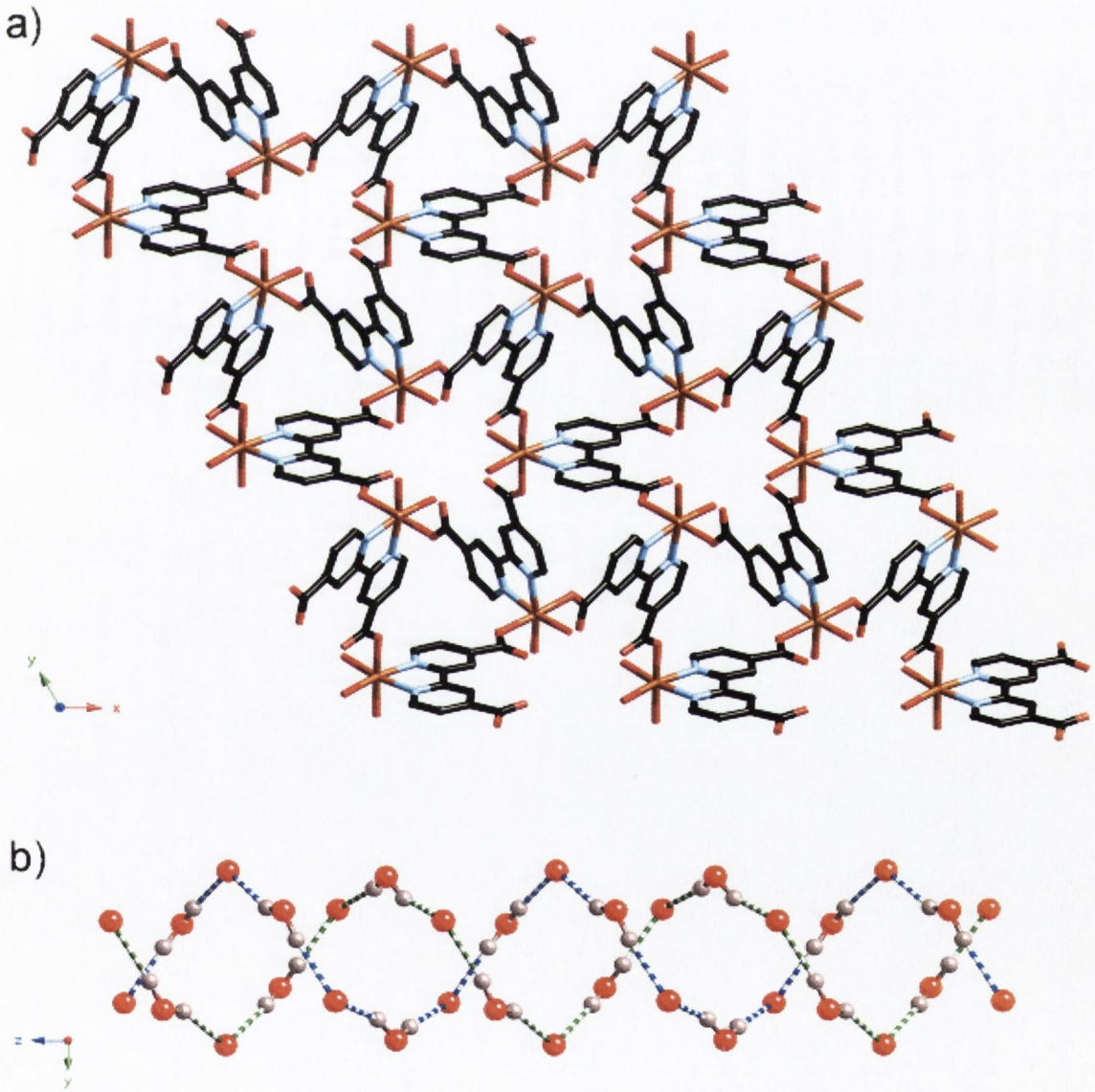

Figure 2.12 – a) Structure of α-[Co(4,4'-dcbp)$(H_2O)_2]_n$ viewed down the *c* direction, where channels are formed. (Hydrogen atoms omitted for clarity). b) Hydrogen bonded water double helix formed in α-[Co(4,4'-dcbp)$(H_2O)_2]_n$ by the interaction of the coordinated water molecules and the noncoordinated carboxylate oxygens.

Both the cobalt atoms and the 4,4'-dcbp ligands serve as 3-connectors in the two polymorphs, and thus both networks belong to the uniform (*n*,3) connected nets. As explained previously, the topology of the network in **2** belongs to the (10,3) class (Figure 2.11), whereas the shortest circuit in the 3D network of the α-polymorph includes twelve nodes and thus a (12,3) net is formed (Figure 2.13). The (12,3) net has the largest value of *n* for the (*n*,3) nets considered by Wells,[85] and is a combination of trigonal and T-shaped nodes. It occupies a unique position amongst all the uniform nets in showing self-entanglement such that some of its shortest circuits have other shortest circuits passing through them ('catenation').

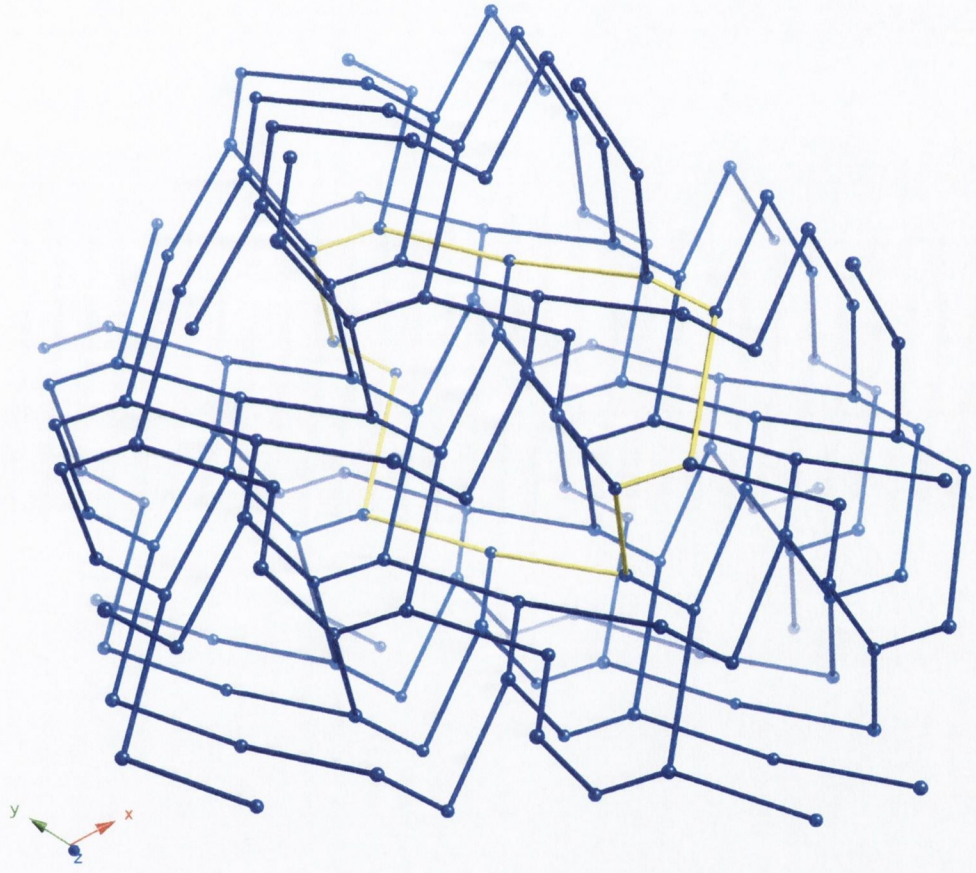

Figure 2.13 – Overall connectivity of the 3D network in α-$[Co(4,4'\text{-dcbp})(H_2O)_2]_n$, showing it to be an example of a (12,3) net. (A single circuit has been highlighted in yellow. One half of the nodes represent Co atoms, the other represents an arbitrary point in the ligand)

2.3.4 Thermal analysis and magnetic properties of α-$[Co(4,4'\text{-dcbp})(H_2O)_2]_n$ and **2**.

The thermal behaviour of the two polymorphs: α-$[Co(4,4'\text{-dcbp})(H_2O)_2]_n$ and **2** was investigated by thermogravimetric analysis. The curve of α-$[Co(4,4'\text{-dcbp})(H_2O)_2]_n$ (Figure 2.14) reveals a weight loss of *ca.* 9% between 190 and 240 °C, consistent with the loss of the coordinated water molecules (calcd. 10.6%). No further weight loss is observed until decomposition begins at 355°C. Samples of **2** did not zero on the

balance and so the thermogravimetric analysis is not as accurate and does not allow calculation of exact weight loss. Some weight loss is observed between 145 and 190°C, most likely indicating the loss of the two coordinated water molecules. Decomposition of the network follows at 355 °C. These are only preliminary results and further analyses are being performed in order to obtain more accurate results for **2**, and thus enable a more precise comparison between the two networks.

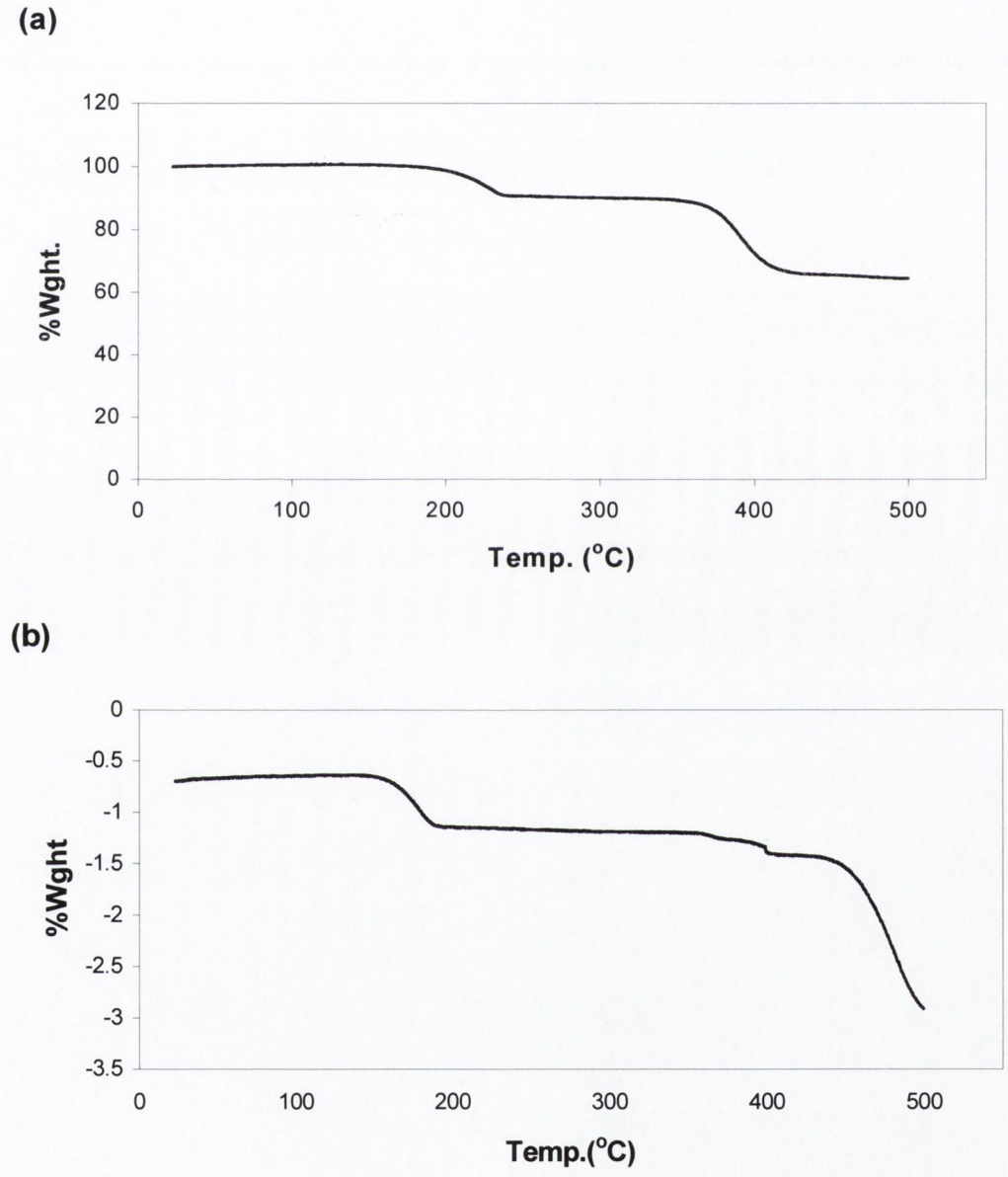

Figure 2.14 – (a) Thermogravimetric analysis curve for α-[Co(4,4'-dcbp)$(H_2O)_2]_n$. 9% weight loss is observed between 190 and 240 °C consistent with the loss of two coordinated water molecules. Decomposition follows at 355 °C. (b) Thermogravimetric anlaysis curve for **2**. Samples did not zero and thus % of mass lost is not accurate. Some weight loss is observed between 140 and 190 °C before decomposition begins at 355°C.

A variable temperature magnetic susceptibility study was performed on a powdered sample of α-[Co(4,4'-dcbp)$(H_2O)_2]_n$. The magnetic data for α-[Co (4,4'-dcbp)$(H_2O)_2]_n$ are shown in Figure 2.15. The magnetic moment (μ_{eff}) decreases from a value of 4.56 BM at 300 K to reach 3.5 BM at 5 K and then, more rapidly to 3.15 BM at 4.2 K. This behaviour is typical for uncoupled high spin octahedral Co(II) centres. The temperature dependence arises from a combination of spin-orbit coupling and low symmetry ligand field effects.[184] Very weak antiferromagnetic coupling may also be occurring but there is no maximum in χ_m down to 4.2 K and thus the coupling occurring via the 4,4'-dcbp bridges is less than $-0.1 cm^{-1}$. **2** displayed similar magnetic behaviour to that observed for α-[Co(4,4'-dcbp)$(H_2O)_2]_n$, the μ_{eff} values at any temperature being a little higher in **2**. The shape of the μ_{eff} *vs.* T plot has also been observed in other six coordinate Co(II) network species, for instance in weakly coupled $\mu_{1,5}$ – dicyanamide species of various dimensionalities.[185, 186] Measurements of magnetization in very low applied fields showed that no long–range magnetic ordering was present in α-[Co(4,4'-dcbp)$(H_2O)_2]_n$ and **2**.

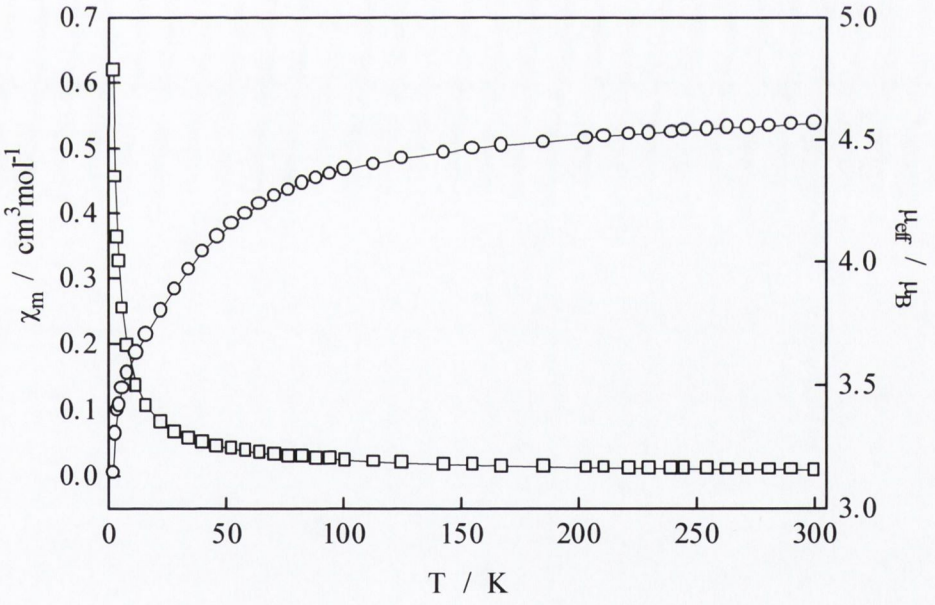

Figure 2.15 – μ_{eff} and χ_m *versus* T plot for α-[Co(4,4'-dcbp)$(H_2O)_2]_n$. (Plots for **2** are almost identical and are not shown)

2.4 Reaction of Mn(II) with 4,4'-dicarboxy-2,2'-bipyridine.

2.4.1 Reaction of $MnCl_2$ with 4,4'-H_2dcbp.

$MnCl_2$ and 4,4'-H_2dcbp (1:2) were placed in Teflon®-lined stainless steel vessel, in a 50:50 (% vol.) solvent mix of H_2O and DMF, and heated to 200 °C for 16 hrs. Yellow plates were obtained directly in approximately 80% yield. An infrared spectrum showed the presence of deprotonated 4,4'-dcbp ($\nu_{as}(CO_2^-)$ 1600 cm^{-1} and $\nu_s(CO_2^-)$

1380 cm^{-1}) and DMF (ν(C=O) 1671 cm^{-1}). A single crystal X-ray diffraction study showed the formation of a porous polymeric network containing DMF in the channels, $\{[Mn(4,4'\text{-dcbp})]\cdot\frac{1}{2}DMF\}_n$ (**3**). The same reaction was then performed employing a 50:50 (% vol.) diethylformamide (DEF)/H_2O mixture with the aim of producing a pseudopolymorph of **3** containing DEF, in place of DMF, in the channels. Yellow needles were obtained directly from the bomb and an infrared spectrum showed the presence of deprotonated 4,4'-dcbp ($\nu_{as}(CO_2^-)$ 1600 cm^{-1} and $\nu_s(CO_2^-)$ 1382 cm^{-1}), and water (3442 cm^{-1}), but no carbonyl stretch for the amide from the DEF. From a single crystal X-Ray diffraction analysis the complex was formulated as $\{[Mn(4,4'\text{-dcbp})]\cdot 2H_2O\}_n$ (**5**), previously reported by Kempe and co-workers.[176] These two complexes, **3** and **5**, are indeed pseudopolymorphs as their networks are made of the same components and they differ only in the solvent molecules within the lattice. The reaction of $MnCl_2$ and 4,4'-H_2dcbp was then carried out in 100% vol. DEF, with no water present, to force the inclusion of this solvent in the channels, producing a yellow powder. On close inspection of the sample some small yellow crystals were also spotted. A preliminary X-ray analysis revealed similar parameters as for **3**, and after a full single crystal X-ray diffraction study the structure of these crystals was indeed found to be a pseudopolymorph of **3**: $\{[Mn(4,4'\text{-dcbp})]\cdot\frac{1}{2}DEF\}_n$ (**4**). Crystals of **4** are only obtained in small yield (*ca.* 5%), however we are currently investigating whether the yellow powder obtained is also **4**, in which case the yield of the reaction would increase dramatically (yellow powder constitutes *ca.* 70%).

Several reactions were set up to determine the threshold of formation for **3** and **5**. $MnCl_2$ and 4,4'-H_2dcbp (1:2) were reacted in a 23ml Teflon-lined stainless steel vessel at 200 °C for 16 hrs, with varying proportions of DMF and water, as shown in Table 2.7. Whenever 50% vol. or more DMF is present, **3** is formed, otherwise **5** is favoured. It is worth noting the high yields (based on $MnCl_2$) obtained for all the reactions regardless of the amount of templating solvent, except when only DMF is used. In this case the yield of $\{[Mn(4,4'\text{-dcbp})]\cdot\frac{1}{2}DMF\}_n$ is only 32%, with the rest of the product being unreacted 4,4'-H_2dcbp. Also, only one of the products is favoured in each reaction, with no mixture of products seen at any time. This was confirmed by microanalysis and random cell checks of the different batches of crystals.

Table 2.7 – Outcome of reactions between $MnCl_2$ and 4,4'-H_2dcbp, depending on solvent and ratio employed.

Solvent	*Solvent ratio (%vol)*	*Product*	*Yield*
DMF	100	$\{[Mn(4,4'\text{-dcbp})]\cdot\frac{1}{2}DMF\}_n$	32%
DMF/H_2O	75:25	$\{[Mn(4,4'\text{-dcbp})]\cdot\frac{1}{2}DMF\}_n$	79%
DMF/H_2O	50:50	$\{[Mn(4,4'\text{-dcbp})]\cdot\frac{1}{2}DMF\}_n$	80%
DMF/H_2O	25:75	$\{[Mn(4,4'\text{-dcbp})]\cdot 2H_2O\}_n$	82%
H_2O	100	$\{[Mn(4,4'\text{-dcbp})]\cdot 2H_2O\}_n$	74%
DEF/H_2O	50:50	$\{[Mn(4,4'\text{-dcbp})]\cdot 2H_2O\}_n$	75%
DEF	100	$\{[Mn(4,4'\text{-dcbp})]\cdot\frac{1}{2}DEF\}_n$	5%

*2.4.2 Crystal structure of $\{[Mn(4,4'\text{-dcbp})]\cdot\frac{1}{2}DMF\}_n$ (**3**).*

The structure of **3** was refined in the monoclinic *C2/c* space group and crystallographic details are shown in Table 2.8. The atom connectivity and labelling scheme of **3** are shown in Figure 2.16. The manganese atom adopts an octahedral geometry and is coordinated by five 4,4'-dcbp ligands. One of the ligands is coordinating through the chelating nitrogen atoms, with the rest of the positions occupied by a single carboxylate oxygen of four other 4,4'-dcbp ligands. Distortion from octahedral symmetry of the coordination sphere can be seen in the coordination angles, with *cis* angles ranging from 71.69(9)° (N1-Mn1-N2) to 98.39(9)° (O1-Mn1-O2), and *trans* coordination angles ranging from 167.31° (N1-Mn1-O2) to 171.11° (O1-Mn1-O3). Selected bond lengths and angles are given in Table 2.9. A striking feature of this complex is the heavy distortion of the 4,4'-dcbp ligand. There is a torsion angle of approximately 21° between the pyridyl rings. In addition to this, the pyridyl rings are at *ca.* 6° to the C5-C6 bond, giving the ligand a 'bent' appearance. The carboxylate group about C11 is twisted 11.0° about the aromatic ring to which it is attached, with the carboxylate group about C12 twisted even further, forming an angle of approximately 33.7° with the aromatic ring.

Table 2.8 - Crystallographic data for **3** and **4**.

Compound		**3**	**4**
Chemical Formula		$MnC_{13.5}H_{9.5}N_{2.5}O_{4.5}$	$MnC_{14.5}H_{11.5}N_{2.5}O_{4.5}$
Formula weight		333.68	347.70
Crystal system		Monoclinic	Monoclinic
Space group		*C*2/*c*	*C*2/*c*
μ (MoK_α)/ mm^{-1}		1.026	1.018
a/Å		15.676(1)	15.6193(9)
b/Å		10.2423(6)	10.3503(6)
c/Å		16.775(1)	16.872(1)
α/°		90	90
β/°		102.249(1)	102.400(1)
γ/°		90	90
V/$Å^3$		2632.2(3)	2664.0(3)
Z		8	8
D_{calc}/gcm^{-3}		1.684	1.734
T/K		153(2)	153(2)
Crystal size	max /mm	0.15	0.18
	mid /mm	0.11	0.17
	min /mm	0.02	0.03
$2\theta_{max}$/°		50.0	50.0
Min/Max trans. Factor		0.897/1.000	0.821/1.000
R_{int}		0.0414	0.0275
R_1, $wR_2[I>2\sigma(I)]$[a]		0.0478, 0.0935	0.0444, 0.0947
R_1, wR_2 (all data)		0.0522, 0.0952	0.0467, 0.0956
Reflections–	collected:	10077	8622
	unique:	2312	2345
	observed:	2182	2269

[a] $R_1 = \Sigma||F_o| - |F_c||/\Sigma|F_o|$, $wR_2 = [\Sigma w(F_o^2 - F_c^2)^2/\Sigma w(F_o^2)^2]^{1/2}$

Table 2.9 – Selected bond lengths (Å) and angles (°) for **3**.

Mn1-O1^{i}	2.158(2)	N1-Mn1-N2	71.69(9)
Mn1-O2^{ii}	2.117(2)	O1^{i}-Mn1-O2^{ii}	98.39(9)
Mn1-O3^{iii}	2.179(2)	N2-Mn1-O1^{i}	88.80(9)
Mn1-O4^{iv}	2.120(2)	N1-Mn1-O1^{i}	81.53(9)
Mn1-N1	2.296(3)	O1^{i}-Mn1-O4^{iv}	87.02(9)
Mn1-N2	2.307(3)	O2^{ii}-Mn-O4^{iv}	95.69(9)
Mn1···Mn1^{v}	4.731(1)	N2-Mn1-O2^{ii}	95.69(9)
Mn1···Mn1^{vi}	4.839(1)	N1-Mn1-O4^{iv}	96.91(9)
		O1^{i}-Mn1-O3^{iii}	171.04(9)
		N1-Mn1-O2^{ii}	167.37(9)
		N2-Mn1-O4^{iv}	168.34(9)

Symmetry codes: i = 0.5-x, 0.5+y, 0.5-z; ii = x, 1-y, z-0.5; iii = 0.5-x, 0.5-y, -z; iv = x-0.5, 0.4+y, z; v = 0.5-x, 1.5-y, -z; vi = -x, 1-y, -z.

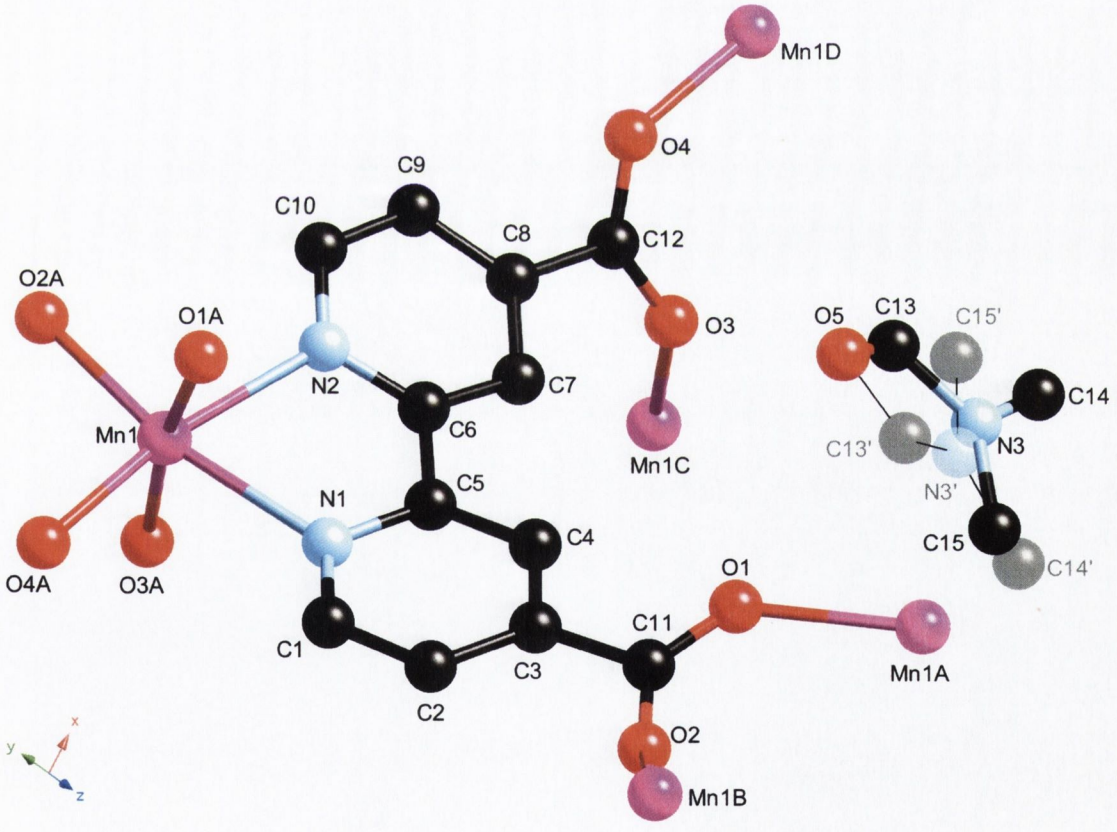

Figure 2.16 – Atom connectivity and labelling scheme for **3**. (Disordered DMF positions (N3', C13', etc.) shown as translucent atoms. Hydrogen atoms omitted for clarity).

The carboxylate groups adopt a bridging bidentate conformation (*anti-syn*) to produce infinite bis-carboxylato bridged manganese chains. These chains are made up of eight-membered rings, at *ca.* 118° to each other. Adjacent rings are non-equivalent crystallographically and give rise to two different metal-to-metal distances along the chains. Metal centres bridged by C11 carboxylate groups are 4.731(1) Å apart, while those bridged by C12 carboxylate groups are further apart at 4.839(1) Å. The rings are not planar and adopt what can be described as a 'chair-like' conformation as seen in Figure 2.17.

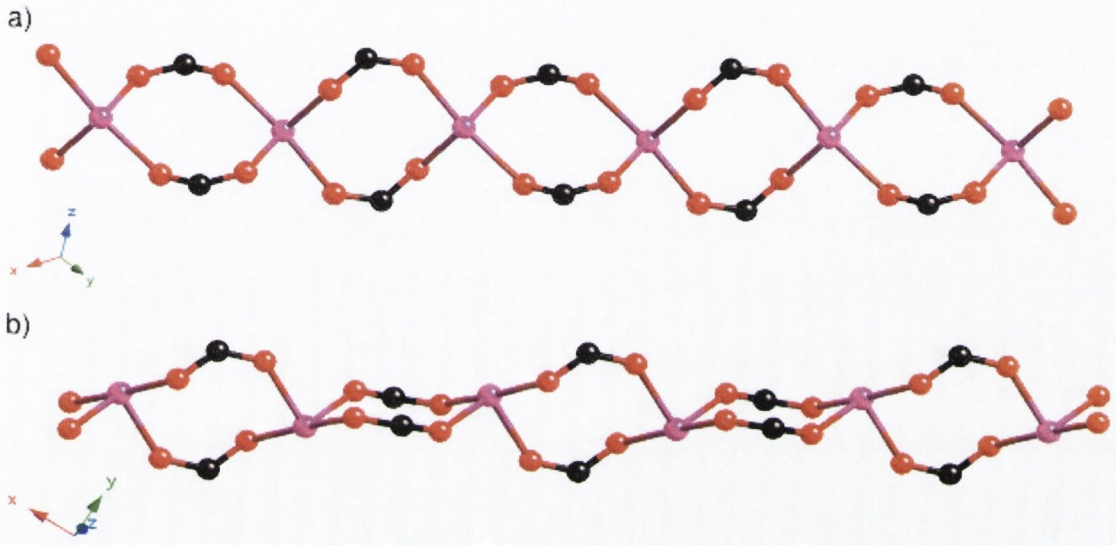

Figure 2.17 – a) The bis-carboxylato bridged manganese chains in **3**, showing the formation of the eight membered rings. Alternate rings are at 118° to each other; b) view of the chains highlighting the chair-like conformation of the eight membered rings.

The manganese-carboxylato chains are cross-linked by the 4,4'-dcbp ligands producing a 3D coordination polymer as shown in Figure 2.18. The 3D network is reinforced by π-π interactions between the 4,4'-dcbp ligands, with the separation at closest contact being 3.377(4) Å. The network in **3** is elaborately perforated with channels along *a*, *b* and *c* with dimensions[$] of 3.38 × 4.54, 2.48 × 7.02 and 3.23 × 6.26 Å^2 respectively. The channels constitute 23.3% of the crystal volume[187-189] and naturally contain larger voids at their points of intersection, where the DMF molecules reside. The DMF molecules are at half-occupancy and are disordered over two positions, related by a two-fold rotation axis, which passes through the oxygen atom and the midpoint between the two nitrogen atoms, as shown in Figure 2.16.

[$] Dimensions given are atom to atom (including hydrogen) as viewed along channels and are *ca.* perpendicular to channel direction.

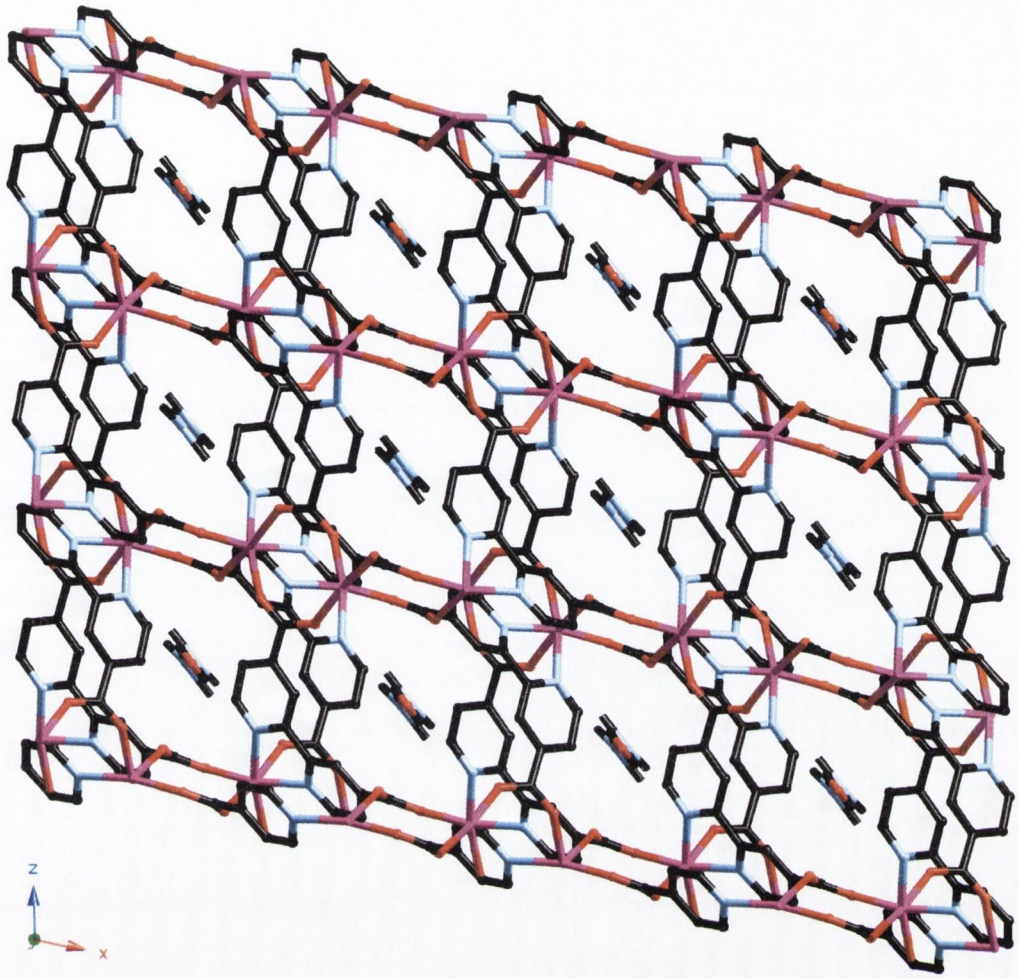

Figure 2.18 – Structure of **3** looking down the (010) direction, showing the channels occupied by disordered DMF molecules. (Hydrogen atoms omitted for clarity)

The overall network resulting from coordination in **3** may be represented by the schematic diagram in Figure 2.19. The red nodes represent the Mn atoms, while the blue and green nodes each represent one half of the 4,4'-dcbp ligand (*i.e.* an isonicotinate subunit). The blue nodes represent the N1 containing isonicotinate subunit, while the green nodes represent the N2 containing subunit. The network consists of 6-connectors (Mn atoms) and 3-connectors (isonicotinate subunits of 4,4'-dcbp) in the ratio 1:2. Although there is only one type of 6-connector, topologically there are two types of 3-connectors arising from the crystallographic inequivalence of each half of the 4,4'-dcbp ligand. In order to differentiate between the two, the nodes representing the N1 containing isonicotinate subunit will be referred to as type I 3-connectors whilst the nodes representing the N2 containing isonicotinate subunit will be referred to as type II 3-connectors.

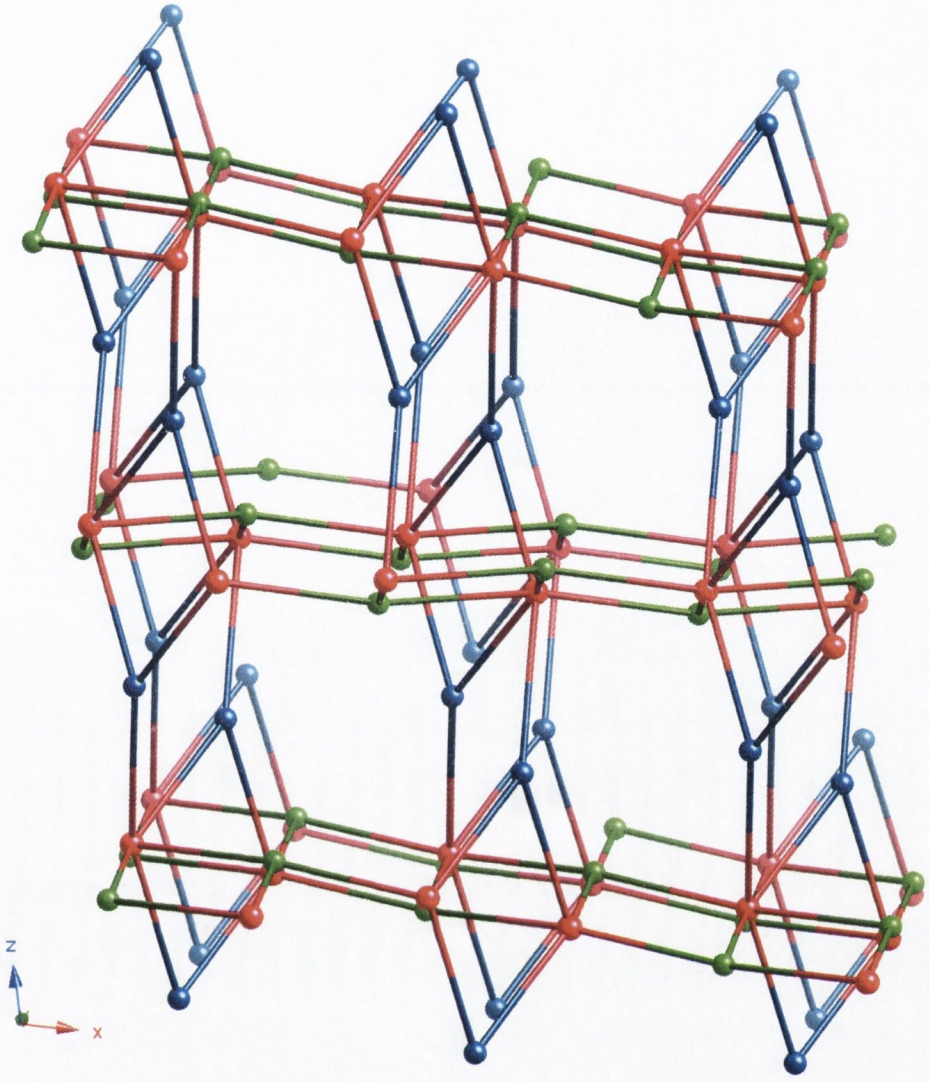

Figure 2.19 – Schematic representation for the overall 3D network of **3**. The 6-connecting nodes (red centres) are the positions of the Mn atoms. There are two types of 3-connecting nodes, each representing one half of the 4,4'-dcbp ligand. The blue centres represent an arbitrary point in the N1 containing isonicotinate subunit of the 4,4'-dcbp ligand, whilst the green centres represent an arbitrary point in the N2 containing isonicotinate subunit. This gives rise to a network with $(4.6^2)(4^2.6)(4^3.6^6.8^6)$ Schläfli notation.

Each 6-connecting node is linked to six other 3-connectors, three of type I and three of type II. Each 3-connector (both type I and II) is linked to three 6-connectors. The three 'shortest circuits' for the type I 3-connector, include two circuits involving six nodes and one involving four nodes, whilst for the type II 3-connectors the 'shortest circuits' include two involving four nodes and one involving six nodes. Analysis of the fifteen 'shortest circuits' for the 6-connectors gives six circuits involving six nodes, another six circuits involving eight nodes, and three circuits involving four nodes. Therefore the Schläfli notation for the network is $(4.6^2)(4^2.6)(4^3.6^6.8^6)$.

*2.4.3 Crystal structure of {[Mn(4,4'-dcbp)]·½(DEF)}$_n$ (**4**).*

The structure of **4** is similar to that of **3** above. In fact **3** and **4** are pseudopolymorphs as they differ only in the solvent within the networks. The structure of **4** was refined in the monoclinic *C*2/*c* space group. Crystallographic details are given in Table 2.8. The cell parameters are similar to those of **3**, but significantly different: *a* decreases by 0.4%, while *b* and *c* lengthen by 1.1% and 0.6% respectively; a slight increase in β is also observed (0.2%). This results in an overall cell volume increase of 1.3%. The coordination sphere around the manganese atom is near identical to that of **3**, with the octahedral metal ion coordinated by five different 4,4'-dcbp ligands in the same fashion as in **3**, shown in Figure 2.20. The bond lengths around the manganese ion are virtually identical to those of **3**, while the angles are slightly different (Table 2.10). The most significantly different angles compared to **3** are O2-Mn1-O4 (96.80(9)°, *cf.* 95.69(9)°) and N2-Mn1-O2 (94.68(9)°, *cf.* 95.69(9)°) for the *cis* angles, and O1-Mn1-O3 (172.24(8)°, *cf.* 171.04(9)°) and N1-Mn1-O2 (166.17(9)°, *cf.* 167.37(9)°) for the *trans* angles. Thus the geometry around the metal ion is distorted.

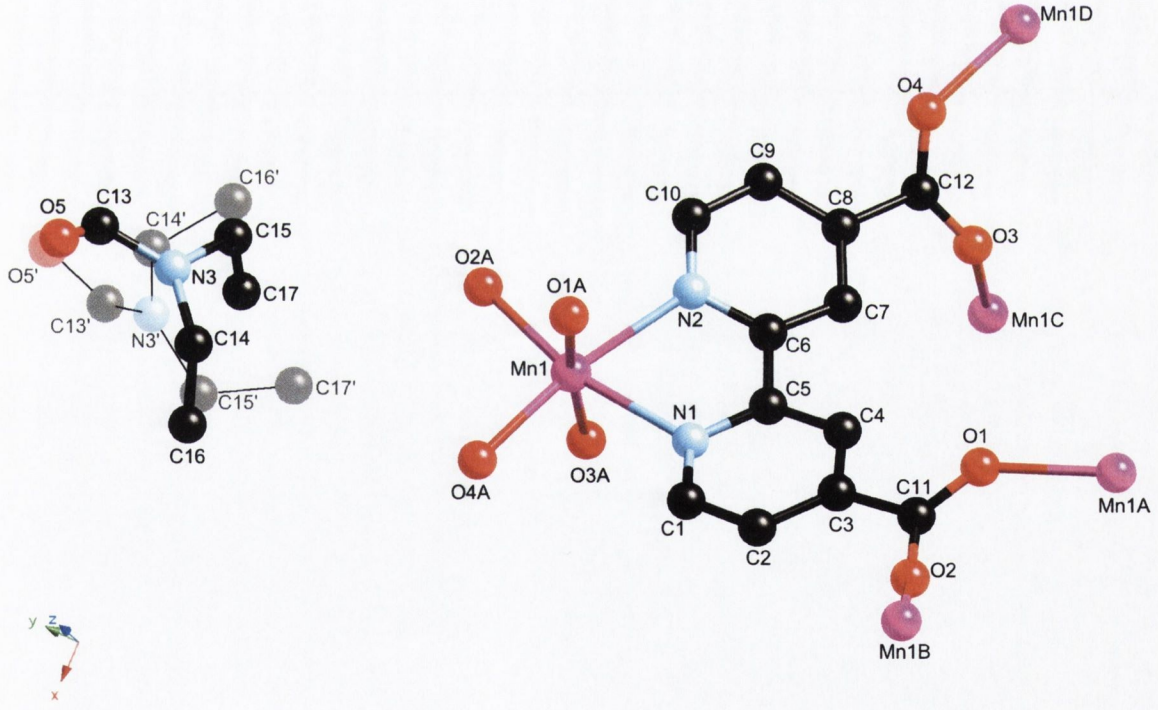

Figure 2.20 – Atom connectivity and labelling scheme for **4**. (Disordered DEF positions (O5', N3', etc.) shown as translucent atoms. Hydrogen atoms omitted for clarity).

Table 2.10 – Selected bond lengths (Å) and angles (°) for **4**.

Mn1-O1^{i}	2.161(2)	N1-Mn1-N2	71.49(9)
Mn1-O2^{ii}	2.117(2)	O1^{i}-Mn1-O2^{ii}	98.18(8)
Mn1-O3^{iii}	2.184(2)	N2-Mn1-O1^{i}	89.32(9)
Mn1-O4^{iv}	2.126(2)	N1-Mn1-O1^{i}	82.07(9)
Mn1-N1	2.298(3)	O1^{i}-Mn1-O4^{iv}	86.80(8)
Mn1-N2	2.313(3)	O2^{ii}-Mn-O4^{iv}	96.80(9)
Mn1···Mn1^{v}	4.7634(9)	N2-Mn1-O2^{ii}	94.68(9)
Mn1···Mn1^{vi}	4.8294(9)	N1-Mn1-O4^{iv}	97.02(9)
		O1^{i}-Mn1-O3^{iii}	172.24(8)
		N1-Mn1-O2^{ii}	166.17(9)
		N2-Mn1-O4^{iv}	168.30(9)

Symmetry codes: i = 0.5-x, y+0.5, 0.5-z; ii = x, -y, z-0.5; iii = 0.5-x, -0.5-y, -z; iv = x-0.5, y+0.5, z; v = -x, -y, -z; vi = 0.5-x, 0.5-y,-z.

The 4,4'-dcbp ligand is heavily distorted, even more so than in **3**. The pyridyl rings are twisted at approximately 23° about the C5-C6 bond (*cf.* 21° for **3**). Additionally the 'bending' of the ligand is more pronounced with C2-C5-C6 172.5° and C9-C6-C5 170.9° (*cf.* 173.6° and 171.6° respectively for **3**). The carboxylate about C11 is twisted 11.5° about the aromatic ring to which it is attached, while that about C12 is twisted significantly more at 32.5°. The C-O bond lengths about C11 are identical (1.252(4) Å) while those about C12 are slightly different (C12-O3 1.258(4) Å, C12-O4 1.245(4) Å).

The *anti-syn* bridging bidentate conformation of the carboxylate groups gives rise to infinite bis-carboxylato bridged manganese chains similar to those in **3** (Figure 2.17). The rings also adopt a chair-like conformation, however, the different angles about the manganese atom and the carboxylate groups give rise to different metal-to-metal distances than in **3**. The manganese ions bridged by C11 carboxylate groups are separated by 4.7634(9) Å (*cf.* 4.731(1) Å in **3**) while those bridged by C12 carboxylate groups are separated by 4.8294(9) Å (*cf.* 4.839(1) Å in **3**). The manganese-carboxylate chains, which run along the (110) and (-110) directions, are cross-linked by the 4,4'-dcbp ligands producing a 3D network similar to that of **3**, as shown in Figure 2.21. As with **3**, offset face-to-face π-π interactions between the pyridyl rings reinforce the network (separation at closest contact 3.398(4) Å). The resulting network is near identical to **3** and also displays channels along the three crystallographic axes, occupied by the DEF molecules. Similarly to **3**, these are at half-occupancy and disordered over two positions, however the two-fold rotation axis which relates these positions does not pass through the oxygen atom but through the

midpoint between the two oxygen atoms and the two nitrogen atoms. The need to accommodate bigger guest molecules forces the expansion of the channels which now have dimensions[#] of 3.33 × 4.57, 2.53 × 7.07 and 3.12 × 6.34 $Å^2$ along *a*, *b* and *c* respectively. This in turn results in the distortion of the coordinated network and in the more pronounced 'bending' of the 4,4'-dcbp ligand. The channels now constitute 24.4% (*cf.* 23.3% for **3**) of the crystal volume.[187-189] As expected the resulting structure is more densely packed than that of **3** (1.734 gcm^{-3}, *cf.* 1.684 gcm^{-3} for **3**).

In terms of topology the coordination network of **4** is identical to that of **3**, since the connectivity is the same, and thus no further discussion will be made here.

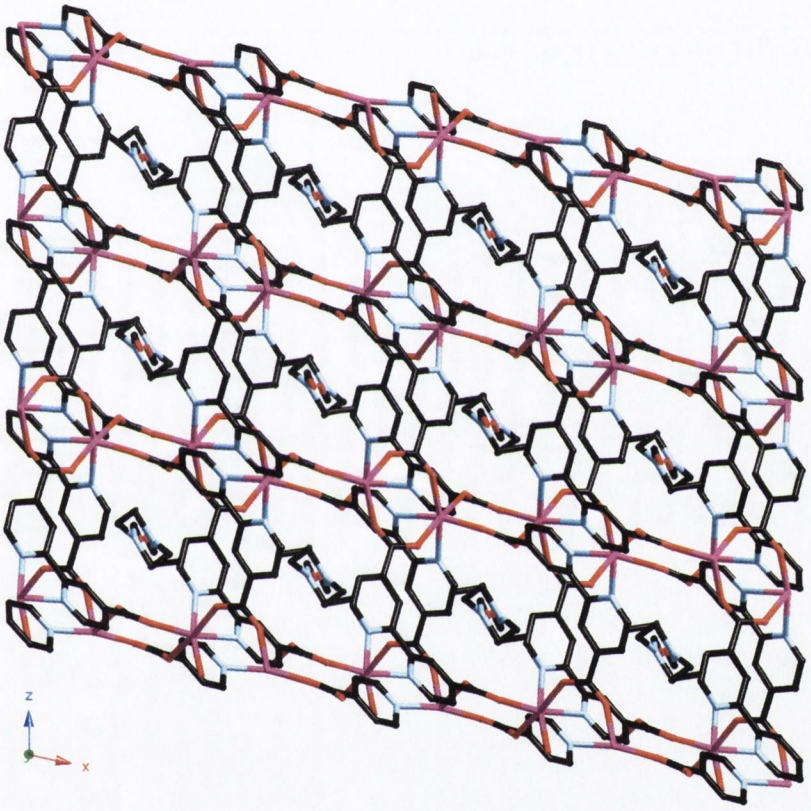

Figure 2.21 – Structure of **4** looking down the (010) direction, showing the channels where the disordered DEF molecules reside. (Hydrogen atoms omitted for clarity)

*2.4.4 Structural comparison of {[Mn(4,4'-dcbp)]·½DMF}$_n$ (**3**) and {[Mn (4,4'-dcbp)]·2H_2O}$_n$ (**5**).*

The structure of {[Mn(4,4'-dcbp)]·2H_2O}$_n$ (**5**), shown in Figure 2.22, has been described by Kempe and co-workers.[176] For comparison with **3** our lower temperature refinement is used in this discussion. Crystallographic details for **5** are shown in Table 2.11. As explained previously, **3** and **5** are pseudopolymorphs, meaning that their 3D networks contain the same components, but they differ in the solvent molecules

[#] Dimensions given are atom to atom (including hydrogen) as viewed along channels and are *ca.* perpendicular to channel direction.

residing in the channels. Both complexes crystallise in the monoclinic *C*2/*c* space group, but despite this **5** effectively has 'more' symmetry than **3** since the unit cell is approximately half the volume. The asymmetric unit of **3** consists of a full Mn(II) metal ion and a 4,4'-dcbp ligand, whereas for **5** only one half of the Mn(II) ion and the 4,4'-dcbp ligand are unique as the complex resides on the two-fold axis.

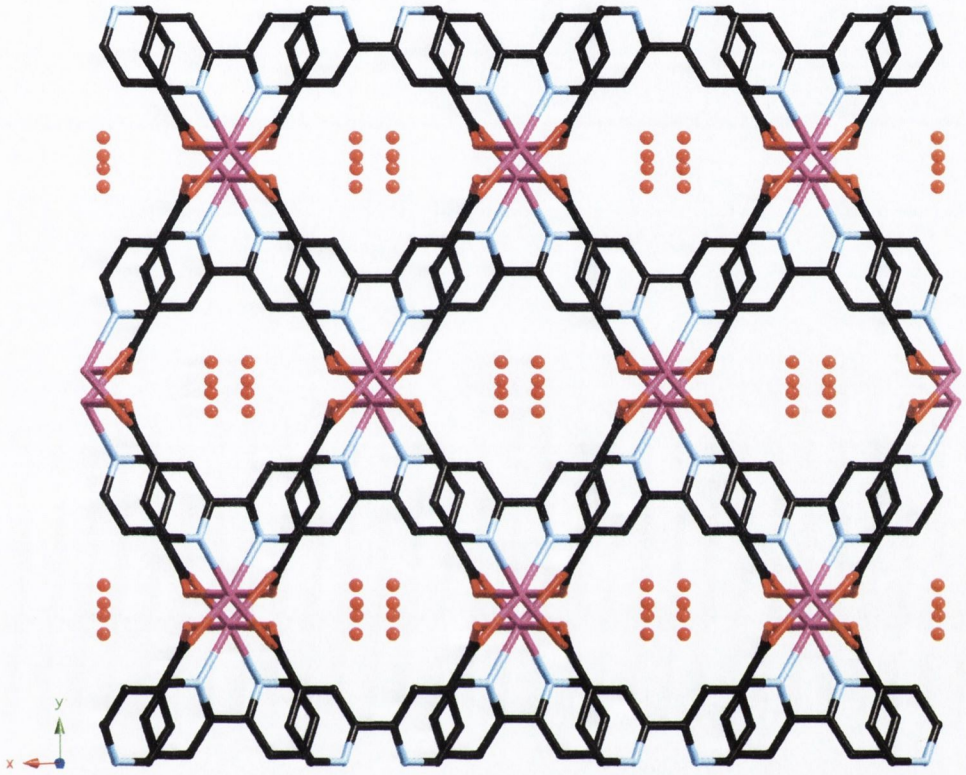

Figure 2.22 – Structure of **5**, viewed down the *c* direction showing the channels extending along this direction. Disordered water molecules reside in the channels. (Hydrogen atoms omitted for clarity)

Apart from small differences in the distortion from octahedral symmetry, the coordination sphere about the Mn(II) ion in **5** is identical to that found in **3**. The coordination mode for the 4,4'-dcbp ligand is identical in the two structures, with the nitrogen atoms chelating to a Mn(II) ion, and the carboxylate oxygen atoms coordinating to four other Mn(II) ions. However, the 4,4'-dcbp ligand is less distorted as exemplified by the 176.4° angle across the central C5–C5A bond (*i.e.* C2–C5–C5A). Symmetry dictates that this distortion buckles the ligand as opposed to bending it, as was observed in **3**. The carboxylate group, which is rotated by *ca.* 42° to the pyridyl ring (*cf.* 11° and 34° in **3**) bridges adjacent Mn centres forming bis-carboxylato bridged chains, similar to those in **3**, that cross-link through 4,4'-dcbp to give a 3D network. The chains in both **3** and **5** consist of eight-membered rings in a chair like conformation, however, because of the higher symmetry of the 4,4'-dcbp ligand in **5**, only one crystallographically unique type of ring exists. Thus all the metal-to-metal

distances along the chain are 4.7345(4) Å (*cf.* 4.731(1) Å and 4.839(1) Å in **3**). It is the way in which these chains are cross-linked by the 4,4'-dcbp ligand that gives rise to the two different network topologies. As seen in Figure 2.23, the manganese atoms are doubly bridged by the carboxylate groups of the 4,4'-dcbp ligand. The black carbon atoms in the chains are pointing in the same direction for both **3** and **5**, whilst the green carbon atoms in **3** are pointing in a different direction to those in **5**. This shows how the 4,4'-dcbp ligands are oriented differently in the two structures and thus link the chains in a different manner, resulting in the formation of two dissimilar but related networks.

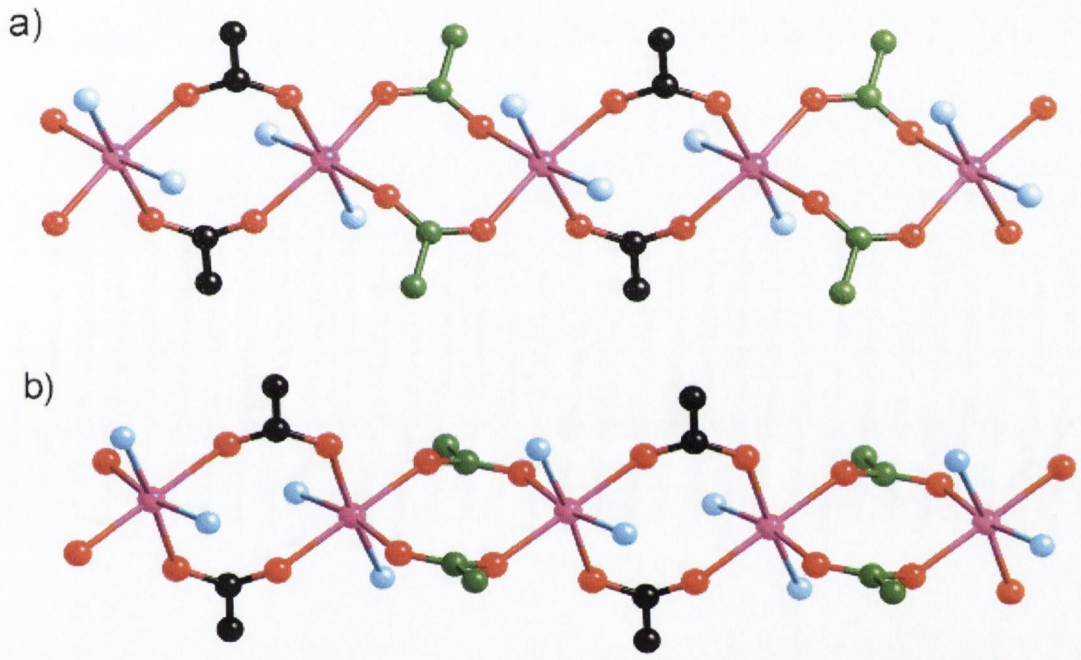

Figure 2.23 –Bis-carboxylato bridged manganese chains in a) $\{[Mn(4,4'\text{-dcbp})]\cdot ½\ DMF\}_n$ (**3**) and b) $\{[Mn(4,4'\text{-dcbp})]\cdot 2H_2O\}_n$ (**5**). The black carbons are oriented in the same direction in the two chains, whereas the green carbons in **3** are pointing in a different direction to those in **5**, thus resulting in a different orientation for the 4,4'-dcbp ligands and hence different linking of the chains in the two structures.

Figure 2.24 and Figure 2.25 are schematic representations of the networks formed in **3** and **5**, respectively. The manganese-carboxylato chains are highlighted in red and/or yellow, and the 4,4'-dcbp ligand is represented as two isonicotinate subunits with a single link from the nitrogen atom to the carbon atom *para* to it (as in Figure 2.10). Layers containing parallel chains in **3** lie in the *ab* plane and are separated by *ca.* 8.6 Å along the *c* direction. Chains in alternate layers all run in the same direction, but at 66° to those in the other layers. In contrast, all the manganese-carboxylato chains in **5** run parallel to each other, extending along the crystallographic *c* direction.

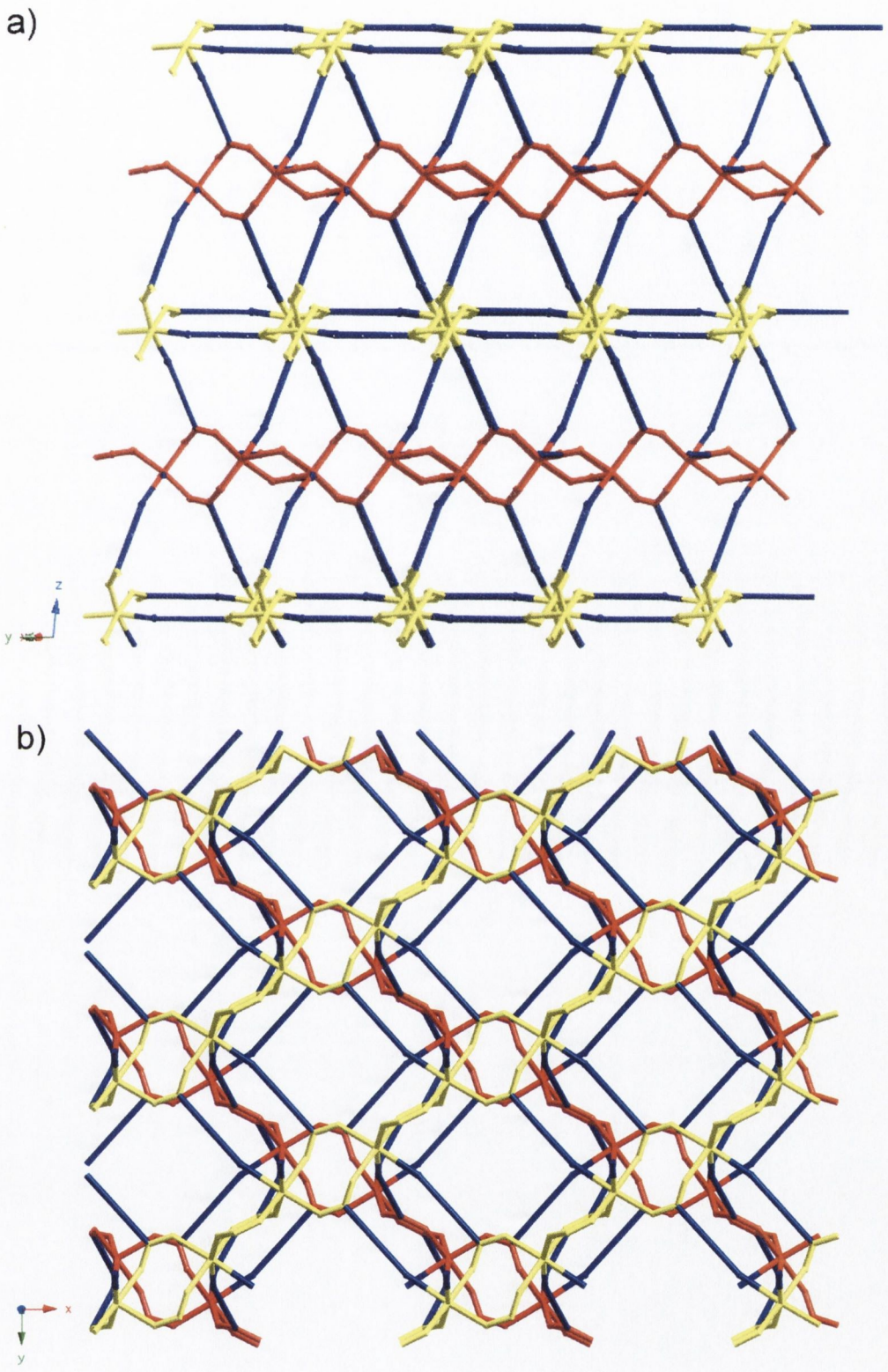

Figure 2.24 – Schematic representation of **3**. The manganese-carboxylato chains are highlighted in red and yellow and the 4,4'-dcbp ligand is represented as two isonicotinate subunits, with a single blue bond from the nitrogen atom to the carbon atom *para* to it. a) View along (110) showing the different chain 'layers', with chains in red runnning parallel to the page, whilst yellow chains extend perpendicular to the page; b) View along (001), showing the 66° angle formed by chains in alternate layers.

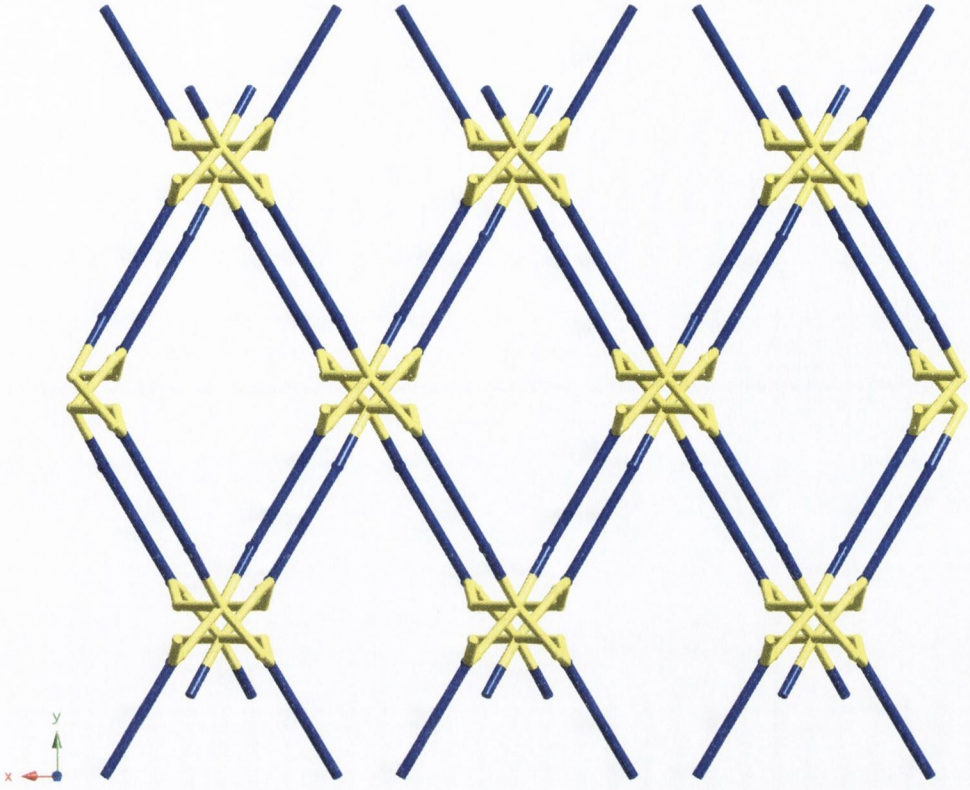

Figure 2.25 – Schematic representation of **5**. The manganese-carboxylato chains are highlighted in yellow and the 4,4'-dcbp ligand is represented as two isonicotinate subunits, with a single blue bond from the nitrogen atom to the carbon atom *para* to it. View along (001), with the chains extending perpendicular to the page.

The network in **5** is not as heavily perforated as **3** with only two directions containing channels of appreciable dimension[§] that measure *ca.* 3.81 × 6.84 Å^2 (down *c*-axis) and 2.3 × 5.7 Å^2 (down 101). The water molecules reside in the former channels, with each disordered over two close positions, and hydrogen bond to each other giving chains extending along the *c* axis. They also hydrogen bond to the carboxylate groups. The channels in **5** constitute 18.2% of the crystal volume.[187-189]

As described in the previous section, the overall network in **3** consists of 6-connecting nodes (Mn atoms) and two types of 3-connecting nodes (4,4'-dcbp ligand). The Schläfli notation was determined as $(4.6^2)(4^2.6)(4^3.6^6.8^6)$. The overall network resulting from coordination in **5** is shown in Figure 2.26, and consists of two types of nodes: 6- and 3-connecting in 1:2 ratio. In comparison to the network in **3**, only one type of 3-connecting node exists, since each isonicotinate subunit of the 4,4'-dcbp ligand is crystallographically equivalent and thus has the same topological environment. The red nodes represent the position of the Mn atoms, while the blue

---

[§] Dimensions given are atom to atom (including hydrogen) as viewed along channels and are *ca.* perpendicular to channel direction.

nodes represent an arbitrary point in the isonicotinate subunit of the 4,4'-dcbp ligand. Each 3-connecting node is linked to three 6-connectors, while each 6-connector is linked to six 3-connectors. The three shortest circuits for the 3-connectors include two circuits involving four nodes and one circuit involving six nodes. The fifteen shortest circuits for the 6-connectors include four circuits involving four nodes, two circuits involving six nodes, eight circuits involving eight nodes and one circuit involving ten nodes. Therefore, the Schläfli notation for the network is $(4^2.6)(4^4.6^2.8^8.10^1)$ (*c.f.* **3**, $(4.6^2)(4^2.6)(4^3.6^6.8^6)$). Thus, the 3-connectors have the same notation as for the type II 3-connectors in **3**, but the 6-connectors in **5** have a more complex notation, involving four different types of circuits.

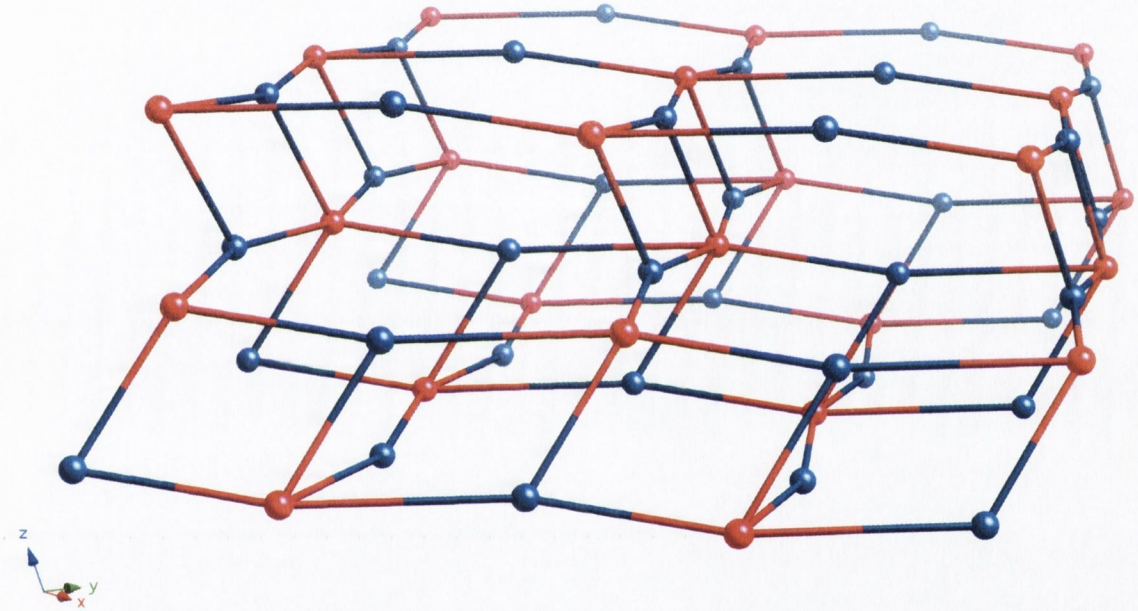

Figure 2.26 – Schematic diagram for the overall 3D network of **5**. The 6-connecting nodes (red centres) are the positions of the Mn atoms. The 3-connecting nodes (blue centres) represent an arbitrary point in each half of the 4,4'-dcbp ligand (*i.e.* an isonicotinate subunit). The Schläfli notation for the network formed is $(4^2.6)(4^4.6^2.8^8.10^1)$.

Table 2.11 - Crystallographic data for **5**[‡] and **5a**.

Compound		**5**	**5a**
Chemical Formula		$MnC_{12}H_{10}N_2O_6$	$MnC_{12}H_6N_2O_4$
Formula weight		333.16	297.13
Crystal system		Monoclinic	Monoclinic
Space group		*C*2/*c*	*C*2/*c*
μ (MoK_α)/ mm^{-1}		1.068	1.104
a/Å		11.9505(9)	12.174(1)
b/Å		14.568(1)	14.632(1)
c/Å		9.2494(7)	9.0078(8)
α/°		90	90
β/°		127.791(1)	131.210(1)
γ/°		90	90
V/Å^3		1272.5(2)	1207.1(2)
Z		4	4
D_{calc}/gcm^{-3}		1.739	1.635
T/K		153(2)	343(2)
Crystal size	max /mm	0.38	0.28
	mid /mm	0.09	0.08
	min /mm	0.08	0.07
$2\theta_{max}$/°		56.58	49.88
Min/Max trans. Factor		0.855/1.000	0.855/1.000
R_{int}		0.0259	0.0260
R_1, wR_2[I>2σ(I)][a]		0.0392, 0.0954	0.0381, 0.0852
R_1, wR_2 (all data)		0.0415, 0.0966	0.0438, 0.0876
Reflections–	collected:	6153	4647
	unique:	1500	1061
	observed:	1439	968

[a] $R_1 = \Sigma||F_o| - |F_c||/\Sigma|F_o|$, $wR_2 = [\Sigma w(F_o^2 - F_c^2)^2/\Sigma w(F_o^2)^2]^{1/2}$

[‡] Crystallographic details for **5** refer to data collection and refinement performed at Trinity College Dublin.

*2.4.5 Thermal analysis and magnetic properties of **3** and **5**.*

The connectivity of the networks, as described above, gives rise to channels in **3**, where the DMF molecules reside. The channels in **3** constitute 23.3% of the total volume, as calculated by the CALCSOLV feature of the PLATON program.[187-189] Thermogravimetric analysis of **3** shows it is exceptionally robust and stable to guest loss up to 410 °C, after which decomposition begins (Figure 2.27). MOF guest loss typically precedes host decomposition, however, it appears that DMF is too large to fit through the apertures of the pores and is therefore irreversibly enclathrated within the host network. The channels in **5**, however, are occupied by water molecules and constitute 18.2% of the crystal volume.[187-189] In contrast to the 'entrapment' of the DMF molecules within the channels in **3**, TGA showed that the water molecules are rather weakly bound and vacate the pores before 65 °C (10%, calcd. 10.8%) with the network remaining intact up to 410 °C (Figure 2.28). **3** and **5** display essentially the same network decomposition temperature (*i.e.* independent of topology) and are, to the best of our knowledge, amongst the most thermally robust MOFs reported to date.[190-191]

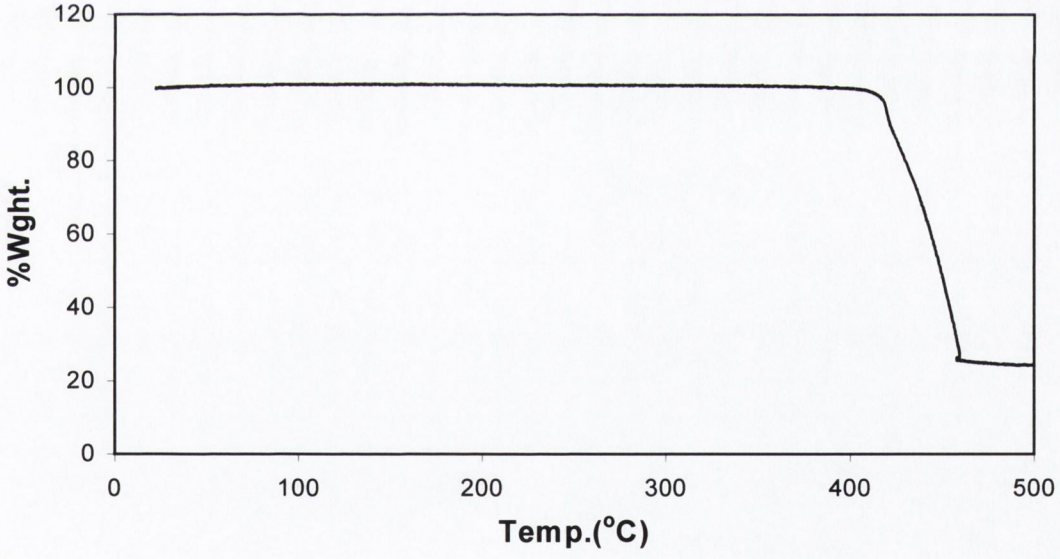

Figure 2.27 –Thermogravimetric analysis curve for **3**. No weight loss is observed until decomposition begins at 410 °C.

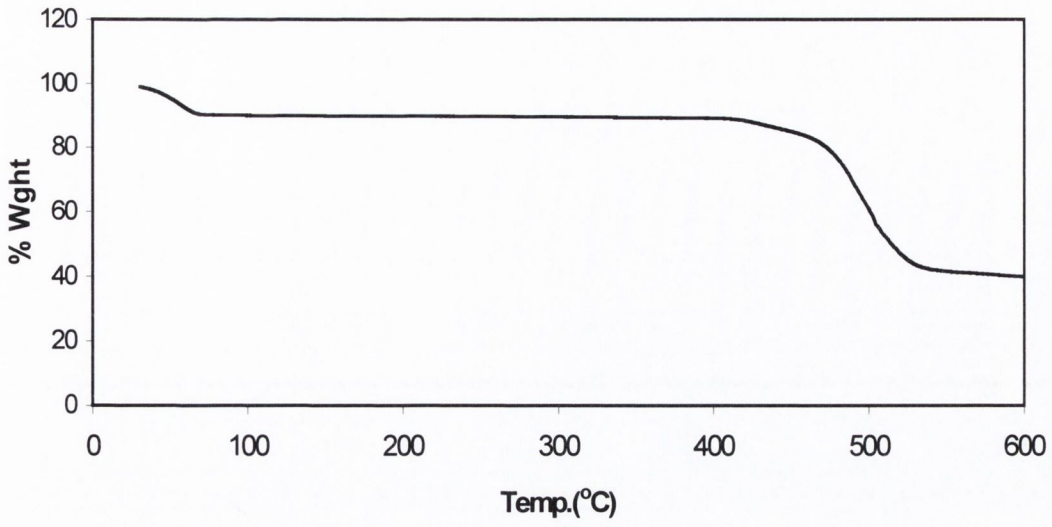

Figure 2.28 - Thermogravimmetric anlaysis curve for **5**. 10% weight loss is observed up to 65 °C consistent with the loss of two water molecules. Decomposition begins at 410 °C.

Notably, **3** and **5** retain crystallinity even after extreme thermal treatment. Indeed, when a single crystal of **5** was heated to 70 °C on the diffractometer and a new data set collected, the structure of the 'guest-free' host $[Mn(4,4'\text{-dcbp})]_n$ (**5a**) was revealed. Crystallographic details for **5a** are shown in Table 2.11. The cell parameters of **5a** *cf.* **5** (153K) vary slightly but significantly: *a* and *b* lengthen by 1.8 and 0.4%, *c* contracts by 2.6% and β increases by 2.6%. Thus the volume decreases by 5.1%. These changes are accompanied by a decrease in the torsion angles between pyridyl rings (*ca.* 18° *cf.* 22° in **5**) and between the carboxylate group and the pyridyl ring (*ca.* 35° *cf.* 42° in **5**)(Figure 2.29). This results in a shorter metal-to-metal distance across the manganese-carboxylato chains (4.601 Å, *cf.* 4.735 Å in **5**). Nevertheless, **5a** retains its porous nature, which now accounts for 17.0% of the cell volume.[187-189] Furthermore, when crystals of **5a** were exposed to air on cooling, **5** was regenerated showing the reversibility of the desorption-adsorption process.

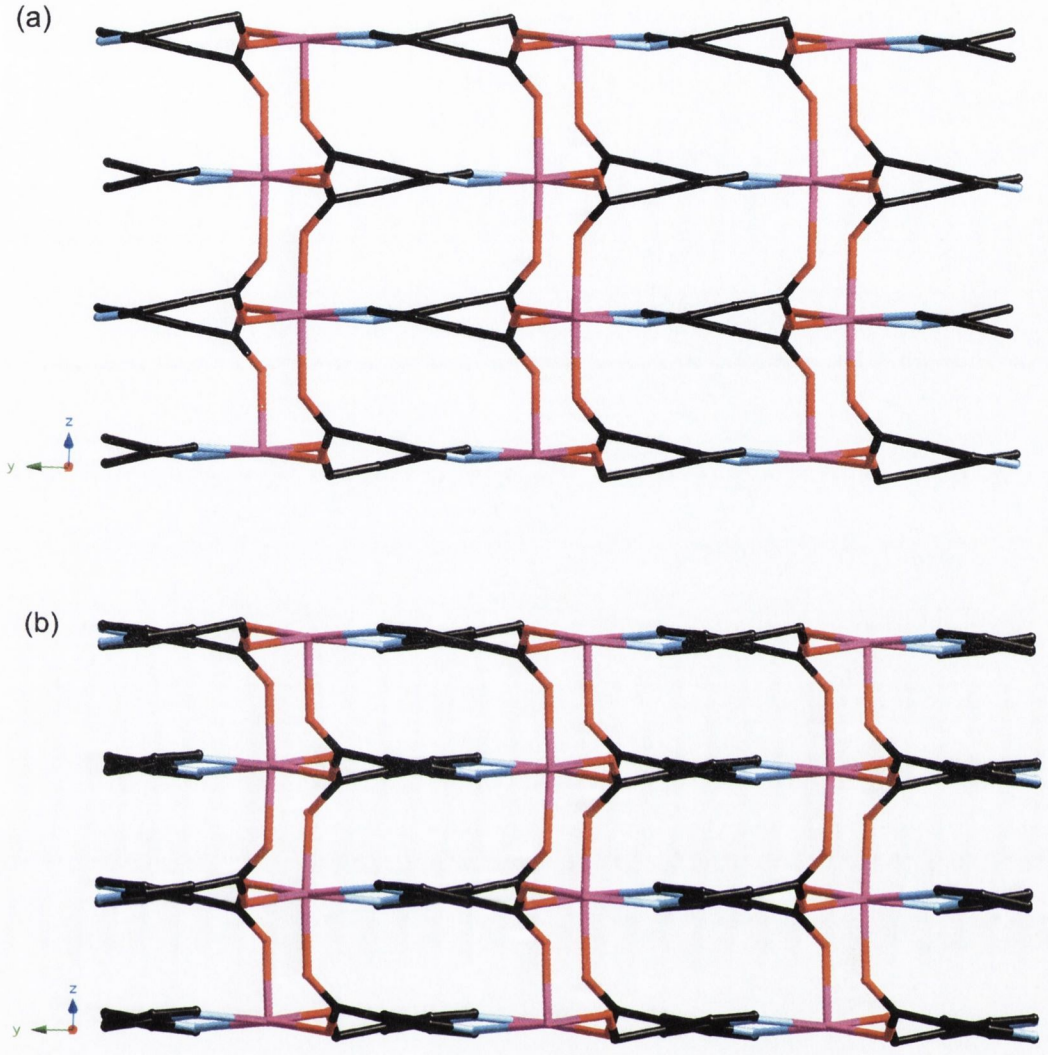

Figure 2.29 – View of **5** (a) and **5a** (b) along the *a* direction. Note the bigger torsion angle between the pyridyl rings in **5** compared to **5a**.

Variable temperature magnetic susceptibility studies were performed on powdered samples of **3** and **5**, over the temperature range 300-4 K. The magnetic data for **3** are shown in Figure 2.30(a). The magnetic moment (μ_{eff}) for **3** decreases gradually from 5.80 BM at 300 K, reaching 5.35 BM at 80 K. The moment then decreases rapidly below 80 K to reach 1.40 BM at 4 K. The plot of χ_m *vs* T goes through a maximum at *ca.* 8 K. This behaviour is typical for high spin octahedral Mn(II) centres with weak antiferromagnetic coupling combined with zero-field splitting at low temperatures. The 100-4 K region was explored further with variable field {20, 100, 1000, and 10000 Oe (= 1 Tesla)} measurements to determine whether any long-range antiferromagnetic order might be occurring. The values were essentially independent of field indicating no such effect. Magnetic data for **5** were similar to those of **3** as shown by Figure 2.30(b). Similarly, χ_m passes through a maximum at *ca.* 5 K, with the magnetic moment (μ_{eff}) decreasing gradually from 5.70 BM at 300 K, reaching 5.50 BM

at 80 K. The moment then decreases rapidly below 80 K to reach 1.75 BM at 4.2 K. The data for **3** and **5** were fitted to a 2D sheet model,[192, 193] for spins of 5/2, yielding a coupling constant, *J*, of -0.35 cm^{-1}, *g* = 1.94 (**3**) and –0.262 cm^{-1}, *g* = 1.95 (**5**), indicative of very weak antiferromagnetic coupling.

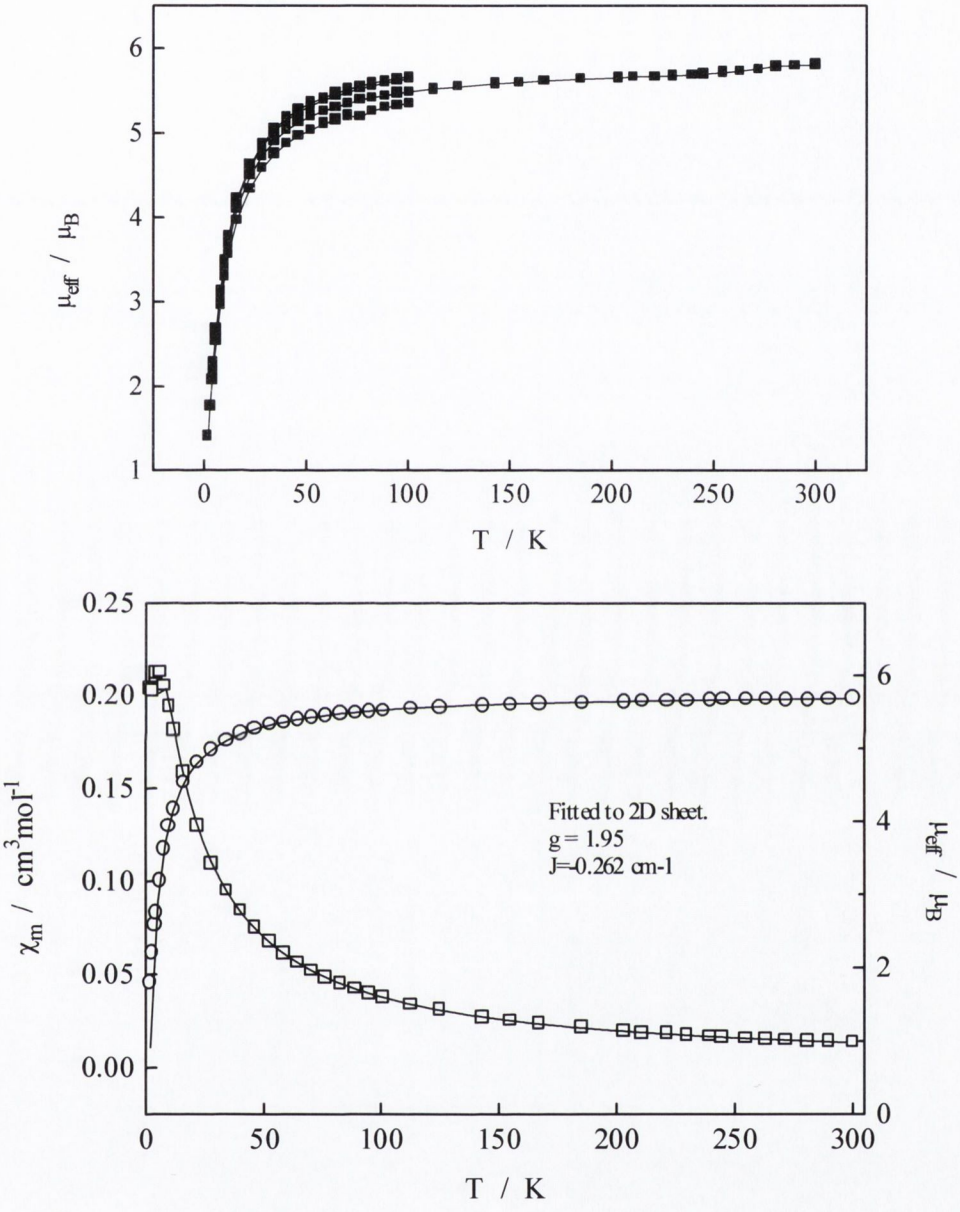

Figure 2.30 – (a) μ_{eff} *versus T* plot for **3**. (b) χ_m and μ_{eff} *versus T* plots for **5**.

2.5 Conclusions

As a result of this study several novel coordination polymers have been synthesised. The use of hydrothermal synthetic techniques has proved successful in the formation of crystalline products. High temperatures and pressures present in the bomb allow for ligands with low solubility, such as 4,4'-H_2dcbp, to be forced into solution and thus participate in the reactions. Another technique used was the employment of base to deprotonate the ligand, producing a soluble salt which could

then be reacted with metal salts. This was the method used in the synthesis of **1**, by reacting 4,4'-Na_2dcbp with $Cu(NO_3)_2$, producing a 2D polymer.

Hydrothermal reaction of Co(II) with 4,4'-H_2dcbp (and pyridine to deprotonate the ligand), produced a mixture of the α- and β-polymorphs of $[Co(4,4'\text{-dcbp})(H_2O)_2]_n$. Whilst the α-polymorph has been reported by Kempe and coworkers, the β-polymorph is a novel compound. It is interesting to note that despite the α-polymorph being reported before the β-polymorph, the latter is the more thermodynamically stable product, since it is much more efficiently packed than the former (density of 1.940 gcm^{-3} *cf.* 1.654 gcm^{-3}). This is consistent with the α-polymorph being the kinetically favoured product.

The hydrothermal reaction of Mn(II) with 4,4'-H_2dcbp produces three pseudo-polymorphs depending on the solvent employed. In H_2O/DMF mixtures, when the major solvent employed is DMF, **3** is produced, whereas **5** is produced when water is the major solvent. **4** is produced when only DEF is employed. All three display channels in their structures, which are occupied by a different solvent in each case. **3** and **4** have the same coordination network and thus topology, while **5** has a different connectivity and topology. Interestingly, the solvent in **5** can be expelled at 65 °C, whereas the solvent in **3** is 'trapped' and no expulsion of the guests occurs. Due to the small amount of **4** obtained no thermogravimmetric analysis was performed, although it would be expected to exhibit a similar behaviour as **3**, since the coordination networks are identical. **5** retains crystallinity after the loss of solvent and the structure of the desolvated host **5a** was obtained. As would be expected, this is very similar to **5** but less dense (1.635 *cf.* 1.739 gcm^{-3}) and with a smaller solvent accessible area (17.0% cf. 18.2%). Thus, **5** is a new member of only a handful of examples of molecular materials to be characterised by single crystal X-ray diffraction in both the presence and absence of guests.[116, 194, 195] We are currently investigating whether the porous network of **5a** adsorbs guests other than water.

The coordination polymers prepared all display different coordination modes for the 4,4'-dcbp ligand. As expected, in all the structures the ligand coordinates through the chelating nitrogen atoms, but differ in the way the coordinate through the carboxylate moieties. The ligand in both **1** and **2** has a coordination number of three, whereas in **3**, **4** and **5** the ligand coordinates to five different metals. In addition to coordination through the chelating site, the two carboxylate groups of the 4,4'-dcbp ligand in **1** are coordinating in a monodentate fashion, whereas in **2** one of the carboxylates coordinates in a bidentate bridging fashion, whilst the other carboxylate is non-coordinating. The coordination mode for **1** is identical to that seen in the α-$[Co(4,4'\text{-dcbp})(H_2O)_2]_n$ polymorph prepared by Kempe an co-workers. In **3**, **4** and **5**

both carboxylate groups of the 4,4'-dcbp ligand coordinate in a bridging bidentate fashion.

The networks formed by coordination in **1**, **2** and α-$[Co(4,4'\text{-dcbp})(H_2O)_2]_n$ all belong to the uniform (*n*,3) connected nets. When both the ligand and metal atoms are considered as nodes, a 2D (6,3) net is formed by **1**. The two polymorphs of $[Co(4,4'\text{-dcbp})(H_2O)_2]_n$ form two different networks: the α-polymorph forms a (12,3) connected net, whilst the β-polymorph forms a (10,3)-a connected net. Both structures were refined in chiral space groups, and thus, as expected, both nets are enantiomorphic. The networks formed by the pseudo-polymorphs **3**, **4** and **5** are more complex than those formed by the other polymers in terms of topology. The networks are identical for **3** and **4** and have Schläfli notation $(4^2.6)(4.6^2)(4^3.6^6.8^6)$, but different for **5** which has Schläfli notation of $(4^2.6)(4^4.6^2.8^8.10^1)$.

In summary, this study shows that 4,4'-H_2dcbp is a versatile ligand, which can adopt a wide array of coordination modes, and is capable of forming multiple types of coordination networks, including polymers displaying channels in their structure, depending on the metal, solvent and conditions employed.

Chapter Three

First Row Transition Metal Complexes Incorporating 4,4'-dicarboxy-2,2'-bipyridine and other Pyridine Based Ligands or Coordinating Anions

3.1 Complexes incorporating 4,4'-dicarboxy-2,2'-bipyridine and other pyridine based ligands.

Preamble

In Chapter 2, several coordination polymers were prepared by the use of 4,4'-dcbp as a connector. The approach adopted in this chapter was to employ 4,4'-bipy as a ligand in conjunction with 4,4'-dcbp. 4,4'-bipy has two linearly disposed coordination sites, and has been extensively used in the preparation of coordination polymers providing many interesting examples.[88, 89, 92, 196, 197] Much less work has been done in systems containing two different organic ligands. However, recently mixed-linker systems of both carboxylate and pyridyls have proved effective in the formation of coordination polymers.[198-203] The basic idea is to exploit the linear coordination sites of these ligands to link 2D sheets formed by carboxylate ligands, creating a 3D network. This approach has been exploited by Rosseinsky and co-workers by linking 2D sheets of Ni-TMA with 4,4'-bipy to create a 3D network.[204] Similarly, replacement of the axially coordinated water molecules in **1** by 4,4'-bipy would then link the 2D sheets into a 3D network. This approach has the advantage that, since 4,4'-bipy is a neutral ligand, no further charge balancing counterions will need to be incorporated into the network.

3.1.1 Reaction of Co(II) with 4,4'-dicarboxy-2,2'-bipyridine and 4,4'-bipyridine.

An aqueous mixture of $CoSO_4$, 4,4'-H_2dcbp and 4,4'-bipy (1:1:1), was reacted hydrothermally, with excess pyridine, at 180 °C for 7 days. Orange crystals were obtained directly in approximately 47% yield. An infrared spectrum clearly showed the presence of deprotonated 4,4'-dcbp ($\nu_{as}(CO_2^-)$ 1614 and 1548 cm^{-1}, $\nu_s(CO_2^-)$ 1376 cm^{-1}) and water (3118 cm^{-1}), plus bands due to aromatic pyridyl ring systems, which were harder to assign to a particular group due to overlap between them. A suitable crystal was selected and a single crystal X-Ray diffraction study performed. From this, the complex was determined to be: $\{[Co(4,4'\text{-dcbp})(py)(H_2O)_2]\cdot(½\ 4,4'\text{-bipy})\ 2H_2O\}_n$ (**6**).

*3.1.2 Crystal structure of $\{[Co(4,4'\text{-dcbp})(py)(H_2O)_2]\cdot(½\ 4,4'\text{-bipy})\cdot 2H_2O\}_n$.(**6**).*

The structure of **6** was refined in the monoclinic $P2_1/c$ space group and crystallographic data are shown in Table 3.2. The molecular structure and labeling scheme for the asymmetric unit can be seen in Figure 3.1. The Co(II) atom adopts an octahedral geometry, with the equatorial positions occupied by the chelating 4,4'-dcbp nitrogen atoms, a carboxylate oxygen atom from an adjacent 4,4'-dcbp ligand, and a coordinated water molecule. The axial positions are occupied by a pyridine nitrogen atom and a second coordinated water molecule. As expected, slight disortion from

octahedral geometry arises from the bite angle of the 4,4'-dcbp nitrogen atoms (N1-Co1-N2 77.2(1)°). See Table 3.1 for selected bond lengths and angles. The 4,4'-dcbp ligand adopts a near planar conformation, with the carboxylate groups twisted less than 7° from the plane of the aromatic ring to which they are attached. Carboxylate C-O bond lengths are similar for both the coordinated (C11-O2 1.260(5) Å) and uncoordinated (C11-O1 1.254(5) Å) oxygens about C11, whereas for both uncoordinated oxygens about C12, C-O distances differ slightly (C12-O3 1.256(5) Å, C12-O4 1.240(5) Å).

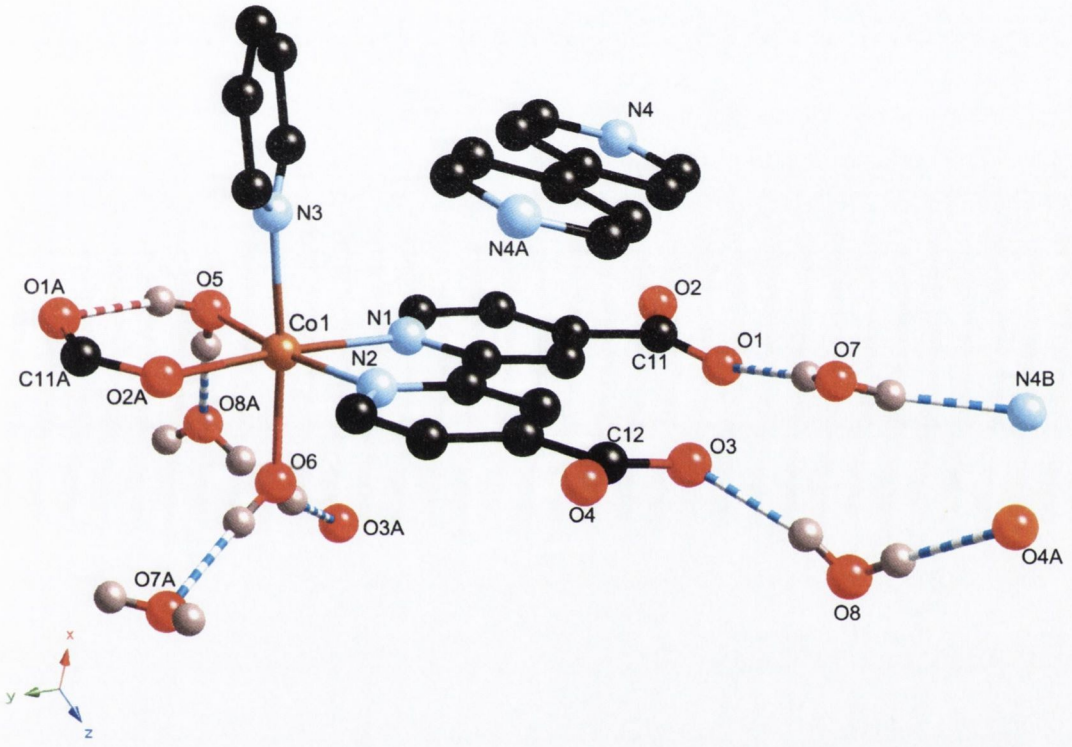

Figure 3.1 – Molecular structure and atomic numbering scheme in **6**. The eight unique hydrogen bonds are shown as dashed bonds, with the intramolecular one shown as red and white, whilst intermolecular ones are shown as blue and white. (Aromatic hydrogen atoms omitted for clarity)

Table 3.1 – Selected bond lengths (Å) and angles(°) for **6**.

Co1–N1	2.127(3)	N1–Co1–N2	77.2(1)
Co1–N2	2.125(3)	O5–Co1–N1	93.0(1)
Co1–O2^{i}	2.089(3)	O2^{i}–Co1–N2	94.4(1)
Co1–O5	2.118(3)	O5–Co1–N2	170.0(1)
Co1–O6	2.061(3)	O2–Co1–N1	171.3(1)
Co1-N3	2.152(4)	O6–Co1–N3	175.0(1)

Symmetry codes: i = 1-x, y+0.5, 0.5-z.

Table 3.2 – Crystallographic data for **6** and **7**.

Compound	**6**	**7**
Chemical Formula	$CoC_{22}H_{23}N_4O_8$	$CuC_{22}H_{25}N_4O_{9.5}$
Formula weight	530.37	561.0
Crystal system	Monoclinic	Monoclinic
Space group	$P2_1/c$	$C2/c$
μ (MoK_α)/ mm^{-1}	0.819	0.925
a/Å	10.419(1)	23.117(5)
b/Å	18.376(2)	12.426(2)
c/Å	12.535(1)	17.652(3)
α/°	90	90
β/°	110.124(2)	95.574(3)
γ/°	90	90
V/$Å^3$	2253.4(4)	5046.8(2)
Z	4	8
D_{calc}/gcm^{-3}	1.563	1.477
T/K	153(2)	153(2)
Crystal size max /mm	0.15	0.43
mid /mm	0.05	0.20
min /mm	0.03	0.13
$2\theta_{max}$/°	57.04	56.50
Min/Max trans. Factor	0.868/1.000	0.713/1.000
R_{int}	0.0806	0.0493
R_1, wR_2[I>2σ(I)][a]	0.0783, 0.1227	0.0422, 0.1062
R_1, wR_2 (all data)	0.1227, 0.1374	0.0541, 0.1108
Reflections – collected:	13903	27592
unique:	5195	5817
observed:	3597	4599

[a] $R_1=\Sigma||F_o|-|F_c||/\Sigma|F_o|$, $wR_2=[\Sigma w(F_o^2-F_c^2)2/\Sigma w(F_o^2)^2]^{½}$

Figure 3.2 shows the 1D chains formed by repetition of the [Co (4,4'-dcbp)(py)(H_2O)$_2$] unit, extending along the *b* direction, with the intramolecular hydrogen bond between O5 and O1 shown as a red and white band. Adjacent units are rotated at 180° to each other such that the coordinated pyridine molecules reside on opposite sides of the chain. The cobalt atoms are linked by 4,4'-dcbp ligands with a metal-to-metal distance of 9.1910(9) Å.

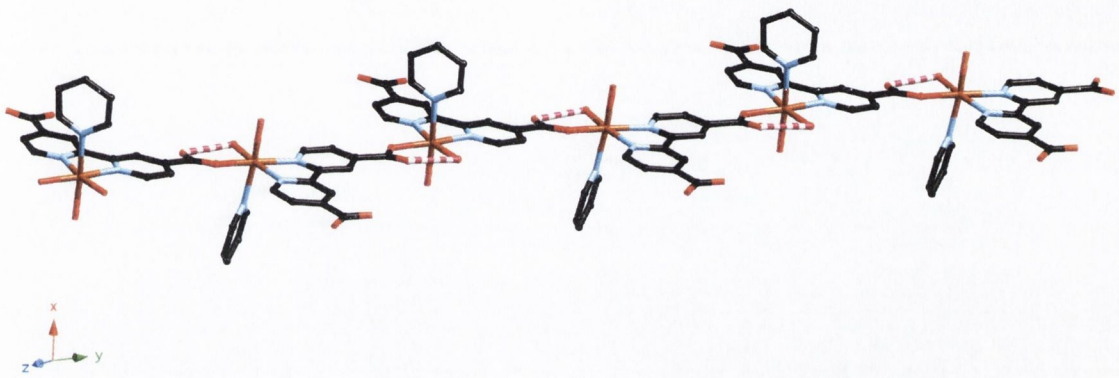

Figure 3.2 – Picture of a single, infinite 1D chain formed in **6**. Adjacent [Co(4,4'-dcbp)(py)(H_2O)$_2$] units are rotated at 180°. (Red and white dashed bonds represent intramolecular hydrogen bonds. Hydrogen atoms, lattice water molecules and 4,4'-bipy omitted for clarity)

There are four water molecules in the structure, two coordinated (O5 and O6) and two in the lattice (O7 and O8). There are eight unique hydrogen bonds in the structure, seven intermolecular and one intramolecular, shown in Figure 3.1, with distances and angles shown in Table 3.3. O5 is a hydrogen bond donor to O1, forming an intramolecular hydrogen bond within the chain, as mentioned above, and to O8, one of the lattice water molecules. O6 is a hydrogen bond donor to the other lattice water molecule, O7, and to a carboxylate oxygen of an adjacent chain, O3. O7 is a hydrogen bond donor to carboxylate oxygen, O1, and to the 4,4'-bipyridine nitrogen N4. O8 donates one hydrogen bond to carboxylate oxygen O3, and another to carboxylate oxygen O4 of an adjacent chain.

The 1D chains are linked into a 2D sheet by hydrogen bonding between the O6 coordinated water and the O3 carboxylate oxygen of an adjacent chain, as shown in Figure 3.3. This is reinforced by offset face-to-face π-π-interactions between 4,4'-dcbp ligands of adjacent chains, with the closest contact being 3.370(6) Å. Weaker edge-to-face C-H···π interactions also exist between the pyridine ring and the 4,4'-dcbp ligand of an adjacent chain, with the separation at closest contact being 3.494(6) Å.

Table 3.3 – Parameters of hydrogen bonding interactions for **6**. (D–H distances are fixed at 0.84(1) Å)

D–H···A	d(H···A)/Å	d(D···A)/Å	<(D–H···A)/°
O5-H5A···O1^{i}	1.85	2.650(4)	158
O5-H5B···O8^{ii}	1.84	2.676(5)	177
O6-H6A···O7^{ii}	1.84	2.671(5)	172
O6-H6B···O3^{ii}	1.85	2.674(4)	171
O7-H7A···O1	2.00	2.832(5)	172
O7-H7B···N4^{iii}	2.03	2.850(5)	166
O8-H8A···O3	1.92	2.707(4)	158
O8-H8B···O4^{iv}	1.94	2.776(5)	177

Symmetry codes: i = 1-x, 0.5+y, 0.5-z; ii = 1-x, -y, -z; iii = x, -0.5-y, z-0.5; iv = -x, -y, -1-z.

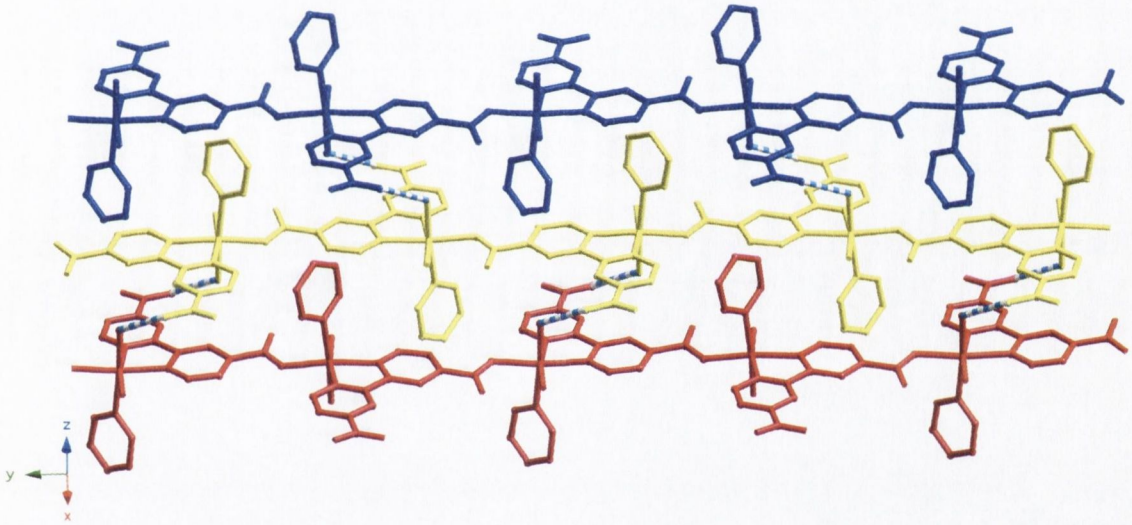

Figure 3.3 - Packing diagram of the 1D chains in **6**, showing the formation of a 2D sheet where three different chains have been highlighted. (Blue and white dashed bonds correspond to hydrogen bonds. Hydrogen atoms, lattice water molecules and 4,4'-bipy molecules omitted for clarity)

The sheets lie in the crystallographic *bc* plane and are further linked down the crystallographic *a* direction to form a hydrogen bonded 3D network, reinforced by π-interactions. Figure 3.4 shows the hydrogen bonding interactions between the chains. Two carboxylate groups on adjacent sheets are connected through hydrogen bonding with two lattice water molecules to form an $R_4^4(12)$ motif. This motif is isographical with the carboxylate-dialkylammonium interaction observed in organic solids.[55, 57] The other main interaction is a hydrogen bond link through a 4,4'-bipy molecule. The O6 coordinated water molecule and the O1 carboxylate oxygen atom of an adjacent chain participate in hydrogen bonding with the O7 lattice water molecule which then hydrogen

bonds to the 4,4'-bipy nitrogen atom on one end of the molecule. As an inversion centre exists in the midpoint of the 4,4'-bipy, this sequence repeats itself on the other end of the 4,4'-bipy, thus linking the chains on adjacent sheets. This link is reinforced by π-π-interactions between 4,4'-dcbp, 4,4'-bipy and pyridine. Offset face-to-face π-π-interactions occur between the 4,4'-bipy and the 4,4'-dcbp ligands. The planes of the interacting rings are at an angle of approximately 21°, with the separation at closest contact being 3.306(6) Å. Edge-to-face π-interactions also exist between the pyridine ring and 4,4'-bipy, with a separation at closest contact of 3.563(7) Å. The overall packing diagram for **6** is shown in Figure 3.5.

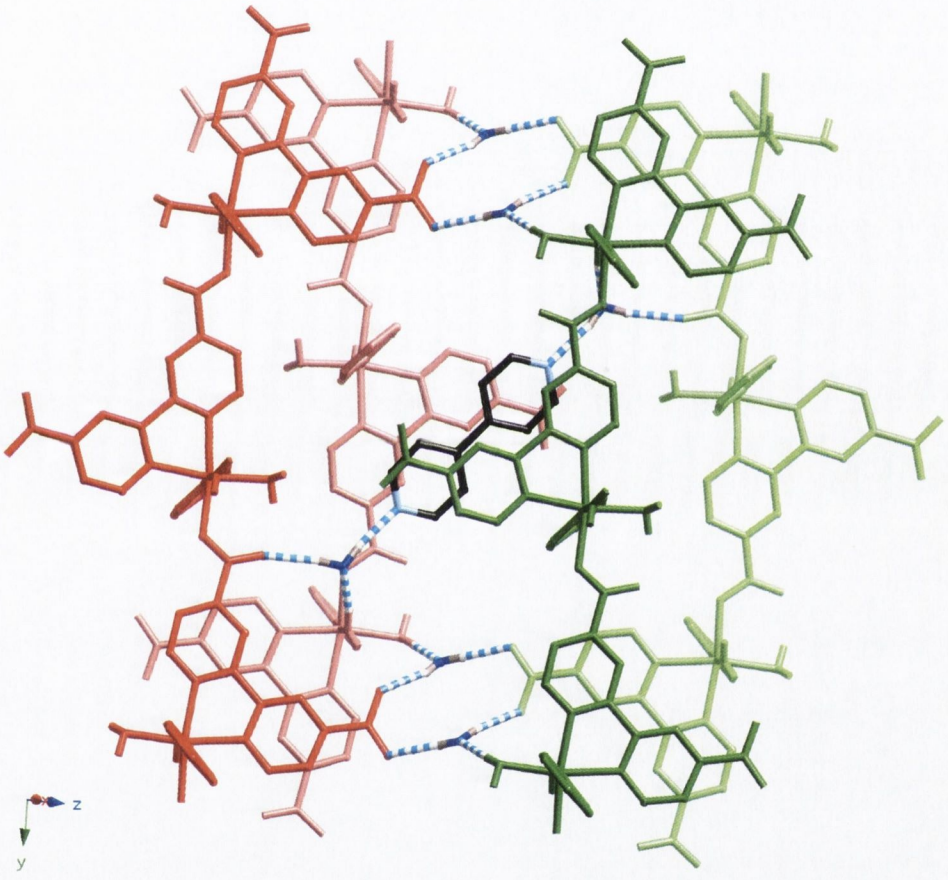

Figure 3.4 – Detail of the hydrogen bonding interactions between the chains in **6**. An $R_4^4(12)$ motif is formed *via* hydrogen bonding between two carboxylate groups of two chains on adjacent sheets and two lattice water molecules, resembling the carboxylate-dialkylammonium interaction. A second interaction involves hydrogen bonding through the 4,4'-bipy molecule, linking the chains on adjacent sheets. The 4,4'-bipy molecule is 'encapsulated' by two 4,4'-dcbp and two pyridine ligands through π-interactions. (The 1D chains extend parallel to the page. Hydrogen bonds represented as blue and white dashed bonds. Aromatic hydrogen atoms omitted for clarity)

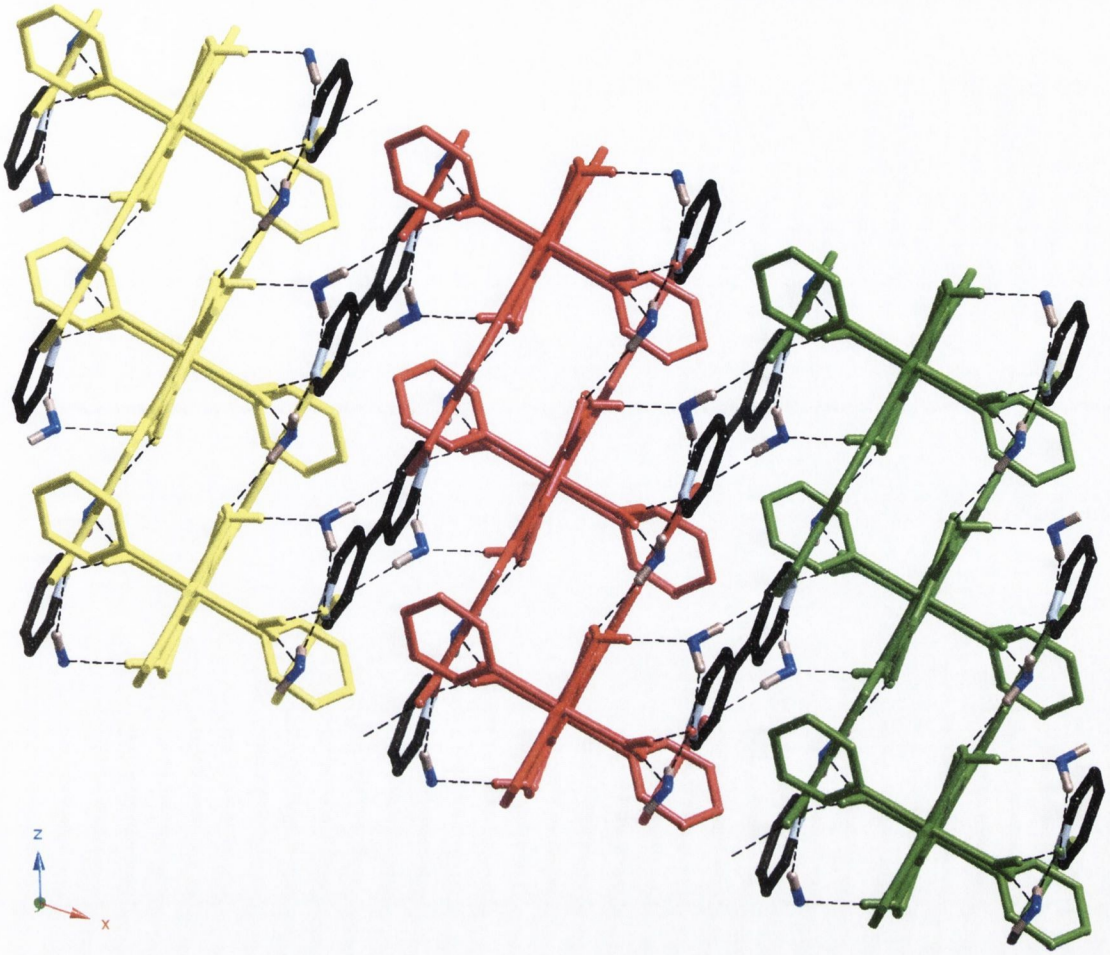

Figure 3.5 – Packing diagram for **6**. The 2D hydrogen bonded sheets, highlighted in three different colours, are extended into a 3D network through hydrogen bonding with the 4,4'-bipy and the lattice water molecules. (View along the *b* direction. The 1D chains are running into the page. Lattice waters are shown in blue. Hydrogen bonds are shown as dashed bonds. Aromatic hydrogens omitted for clarity.)

After looking at the structure of **6** it was thought that substitution of the pyridine by coordinating 4,4'-bipyridine might create a higher dimensionality network, and with this in mind the same reaction was performed in the absence of pyridine. $CoSO_4$, 4,4'-H_2dcbp and 4,4'-bipy (1:1:1) were reacted hydrothermally at 180 °C for 5 days, directly yielding orange crystals. The infrared spectrum looked very similar to that of **6**, clearly indicating the presence of 4,4'-dcbp as well as H_2O, but a single crystal X-ray diffraction study determined the crystals to be α-[Co(4,4'-dcbp)$(H_2O)_2]_n$, as discussed in Chapter 2. In a parallel study pyrazine was used with the view of incorporating it as a bridging ligand.[205-207] An aqueous mixture of $CoSO_4$, 4,4'-H_2dcbp and pyrazine (1:1:1) was reacted hydrothermally at 180 °C for 5 days, producing orange crystals directly, which were confirmed as α-[Co(4,4'-dcbp)$(H_2O)_2]_n$, as above, from a single crystal X-Ray diffraction analysis.

3.1.3 Reaction of Cu(II) with 4,4'-dicarboxy-2,2'-bipyridine and 4,4'-bipyridine.

$Cu(NO_3)_2$, 4,4'-H_2dcbp and 4,4'-bipy (1:1:1) were reacted hydrothermally, with excess pyridine, at 180 °C for 7 days. After filtering a blue powder, the remaining green solution was left to evaporate producing blue crystals within two weeks. An infrared spectrum of these showed the presence of 4,4'-dcbp as well as 4,4'-bipy. A single crystal X-Ray diffraction study revealed these crystals to be a 1D polymeric complex of formula $[Cu(4,4'\text{-dcbp})(4,4'\text{-bipy})(H_2O)]\cdot 4\frac{1}{2}H_2O$ (**7**). In an attempt to 'force' the 4,4'-bipy to use both nitrogens as coordination sites, and thus create a polymer with higher dimensionality, the starting materials were again reacted in a 2:2:1 ratio, but this produced the same complex. Complex **7** could also be obtained using the same reaction conditions without the use of pyridine, showing that base is not essential for the deprotonation of the 4,4'-H_2dcbp ligand under hydrothermal conditions. Pyrazine was also employed in place of 4,4'-bipy to create similar networks but no identifiable products were isolated from these reactions.

Several repetitions of the original reaction gave the same result, except in one instance when blue crystals were also formed, and a single crystal X-Ray diffraction study revealed these to be a different complex, of formula $\{[Cu_2(OH)_2(2,2'\text{-bipy})_2(\mu\text{-}4,4'\text{-bipy})]_2[[Cu_2(OH)_2(2,2\text{-bipy})_2(4,4'\text{-bipy})]_2\text{-}\mu\text{-}(4,4'\text{-bipy})]\}\cdot(NO_3)_4\cdot xH_2O$ (**8**). Decarboxylation of the 4,4'-H_2dcbp ligand occurred to produce 2,2-bipyridine, an unexpected result, although decarboxylation of heteroaryl carboxylic acids has been previously reported.[208-213] A more 'direct' route to complex **8** was attempted by using 2,2'-bipyridine directly in place of 4,4'-H_2dcbp but this proved unsuccessful. Another attempt involved the synthesis of $[Cu(OH)(2,2'\text{-bipy})]_2\cdot(NO_3)_2$ first, and then further reaction with 4,4'-bipy, in both the bomb and at ambient conditions, but no identifiable product was isolated in either case. As explained before, hydrothermal synthesis produces conditions that cannot be reproduced otherwise and it has allowed, in this case, for the formation of a complex which could not be synthesised, to the best of our ability, by any other method, including direct use of 2,2'-bipy.

*3.1.4 Crystal structure of $\{[Cu(4,4'\text{-dcbp})(4,4'\text{-bipy})(H_2O)]\cdot 4\frac{1}{2}H_2O\}_n$ (**7**).*

The structure of **7** was refined in the monoclinic *C*2/*c* space group and crystallographic data are shown in Table 3.2. The structure of **7** is similar to that of **6** and consists of a 1D coordination polymer extending along the crystallographic *c* axis. The atomic labelling scheme and atom connectivity for the asymmetric unit in **7** are shown in Figure 3.6. The Cu(II) atom is chelated by the nitrogen atoms of 4,4'-dcbp, coordinated by a carboxylate oxygen atom from an adjacent 4,4'-dcbp , a nitrogen atom from 4,4'-bipy and an oxygen atom from a coordinated water molecule. The geometry around the Cu(II) atom is square pyramidal, with the basal plane occupied by the

4,4'-dcbp nitrogen atoms, the 4,4'-bipy nitrogen atom and the carboxylate oxygen atom, and the apical position occupied by the coordinated water oxygen atom. Slight distortion in the plane arises from the large N3-Cu1-O5 angle (100.85(7)°), and this gives a mean plane deviation of 0.0925 Å for the copper atom. Bond lengths around the Cu(II) centre vary according to donor atom and position and typical Jahn–Teller distortion is displayed with equatorial bond lengths ranging from 1.931(2) Å for Cu1-O2 and 2.014(2) Å for Cu1-N3, and an axial bond length of 2.204(2) Å (Cu1-O5). See Table 3.4 for selected bond lengths and angles. The pyridyl rings of the 4,4'-dcbp ligand are coplanar, and so are the carboxylate moieties with respect to the aromatic ring to which they are attached. The 4,4'-dcbp ligand is fully deprotonated and delocalisation results in similar C-O bond lengths about C12 (C12-O4 1.236(3) Å, C12-O3 1.256(3) Å), while C-O bond lengths about C11 differ more slightly due to the coordination of one of the oxygens to the copper ion (C11-O1 1.217(3) Å, C11-O2 1.271(3) Å). In contrast to the planarity of the 4,4'-dcbp ligand, the pyridine rings of the 4,4'-bipy ligand are twisted at *ca.* 44°. Only one of the 4,4'-bipy nitrogen atoms is coordinating to Cu(II), with the other participating in hydrogen bonding. This allows larger 'movement' for the atoms on the 4,4'-bipy pyridyl ring not coordinated to the copper atom, which can be seen in the larger thermal parameters for these atoms compared to those in the coordinated pyridyl ring.

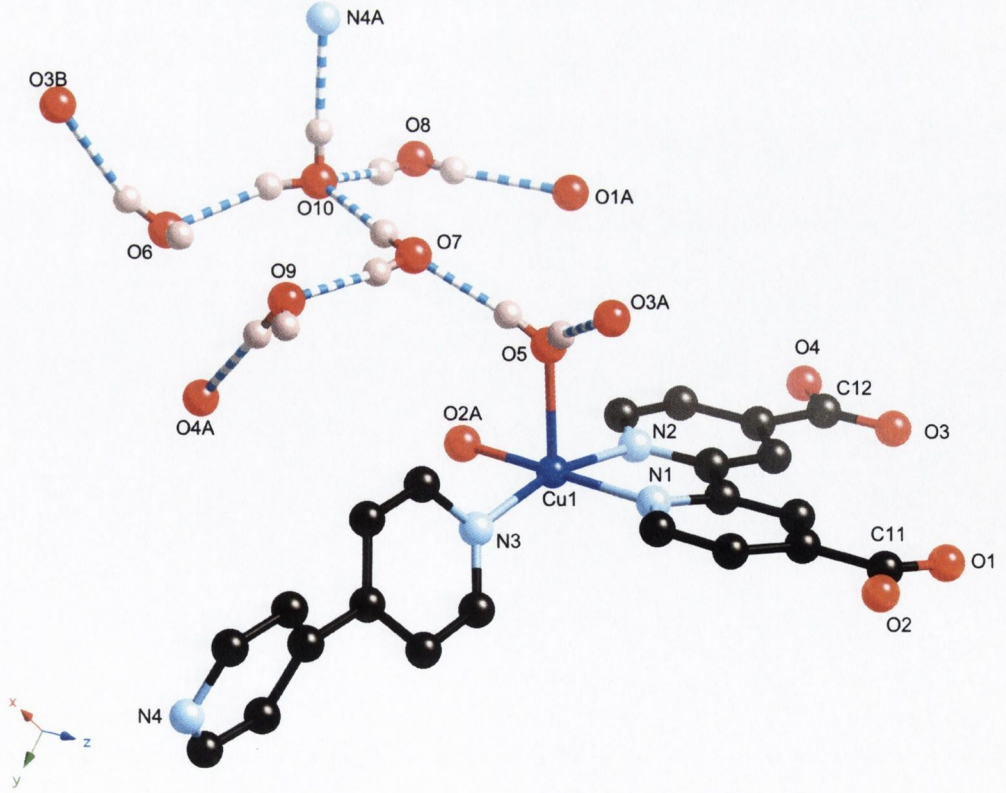

Figure 3.6 - Molecular structure and atomic numbering scheme for **7**. The blue and white dashed bonds depict the ten unique hydrogen bonds. (Bipyridyl hydrogen atoms omitted for clarity.)

Table 3.4 Selected bond lengths (Å) and angles (°) for **7**.

Cu1-N1	2.003(2)	O5-Cu1-N1	94.67(6)
Cu1-N2	2.007(2)	O5-Cu1-N2	93.95(7)
Cu1-N3	2.014(2)	O5-Cu1-N3	100.85(7)
Cu1-O2^{i}	1.931(2)	O5-Cu1-O2^{i}	88.13(6)
Cu1-O5	2.204(2)	N2-Cu1-N3	164.83(7)
		N1-Cu1-O2^{i}	174.43(7)
		N1-Cu1-N2	81.02(7)

Symmetry codes: i = x, -y, z+0.5

Repetition of the asymmetric unit results in infinite 1D linear chains running down the *c* direction (Figure 3.7), similar to those in **6**, but while in the former, adjacent units are rotated at 180°, in this structure the [Cu(4,4'-dcbp)(4,4'-bipy)(H_2O)] units are related by a *c* glide plane. In contrast to the chains in **6**, this results in an arrangement where the 4,4'-bipy ligands on adjacent complexes are at approximately 90°. Furthermore, adjacent units in the chain are of opposite handedness and as each chain contains equal numbers of each hand, the overall structure is achiral. The copper atoms are linked by the 4,4'-dcbp ligand with a metal-to-metal distance of 8.838(2) Å. This is shorter than in **6** (9.1910(9) Å), due to the compression of the equatorial bond lengths around the copper atom.

There are five water molecules in the lattice, with O9 sitting on a two-fold screw axis and is therefore at half-occupancy. The ten unique hydrogen bonds are depicted in Figure 3.6. The coordinated water molecule O5, is a hydrogen bond donor to lattice water molecule O7, and to a carboxylate oxygen atom, O3. O6 accepts a hydrogen bond from O10 and is a hydrogen bond donor to a carboxylate oxygen atom (O3). O7 donates two hydrogen bonds, one to O9 and one to O10. O8 is a hydrogen bond donor to a carboxylate oxygen atom, O1, and to lattice water molecule O10. O9 sits on a special position and thus donates two hydrogen bonds to two symmetry equivalent carboxylate oxygen atoms, O4, and accepts two hydrogen bonds from two symmetry equivalent O7 lattice water molecules, thus engaging in the maximum number of hydrogen bonds possible. Lattice water molecule O10 is also participating in four hydrogen bonds: it donates a hydrogen bond to lattice water molecule O6, and another to N4, and is accepting hydrogen bonds from two lattice water molecules, O8 and O7. Distance and angles for the ten unique hydrogen bonds are shown in Table 3.5. This arrangement connects the 1D linear chains into a 3D hydrogen-bonded network.

Table 3.5 – Parameters of hydrogen bonding interactions for **7** (D–H distances are fixed at 0.84(1) Å).

D–H···A	d(H···A)/Å	d(D···A)/Å	<(D–H···A)/°
O5-H5A···O7	1.84	2.673(3)	174
O5-H5B···O3^{i}	1.93	2.750(2)	167
O6-H6A···O3^{ii}	2.04	2.848(3)	162
O7-H7A···O9	1.94	2.779(3)	175
O7-H7B···O10	1.94	2.782(3)	178
O8-H8A···O10	1.98	2.792(3)	163
O8-H8B···O1^{i}	2.04	2.848(3)	160
O9-H9A···O4^{iii}	1.88	2.708(2)	168
O10-H10A···O6	1.91	2.708(3)	160
O10-H10B···N4^{iv}	1.92	2.758(3)	178

Symmetry codes: i = 0.5-x, -0.5-y, -z; ii = x-0.5, -0.5-y, 0.5+z; iii = 0.5-x, 0.5+y, 0.5-z; iv = -x, y-1, 0.5-z.

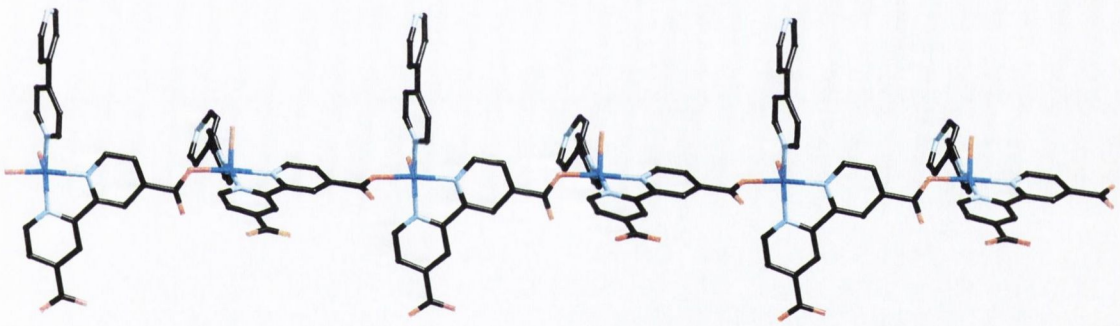

Figure 3.7 - Picture of a single 1D linear chain in the structure of **7** viewed parallel to the chain. (Hydrogen atoms and lattice water molecules omitted for clarity)

As shown in Figure 3.8(a), the 1D chains pack through hydrogen bonding and π-interactions to produce 2D sheets along the crystallographic *bc* plane, in a similar fashion to the packing in **6**. The coordinated water molecule, O5, is hydrogen bonded to a carboxylate oxygen (O3) of an adjacent chain, and this is reinforced by offset face-to-face π-π interactions between 4,4'-dcbp ligands of adjacent chains (separation at closest contact 3.362(3) Å). Weaker edge-to-face C-H···π close contacts exist between 4,4'-bipy and two 4,4'-dcbp ligands on an adjacent chain (separation at closest contact 3.801(3) Å).

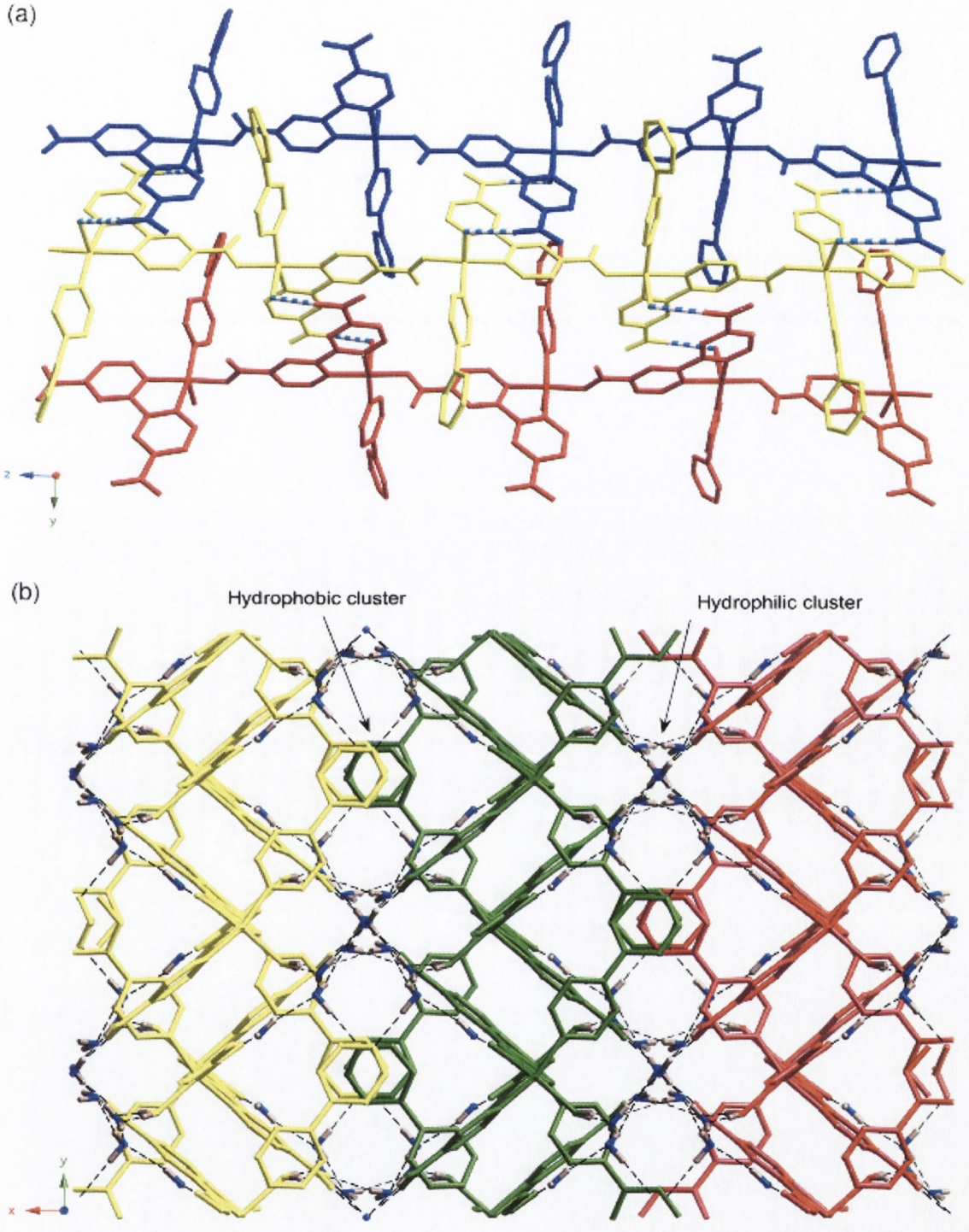

Figure 3.8 – (a) Picture of a single 2D sheet formed along the *bc* plane in **7**, by linking of the 1D chains through hydrogen bonding and π-interactions. (b) Packing diagram of the 2D sheets in **7** looking down the c direction. Three different sheets have been highlighted, in which the chains run into the paper. The lattice waters (blue) link these sheets into a 3D network through hydrogen bonding. Hydrophobic clusters and hydrophilic clusters are formed between the sheets. (Hydrogen bonds are represented as dashed bonds. Bipyridyl hydrogen atoms omitted for clarity)

The 2D sheets are then linked into a 3D network through hydrogen bonding with the lattice water molecules. This creates a network with hydrophobic clusters, where the aromatic pyridyl rings reside, and hydrophilic clusters, where the lattice water molecules reside, between the sheets, as shown in Figure 3.8(b). Within the hydrophobic clusters, weak offset face-to-face π-π interactions exist between every other pair of pyridyl rings, with a separation at closest contact of 3.620(6) Å. The hydrogen bonded network is reinforced by edge-to-face C-H$\cdots\pi$-interactions between 4,4'-bipy and the 4,4'-dcbp ligand on adjacent sheets (closest contact 3.539(4) Å).

3.1.5 Crystal structure of $[Cu_4(OH)_4(2,2'\text{-bipy})_4)(\mu\text{-}4,4'\text{-bipy})_2][Cu_4(OH)_4(2,2\text{-bipy})_4(4,4'\text{-bipy})_2(\mu\text{-}4,4'\text{-bipy})]\cdot(NO_3)_8\cdot xH_2O$ (**8**).

The structure of **8** was refined in the *P*-1 space group and crystallographic data are shown in Table 3.6. The structure of **8** consists of two components, both made up of the classical $[Cu_2(\mu\text{-}OH)_2(2,2'\text{-bipy})_2]^{2+}$ species, but doubly bridged by 4,4'-bipy in one instance, forming a metallocyclophane, and bridged by a single 4,4'-bipy in the other. There are eight nitrate anions to balance the charge and several water molecules within the lattice. These are disordered and the exact location of the water molecules could not be determined, but despite this the refinement of the structure is quite good (R_1 = 0.0680). For the purpose of this discussion the counterions and lattice water molecule will be left out. The two components will be described separately first followed by discussion of the overall structure.

The metallocyclophane has the formula: $[Cu_4(OH)_4(2,2'\text{-bipy})_4(\mu\text{-}4,4'\text{-bipy})_2]^{2+}$, and it is built up of two $[Cu_2(\mu\text{-}OH)_2(2,2'\text{-bipy})_2]$ units bridged by two 4,4'-bipy ligands. The atomic labelling scheme is shown in Figure 3.9. There is an inversion centre between the 4,4'-bipyridines, in the 'middle' of the metallocyclophane, and thus only half of the molecule is unique. There are two unique copper atoms and both have the same coordination sphere. The geometry around both metal ions is square pyramidal with the two nitrogen atoms of the 2,2'-bipy ligand occupying the basal positions *trans* to the two hydroxyl oxygen atoms. The apical position is occupied by a nitrogen atom of 4,4'-bipy. Jahn-Teller distortion is evident from the bond lengths, with equatorial bond lengths of 1.931(4) Å (Cu1-O1), 1.917(4) Å (Cu2-O1), 2.020(4) Å (Cu1-N1) and 2.022(4) Å (Cu2-N4), and considerably longer apical bond lengths of 2.268(4) Å (Cu1-N5) and 2.286(4) Å (Cu2-N6). Selected bond lengths and angles are shown in Table 3.7.

Table 3.6 – Crystallographic data for **8**.

Compound	**8**
Chemical Formula[¶]	$Cu_8C_{130}H_{132}N_{34}O_{42}$
Formula weight[¶]	3351.02
Crystal system	Triclinic
Space group	*P*-1
$\mu(MoK_\alpha)$/ mm^{-1}	1.248
a/Å	15.431(2)
b/Å	15.441(2)
c/Å	17.314(2)
α/°	110.336(2)
β/°	99.593(2)
γ/°	103.977(2)
V/$Å^3$	3608.7(8)
Z	1
D_{calc}/gcm^{-3}	1.542
T/K	153(2)
Crystal size max /mm	0.43
mid /mm	0.28
min /mm	0.05
$2\theta_{max}$/°	56.80
Min/Max trans. Factor	0.770/1.000
R_{int}	0.0639
R_1, $wR_2[I>2\sigma(I)]$[a]	0.0680, 0.1733
R_1, wR_2 (all data)	0.1101, 0.1895
Reflections – collected:	61092
unique:	16073
observed:	9795

[a] $R_1=\Sigma||F_o|-|F_c||/\Sigma|F_o|$, $wR_2=[\Sigma w(F_o^2-F_c^2)2/\Sigma w(F_o^2)^2]^{½}$

[¶] Formula based on x = 10, i.e. ten lattice water molecules.

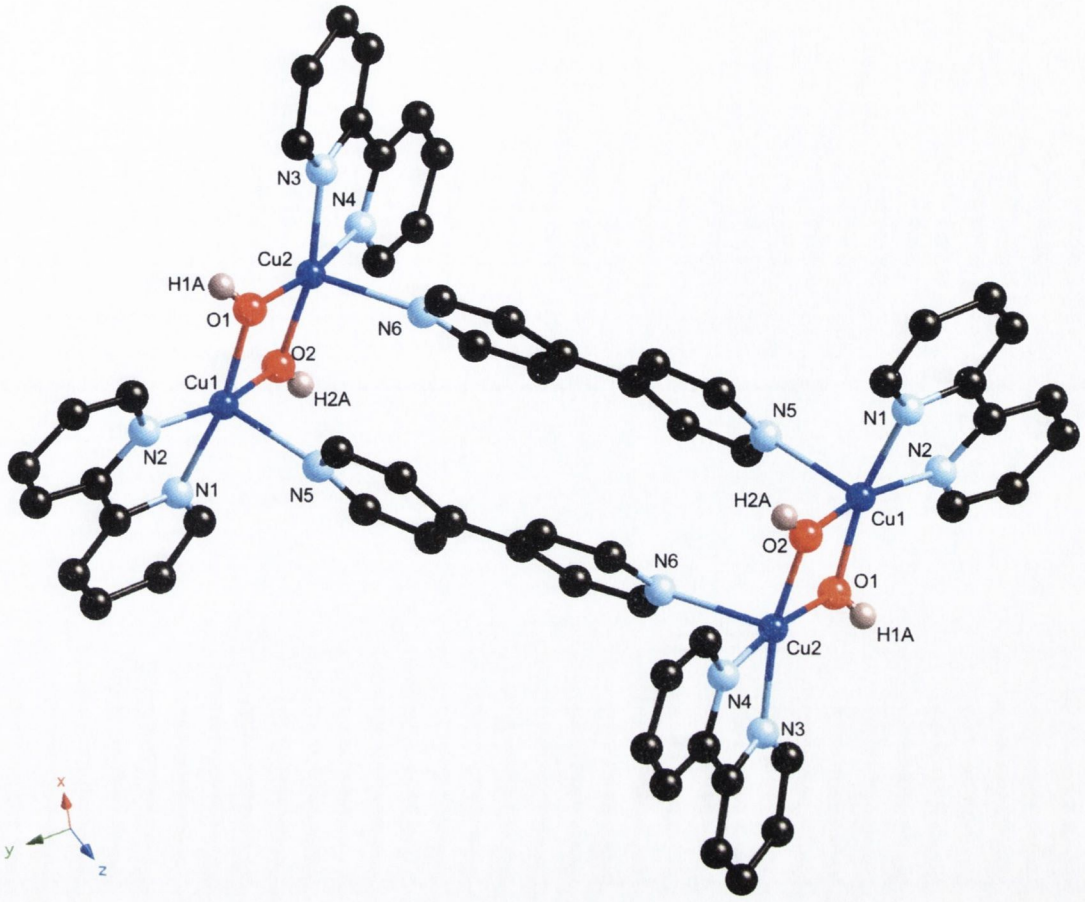

Figure 3.9 – Molecular structure and atomic labelling scheme for the $[Cu_4(OH)_4(2,2'\text{-bipy})_4(\mu\text{-}4,4'\text{-bipy})_2]$ metallocyclophane unit in **8**. (Bipyridyl hydrogen atoms omitted for clarity)

Table 3.7 - Selected bond lengths (Å) and angles (°) for **8**.

Cu1-O1	1.931(4)	N5-Cu1-N1	98.6(1)
Cu1-O2	1.947(4)	N5-Cu1-N2	97.2(2)
Cu1-N1	2.020(4)	N5-Cu1-O1	93.7(2)
Cu1-N2	2.006(4)	N5-Cu1-O2	98.8(2)
Cu1-N5	2.268(4)	N6-Cu2-N3	93.9(2)
Cu2-O1	1.917(4)	N6-Cu2-N4	91.3(1)
Cu2-O2	1.953(4)	N6-Cu2-O1	97.8(2)
Cu2-N3	2.008(4)	N6-Cu2-O2	100.1(2)
Cu2-N4	2.022(4)	Cu1-O1-Cu2	97.4(2)
Cu2-N6	2.286(4)	Cu1-O2-Cu2	95.7(2)
		O2-Cu1-O1	83.2(2)
		O2-Cu2-O1	83.4(2)

The 2,2'-bipy attached to Cu1 is 'bent' outwards giving a N5-Cu1-N2 angle of 97.2(2)° and a N5-Cu1-N1 angle of 98.6(1)°, while the 2,2'-bipyridine attached to Cu2 is more coplanar with the N_2O_2 basal plane, with N6-Cu2-N3 93.9(2)° and N6-Cu2-N4 91.3(1)°. This results in the metal atoms being slightly shifted from the basal plane with Cu1 displaced 0.078 Å and Cu2 0.065 Å. Whilst there is a small dihedral O-Cu-O angle of approximately 6°, the dihedral angle between the two CuN_2O_2 planes is 11.5°. There is a dihedral angle of *ca.* 7° between the Cu-O-Cu planes resulting in a separation of 2.574(6) Å between the two hydroxyl oxygen atoms. The two hydroxyl protons are pointing away from their respective Cu-O-Cu plane in a *trans* conformation. H1A is pointing 'downwards' at approximately 64° from the Cu1-O1-Cu2 plane, whereas H2A is pointing 'upwards' at approximately 48° to the Cu1-O2-Cu2 plane. The metal-to-metal distance across the hydroxide bridge is 2.8916(8) Å, while that across the 4,4'-bipy bridge is 11.604(1) Å. Face-to-face π-π interactions exist between the bridging 4,4'-bipy ligands, with the separation at closest contact being 3.39(1) Å. The 4,4'-bipyridyl rings are not parallel with an angle of 8.2° between the planes of the rings. A small torsion angle of *ca.* 6.5° is observed between the pyridyl rings of 4,4'-bipy.

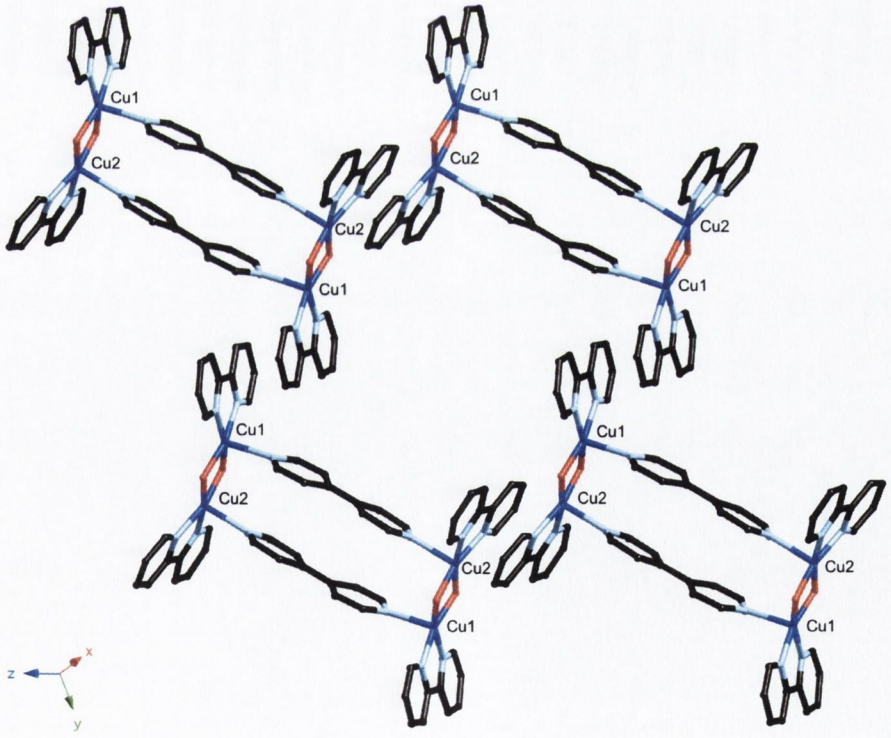

Figure 3.10 – Picture showing the π-interactions between four metallocyclophane units in **8**. (Hydrogen atoms omitted for clarity)

The metallocyclophane units pack, through π-interactions between the bipyridine rings, to form 2D sheets extending along the *bc* plane, separated by a distance equivalent to the length of the *a* axis (~15 Å). Each 2,2'-bipy is π-π stacking in an offset face-to-face manner with a symmetry equivalent 2,2'-bipy on an adjacent metallocyclophane (Figure 3.10). Close contacts between the 2,2'-bipyridine rings attached to Cu2 exist with a shortest distance of 3.449(8) Å. Slightly weaker π-π interactions exist between the 2,2'-bipyridine rings attached to Cu1, with the closest contact being 3.505(7) Å. The 2,2'-bipy attached to Cu1 also participates in edge-to face C-H···π interactions with the N5 containing pyridyl ring of a 4,4'-bipy on an adjacent metallocylophane. The planes of the rings are at an angle of 63° with the closest contact being 3.588(7) Å. If the centre point of the metallocyclophane, the inversion centre, is taken as the node, then π-interactions connect these into a (4,4) 2D sheet. This arrangement gives rise to channels, with approximate dimensions of 14.86 Å X 10.00 Å, running along the *a* direction (Figure 3.11).

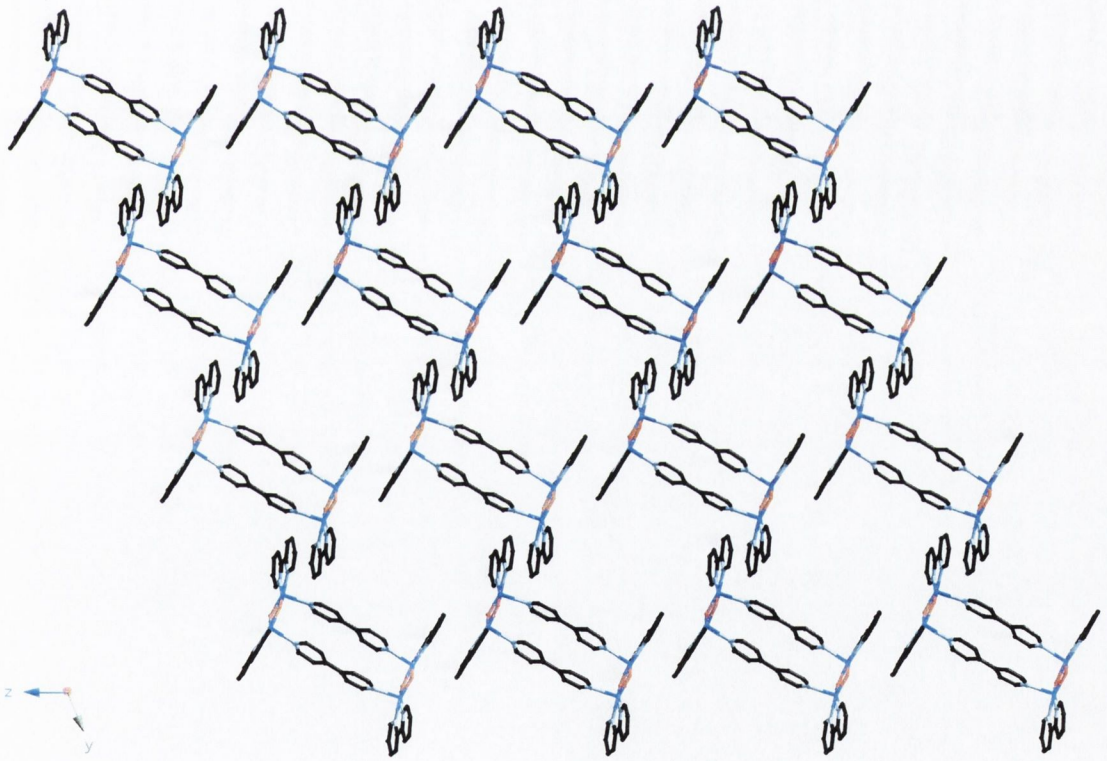

Figure 3.11 – Packing diagram of the metallocylophanes in **8** to form a (4,4) 2D sheet through π-interactions of the bipyridines, forming channels down the *a* direction. (Hydrogen atoms omitted for clarity)

The second component of **8** has formula: $[Cu_4(OH)_4(2,2\text{-bipy})_4(4,4'\text{-bipy})_2(\mu\text{-}(4,4'\text{-bipy})]$, and from here on will be referred to as unit 2. This is quite similar to the metallocyclophane unit in that it is also built of $[Cu_2(\mu\text{-}OH)_2(2,2'\text{-bipy})_2]$ units, but now

only one of the 4,4'-bipy ligands is bridging them and thus, the cyclic motif is lost. Instead, the bridging 4,4'-bipy is sitting between two other monodentate 4,4'-bipy ligands and a sandwich-type complex is formed. The atomic labelling scheme and atom connectivity are shown in Figure 3.12. As with the metallocyclophane, an inversion centre exists in the midpoint of the bridging 4,4'-bipy and so only half the molecule is unique. There are two unique copper atoms and both have square pyramidal geometry with a similar coordination sphere to the metallocyclophane unit copper atoms. The bond lengths around the copper atoms vary with donor atom and position. For Cu3 equatorial bond lengths range from 1.930(4) Å (Cu3-O3) to 2.014(4) Å (Cu3-N8), with an axial bond length of 2.292(4) Å (Cu3-N11), and so Jahn-Teller distortion is evident. This type of distortion is even more pronounced for Cu4 with equatorial bond lengths ranging from 1.931(4) Å (Cu4-O3) to 2.023(4) Å (Cu4-N9), and an axial bond length of 2.585(4) Å (Cu4-N13). Selected bond lengths and angles are shown in Table 3.8. The Cu3 atom is displaced 0.133 Å from the basal plane towards the axially coordinated 4,4'-bipy nitrogen (N11), while the Cu4 atom is only displaced 0.078 Å towards N13.

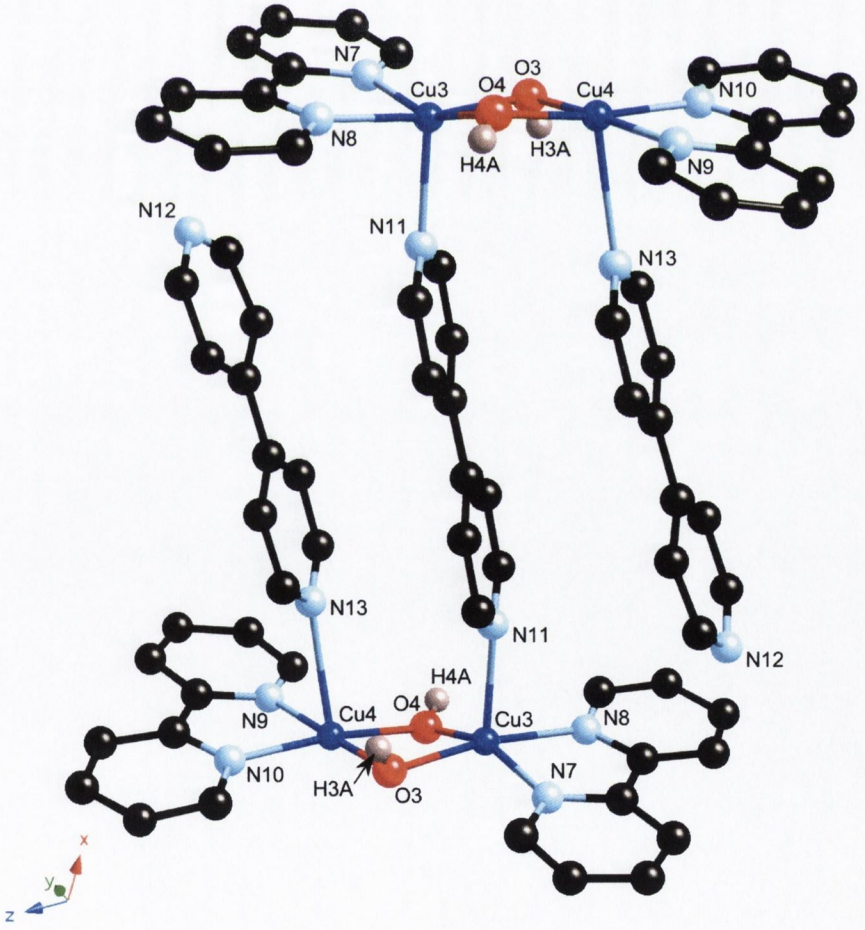

Figure 3.12 – Molecular structure and atomic labelling scheme for the $[Cu_2(OH)_2(2,2'\text{-bipy})_2(4,4'\text{-bipy})]_2$-μ-(4,4'-bipy) unit of **8**. (Bipyridyl hydrogen atoms omitted for clarity)

Table 3.8 – Selected bond lengths (Å) and angles (°) for **8**.

Cu3-O3	1.930(6)	N11-Cu3-N7	97.3(2)
Cu3-O4	1.958(4)	N11-Cu3-N8	91.3(1)
Cu3-N7	2.013(4)	N11-Cu3-O3	98.1(2)
Cu3-N8	2.014(4)	N11-Cu3-O4	105.2(2)
Cu3-N11	2.292(4)	N13-Cu4-O3	97.4(1)
Cu4-O3	1.931(4)	N13-Cu4-O4	101.1(1)
Cu4-O4	1.937(4)	N13-Cu4-N10	86.6(2)
Cu4-N9	2.023(4)	N13-Cu4-N9	79.4(2)
Cu4-N10	2.003(4)		
Cu4-N13	2.585(4)		

The metal-to-metal distance across the hydroxide bridge is 2.9274(9) Å, slightly longer than that of the metallocyclophane (*c.f.* 2.8916(8) Å). There is a large dihedral angle between the two O-Cu-O planes of *ca.* 16°, and also a large bending of the Cu-O-Cu planes with a dihedral angle of *ca.* 18°, which results in a slightly shorter separation between the hydroxyl oxygen atoms (2.512(5) Å) than that of the metallocyclophane (*c.f.* 2.574(6)). Whilst the bending in the Cu_2O_2 unit is more pronounced here than in the metallocyclophane unit, the dihedral angle of 3.5° between the CuN_2O_2 planes is considerably smaller (*c.f.* 11.5°). As in the metallocyclophane unit, the hydroxyl hydrogen atoms are pointing away from their respective Cu-O-Cu plane, but here they are arranged in a *cis* conformation. Both hydrogens are pointing 'inwards', with H3A at approximately 70° from the Cu4-O3-Cu3 plane, and H4A at approximately 65° from the Cu4-O4-Cu3 plane. As mentioned above, there is only a single 4,4'-bipy bridge between the $[Cu_2(\mu\text{-}OH)_2(2,2'\text{-bipy})_2]^{2+}$ units and as only half of the ligand is unique, it bridges two symmetry equivalent Cu3 centres with a copper-to-copper separation of 11.599(2) Å. The other 4,4'-bipy ligand is only monodentate and is coordinating to Cu4 through N13, with the other nitrogen atom (N12) participating in hydrogen bonding with the lattice water molecules. This results in the bridging 4,4'-bipy ligand being sandwiched between two other symmetry equivalent monodentate 4,4'-bipy ligands. As with the metallocyclophane unit, the 4,4'-bipy ligands are participating in π-π interactions through the N11 and N13 containing pyridyl rings. The planes of the interacting pyridyl rings are at a smaller angle than in the metallocyclophane unit, 6.7°, with the separation at closest contact being 3.45(1) Å. While the pyridyl rings of the bridging 4,4'-bipy ligand are coplanar, there is a small torsion angle between the pyridyl rings of the monodentate 4,4'-bipy ligand (~4°). Edge-to face C-H$\cdots\pi$ interactions also exist between the 'free' pyridyl ring of the monodentate 4,4'-bipy and the 2,2'-bipyridine attached to Cu3, with the separation at closest contact being 3.429(7) Å.

These units stack on top of each other through π-π interactions of the 2,2'-bipyridines to form infinite 1D chains extending along the *a* direction, as shown in Figure 3.13. The 2,2'-bipy attached to Cu4 is π-π stacking with a Cu3 attached 2,2'-bipy from an adjacent complex in an offset face-to-face manner, with the separation at closest contact being 3.234(7) Å. In addition, a close contact exists between Cu4 and the O4 hydroxyl oxygen atom from an adjacent unit (Cu4···O4* 2.733(3) Å).

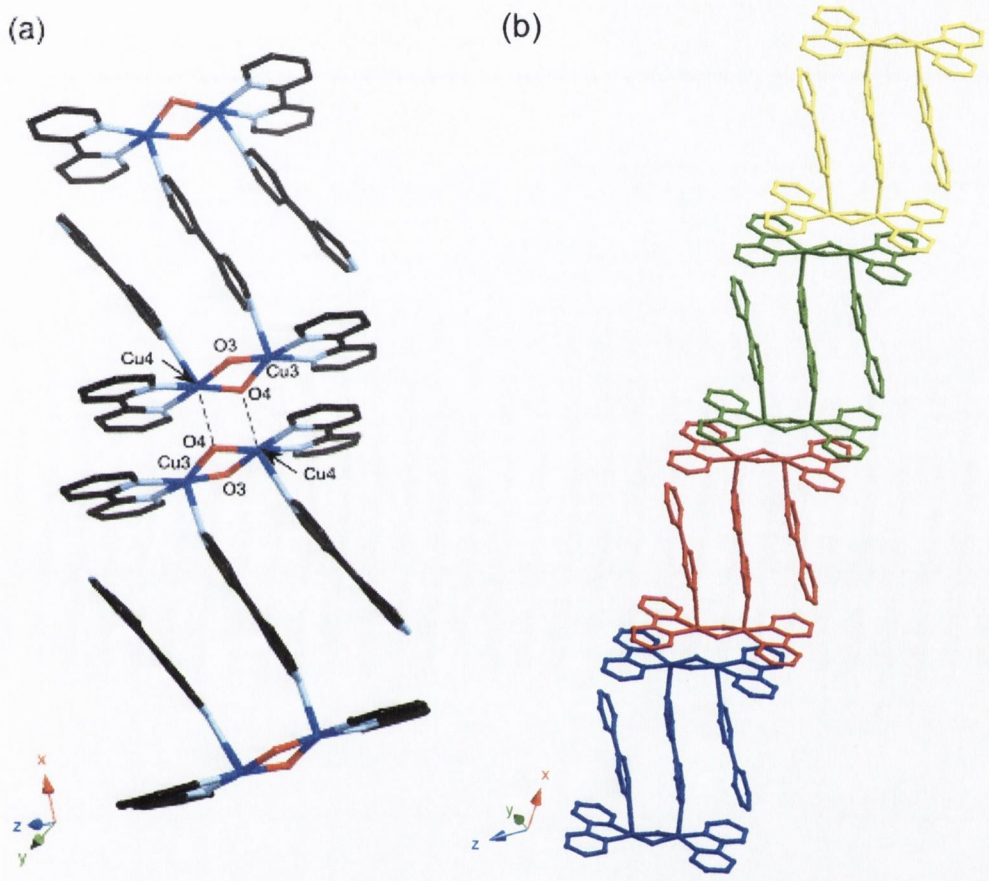

Figure 3.13 – (a) Picture showing the close contacts between two units in **8**. The Cu4-O4 close contact is shown as a dashed bond. (b) Packing diagram of unit 2 in **8** showing a single 1D chain, where four different complexes have been highlighted, stacked together through π-interactions. (Hydrogen atoms omitted for clarity)

The 1D chains formed by unit 2 penetrate the channels formed by the (4,4) 2D metallocyclophane sheets. There is a separation of *ca.* 15 Å between the 2D sheets, and while the 4,4'-bipy ligands of unit 2 are sitting in the middle of channels formed by the metallocyclophanes, the 2,2'-bipy ligands sit above and below these 2D sheets (Figure 3.14). The lattice water molecules and the nitrate counterions reside within the remaining voids in the network.

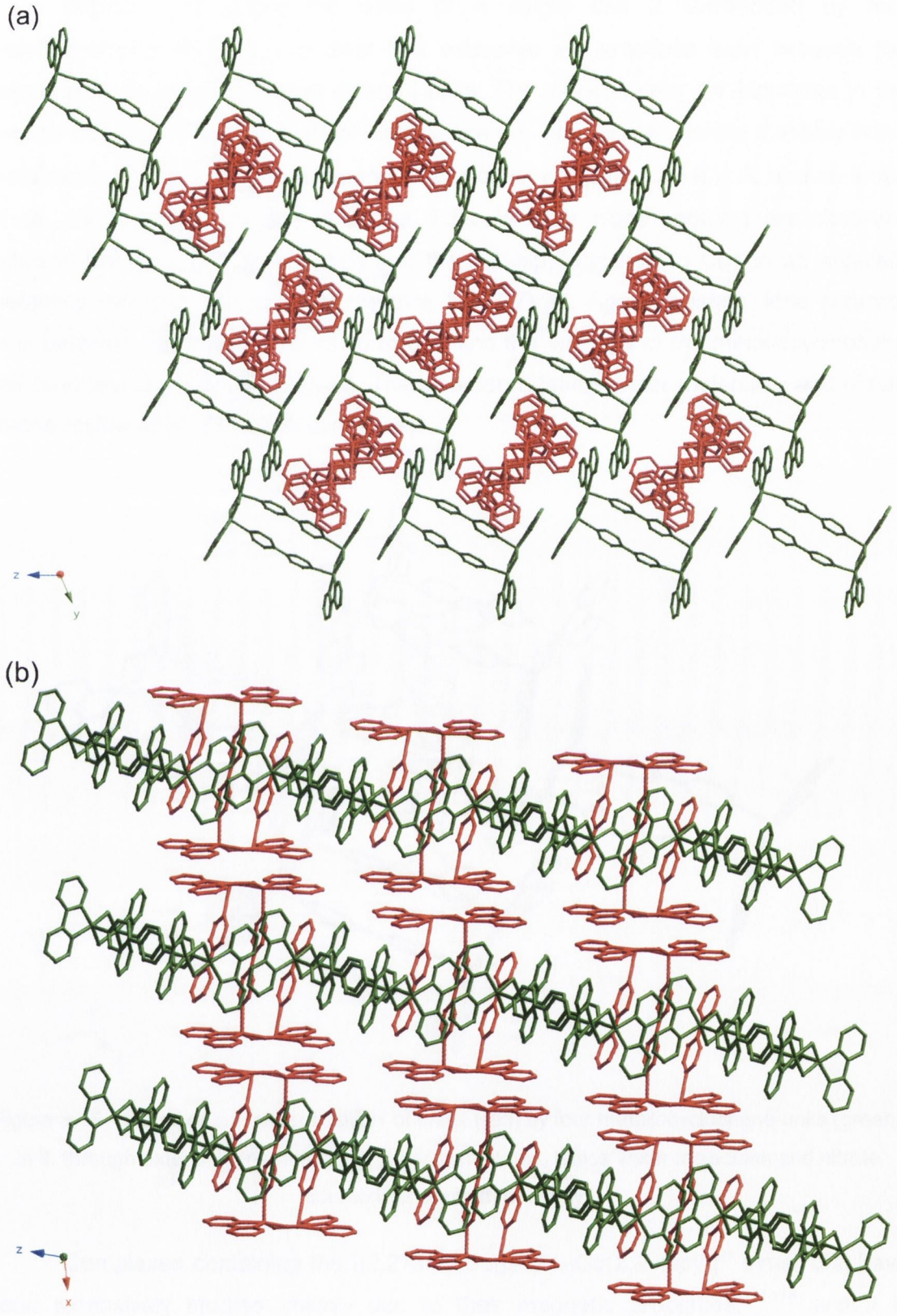

Figure 3.14 – Overall packing diagrams of **8**. The metallocylophanes are highlighted in green and unit 2 in red. (a) View along (100). Penetration of the 1D chains into the channels formed by the metallocyclophane 2D sheet. (b) View along (010). The 4,4'-bipyridines of unit 2 lie in the channels of the 2D sheets, whilst the 2,2'-bipyridine groups of the 1D chains lie in between the 2D sheets. (Hydrogen atoms, lattice water molecules and nitrate counterions omitted for clarity)

Figure 3.15 shows the detail of a single unit 2 surrounded by four metallocyclophanes, and it is clear that extensive π-interactions exist between the heteroaromatic rings of the two different units. The monodentate 4,4'-bipyridine in the second unit is participating in offset face-to-face π-π-interactions with the 4,4'-bipy in the metallocyclophane unit, with a separation at closest contact of 3.54(1) Å, and an angle of *ca.* 13° between the planes of the rings. Weaker close contacts are observed between the monodentate 4,4'-bipy and the 2,2'-bipy attached to Cu1 in an adjacent metallocyclophane unit (shortest distance 3.837(7) Å). Again, weaker close contacts exist between the 2,2'-bipy attached to Cu4 and the 4,4'-bipy of the metallocyclophane unit (shortest distance 3.702(8) Å). The disordered lattice water molecules and nitrate anions reside within the metal complexes.

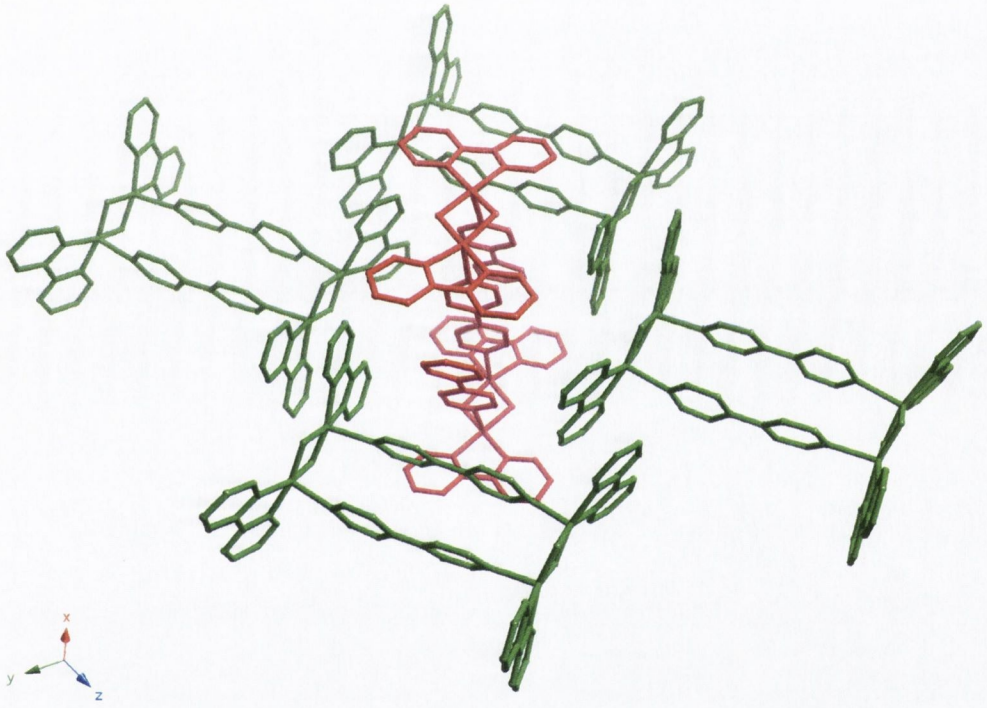

Figure 3.15 – Detail of the 'encapsulation' of unit 2 (red) by four metallocyclophane units (green) in **8**, through extensive π-interactions. (Hydrogen atoms, lattice water molecules and nitrate counterions omitted for clarity)

Complexes containing the $[(2,2'\text{-bipy})Cu(\mu\text{-}OH)_2Cu(2,2'\text{-bipy})]^{2+}$ dimer unit have been extensively studied, mainly due to their magnetic properties,[214-218] and it is interesting to compare these with the dimeric units in **8**. Figure 3.16 shows the environment of the copper atoms in unit 1 (dimer 1) and unit 2 (dimer 2) of **8**. For comparison, the previously reported $[Cu(2,2'\text{-bipy})(\mu\text{-}OH)(NO_3)]_2$ (dimer 3)[219] and $[(H_2O)(2,2'\text{-bipy})Cu(\mu\text{-}OH)_2Cu(2,2'\text{-bipy})(OSO_3)]\cdot 4H_2O$ (dimer 4)[220] complexes are also shown.

For each structure, the four equatorial bond lengths occur in sets of two: the copper to hydroxyl oxygen distances average 1.94 Å, while the copper to bipyridine nitrogen distances average 2.01 Å for both dimer 1 and 2. This is comparable to the average of 1.92 Å / 2.00 Å and 1.93 Å / 2.00 Å respectively for dimer 3 and 4. All copper atoms adopt a Jahn-Teller distorted square pyramidal geometry, and apical distances for dimer 1 and 2 are typical of these type of complexes. Cu4-N13 (2.585(4) Å) for dimer 2 is longer than the average length of 2.28 Å for the other axial positions. In dimers 3 and 4 the axial positions are occupied by charge balancing anions in a *trans* arrangement, whereas for dimer 1 and 2 the axial positions are occupied by the neutral 4,4'-bipy bridging ligand in a *cis* arrangement. This results in the copper atoms in dimer 1 and 2 being shifted away from the N_2O_2 basal plane in the same direction, whereas in dimer 3 and 4 the copper atoms are shifted away in opposite directions. It is worth noting that the copper atoms in dimers 1 and 2 are only shifted 0.07 Å on average above the basal of the pyramid, with the exception of Cu3 which is shifted 0.13 Å, while the copper atoms in the other dimers are shifted considerably more (0.18-0.23 Å). As expected, in all the complexes the N-Cu-N chelating angle is significantly deviated (79.9(3)°-81.0(3)°) from the ideal value of 90° due to the bite angle of the bipyridine nitrogens.

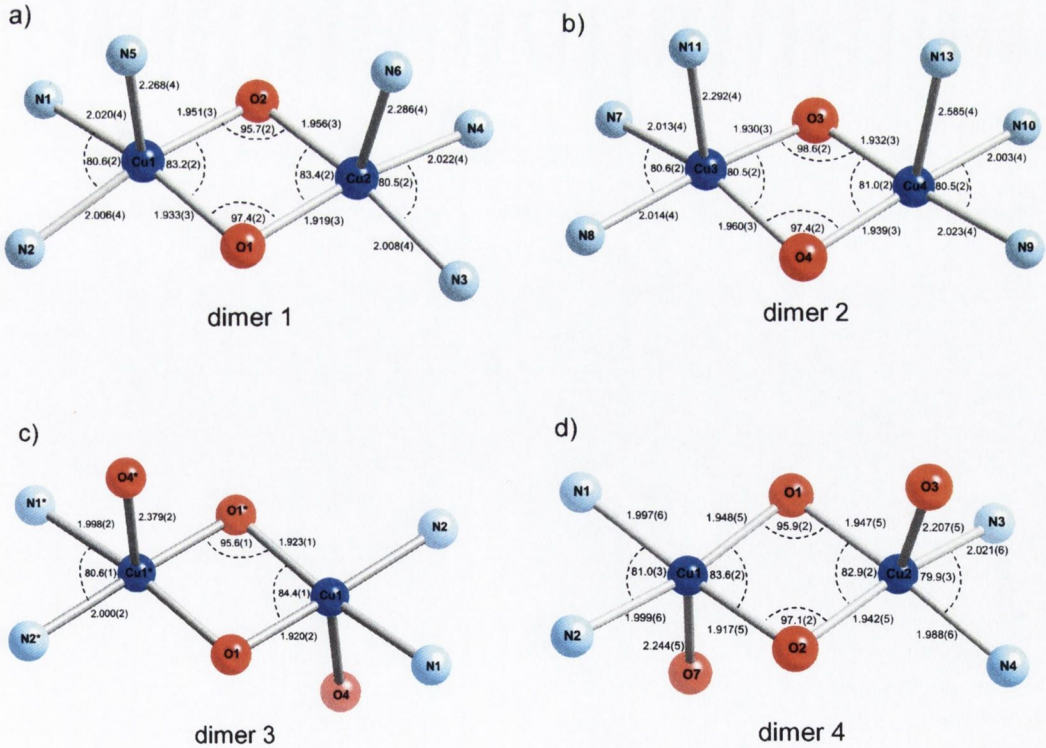

Figure 3.16 – The environment of the copper atoms in various μ-hydroxo-bridged dimers, with selected bond lengths (Å) and angles (°). a) dimer in unit 1 of **8**; b) dimer in unit 2 of **8**; c) dimer in $[Cu(2,2'\text{-bipy})(\mu\text{-OH})(NO_3)]_2$;[219] d) dimer in $[(H_2O)(2,2'\text{-bipy})Cu(\mu\text{-OH})_2Cu(2,2'\text{-bipy})(OSO_3)]\cdot 4H_2O$.[220]

The Cu-O-Cu angles of dimer 1 (95.7(2)°-97.4(2)°) are comparable to those of dimer 3 and 4 (95.6(1)°-97.1(2)°), and are only slightly bigger in dimer 2 (97.4(2)°-98.6(2)°). The O-Cu-O angles in dimer 1 (83.2(2)°-83.4(2)°) are comparable to those of dimer 3 and 4 (82.9(2)°-84.4(1)°), with those in dimer 2 slightly smaller (80.5(2)°-81.0(2)°). The metal-to-metal distance across the hydroxyl bridge for dimer 1 and 2 (2.892(8) Å and 2.927(9) Å respectively) is within the expected 2.78-3.00 Å range for these type of complexes. The O-Cu-O dihedral angle for dimer 1 is comparable to that in dimer 3 with both at 6.1°, whilst for dimer 2 this angle is considerably larger with a value of *ca.* 16°. The same occurs with the Cu-O-Cu dihedral angle, which is *ca.* 7° for dimer 1 and *ca.* 18° for dimer 2. The hydroxyl-to-hydroxyl oxygen separation is 2.574(6) Å for dimer 1, comparable to the separation in dimer 3 and 4 (2.581 and 2.576(8) Å), whereas the separation in dimer 2 is shorter, 2.512(5) Å, probably due to the heavy distortion within the Cu_2O_2 unit.

3.1.6 Conclusions

As a result of this study, several novel coordination compounds have been synthesized. The use of hydrothermal techniques has again proved successful in the formation of crystalline products with low solubility.

While 4,4'-bipy has been employed successfully in combination with carboxylate ligands such as 1,4-benzenedicarboxylate to form high dimensionality coordination networks,[198, 200] in our study 1D coordination polymers have been formed.

In the structure of **6** the 4,4'-dcbp ligand only coordinates through one of its carboxylate sites, in addition to coordination through the chelating site, and thus only acts as a 2-connector, losing its 3-connecting capability shown in Chapter 2. The pyridine is coordinating to the cobalt(II) ion, whilst the 4,4'-bipy sits in the lattice. This only allows for a 1D coordination polymer to be formed. It was initially thought that substitution of the pyridine by 4,4'-bipy might then link the 1D chains into a higher dimensionality network. When the metal employed was Co(II), a 3D 4,4'-H_2dcbp polymer, not incorporating 4,4'-bipy was formed, whereas when the metal employed was Cu(II) a polymer containing 4,4'-dcbp and 4,4'-bipy was formed (**7**). However, the 4,4'-bipy coordinates through only one of its donor sites, and thus produces a similar 1D polymer to that in **6**. Again, in **7**, the 4,4'-H_2dcbp acts as a 2-connector and links the copper atoms, while the 4,4'-bipy acts as a terminating ligand. Similar 2D sheets are formed in **6** and **7** through hydrogen bonding an π-stacking, and different hydrogen bonding interactions link these into a 3D network.

The harsh conditions obtained from hydrothermal synthesis have allowed for the formation of **8**. Decarboxylation of 4,4'-H_2dcbp occurred to produce 2,2'-bipyridine. Decarboxylation is favoured upon heating, and thus, hydrothermal conditions present

an ideal environment for such reactions to occur. The pyridine ring system is believed to play a key role in the decarboxylation reaction due to resonance stabilisation.[208, 210-213] The reaction takes place more rapidly in basic media, since deprotonation of the acid increases the positive potential on the ring nitrogen, which then decreases the electron density on the α-carbon, thus facilitating heterolysis of the carbon to carboxy bond. The intermediate involved is believed to be a zwitterion (Scheme 1), although the precise mechanism of the reaction is not clear. Further studies of this reaction are being currently performed.

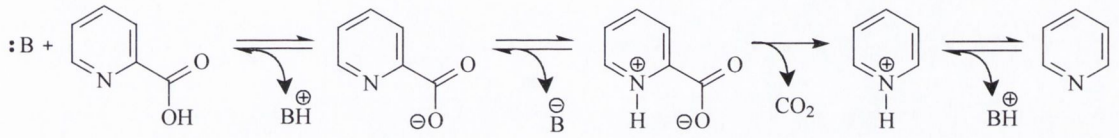

Scheme 1

3.2 Complexes incorporating 4,4'-dicarboxy-2,2'-bipyridine and coordinating inorganic anions.

Preamble

As part of our studies, it was attempted to synthesize tris-chelated metal complexes of 4,4'-H_2dcbp by following the procedure previously described by Pakkanen and co-workers[174] to synthesize $[Ru(4,4'\text{-}H_2dcbp)_3]Cl_2$. This involved perfoming hydrothermal reactions under acidic conditions to keep the ligand protonated. While the initial targets were Fe(II) and Co(II) complexes, attempts at isolating these were unsuccessful. However, reactions using Cu(II) proved successful and prompted the following study.

3.2.1 Reaction of Cu(II) and 4,4'-H_2dcbp under acidic conditions.

$CuCl_2$ and 4,4'-H_2dcbp (1:2) were reacted hydrothermally in an aqueous solution made acidic with conc. HCl, at 200 °C for 5 hrs. Green crystals were obtained directly in approximately 87% yield based on copper. An infrared spectrum showed the presence of 4,4'-H_2dcbp (ν(OH) 2519 cm^{-1}, ν(C=O) 1730 cm^{-1}). After a single crystal X-Ray diffraction analysis, the structure was determined to be a chloride-bridged dimer of formula $[Cu(4,4'\text{-}H_2dcbp)Cl_2]_2 \cdot 2H_2O$ (**9**). The same reaction was performed varying the copper salt employed and keeping the same mineral acid (HCl). In all instances the chloride-bridged dimer was produced and thus, it is the acid that provides the anion regardless of the metal salt employed. A study was then undertaken using the different types of available mineral acids in the reaction. $CuSO_4$ and 4,4'-H_2dcbp (1:1) were reacted hydrothermally in an aqueous mixture made acidic with conc. H_2SO_4, at 200 °C

for 5 hrs. Blue crystals were obtained directly in *ca.* 70% yield. An infrared spectrum showed the presence of 4,4'-H_2dcbp (ν(OH) 2873 cm^{-1}, ν(C=O) 1735 cm^{-1}) and coordinating sulfate (1187, 1104 and 991 cm^{-1}). From a single crystal X-ray diffraction study the structure was determined to be a 1D polymer consisting of sulfate-bridged copper atoms, $\{[Cu(4,4'\text{-}H_2dcbp)(SO_4)]\cdot\frac{1}{3}H_2O\}_n$ (**10**). On reacting $Cu(NO_3)_2$ and 4,4'-H_2dcbp hydrothermally, as above, in a H_2O/HNO_3 mixture, a blue solution was obtained. On evaporation, small blue crystals grew in *ca.* 33% yield. From an X-ray diffraction study these were determined to be discrete metal complexes of formula $[Cu(4,4'\text{-}H_2dcbp)(NO_3)_2(H_2O)]$ (**11**). The same reaction was performed using glacial acetic acid, which produced the polymeric $\{[Cu(4,4'\text{-}dcbp)(H_2O)_2]\cdot 2H_2O\}_n$ complex reported in Chapter 2. Despite the presence of acid, the ligand was deprotonated during the reaction, and this can be attributed to the fact that acetic acid is a considerably weaker acid than sulfuric, hydrochloric and nitric acids.

*3.2.2 Crystal structure of $[Cu(4,4'\text{-}H_2dcbp)Cl_2]_2\cdot 2H_2O$ (**9**).*

This structure was refined in the triclinic *P*-1 space group. Crystallographic data are given in Table 3.10. The structure of **9** consists of neutral chloride-bridged copper dimers, where the 4,4'-H_2dcbp ligand is protonated and is acting as a terminal ligand. The molecular structure and numbering scheme are shown in Figure 3.17. The geometry around the copper atom is square pyramidal with the equatorial positions occupied by the chelating 4,4'-H_2dcbp nitrogen atoms, a bridging chloride atom and a monodentate chloride atom, and the apical position occupied by another bridging chloride atom. Equatorial bond lengths come in sets of two, the copper to bipyridyl nitrogen, which average 2.03 Å, and the copper to chloride, which average 2.27 Å. Jahn-Teller distortion is present with the axial bond length (2.6929(8) Å) considerably longer than the equatorial bond lengths (Table 3.9). Further distortion from ideal square based pyramidal geometry, arises from the bite angle of the 4,4'-H_2dcbp nitrogen atoms (N1-Cu1-N2 79.77(7)°). The copper atom is only slightly shifted from the N_2Cl_2 basal plane, being displaced 0.053 Å towards the axially coordinated chloride atom. The two halves of the dimer unit are related by inversion, with the inversion center being at the midpoint between the two copper atoms. The chloride atoms bridge the two halves of the complex in a step-wise fashion, where the bipyridine rings are sitting perpendicular to the Cu_2Cl_2 plane. The metal-to-metal separation in the dimer unit is 3.4441(8) Å. The copper atoms and the bridging chloride atoms sit in the same plane, with no deviation from planarity, and this results in a chloride-to-chloride separation of 3.617(3) Å.

Table 3.9 – Selected bond lengths (Å) and angles (°) for **9**.

Cu1-N1	2.024(2)	N1-Cu1-N2	79.77(7)
Cu1-N2	2.035(2)	Cl1-Cu1-N1	95.33(6)
Cu1-Cl2	2.2461(7)	Cl1-Cu1-Cl2	95.44(3)
Cu1-Cl1^{i}	2.2846(7)	Cl1-Cu1-N2	94.20(6)
Cu1-Cl1	2.6929(8)	Cl1-Cu1-Cl1^{i}	92.84(2)
Cu ··· Cu^{i}	3.4441(8)	N1-Cu1-Cl1^{i}	169.97(6)
Cl ··· Cl^{i}	3.617(1)	N2-Cu1-Cl2	168.98(6)
		Cu1-Cl1-Cu1^{i}	87.16(2)

Symmetry codes: i = -x, -y, -z.

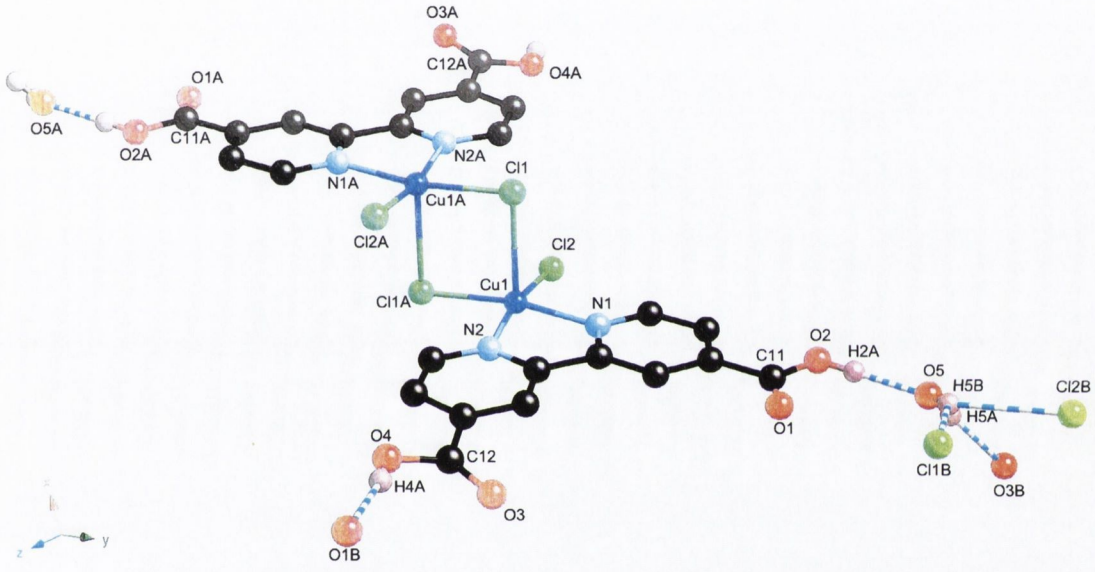

Figure 3.17 – Molecular structure and atomic numbering scheme in **9**. Hydrogen bonds are represented as blue and white dashed bonds. (Bipyridyl hydrogen atoms omitted for clarity)

The bipyridine rings of 4,4'-H_2dcbp are virtually coplanar, with a negligible torsion angle of 0.8°. The carboxylate group about C11 is coplanar with the aromatic ring to which it is attached, whereas the carboxylate group about C12 is twisted at approximately 15.0° to its corresponding aromatic ring. In contrast to the deprotonated complexes, and as expected for protonated carboxylic acids, there are two sets of C-O bond lengths: the carbon to hydroxyl oxygen single bond, which average 1.32 Å, and the carbon to carbonyl oxygen double bond, which average 1.21 Å.

Table 3.10 – Crystallographic data for **9** and **10**.

Compound	**9**	**10**
Chemical Formula	$CuC_{12}H_{10}N_2O_5Cl_2$	$CuC_{12}H_{8.6}N_2O_{8.3}S$
Formula weight	396.66	409.81
Crystal system	Triclinic	Trigonal
Space group	*P*-1	*R*32
μ (MoK_α)/ mm^{-1}	1.996	1.708
a/Å	7.250(2)	23.060(7)
b/Å	9.346(2)	23.060(7)
c/Å	11.785(3)	7.053(2)
α/°	108.400(3)	90
β/°	98.483(3)	90
γ/°	108.720(3)	120
V/$Å^3$	689.6(3)	3248.1(2)
Z	2	9
D_{calc}/gcm^{-3}	1.910	1.886
T/K	153(2)	153(2)
Crystal size max /mm	0.30	0.43
mid /mm	0.13	0.38
min /mm	0.12	0.38
$2\theta_{max}$/°	55.96	56.66
Min/Max trans. Factor	0.570/1.000	0.676/1.000‡
R_{int}	0.0323	0.0604
R_1, $wR_2[I>2\sigma(I)]$[a]	0.0337, 0.0933	0.0465, 0.1313
R_1, wR_2 (all data)	0.0364, 0.0947	0.0528, 0.1406
Twin components (BASF)	n/a	
Ob./rev. twin:		0.0001
Racemic:		0.0730
Ob./rev. with racemic:		0.4276
Reflections – collected:	7458	17801
unique:	2962	6366
observed:	2725	5730

[a] $R_1=\Sigma||F_o|-|F_c||/\Sigma|F_o|$, $wR_2=[\Sigma w(F_o^2-F_c^2)2/\Sigma w(F_o^2)^2]^{½}$

‡ Absorption correction was performed with the TWINABS program.

Table 3.11 – Parameters of hydrogen bonding interactions for **9**. (D-H distances fixed at 0.84(1) Å)

D–H···A	d(H···A)/Å	d(D···A)/Å	<(D–H···A)/°
O2-H2A···O5	1.69	2.525(3)	174
O4-H4A···O1^{i}	1.85	2.660(2)	167
O5-H5A···O3^{ii}	2.18	3.008(3)	177
O5-H5B···Cl1^{iii}	2.50	3.209(2)	145
O5-H5B···Cl2^{iv}	2.64	3.300(2)	137

Symmetry codes: i = -2-x, -1-y, -1-z; ii = -2-x, -y, -1-z; iii = -1-x, -y, -1-z; iv = x-1, y, z-1.

The dinuclear complexes are linked into a 3D network through hydrogen bonding interactions. There are five unique hydrogen bonds and these are shown in Figure 3.17. The protonated carboxylic oxygen atom, O4, donates a hydrogen bond to the O1 carboxylic acid oxygen atom of an adjacent complex, while the protonated carboxylic O2 oxygen atom donates a hydrogen bond to the lattice water molecule, O5. The lattice water molecule, O5, is a hydrogen bond donor to the O3 carboxylic acid oxygen atom on an adjacent complex, and to two chloride atoms on adjacent complexes in a bifurcated manner. The H5B proton sits between a bridging chloride atom, Cl1, and a monodentate chloride atom, Cl2, on that same complex. According to hydrogen-acceptor distances, the former is the major component of the bifurcated hydrogen bond (H5B···Cl1 2.50 Å, H5B···Cl2 2.64 Å). The first three hydrogen bonds can be described as moderate, whereas the last two fall into the weak hydrogen bond category. Bond distances and angles for all the hydrogen bonds are shown in Table 3.11.

The catemeric carboxylic acid interaction (O4-H4A···O1) links the complexes into infinite 1D chains as shown in Figure 3.18. These chains are stepped due to the nature of the dinuclear species. Coplanar 4,4'-H_2dcbp ligands on adjacent complexes are doubly hydrogen bonded forming a centrosymmetric $R_2^2(22)$ motif, with the two O3 carboxylic acid oxygens pointing into the middle of the ring. This results in steric repulsion, which forces the carboxylic acids to twist with respect to the aromatic ring they are attached to. Weaker hydrogen bonds of the C-H···O type reinforce this interaction.

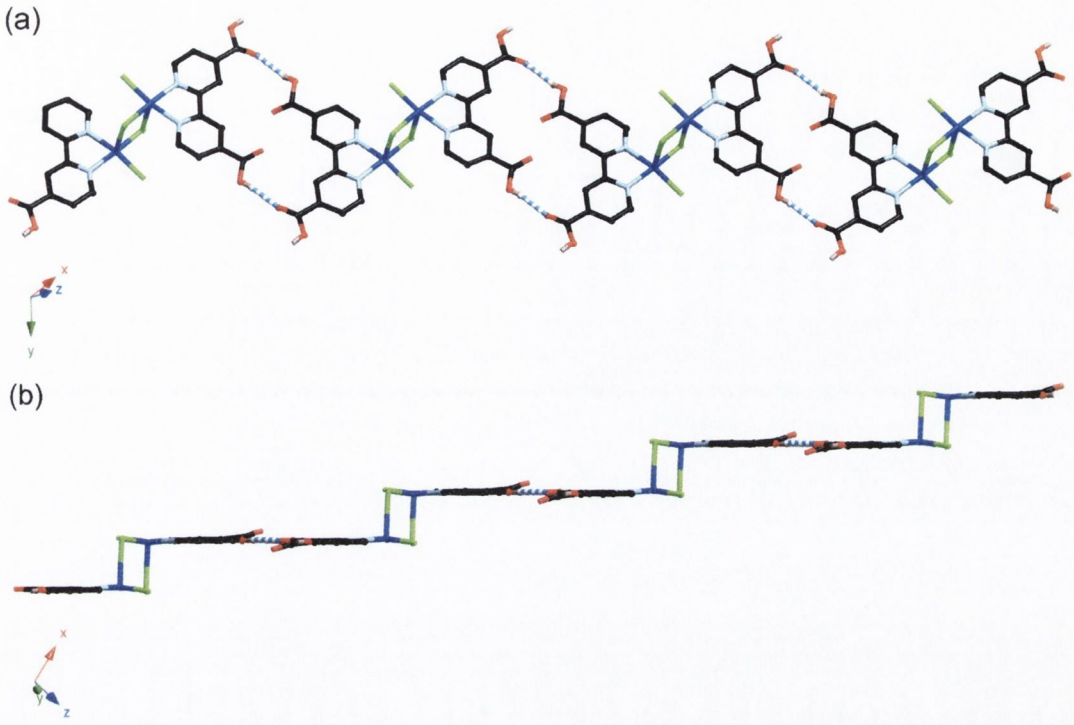

Figure 3.18 – Picture of a single hydrogen bonded chain in **9**. (a) View looking down on the chain showing the $R_2^2(22)$ motif formed between adjacent complexes. (b) View of the chain rotated 90°, highlighting its stepped nature. Note how the carboxylic oxygen atoms in the middle of the hydrogen bonded ring shown above are pointing away from the plane of the aromatic ligands.

Figure 3.19 shows how the chains are then hydrogen bonded through the lattice water molecule (O2···O5···Cl1/Cl2) to form stepped 2D sheets. Small overlap of the 4,4'-H_2dcbp ligands on adjacent chains gives rise to π-interactions, with a closest contact of 3.277(3) Å, which reinforce the hydrogen bonding network. Hydrogen bonding between the carboxylic acids and the lattice water molecule (O2···O5···O3) propagates the sheets into a 3D hydrogen bonded network as shown in Figure 3.20.

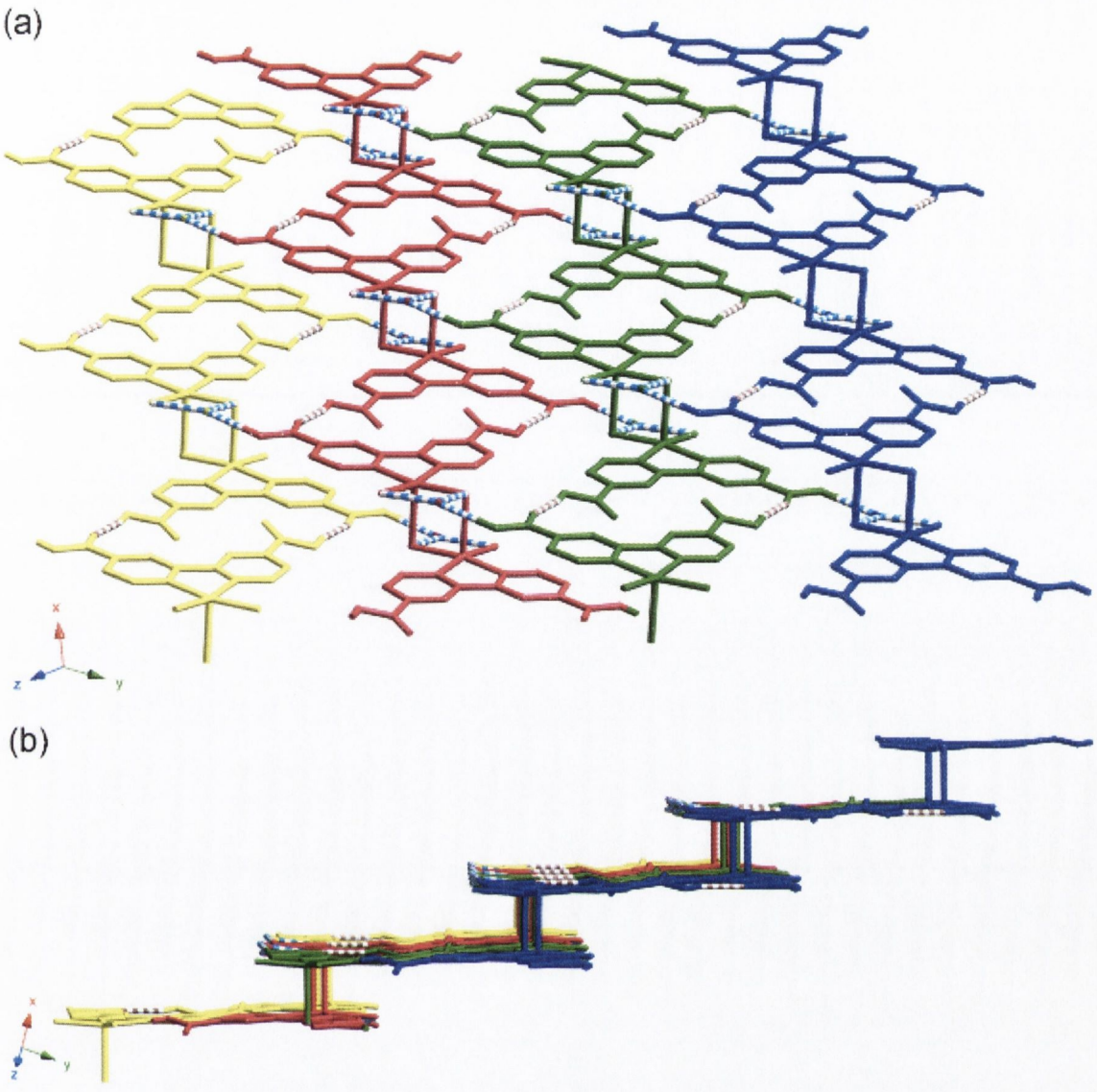

Figure 3.19 – Packing diagram of the 1D chains in **9** into a hydrogen bonded stepped 2D sheet. (a) View along (101), highlighting four different chains in a single sheet; (b) View of the single 2D sheet looking approximately from the right hand corner of the picture above, emphasizing the stepped nature of the sheet. (Hydrogen bonds linking the complexes into 1D chains are shown as brown and white dashed bonds, with hydrogen bonds linking the chains into a 2D sheet shown as blue and white dashed bonds. Hydrogen atoms not participating in hydrogen bonds have been omitted for clarity.)

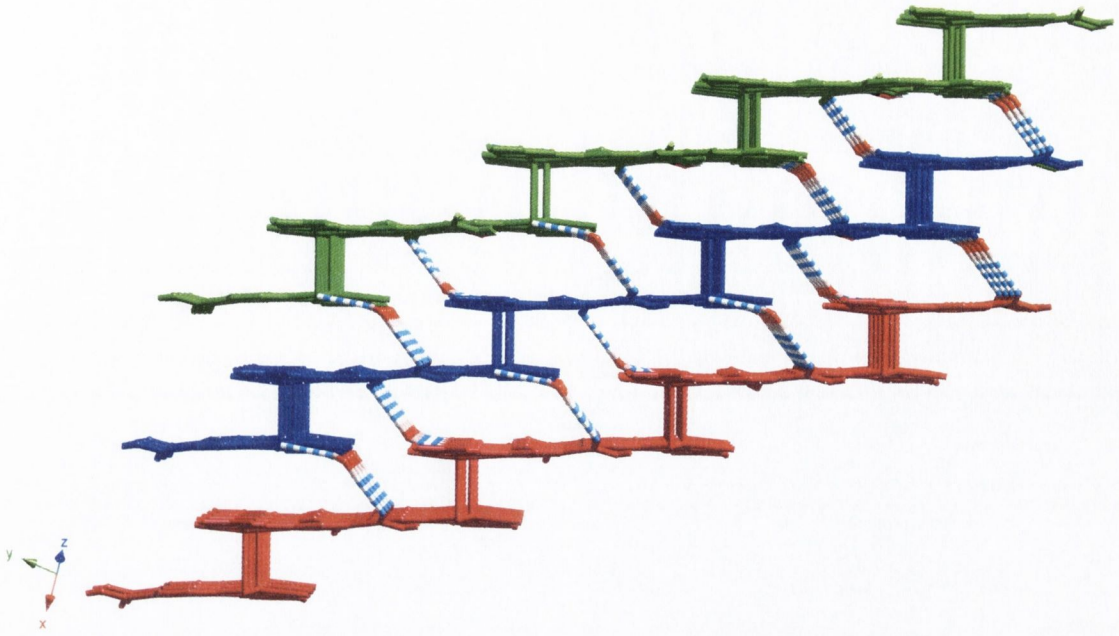

Figure 3.20 – Packing diagram for **9**, showing three different stepped 2D sheets linked through hydrogen bonds to produce a 3D network. (Hydrogen bonds are shown as blue and white dashed bonds. Hydrogen atoms not participating in hydrogen bonding omitted for clarity)

A variable temperature magnetic susceptibility study on powdered samples of **9** over the temperature range 300-2 K was undertaken in order to elucidate the nature of any interaction across the chloride bridge. The magnetic data are shown in Figure 3.21. The magnetic moment, μ_{eff}, decreases very slightly from 1.96 BM to reach 1.9 BM at *ca.* 50 K and then more rapidly to 0.80 BM at 2 K. Such behaviour is typical of weak antiferromagnetic coupling. The data were adequately fit to an S = ½ dimer model[183] yielding J = -2.20 cm^{-1}, g = 2.2.

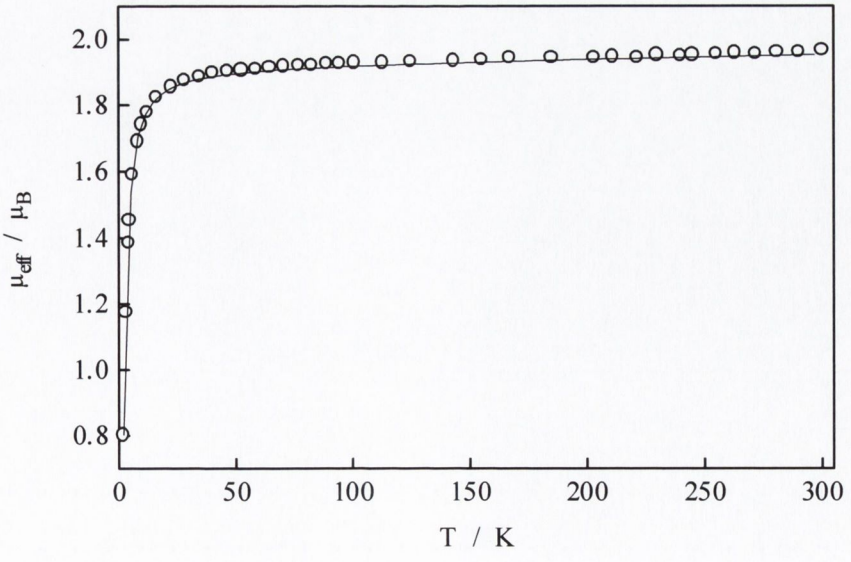

Figure 3.21 – μ_{eff} *versus* T plot for **9**. Curve is characterisitic of weak antiferromagnetism.

*3.2.3 Crystal structure of {[Cu(4,4'-H_2dcbp)(SO_4)]·⅓H_2O}$_n$ (**10**).*

The structure of **10** was refined in the chiral *R*32 space group. The crystals were found to be non-merohedral racemic twins. There are two domains related by rotation (non-merohedral twinning) with each of these containing two further sub-domains related by inversion (racemic twins). Crystallographic details are shown in Table 3.10. The structure of **10** consists of a 1D polymer extending along the crystallographic *c* axis. The atomic labelling scheme and atom connectivity for a single [Cu (4,4'-H_2dcbp)(SO_4)]·⅓H_2O are shown in Figure 3.22. The copper atom sits on a two-fold rotation axis, which also passes through the midpoint of the C5-C5A bond, and thus half of the coordination sphere around the metal atom is related to the other by two-fold rotation. The copper atom adopts a distorted octahedral geometry, with two of the equatorial positions occupied by the chelating nitrogen atoms of the 4,4'-H_2dcbp ligand, and the remaining equatorial and the two axial positions occupied by oxygen atoms of four adjacent sulfate anions. Equatorial bond lengths about the Cu(II) ion are considerably shorter (Cu1-N1 1.963(2) Å, Cu1-O1 1.967(2) Å) than the axial bond lengths (Cu1-O1 2.493(2) Å) as might be anticipated by the Jahn-Teller theorem. Further distortion can be seen in the *cis* bond angles, which range from 82.8(1)° (N1-Cu1-N1A) to 96.12(8)° (N1A-Cu1-O1B). Selected bond lengths and angles are shown in Table 3.12.

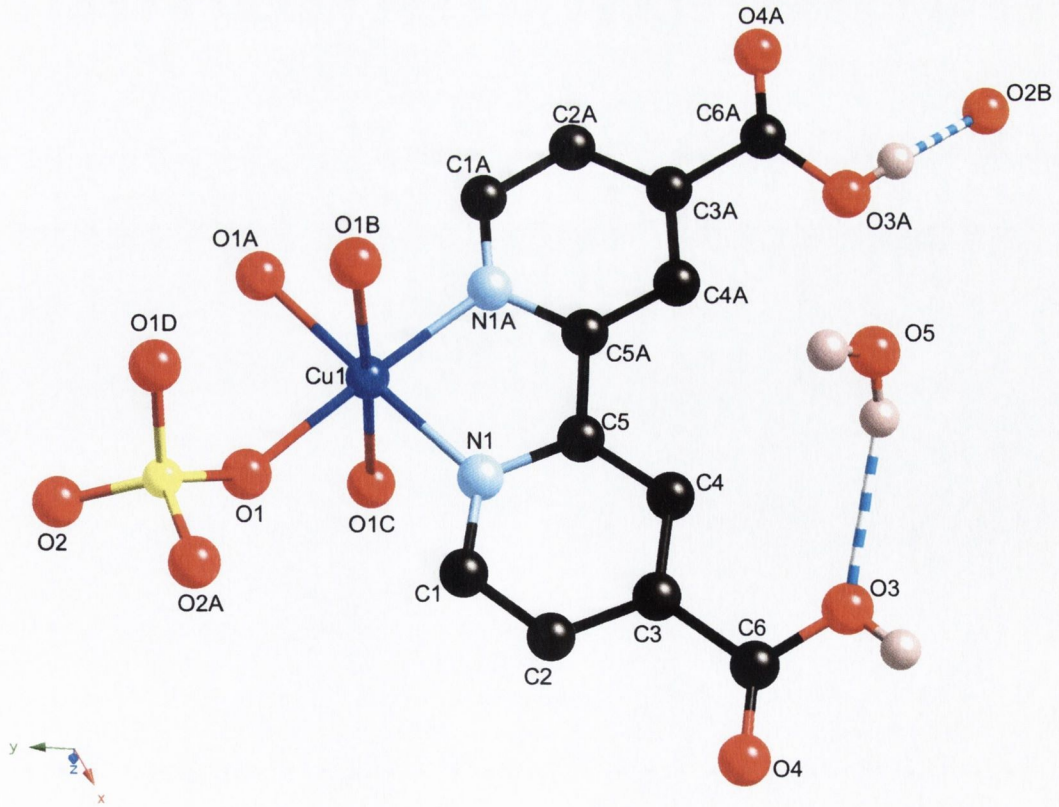

Figure 3.22 – Molecular structure and atomic labelling diagram for **10**. The unique hydrogen bonds are shown as blue and white dashed bonds. (Bipyridyl hydrogen atoms omitted for clarity)

Table 3.12 – Selected bond lengths (Å), distance (Å) and angles (°) for **10**.

Cu1-N1	1.963(2)	N1-Cu1-N1^{ii}	82.8(1)
Cu1-O1	1.967(2)	N1-Cu1-O1^{i}	96.12(8)
Cu1-O1^{i}	2.493(2)	N1-Cu1-O1^{iii}	85.70(8)
S1-O1	1.491(2)	O1-Cu1-O1^{i}	95.45(7)
S1-O2	1.446(2)	N1-Cu1-O1	95.36(8)
O3···O2^{iv}	2.599(3)	O1-Cu1-O1^{ii}	86.5(1)
O5···O3	3.103(8)	N1-Cu1-O1^{ii}	177.95(8)
		O1^{i}-Cu1-O1^{iii}	177.59(9)
		O3-H3···O2^{iv}	165
		O5-H5···O3	155
		O1^{v}-S1-O2^{v}	108.2(1)
		O2-S1-O1^{v}	108.9(1)
		O1-S1-O1^{v}	110.4(2)
		O2-S1-O2^{v}	112.2(2)

Symmetry codes: i = -y-0.333333, x-y+0.333333, z+0.333333; ii = x+0.333333, y-0.333333, 0.333333-z; iii = x-y, -y, -z; iv = y+0.333333, x+0.666667, 0.666667-z; v = -x-0.666667, y-x-0.333333, 0.666667-z.

The 4,4'-H_2dcbp ligand is protonated and is acting as a terminal ligand, coordinating only through the chelating nitrogen atoms. The 4,4'-H_2dcbp ligand is almost planar with only a small torsion angle of *ca.* 7.8° between the pyridyl rings, and with the carboxylic acid group twisted at 11.0° with respect to the aromatic ring. As expected for protonated carboxylic acids groups, and as in **9**, bond lengths about C6 differ for the carbon to hydroxyl oxygen bond (C6-O3 1.315(4) Å) and for the carbon to carbonyl oxygen double bond (C6-O4 1.189(4) Å).

The two-fold rotation axes also pass through the sulfur atom of the sulfate anions, and thus relate each half of the sulfate molecules. Two of the oxygen atoms (O1) are coordinating to the Cu(II) ions while the other oxygen atoms (O2) participate in hydrogen bonding interactions and are not directly bound to the copper atoms. As expected, the S-O bond lengths for the coordinating oxygen atoms are longer (S1-O1 1.491(2) Å) than the bond lengths for the non-coordinating oxygen atoms (S1-O2 1.446(2) Å). Each of the coordinating sulfate oxygen atoms does so in a bidentate fashion, and hence each sulfate anion bridges four copper centres. Bridging of the metal centres by sulfate anions gives rise to a 1D polymer extending along the crystallographic *c* axis, shown in Figure 3.23. Adjacent [Cu(4,4'-H_2dcbp)(SO_4)] units are related by 3_1 screw axes, thus forming left-handed helices. All chains within the structure are left-handed and therefore the structure of **10** is chiral. The Cu(II) ions are solely bridged by the anions, with 4,4'-H_2dcbp merely acting as a terminating ligand.

Thus, this complex belongs to the organic-inorganic hybrid materials class[221] rather than the 'pure' coordination polymers or metal-organic frameworks.[32]

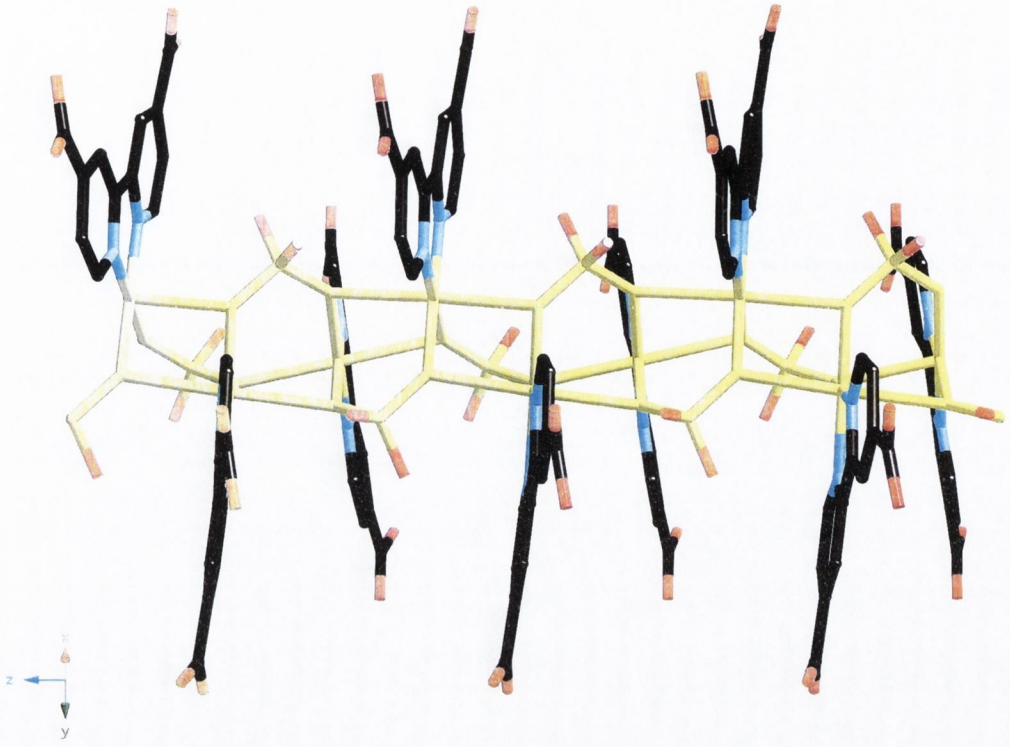

Figure 3.23 –1D polymer formed in **10**. The copper-sulfate chains are highlighted in yellow. The sulfate anions link the copper centres along the crystallographic *c* axis, while 4,4'-H_2dcbp is acting as a terminating ligand. (Hydrogen atoms and lattice water molecules omitted for clarity)

The 1D polymer consists of tris-sulfato bridged Cu(II) ions: two sulfate anions link the copper centres through a single bidentate oxygen atom, while the other links them through an O-S-O bridge, as shown in Figure 3.24. This gives rise to a metal-to-metal distance of 3.2426(8) Å between adjacent copper atoms.

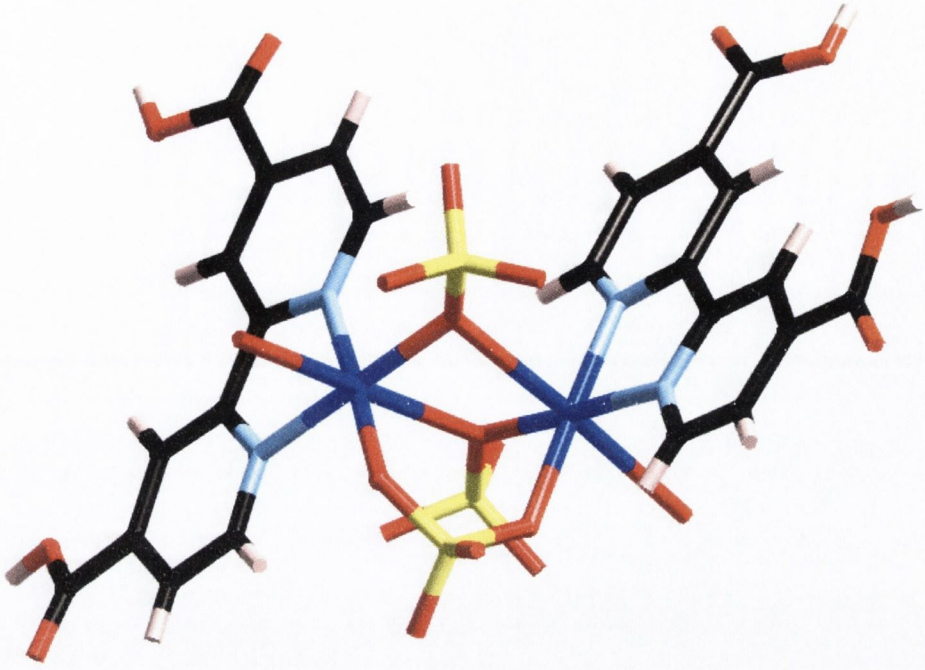

Figure 3.24 – Detail of a tris-sulfate bridged Cu(II) dimer in **10**. Two of the sulfate anions link the copper centres through an oxo-bridge (*i.e.* a single oxygen atom), whilst the third links the copper atoms through a longer O-S-O bridge.

Packing of the 1D polymer gives rise to channels running down the *c* direction, as shown in Figure 3.25. This is furnished by hydrogen bonding and π-π interactions between adjacent polymers. The protonated oxygen atom of the carboxylic acid group in 4,4'-H_2dcbp is a hydrogen bond donor to the non-coordinating sulfate oxygen atom of an adjacent chain (O3···O2 2.599(3) Å). Overlap of the 4,4'-H_2dcbp ligands on adjacent polymeric chains gives rise to offset face-to-face π-π interactions between the pyridyl rings with a separation at closest contact of 3.490(4) Å. There are two types of channels in the structure: those that lie on 3-fold axes and those that lie on 3_1 screw axes. The channels on the 3-fold axes have dimensions[§] of 4.00 x 5.14 Å^2, while those on the 3_1 axes are slightly smaller with dimensions[§] of 4.24 x 4.47 Å^2. Together they constitute 8.5% of the total crystal volume.[187-189] While the former channels are void of solvent, in the latter reside the water molecules. These are disordered over three positions, related by 3_1 screw axes. The water molecules are hydrogen bonding to the carboxylic acid groups as shown in Figure 3.25.

[§] Dimensions given are atom-to-atom (including hydrogen) as viewed along channels and are *ca.* perpendicular to channel direction.

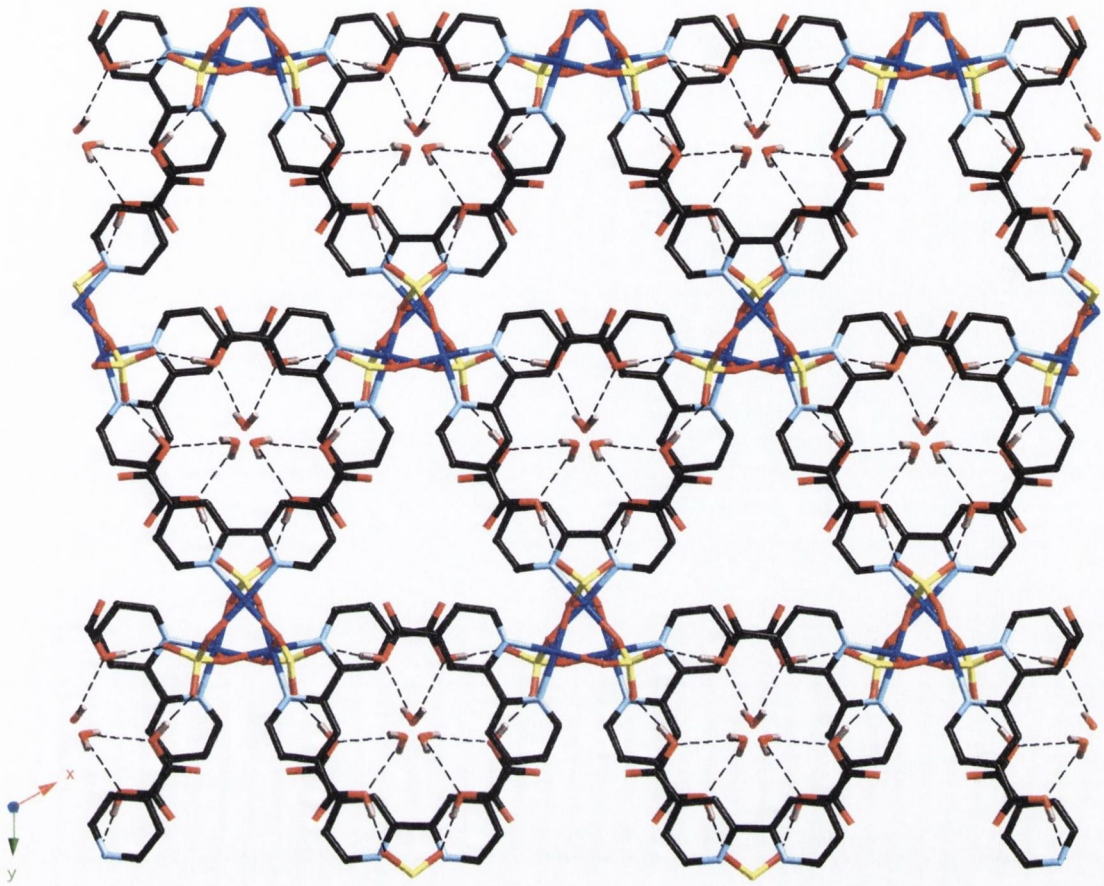

Figure 3.25 – 3D structure of **10**. Hydrogen bonding and π-π interactions between adjacent 1D polymers give rise to channels along the *c* direction. Channels on the 3_1 axes are occupied by disordered water molecules, while those on the 3-fold rotation axes are void of solvent. (Hydrogen bonds shown as dashed bonds. Aromatic hydrogen atoms omitted for clarity)

*3.2.4 Thermal analysis and magnetic properties of **10**.*

Thermogravimetric analysis of **10** revealed a weight loss of 1.5% up to 100°C, consistent with the loss of the guest water molecules (calcd. 1.46% for ⅓ H_2O)(Figure 3.26). No further weight loss is observed until decomposition begins at 380°C. A sample of **10** was heated to 150 °C for 2 hours, maintaining crystallinity, suggesting the network is retained even in the absence of water. Furthermore, a low temperature crystal data collection was performed on a heated crystal, yielding almost identical cell parameters (see Appendix). A very slight increase in *a* and *b* (0.2%), and consequently in the volume (0.4%) is observed. The new structure, **10a**, displays the same 3D network as **10**. A residual of 0.9 e.Å^{-3} was still observed in the same position as the water peak was in **10**, and although small, it suggests that perhaps some residual water is still present in the network. Whether this water is a residue from the original network or has been reabsorbed by the crystal while handling or on the cryostream has yet to be determined.

Studies on the reabsorption of water and other solvents and gases by **10a** are currently being performed.

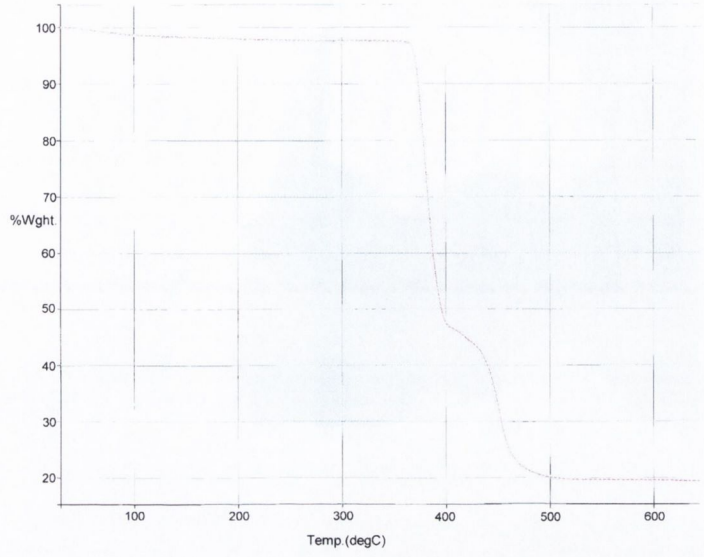

Figure 3.26 –Thermogravimetric analysis curve for **10**. 1.5% weight loss is observed up to 100 °C, corresponding to the loss of the lattice water molecules. The network is then stable up to 380 °C.

A variable temperature magnetic susceptibility study was performed on powdered samples of **10** over the temperature range 300-4.2 K. The $\chi_m T$ *vs.* T plot for **10** is shown in Figure 3.27. At high temperature, $\chi_m T$ is essentially independent of temperature with a gradual decrease from 0.424 $cm^3mol^{-1}K$ (1.84 BM) at 300 K down to 0.410 (1.81 BM) at 50 K followed by a rapid decrease to 0.182 (1.21 BM) at 4.2 K. This behaviour is typical of weak antiferromagnetic coupling between S = ½ Cu(II) centres. The data were fit to a regular chain model, taking only into account the Cu-O2-Cu pathway and neglecting the longer Cu-OSO-Cu one, yielding values of J = -1.90 cm^{-1}, g = 2.10.

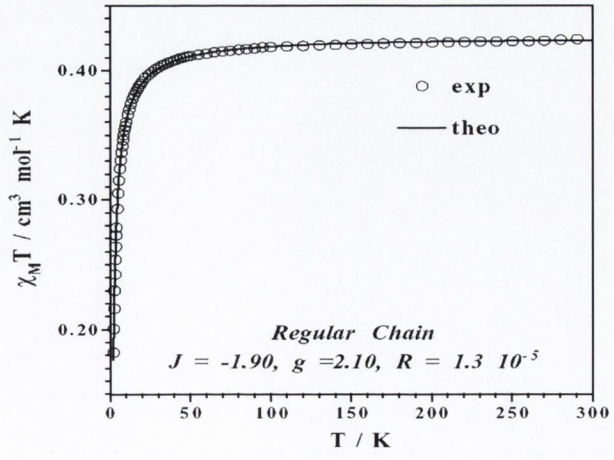

Figure 3.27 – $\chi_m T$ *versus* T plot for **10**. The curve is indicative of weak antiferromagnetic coupling.

*3.2.5 Crystal structure of [Cu(4,4'-H_2dcbp)(NO_3)$_2$(H_2O)] (**11**).*

The structure of **11** was refined in the triclinic *P*-1 space group. Crystallographic details are shown in Table 3.14. Despite the goodness of the refinement (R_1 = 0.0476) a large residual peak of 3 e.Å^{-3} was still observed. This could not be assigned to any real atom and is perhaps an indicator that there is some sort of twinning present in the crystal. The structure of **11** consists of discrete [Cu(4,4'-H_2dcbp)(NO_3)$_2$(H_2O)] complexes, shown in Figure 3.28.

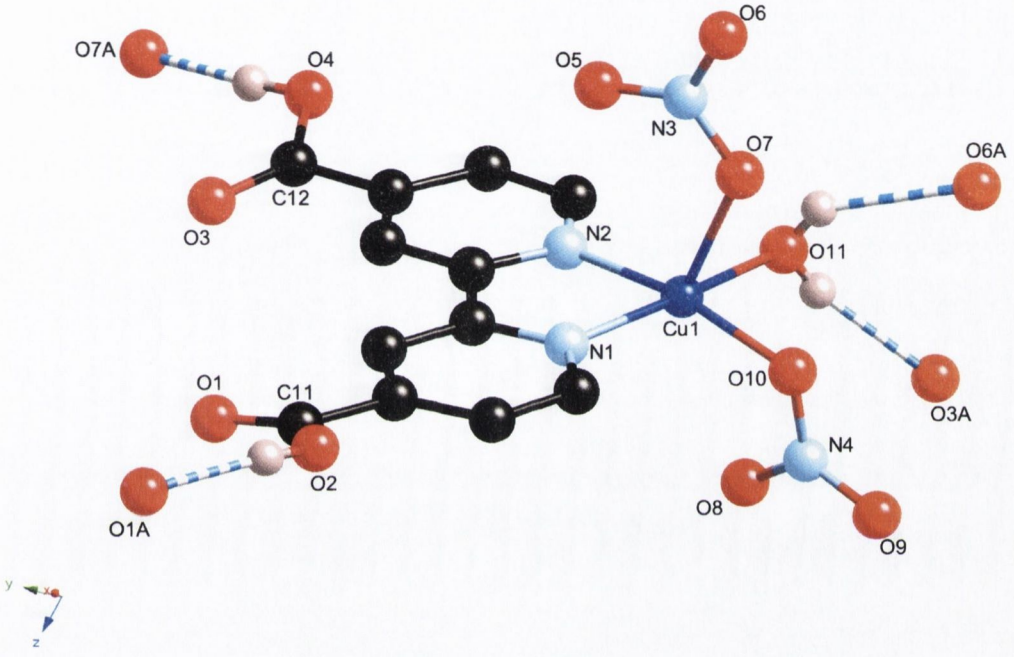

Figure 3.28 – Molecular structure and atomic labelling scheme of **11**. Unique hydrogen bonds are depicted as blue and white dashed bonds.

Table 3.13 – Selected bond lengths (Å) and angles (°) for **11**.

Cu1-N1	1.986(2)	N1-Cu1-N2	81.78(9)
Cu1-N2	1.986(2)	O7-Cu1-N2	112.66(8)
Cu1-O7	2.231(2)	O7-Cu1-O10	78.57(8)
Cu1-O10	1.984(2)	O7-Cu1-O11	89.41(9)
Cu1-O11	1.983(2)	O7-Cu1-N1	96.46(9)
		O10-Cu1-N1	95.94(9)
		N2-Cu1-O10	168.69(9)
		N1-Cu1-O11	172.21(9)

Table 3.14 – Crystallographic data for **11**.

Compound	**11**
Chemical Formula	$CuC_{12}H_{10}N_4O_{11}$
Formula weight	449.78
Crystal system	Triclinic
Space group	*P*-1
$\mu(MoK_\alpha)$/ mm^{-1}	1.421
a/Å	6.4404(4)
b/Å	9.7045(6)
c/Å	13.6309(8)
α/°	76.339(1)
β/°	84.205(1)
γ/°	78.894(1)
V/$Å^3$	810.96(9)
Z	2
D_{calc}/gcm^{-3}	1.842
T/K	153(2)
Crystal size max /mm	0.48
mid /mm	0.08
min /mm	0.07
$2\theta_{max}$/°	59.96
Min/Max trans. Factor	0.770/1.000
R_{int}	0.0324
R_1, $wR_2[I>2\sigma(I)]$[a]	0.0478, 0.1221
R_1, wR_2 (all data)	0.0547, 0.1255
Reflections – collected:	8948
unique:	4456
observed:	3899

[a] $R_1=\Sigma||F_o|-|F_c||/\Sigma|F_o|$, $wR_2=[\Sigma w(F_o^2-F_c^2)2/\Sigma w(F_o^2)^2]^{½}$

The geometry around the Cu(II) ion is distorted square pyramidal with the basal positions occupied by the chelating nitrogen atoms *trans* to the oxygen atoms of a coordinated water molecule and a coordinated nitrate anion. The apical position is occupied by the oxygen atom of a second coordinated nitrate anion. As anticipated by the Jahn-Teller theorem, the axial bond length (Cu1-O7 2.231(2) Å) is longer than the equatorial bond lengths (average 1.985 Å). Selected bond lengths and angles are shown in Table 3.13. The apical oxygen atom, O7, is not perpendicular to the basal plane (O7-Cu1-N2 112.66(8)°, O7-Cu1-N1 96.46(9)°) and this, in combination with the bite angle of the 4,4'-H_2dcbp ligand, results in further distortion from square pyramidal geometry. In addition, the copper atom is displaced 0.070 Å from the basal plane towards the O7 oxygen atom. The pyridyl rings of the 4,4'-H_2dcbp ligand are twisted *ca.* 2.4°. More pronounced distortion from planarity arises from the twisting of the carboxylate groups with respect to the aromatic rings, with C11 twisted *ca.* 13.2° and C12 *ca.* 15.2°. The 4,4'-H_2dcbp ligand is protonated, evident from the C-O bond lengths, with carbon to hydroxyl oxygen distances (C11-O2 1.284(3) Å, C12-O4 1.314(3) Å) longer than carbon to carbonyl oxygen ones (C11-O1 1.247(3) Å, C12-O3 1.213(3) Å).

Two coordinating nitrate anions provide the balance charge for the complex. Unlike **9** and **10**, where the inorganic anions bridge the copper atoms, in **11** both nitrate anions adopt a unidentate coordination mode and thus only discrete metal complexes are formed. The N-O bond lengths are longer for the coordinated oxygen atoms (N3-O7 1.287(3) Å, N4-O10 1.293(3) Å) than for the non-coordinating oxygen atoms, which have similar bond lengths due to delocalisation (N3-O5 1.232(3) Å, N3-O6 1.235(5) Å, N4-O8 1.240(3) Å, N4-O9 1.231(3) Å).

There are four unique hydrogen bonds in **11** and hydrogen bond distances and angles are shown in Table 3.15. The O2 oxygen atom is a hydrogen bond donor to O1 forming a self-complementary carboxylic acid hydrogen bond. O4 is a hydrogen bond donor to nitrate oxygen atom O7. The coordinated water molecule donates two hydrogen bonds: one to a nitrate oxygen atom, O6, and another to a carboxylic acid oxygen, O3. Two [Cu(4,4'-H_2dcbp)(NO_3)$_2$(H_2O)] complexes are connected through the self-complementary carboxylic acid synthon. These are extended into a 1D ladder through hydrogen bonding of the other carboxylic acid with a nitrate anion of an adjacent complex, as shown in Figure 3.29.

Table 3.15 – Parameters of hydrogen bonding interactions for **11**. (D-H distances are fixed at 0.84 Å)

D–H···A	d(H···A)/Å	d(D···A)/Å	<(D–H···A)/°
O2-H2A···O1^{i}	1.77	2.611(3)	175
O4-H4A···O7^{ii}	1.79	2.622(3)	171
O11-H11A···O3^{iii}	1.87	2.687(3)	163
O11-H11B···O6^{iv}	2.10	2.802(3)	141

Symmetry codes: i = -1-x, 1-y, -z; ii = x+1, y-1, z; iii = x, y+1, z; iv = -x, 2-y, 1-z.

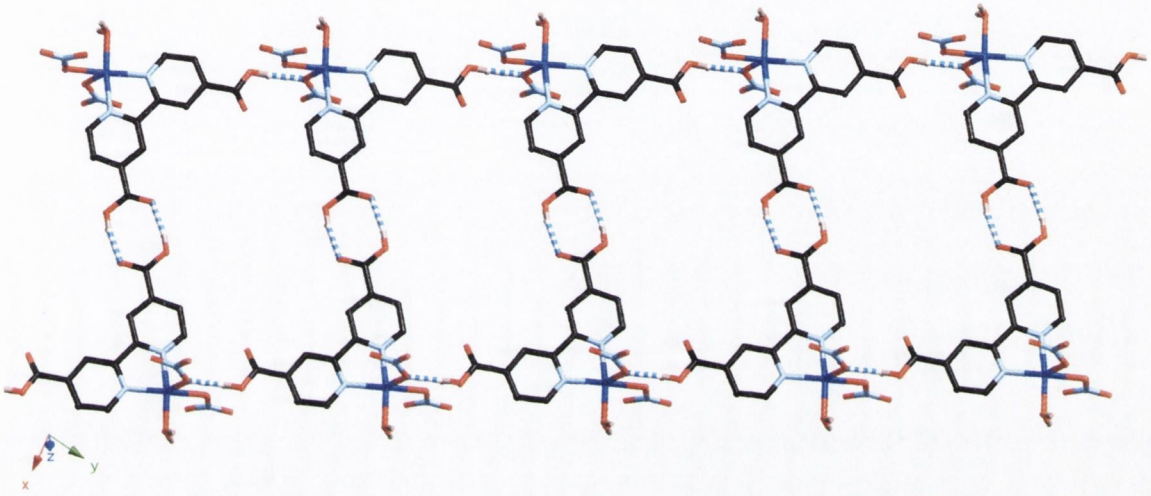

Figure 3.29 – 1D stepped ladder formed in **11**. The classical $R_2^2(8)$ carboxylic acid motif assembles the complexes into dimers which are then linked through hydrogen bonding of the remaining carboxylic acid with the nitrate anion of an adjacent dimeric unit. (Bipyridyl hydrogen atoms omitted for clarity)

Further hydrogen bonding between the coordinated water molecule and a carboxylic acid group (O11-H11A···O3) of an adjacent 1D ladder, and between that water and the nitrate anion (O11-H11B···O6) of another adjacent 1D ladder, links these into a 3D network, shown in Figure 3.30. Offset face-to-face π-π interactions occurs between the pyridyl rings of adjacent stacked ladders with a separation at closest contact of 3.515(4) Å.

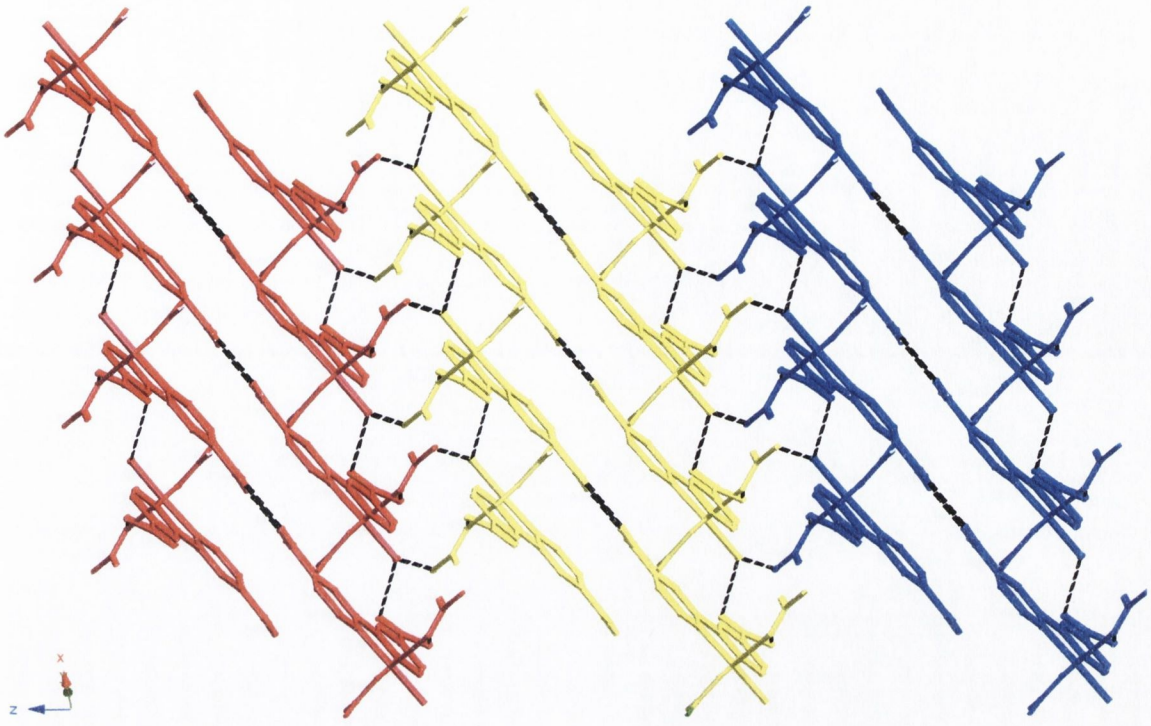

Figure 3.30 – Overall packing diagram for **11**. The 1D ladders are highlighted in different colours. π-π stacking occurs between ladders of the same colour. (Hydrogen atoms omitted for clarity. Hydrogen bonds represented as dashed bonds.)

Each metal complex participates in a total of eight hydrogen bonds (each of the carboxylic acid groups donates one and accepts another, the coordinated water molecule donates two and the nitrate anions accept two). Through self-complementary carboxylic acid dimer formation, a double 'bridge' exists between two adjacent complexes, accounting for two hydrogen bonds. Additional double 'bridges' also exist between two other neighbouring complexes *via* hydrogen bonding between the coordinated water molecules and the nitrate anions, thus accounting for a further two hydrogen bonds. The remaining four 'bridges' for each complex connect to four other metal complexes. Thus, each metal complex is connected to six others *via* hydrogen bonding.

3.2.6 Conclusions

While all reactions discussed previously have been carried out in neutral or basic conditions, the complexes discussed in this section were prepared in acidic solutions. It is well known that pH has an effect on dimensionality of the resulting structure[222] with low pH values leading to low dimensional structures, while higher pH values result in higher dimensionality networks. Under acidic conditions the 4,4'-H_2dcbp ligand is not deprotonated and therefore cannot coordinate to metal ions through the carboxy groups. Thus **9**, **10** and **11** are low dimensionality coordination complexes (**9**

and **11**) or polymers (**10**). Furthermore, the polymeric nature of **10** arises from the bridging of the copper atoms by sulfate anions, not by the 4,4'-H_2dcbp ligand.

Unlike in the complexes prepared in previous sections where the 4,4'-dcbp ligand provides the charge balance, in **9**, **10** and **11**, the 4,4'-H_2dcbp ligand is protonated and therefore further anions are needed. These are provided by the mineral acids used in each reaction: chloride in **9**, sulfate in **10** and nitrate in **11**. In **9** the chloride bridges two Cu(II) ions to form a dimer, while in **10** bridging of the Cu(II) ions by sulfate anions results in a 1D polymer. In contrast, the nitrate anions, while known to bridge metal ions,[223] adopt a unidentate coordination mode in **11** resulting in a 0D complex formed.

The 4,4'-H_2dcbp ligand, while not coordinating through the carboxylic acid groups, retains its capacity to participate in hydrogen bonding, and thus, the low dimensional complexes are linked into 3D networks through hydrogen bond interactions. In **9** and **11** hydrogen bonding between the carboxylic acid groups is observed, with the carboxyl dimer being formed in **11**, and a non-cyclic catemeric arrangement formed in **9**. This type of interaction is, however, not observed in **10** where the carboxylic acid groups only hydrogen bond with the sulfate anions instead. Steiner carried out a database study where he determined the success of formation of either dimer or catemer carboxylic acid motifs against other competitors.[224] He determined that groups such as H_2O and S-O^- are more likely to be favoured as acceptors for the COOH group over itself. Thus COOH-SO_4 interactions are observed in **10**.

Hydrogen bonding and π-π stacking interactions result in a 3D porous network in **10**, which contains water molecules in the channels. Notably **10** retains crystallinity after heating to 100°C, at which point the water molecules are lost. Porous hydrogen bonded networks are generally regarded as being less able to withstand guest loss in comparison to coordination polymers, however, some examples of crystalline hydrogen bonded materials robust to guest evacuation are known.[225] The porous nature of **10** arises from hydrogen bonding of 1D coordination polymers and thus it would be expected to be more stable than solely hydrogen bonded materials. In addition, the channels in **10** constitute a small percent of the total crystal volume (8.7%), and thus the network is not as prone to collapse in the absence of the guest molecules, despite being held by so-called weak interactions.

Chapter Four

Hydrogen Bonded Complexes of 4,4'-dicarboxy-2,2'-bipyridine with First Row Transition Metals.

Preamble.

As mentioned in Chapter 1, carboxylic acids are well known to participate in self-complementary hydrogen bonding through the carboxy dimer or catemer, or forming the strong carboxylic acid-carboxylate pair. 4,4'-H_2dcbp has a primary chelating site which can be employed to strongly bind metal ions while the peripheral carboxylic acid sites can then be used to propagate the geometry around the metal ion through hydrogen bonding. Thus, the use of an octahedral tris-4,4'-H_2dcbp metal complex as a building block may then form an octahedral network.

4.1 Reaction of Co(II) with 4,4'-dicarboxy-2,2'-bipyridine.

4.1.1 Reaction of Co(II) with 4,4'-H_2dcbp.

In an attempt to prepare the tris-4,4'-dcbp complex of Co(II), triethylamine was added to an aqueous suspension of $CoSO_4$ and 4,4'-H_2dcbp (1:3), and this mixture was heated to reflux producing a yellow solution, from which yellow needles grew on slow evaporation. An infrared spectrum showed the presence of deprotonated 4,4'-dcbp (ν_{as}(C-O) 1543 cm^{-1}, ν_s(C-O) 1379 cm^{-1}) as well as a strong, broad band at 3237 cm^{-1}, corresponding to water. This would be consistent with a tris-4,4'-dcbp Co(II) complex with water in the lattice, however, a single crystal X-ray diffraction study showed the structure of these to be [Co(4,4'-dcbp)(H_2O)$_4$].4H_2O (**12**). Only one of the ligands had complexed to the metal despite the 1:3 metal-to-ligand ratio employed. Thus, in order to force the complexation of further ligands, the reaction was performed under solvothermal conditions. A DMF/H_2O mixture of $CoCl_2$ and 4,4'-H_2dcbp (1:3) was heated to 200°C for 36hrs, yielding orange needles in an orange/brown solution. A preliminary X-ray analysis of the orange needles confirmed these to be the previously reported α-[Co(4,4'-dcbp)(H_2O)$_2$]$_n$, as described in Chapter 2. On further evaporation of the orange/brown solution, brown crystals grew in approximately 25% yield of the total reaction. These crystals are very unstable and lose crystallinity within minutes of being exposed to air, thus handling of the crystals was done under extreme care. A suitable crystal was picked from the mother liquor for structure determination by X-ray diffraction and the compound [Me_2NH_2]$_{1.5}$[Co(4,4'-$H_{5/6}$dcbp)$_3$]·10½H_2O (**13**) was formulated.

*4.1.2 Crystal structure of [Co(4,4'-dcbp)(H_2O)$_4$]·4H_2O (**12**).*

The structure of **12** was refined in the orthorhombic *Pccn* space group. Crystallographic details are shown in Table 4.2. The structure of **12** contains neutral [Co(4,4'-dcbp)(H_2O)$_4$] units and four lattice water molecules which are linked together through extensive hydrogen bonding into a 3D network. A single complex is shown in

Figure 4.1 along with the eight crystallographically unique hydrogen bonds. One half of the octahedral Co(II) complex is related to the other by a 2-fold rotation axis which passes through the metal centre and the midpoint of the C5–C5A bond. The bond lengths about Co1 vary with donor type and position with Co1–O3 2.043(2) Å, Co1–O4 2.096(2) Å and Co1–N1 2.119(2) Å, so distortion from ideal octahedral geometry is evident. More significant distortion from octahedral symmetry is observed in the coordination bond angles, with the chelating 4,4'-dcbp ligand giving a bite angle, N1–Co1–N1A, of 77.7(1)°. The 4,4'-dcbp ligand adopts a near planar conformation with the carboxylate group twisted less than 15° from the plane of the aromatic ring to which it is attached. As expected for deprotonated carboxylic acids, delocalisation results in identical C–O bond lengths about C6 (C6–O1 1.251(3) Å, C6–O2 1.255(3) Å).

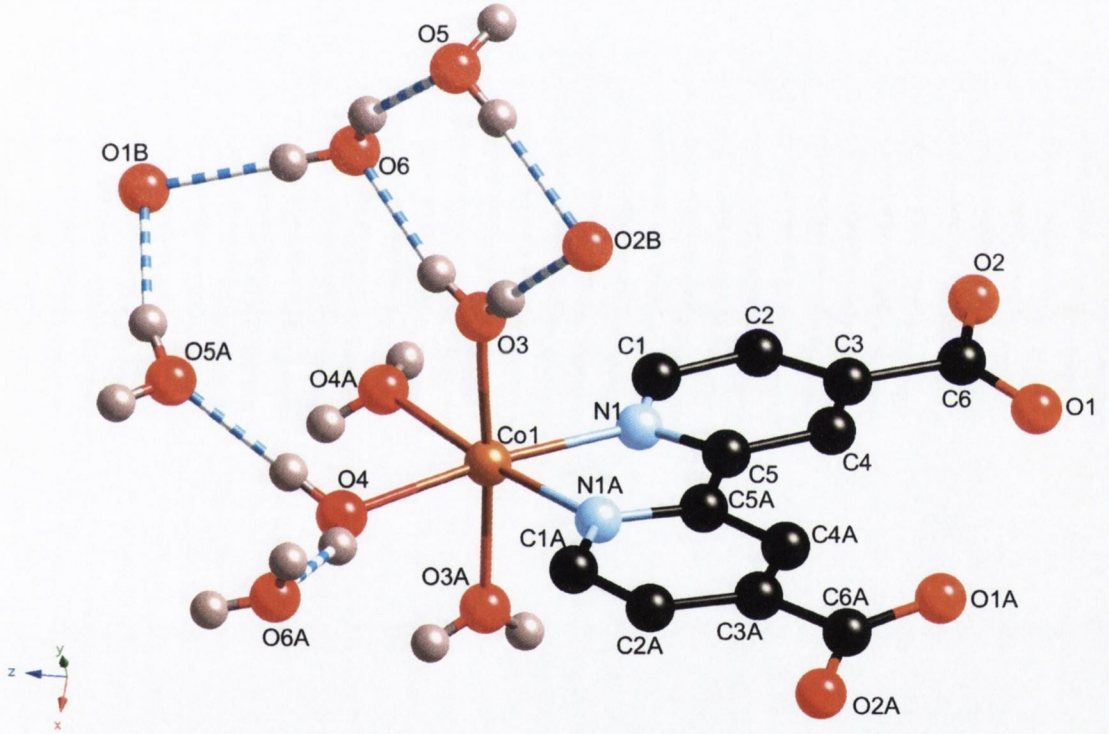

Figure 4.1 – Molecular structure and atomic labelling scheme in **12**. The blue and white dashed bonds depict the eight unique hydrogen bonds. (Bipyridyl hydrogen atoms omitted for clarity)

Table 4.1 – Selected bond lengths (Å) and angles (°) for **12**.

Co1-N1	2.119(2)	N1-Co1-N1^{i}	77.7(1)
Co1-O3	2.043(2)	N1-Co1-O3	92.69(8)
Co1-O4	2.096(2)	N1-Co1-O4^{i}	100.37(7)
		O4-Co1-O3	93.15(8)
		O4-Co1-O4^{i}	82.2(1)
		N1-Co1-O4	173.85(7)
		O3-Co1-O3^{i}	176.4(1)

Symmetry codes: i = 0.5-x, 0.5-y, z.

Table 4.2 – Crystallographic data for **12** and **13**.

Compound		**12**	**13**
Chemical Formula		$CoC_{12}H_{22}N_2O_{12}$	$CoC_{39}H_{53.5}N_{7.5}O_{22.5}$
Formula weight		445.25	1046.32
Crystal system		Orthorhombic	Trigonal
Space group		*Pccn*	*R*-3
μ (MoK_α)/ mm^{-1}		1.032	0.451
a/Å		6.378(1)	14.822(2)
b/Å		12.938(2)	14.822(2)
c/Å		21.558(3)	37.527(5)
α/°		90	90
β/°		90	90
γ/°		90	120
V/$Å^3$		1778.9(5)	7139.8(17)
Z		4	6
D_{calc}/gcm^{-3}		1.662	1.460
T/K		173(2)	153(2)
Crystal size –	max /mm	0.40	0.20
	mid /mm	0.10	0.18
	min /mm	0.10	0.06
$2\theta_{max}$/°		56.84	50
Min/Max trans. Factor		0.842/1.000	0.874/1.000
R_{int}		0.0380	0.0575
R_1, $wR_2[I>2\sigma(I)]$[a]		0.0413, 0.0973	0.0775, 0.1984
R_1, wR_2 (all data)		0.0572, 0.1022	0.0953, 0.2091
Reflections –	collected:	20361	22589
	unique:	2151	2802
	observed:	1661	2161

[a] $R_1=\Sigma||F_o|-|F_c||/\Sigma|F_o|$, $wR_2=[\Sigma w(F_o^2-F_c^2)2/\Sigma w(F_o^2)^2]^{½}$

The water hydrogen atoms are ordered throughout the structure as a result of hydrogen bonding. The coordinated water molecule O3, is a hydrogen bond donor to lattice water molecule O6, and to carboxylate oxygen atom O2, of an adjacent 4,4'-dcbp ligand. The other coordinated water molecule, O4, is also a hydrogen bond donor to lattice water molecules O5 and O6. The lattice water molecules themselves exist as hydrogen bonded pairs. Lattice water molecule O5 donates two hydrogen bonds to carboxylate oxygen atoms O1 and O2 of two adjacent 4,4'-dcbp ligands, while accepting one hydrogen bond from lattice water molecule O6, and another from a coordinated water molecule, O4. Lattice water molecule O6 is a hydrogen bond donor to carboxylate oxygen O1, and acceptor from both coordinated water molecules, O3 and O4. Distances and angles for the eight unique hydrogen bonds are listed in Table 4.3. The overall result of the interactions is a complicated 3D hydrogen bonded network, Figure 4.2.

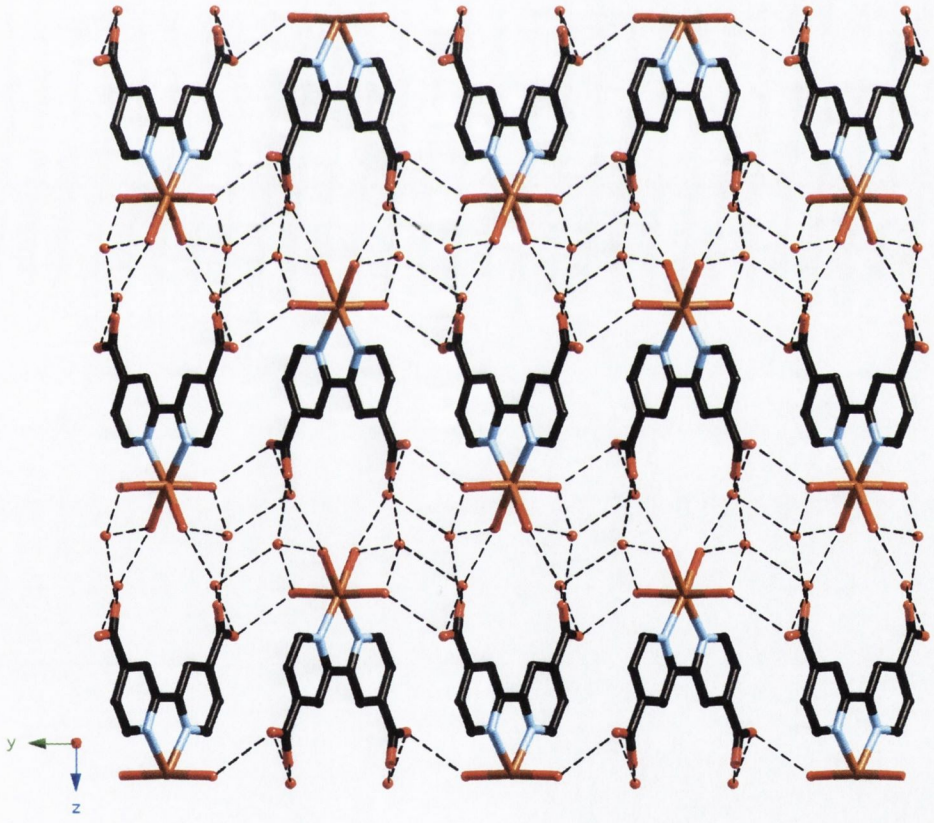

Figure 4.2 - Packing diagram of **12** as viewed along (100), showing the extensive hydrogen bonding between the [Co(4,4'-dcbp)(H_2O)$_4$] units and the lattice waters. Offset face-to-face π-π interactions exist between the 4,4'-dcbp ligands along the *ab* plane. (Hydrogen atoms omitted for clarity)

Table 4.3 – Parameters of hydrogen bonding for **12**.

D-H···A	D-H/Å	d(H···A)/Å	d(D···A)/Å	<(DH···A)/°
O3-H3A···O2^{i}	0.81	1.95	2.757(3)	169
O3-H3B···O6	0.81	1.90	2.693(3)	168
O4-H4A···O5^{ii}	0.85	1.87	2.697(3)	166
O4-H4B···O6^{iii}	0.83	1.94	2.732(3)	159
O5-H5A···O1^{iv}	0.84	1.91	2.712(3)	161
O5-H5B···O2^{i}	0.81	2.01	2.815(3)	173
O6-H6A···O1^{v}	0.83	1.86	2.690(3)	174
O6-H6B···O5	0.83	2.04	2.817(3)	156

Symmetry codes: i = 0.5+x, y-0.5, 1-z; ii = 0.5+x, -y, 0.5-z; iii = 1+x, y, z; iv = x-0.5, y-0.5, 1-z; v = x, 0.5-y, z-0.5.

The $[Co(4,4'\text{-dcbp})(H_2O)_4]$ unit participates in sixteen hydrogen bonds (four coordinated water molecules and four carboxylate oxygen atoms donate and accept, respectively, two hydrogen bonds each). Double 'bridges' exist between each complex and two other neighbouring complexes accounting for four of the sixteen hydrogen bonds emanating from each complex. The remaining twelve 'bridges' for each complex connect to twelve different lattice water molecules. If a single node represents each pair of lattice water molecules, then the network consists of 14-connecting nodes (complexes) and 6-connecting nodes (pairs of lattice waters) in the ratio 1:2. The 14-connecting nodes are joined to two other 14-connectors and twelve 6-connectors while each 6-connector is joined to six different 14-connectors.

The 4,4'-dcbp ligands also participate in offset face-to-face π-π interactions (3.512(5) Å) which form stepped chains propagating in the *a* direction. Weaker π-π interactions (3.644(3) Å), with less overlap of the aromatic rings, are observed between adjacent stepped chains giving 2D π-stacked sheets in the *ab* plane (Figure 4.2).

*4.1.3 Crystal structure of $[Me_2NH_2]_{1.5}[Co(4,4'\text{-}H_{5/6}dcbp)_3]\cdot 10½H_2O$ (**13**).*

Complex **13** crystallises in the trigonal *R*-3 space group and crystallographic details are shown in Table 4.2. The structure of **13** consists of $[Co(4,4'\text{-dcbp})_3]$ complexes. Within the lattice there are ten and a half water molecules, which are heavily disordered and consequently no protons were located. Additional residual peaks were still observed within the lattice, calculated as approximately 27 e.Å^{-3} with the SQUEEZE program in PLATON.[187-189] These were assigned as dimethylammonium cations (31 e.Å^{-3}). Overall there are one and a half dimethylammonium cations *per* metal complex and thus, there must be 5/6 of a proton *per* 4,4'-dcbp ligand. Thus, the formula for **13** is: $[Me_2NH_2]_{1.5}[Co(4,4'\text{-}H_{5/6}dcbp)_3]\cdot 10½H_2O$. A single metal complex with the dimethylammonium cations is shown in Figure 4.3. As is usual for tris-2,2'-bipy

complexes and derivatives, only one third of the complex is unique, the rest is related by a three-fold axis. The Co(II) centre adopts an octahedral geometry with three 4,4'-$H_{5/6}$dcbp ligands chelating through the nitrogen atoms. The bite angle of the ligand (N1-Co1-N2 81.0(1)°) gives rise to slight distortion from ideal octahedral geometry. Selected bond lengths and angles are shown in Table 4.4. The 4,4'-$H_{5/6}$dcbp is nearly planar with the carboxylate groups about C11 and C12 twisted 8.1° and 14.6°, respectively, to the aromatic ring to which they are attached. The dimethylammonium cations are disordered over two positions related by an inversion centre, as shown in Figure 4.3.

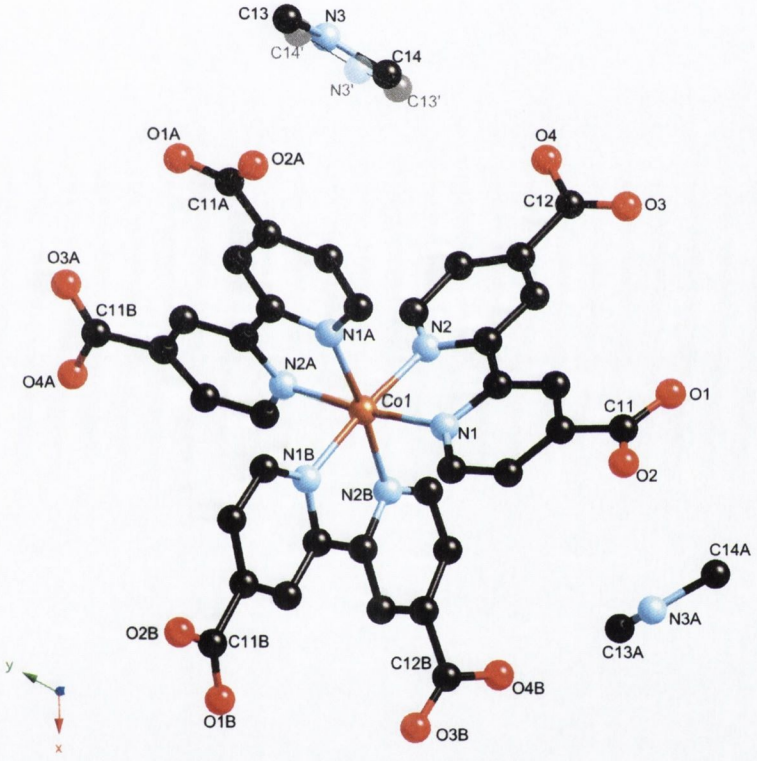

Figure 4.3 – Molecular structure and atomic labelling scheme for **13**. The translucent atoms represent disordered positions. (Lattice water molecules omitted for clarity)

Table 4.4 – Selected bond lengths (Å) and angles (°) for **13**.

Co1-N1	2.010(3)	N1-Co1-N2	81.0(1)
Co1-N2	1.993(3)	N1-Co1-N2^{i}	89.0(1)
		N2-Co1-N2^{i}	95.8(1)
		N1-Co1-N1^{i}	94.6(1)
		N1-Co1-N2^{ii}	174.6(1)

Symmetry codes: i = -y, x-y, z; ii = -x+y, -x, z.

There are ten and a half lattice water molecules in the structure of **13**. O6 and O8 are ordered and are at full occupancy. O5 is also ordered but sits on a three-fold rotation axis and is thus at one-third occupancy. The rest of the water molecules are disordered. O7 is at half-occupancy, and is disordered over six positions related by both inversion and rotation. O9, O10, O11 and O12 are at one-sixth occupancy and are disordered over two positions each, related by inversion. Since the protons were not located the hydrogen bonded network formed cannot be described in terms of donors and acceptors, but in terms of interactions. Distances between atoms participating in hydrogen bonding are given in Table 4.5. O5 participates in hydrogen bonding with three crystallographically equivalent O1 carboxylate oxygen atoms, and with another lattice water molecule, O12. O6 also participates in four hydrogen bonds: two with two crystallographically equivalent O7 lattice water molecules, a third with another lattice water molecule O8, and a fourth with a carboxylate oxygen atom, O2. In addition to hydrogen bonding with two O6 lattice water molecules, O7 also participates in hydrogen bonding with two adjacent crystallographically equivalent lattice water molecules (O7). O8 participates in three hydrogen bonds: one, as described, with lattice water molecule, O8, and another two with carboxylate oxygen atoms, O3 and O4. O9 participates in two hydrogen bonds with two lattice water molecules, O10 and O11. Lattice water molecule O10 participates in three hydrogen bonds: two with two lattice water molecules, O9 and O12, and a third with carboxylate oxygen atom, O4. O11 also participates in hydrogen bonding with O4, as well as with lattice water molecule O9. As described above, O12 participates in hydrogen bonding with lattice water molecules O10 and O5. As a consequence of the heavy disorder of the lattice water molecules, the resulting hydrogen bonded network is also disordered, therefore a detailed discussion will not be presented here.

The metal complexes stack to form a 2D layer extending along the *bc* plane, shown in Figure 4.4, with the molecular C_3 axis perpendicular to this plane and parallel to *a*. Offset face-to-face π-π interactions occur between the 4,4'-$H_{5/6}$dcbp ligands on neighbouring complexes, with a separation at closest contact of 3.696(3) Å. Both Δ and Λ isomers are present, with adjacent complexes in the 2D layer being of opposite chirality. Thus each Δ isomer is surrounded by three Λ isomers, and viceversa. This arrangement gives rise to a (6,3) net, in the voids of which lie lattice water molecules O5, O9, O10, O11 and O12. These are hydrogen bonding with each other as well as with the carboxylate groups which point directly into the cavities. Additional O5 lattice water molecules lie directly above and below the Co(II) ions (i.e. three-fold axes), and are hydrogen bonding with the carboxylate groups pointing away from the cavities.

Table 4.5 – Oxygen-oxygen/nitrogen distances (Å) for hydrogen bonding in **13**.

O1···O5	2.542(4)	O6···O7	2.80(4)
O2···O6	2.754(7)	O6···O7^{iii}	2.88(4)
O3···O8	2.741(5)	O6···O8^{iv}	2.809(8)
O4···O8^{i}	2.876(6)	O7···O7^{v}	2.87(3)
O4···O10	2.739(6)	O9···O10^{vi}	2.43(3)
O4···O11	2.753(5)	O9···O11	2.73(3)
O5···O12^{ii}	2.78(3)	O10···O12	2.97(4)
		O2···N3	3.03(1)

Symmetry codes: i = 1-y, x-y, z; ii = x-0.333333, 0.333333+y, 0.333333+z; iii = y, y-x, 1-z; iv = 0.666667-y, 0.333333+x-y, 0.333333+z; v = -y, x-y, z; vi = 1.333333-x, 0.666667-y, 0.666667-z.

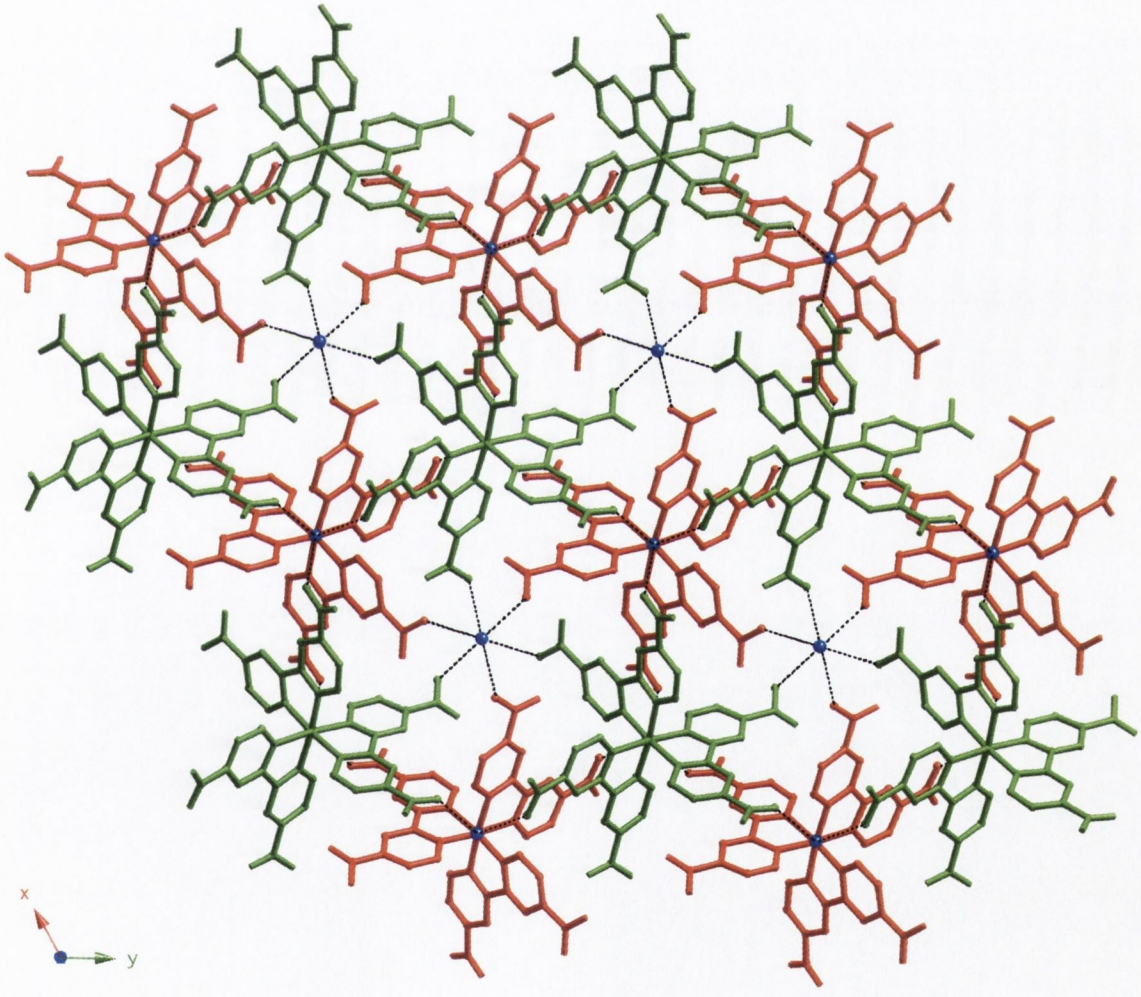

Figure 4.4 – 2D layer formed by the metal complexes in **13**. Adjacent complexes are of opposite chirality: Δ complexes are highlighted in green, while Λ complexes are shown in red. O5, O9, O10, O11 and O12 lattice water molecules (shown in blue) sit on the voids formed by the layer and are hydrogen bonding with the carboxylate groups. Hydrogen bonds are represented as dashed bonds. (Bipyridyl hydrogen atoms, O6, O7, O8 lattice water molecules and dimethylammonium cations omitted for clarity)

As shown in Figure 4.5 these layers stack along the *c* direction, separated by *ca.* 10.7 Å (~*c*/3). There are no direct interactions between the layers. Instead, extensive hydrogen bonding with the lattice waters and dimethylammonium cations links the metal complexes into a 3D network. Hydrogen bonding with lattice water molecules O5, O9, O10, O11 and O12 has been already described and so only interactions with O6, O7 and O8 lattice water molecules are shown. Consecutive layers are offset so that the metal complexes of a layer lie directly on top of the cavities of the next, and so no channels are formed within the network of **13**.

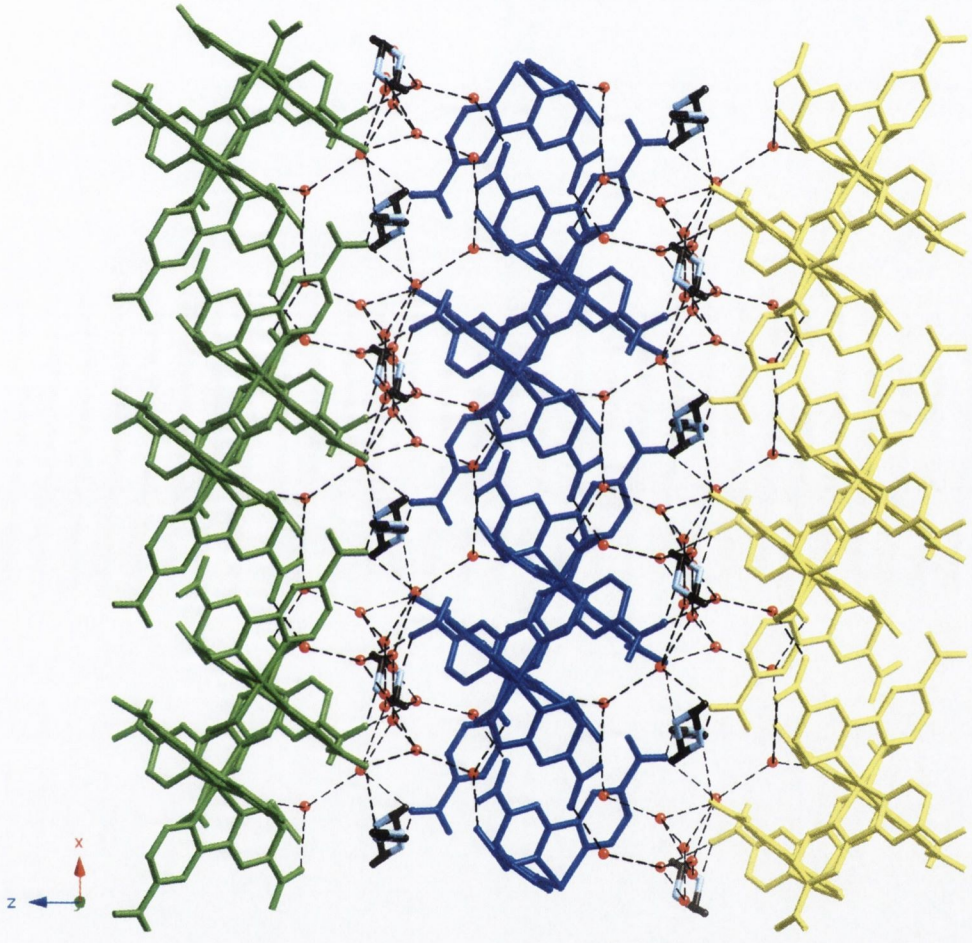

Figure 4.5 – Overall packing diagram for **13**. Three 2D layers have been highlighted. O6, O7 and O8 lattice waters shown in red. Hydrogen bonding shown as dashed bonds. (O5, O9, O10, O11 and O12 lattice water molecules omitted for clarity)

4.2 Reaction of Cu(II) with 4,4'-dicarboxy-2,2'-bipyridine.

4.2.1 Reaction of Cu(II) with 4,4'-H_2dcbp.

A H_2O/DMF mixture of $CuCl_2$ and 4,4'-H_2dcbp (1:2) was heated to 200 °C for 36 hrs, producing a dark brown solution with some brown precipitate in it. After filtering the brown solid, the remaining brown solution was left to evaporate. After a few days the solution had turned deep green, and after a week blue/green crystals grew in *ca.* 19%

yield. An infrared spectrum showed the presence of 4,4'-dcbp stretches ($\nu_{as}(CO_2^-)$ 1617, $\nu_s(CO_2^-)$ 1363 cm^{-1}) as well as amine bands ($\nu_{as}(NH_2)$ 3433 cm^{-1}, $\nu_s(NH_2)$ 3059 cm^{-1}). The presence of an amine in the compound was surprising. An X-ray diffraction study showed the complex to be $[Me_2NH_2]_2[Cu(4,4'\text{-dcbp})_2(H_2O)]\cdot 4H_2O$ (**14**), confirming the presence of an amine. The source of the dimethylammonium cation was DMF, which hydrolysed under the conditions generated in the bomb.

Carrying on from studies describe in Chapter 2 to create Cu(II) complexes of 4,4'-dcbp, $Cu(NO_3)_2$ and 4,4'-Na_2dcbp (1:2) were stirred in an aqueous solution and adjusted to pH ~9.5 with NaOH producing a blue solution from which small, blue crystals grew on evaporation in *ca.* 32% yield. An infrared spectrum showed 4,4'-dcbp stretches ($\nu_{as}(CO_2^-)$ 1610, $\nu_s(CO_2^-)$ 1377 cm^{-1}) and a strong broad band at 3326 cm^{-1}, corresponding to water. An X-Ray diffraction study showed these crystals to be a discrete coordination complex of formula $[Na_2][Cu(4,4'\text{-dcbp})_2(H_2O)]\cdot 10H_2O$ (**15**).

*4.2.2 Crystal structure of $[Me_2NH_2]_2[Cu(4,4'\text{-dcbp})_2(H_2O)]\cdot 4H_2O$ (**14**).*

The structure of **14** was refined in the monoclinic *C2/c* space group and crystallographic details are shown in Table 4.6. The structure of **14** consists of $[Cu(4,4'\text{-dcbp})_2(H_2O)]^{2-}$ units, two dimethylammonium cations and four lattice waters linked together into a 3D network. A single complex is shown in Figure 4.6. One half of the Cu(II) complex is related to the other by a two-fold rotation axis which passes through the metal centre and the coordinated water oxygen atom. The geometry around the Cu(II) centre is trigonal bipyramidal with the axial positions occupied by two crystallographically equivalent nitrogen atoms of two 4,4'-dcbp ligands, and the equatorial positions occupied by the other two 4,4'-dcbp nitrogen atoms and a coordinated water molecule. Analysis of the shape determining angles using the approach of Addison and co-workers[226] yields a τ value of 0.79 (τ = 0 for perfect square pyramidal and 1 for trigonal bipyramidal geometries). Bonding about the Cu(II) centre is as expected for trigonal bipyramidal geometry and varies with donor type and position. Slight distortion from ideal trigonal bipyramidal geometry arises from the bite angle of the 4,4'-dcbp ligand (N1-Cu1-N2 81.5(2) Å). See Table 4.7 for selected bond lengths for **14**. The 4,4'-dcbp ligand is almost planar with only slight distortion arising form the twist of the carboxylate group about C12 with respect to the aromatic ring to which it is attached (*ca.* 6.5°). The 4,4'-dcbp ligand is fully deprotonated and delocalisation results in similar C-O bond lengths about the carboxylate groups (C12-O3 1.242(6) Å, C12-O4 1.251(6) Å, C11-O1 1.255(5) Å, C11-O2 1.237(5) Å).

Table 4.6 – Crystallographic data for **14** and **15**.

Compound	**14**	**15**
Chemical Formula	$CuC_{28}H_{38}N_6O_{13}$	$CuC_{24}H_{34}N_4O_{19}Na_2$
Formula weight	730.18	792.07
Crystal system	Monoclinic	Monoclinic
Space group	*C*2/*c*	$P2_1/c$
μ (MoK_α)/ mm^{-1}	0.793	0.810
a/Å	31.13(1)	14.507(3)
b/Å	7.174(2)	7.007(2)
c/Å	14.457(5)	31.118(5)
α/°	90	90
β/°	108.528(6)	90.015(3)
γ/°	90	90
V/$Å^3$	3061(2)	3163.2(12)
Z	4	4
D_{calc}/gcm^{-3}	1.585	1.663
T/K	153(2)	153(2)
Crystal size max /mm	0.23	0.35
mid /mm	0.11	0.08
min /mm	0.01	0.05
$2\theta_{max}$/°	45.00	50.00
Min/Max trans. Factor	0.793/1.000	0.898/1.000
R_{int}	0.0865	0.0787
R_1, $wR_2[I>2\sigma(I)]$[a]	0.0598, 0.1323	0.0814, 0.1851
R_1, wR_2 (all data)	0.0859, 0.1442	0.0947, 0.1906
Reflections – collected:	10898	29738
unique:	2000	5548
observed:	1511	4777

[a] $R_1=\Sigma||F_o|-|F_c||/\Sigma|F_o|$, $wR_2=[\Sigma w(F_o^2-F_c^2)2/\Sigma w(F_o^2)^2]^{½}$

Table 4.7 – Selected bond lengths (Å) and angles (°) for **14**.

Cu1–N1	2.048(4)	N1-Cu1-N2	81.5(2)
Cu1–N2	1.971(3)	N2-Cu1-O5	87.9(1)
Cu1–O5	2.102(5)	N1-Cu1-O5	115.8(1)
		N1-Cu1-N2^{i}	100.4(2)
		N1-Cu1-N1^{i}	128.4(2)
		N2-Cu1-N2^{i}	175.9(3)

Symmetry codes: i = -x, y, 0.5-z.

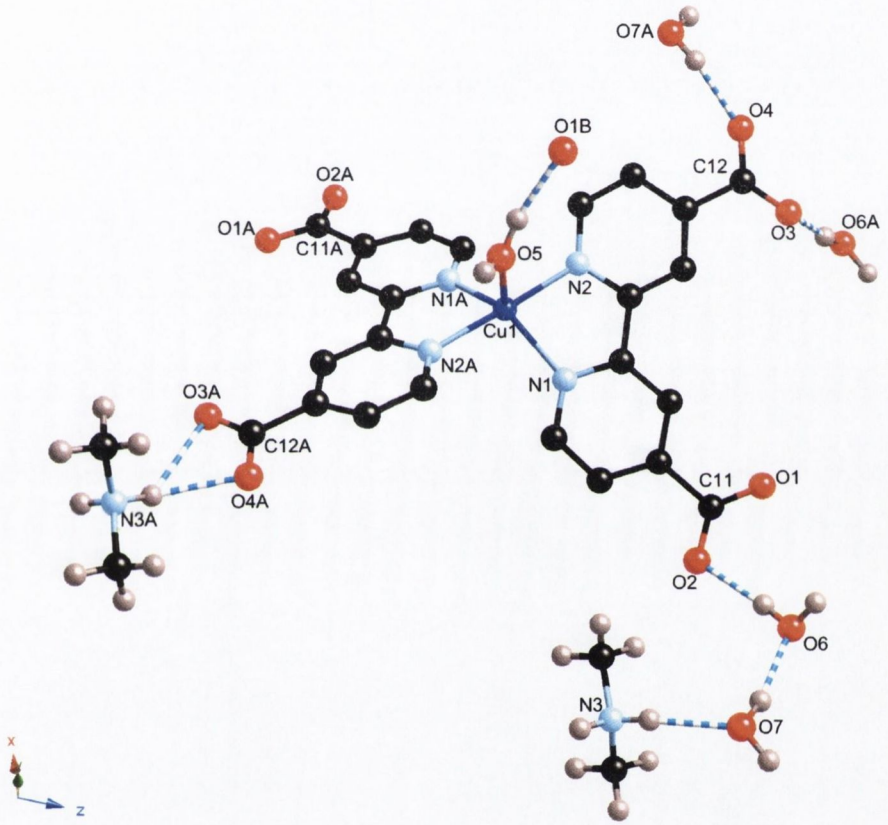

Figure 4.6 – Molecular structure and atomic labelling scheme for **14**. The eight unique hydrogen bonds are shown as blue and white dashed bonds. (Bipyridyl hydrogen atoms omitted for clarity)

There are eight unique hydrogen bonds in **14**. The coordinated lattice water molecule O5 sits on a two-fold rotation axis and since its two protons are crystallographically equivalent, it donates two hydrogen bonds to two crystallographically equivalent carboxylate oxygen atoms (O1). The two lattice water molecules, O6 and O7, both donate two hydrogen bonds and accept one. O6 donates one hydrogen bond to carboxylate oxygen O2, and another to carboxylate oxygen O3, and accepts a hydrogen bond from O7, which is also donating a hydrogen bond to carboxylate oxygen O4. The dimethylammonium cation is a hydrogen bond donor to lattice water molecule O7, and to carboxylate oxygen atoms O3 and O4. This latter is a bifurcated hydrogen bond. According to H···A distances the N3-H3B···O4 bond may be

considered the major component (H3B···O4 2.09 Å) while the N3-H3B···O3 interaction is the minor component (2.38 Å). Hydrogen bond distances and angles are shown in Table 4.8.

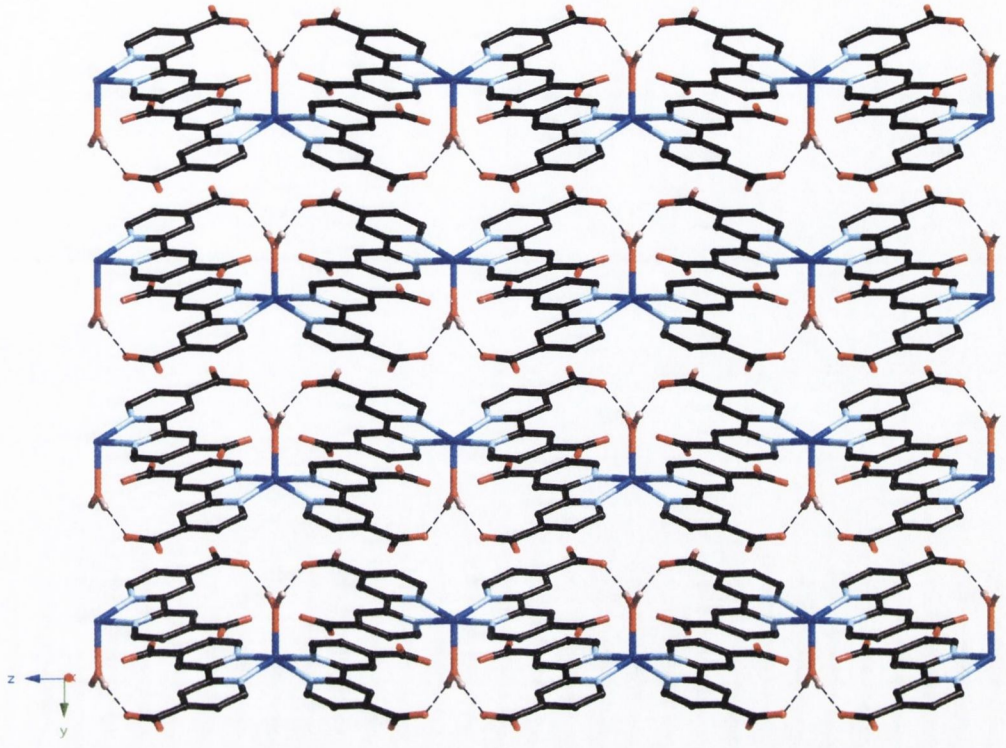

Figure 4.7 – 2D sheet formed in the structure of **14** *via* hydrogen bonding and π-π stacking interactions. View along (100). (Bipyridyl hydrogen atoms omitted for clarity)

Table 4.8 – Parameters of hydrogen bonding interactions for **14**.

D–H···A	D-H/Å	d(H···A)/Å	d(D···A)/Å	<(D–H···A)/°
O5-H5··O1^{i}	0.88	1.81	2.654(5)	160
O6-H6A···O2	0.90	1.84	2.714(5)	165
O6-H6B···O3^{ii}	0.91	1.87	2.779(6)	173
O7-H7A···O4^{iii}	0.91	1.84	2.694(7)	154
O7-H7B···O6	0.91	1.83	2.691(7)	157
N3-H3A···O7	0.92	1.95	2.827(8)	158
N3-H3B···O4^{iv}	0.92	2.09	2.823(7)	136
N3-H3B···O3^{iv}	0.92	2.38	3.145(7)	140

Symmetry codes: i = x, 1-y, 0.5+z; ii = -x, y, -0.5-z; iii = 0.5+x, y-0.5, z; iv = 0.5+x, 0.5-y, 0.5+z.

Adjacent $[Cu(4,4'\text{-dcbp})_2(H_2O)]^{2-}$ units are linked *via* hydrogen bonding between the coordinated water molecule and one of the carboxylate groups, as shown in Figure 4.7. This is reinforced by offset face-to-face π-π interactions between the pyridyl rings of adjacent complexes, with a separation at closest contact of 3.387(6) Å. This results in 'double tapes' running along the *c* direction, which are then stacked along the *b*

direction through further offset face-to-face π-π interactions between the aromatic rings of adjacent tapes to form 2D sheets, as shown in Figure 4.7 (separation at closest contact 3.249(9) Å). The metal-to-metal separation along the 1D chains is 7.384(3) Å, while that along the *b* direction in the 2D sheet is 7.174(2) Å.

The 2D layers pack along the *a* direction, separated by *ca. a*/2. In between lie the DMA cations and lattice water molecules, which link the layers into a hydrogen bonded 3D network, as shown in Figure 4.8.

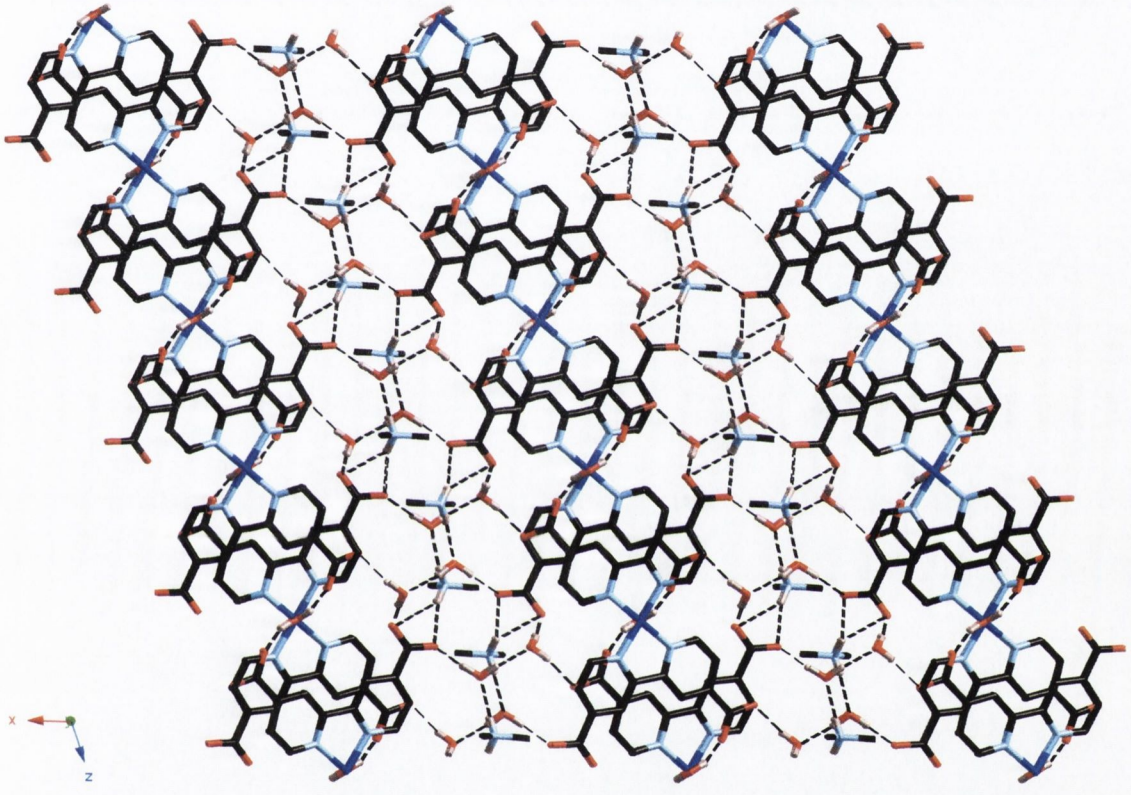

Figure 4.8 – Overall packing of **14**. View along (010). The π-stacked 2D sheets are linked to form a 3D network *via* hydrogen bonding with the lattice water molecules and DMA cations. (Bipyridyl hydrogen atoms omitted for clarity)

Each $[Cu(4,4'\text{-dcbp})_2(H_2O)]^{2-}$ unit participates in fourteen hydrogen bonds (the coordinated water molecule donates two hydrogen bonds, two of the carboxylate groups accept two hydrogen bonds while the other two accept four hydrogen bonds each). Double 'bridges' exist between each complex and two adjacent ones, accounting for four of the hydrogen bonds (O5-H5···O1). The bifurcated hydrogen bond from the dimethylammonium cation to one of the carboxylate groups (N3-H3B···O4/O3) doubly 'bridges' these, accounting for another four hydrogen bonds emanating from each complex. The remaining six 'bridges' connect to six different lattice water molecules. The crystallographically unique lattice water molecules and the dimethylammonium cation are taken as a single node, and thus the network consists of 10-connecting

nodes (metal complexes) and 4-connectors (lattice water molecules and dimethylammonium cation). Each 10-connector is joined to two other 10-connectors and to eight 4-connectors, while each 4-connector is joined to four 10-connectors.

*4.2.3 Crystal structure of $[Na_2][Cu(4,4'\text{-dcbp})_2(H_2O)].10H_2O$ (**15**).*

The structure of **15** was refined in the monoclinic $P2_1/c$ space group. Crystallographic details are shown in Table 4.6. As is common in monoclinic crystals with a β angle close to 90°, the crystals of **15** display pseudo-merohedral twinning. Thus, the twin law (100, 0-10, 00-1), i.e. two-fold rotation about *a*, was applied to the data during refinement, greatly improving the model (R_1 = 0.0814). The molecular structure and atomic labelling scheme for **15** are shown in Figure 4.9. The structure of **15** is somewhat similar to that of **14**, in that it consists of $[Cu(4,4'\text{-dcbp})_2(H_2O)]^{2-}$ units, however, in **15** sodium ions provide the charge balance (*cf.* dimethylammonium cations for **14**). Additionally the whole $[Cu(4,4'\text{-dcbp})_2(H_2O)]$ units in **15** are unique, while in **14** half of the unit is related to the other by two-fold rotation, and thus **15** has lower symmetry than **14**.

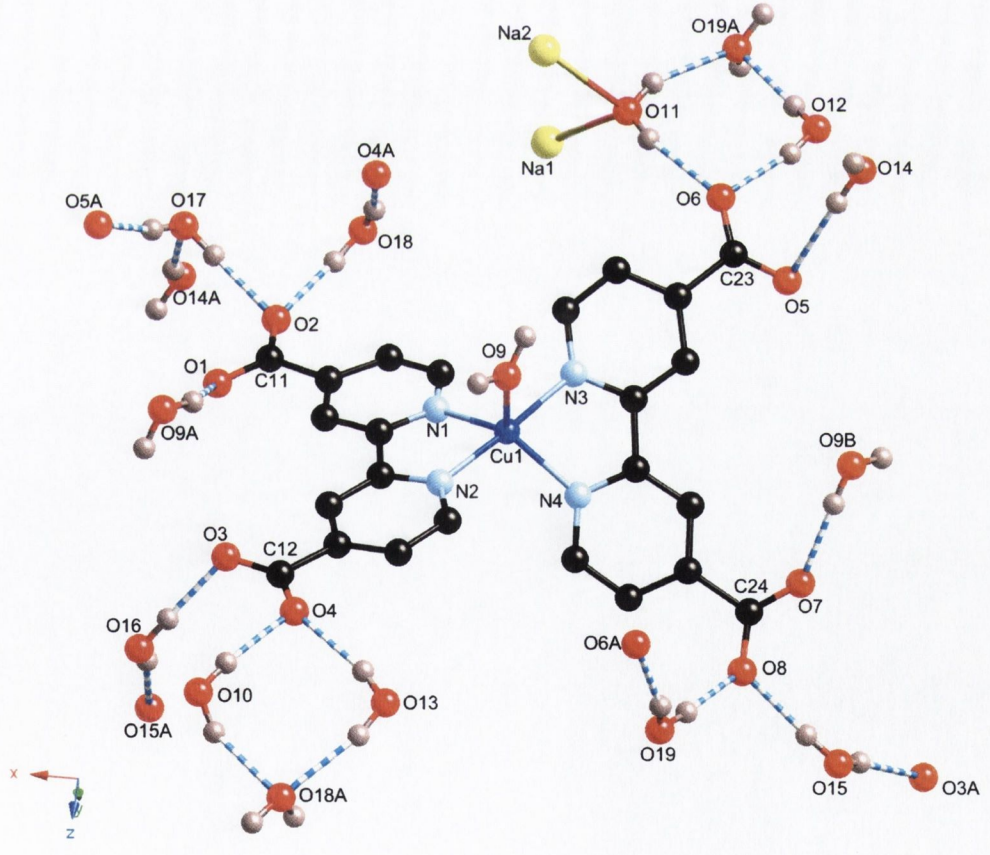

Figure 4.9 – Molecular structure and atomic labelling scheme for **15**. The blue and white dashed bonds depict the unique hydrogen bonds. (Bipyridyl hydrogens omitted for clarity)

Table 4.9 – Selected bond lengths (Å) and angles (°) for **15**.

Cu1-N1	2.023(7)	N1-Cu1-N2	80.9(3)
Cu1-N2	1.962(6)	N3-Cu1-N4	81.1(3)
Cu1-N3	1.955(7)	N1-Cu1-N3	102.0(3)
Cu1-N4	2.028(7)	N2-Cu1-N4	102.0(3)
Cu1-O9	2.086(5)	N1-Cu1-N4	130.9(3)
Na1-O10	2.356(8)	N2-Cu1-N3	173.0(3)
Na1-O11	2.523(8)	N4-Cu1-O9	115.3(3)
Na1-O12	2.368(7)	N2-Cu1-O9	88.0(3)
Na1-O13	2.492(8)	N3-Cu1-O9	85.0(3)
Na1-O14	2.335(6)	N1-Cu1-O9	113.8(3)
Na1-O15	2.394(6)		
Na2-O10	2.358(8)		
Na2-O11	2.451(8)		
Na2-O12^{i}	2.346(8)		
Na2-O13^{i}	2.490(8)		
Na2-O16	2.365(6)		
Na2-O17	2.427(6)		

Symmetry codes: i = x, y-1, z.

The geometry around the metal ion in **15** is trigonal bipyramidal with the equatorial positions occupied by the nitrogen atoms of two 4,4'-dcbp ligands and the oxygen atom of the coordinated water molecule. The axial positions are occupied by the other two nitrogen atoms of the 4,4'-dcbp ligands. Analysis of the shape determining angles using the approach of Addison and co-workers[226] yields a τ value of 0.70. This is slightly less than the value obtained for **14** (0.79), which indicates that the geometry around the Cu(II) ion in **15** is shifted more towards square pyramidal when compared to that in **14**, but is still clearly a trigonal bipyramid (τ = 0 for perfect square pyramidal and 1 for trigonal bipyramidal geometries). Bonding about the Cu(II) centre is as expected for trigonal bipyramidal geometry and varies with donor type and position. Selected bond lengths and angles for **15** are shown in Table 4.9. Slight distortion from ideal trigonal bipyramidal geometry arises from the bite angle of the 4,4'-dcbp ligands (N1-Cu1-N2 80.9(3) Å, N3-Cu1-N4 81.1(3) Å)).

As in **14**, the 4,4'-dcbp ligands in **15** are almost planar with only slight distortion arising from the twist of the carboxylate groups with respect to the aromatic ring to which they are attached. The carboxylate groups about C11 and C12 are twisted 7.1° and 7.7° respectively, while those about C23 and C24 are more planar, only twisted 3.7° and 2.4° respectively. As expected, delocalisation results in similar C-O bond

lengths about the carboxylate groups (C11-O1 1.244(9) Å, C11-O2 1.251(8) Å, C12-O3 1.232(8) Å, C12-O4 1.262(8) Å, C23-O5 1.262(8) Å, C23-O6 1.242(8) Å, C24-O7 1.244(9) Å, C24-O8 1.262(8) Å).

There are ten unique lattice water molecules in **15** in addition to the coordinated water molecule already mentioned. Thus, extensive hydrogen bonding occurs within the structure. The twenty-two unique hydrogen bonds are shown in Figure 4.9, with donor-acceptor distances shown in Table 4.10. The coordinated water molecule, O9, is a hydrogen bond donor to carboxylate oxygens O1 and O7. The remaining lattice water molecules all donate two hydrogen bonds each. O10 donates a hydrogen bond to a carboxylate oxygen atom, O4, and to another lattice water molecule, O18. O11 and O12 donate each one hydrogen bond to carboxylate oxygen atom O6, and another to lattice water molecule, O19. O13 also donates a hydrogen bond to a carboxylate oxygen atom, O4, and a second to another lattice water molecule, O18. O14 is a hydrogen bond donor to carboxylate oxygen atom O5, and to lattice water molecule O17. O15 is a hydrogen bond donor to two carboxylate oxygen atoms, O3 and O8. O16 donates a hydrogen bond to a carboxylate oxygen atom, O3, and to a lattice water molecule, O15. The remaining water molecules donate each two hydrogen bonds to two carboxylate oxygen atoms. O17 is a hydrogen bond donor to O2 and O5, while O18 donates one hydrogen bond to O2 and another to O4. O19 is a hydrogen bond donor to O6 and O8.

The $[Cu(4,4'\text{-dcbp})_2(H_2O)]^{2-}$ units effectively pack in the same way as those in **14**. Adjacent metal complexes are linked *via* hydrogen bonding between the coordinated water molecule and two carboxylate groups (O9···O1, O9···O7). This is reinforced by offset face-to-face π-π stacking of the 4,4'-dcbp ligands on adjacent units, with a separation at closest contact of 3.23(1) Å for the N1 and N2 containing ligands, and 3.39(1) Å for the N3 and N4 containing ligands. These 'double tapes' extend along the *a* direction (*cf. c* for **14**), and form a 2D sheet along the *ab* plane through further offset face-to-face π-π stacking of the 4,4'-dcbp ligands, with a separation at closest contact of 3.16(2) Å for the N1 and N2 containing ligands and 3.22(2) Å for the N3 and N4 containing ligands (Figure 4.10). The metal-to-metal distance along the chains is 7.462(3) Å, slightly more than that in **14** (7.384(3) Å), while the metal-to-metal distance of adjacent chains along the sheet is 7.007(2) Å, shorter than in **14** (7.174(2) Å).

Table 4.10 – Donor-Acceptor distances (Å) for hydrogen bonding in **15**.

O9···O1^{i}	2.680(8)	O14···O17	2.834(9)
O9···O7^{ii}	2.754(8)	O14···O5^{v}	3.116(9)
O10···O4^{i}	2.774(8)	O15···O3^{i}	3.075(8)
O10···O18^{iii}	2.843(9)	O15···O8^{vii}	2.795(8)
O11···O6	3.060(8)	O16···O3^{i}	2.753(8)
O11···O19^{iv}	2.899(8)	O16···O15^{viii}	3.097(8)
O12···O6^{v}	2.780(7)	O17···O2^{iii}	2.782(8)
O12···O19	2.773(8)	O17···O5^{iv}	2.772(9)
O13···O4^{vi}	2.932(8)	O18···O4^{i}	2.949(9)
O13···O18	2.958(8)	O18···O2	2.773(7)
		O19···O8^{vii}	2.759(8)
		O19···O6^{ix}	2.728(8)

Symmetry codes: i = -x, -y, -z; ii = 1-x, -y, -z; iii = -x, y-0.5, 0.5-z; iv = 1-x, y-0.5, 0.5-z; v = 1-x, 0.5+y, 0.5-z; vi = x, 0.5-y, 0.5+z; vii = 1-x, 1-y, -z; viii = x, y-1, z; ix = x, y+1, z.

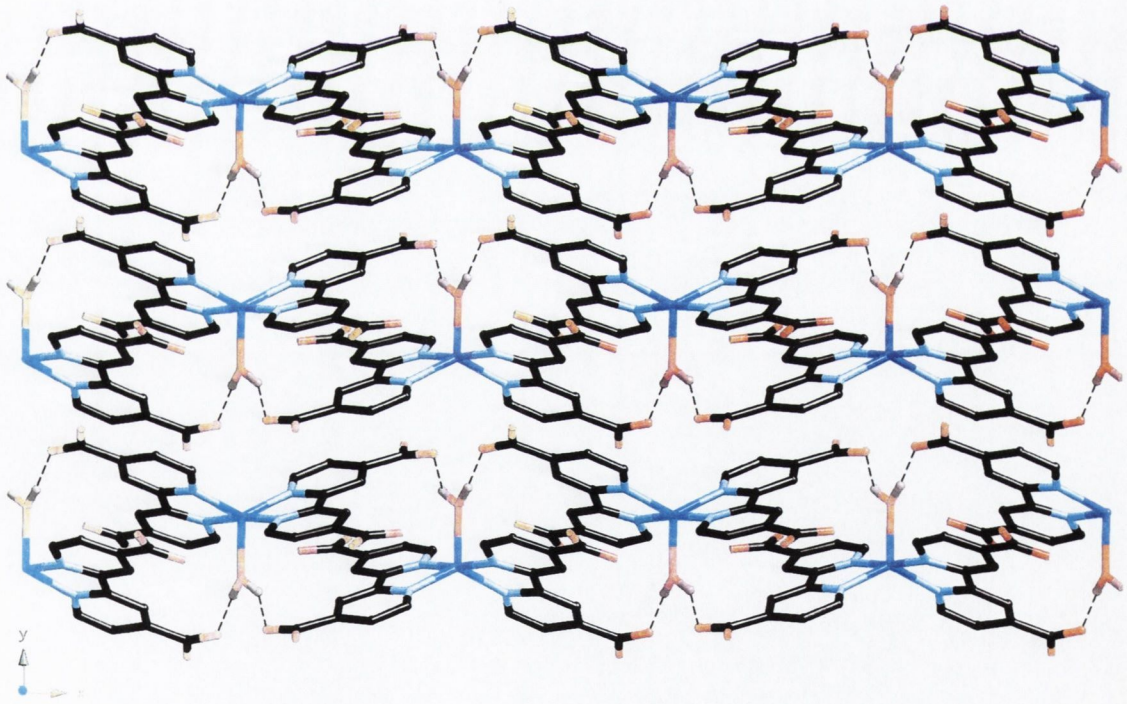

Figure 4.10 - 2D sheet formed in **15** *via* hydrogen bonding and π-π stacking of the metal complexes. (Bipyridyl hydrogen atoms omitted for clarity)

There are two unique sodium cations providing the balance charge within the lattice in **15**. Eight of the lattice water molecules are coordinating to the sodium ions, creating a 1D array of hexacoordinated sodium ions extending along the crystallographic *b* direction, as shown in Figure 4.11. Bond lengths are shown in Table 4.9. Within these chains, intramolecular hydrogen bonding occurs between O15 and O16, and between O14 and O17 water molecules.

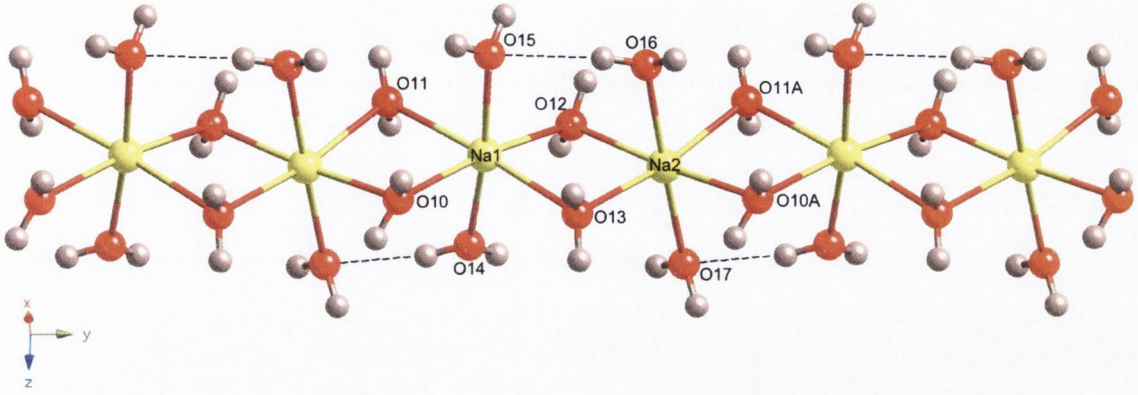

Figure 4.11 – 1D array of hexacoordinated sodium ions and lattice water molecules formed in **15**. Intramolecular hydrogen bonds within the chain are shown as dashed bonds.

Overall the $[Cu(4,4'\text{-dcbp})_2(H_2O)]^{2-}$ complexes participate in eighteen hydrogen bonds each (the coordinated water molecule donates two hydrogen bonds, the carboxylate groups about C12 and C23 accept five each, while those about C11 and C24 accept three each). As in **14**, double 'bridges' exist between each complex and two adjacents ones, accounting for four hydrogen bonds (O9···O1, O9···O7), which form the 1D chains already described. The remaining fourteen hydrogen bonds link the metal complexes with the sodium-lattice water array forming a 3D network, in which alternate layers of metal complexes and sodium/lattice water molecules are formed, as shown in Figure 4.12. The overall packing of **15** is very similar to that of **14**, with the 2D sheets separated by *ca. c*/2 (*cf. a*/2 for **14**).

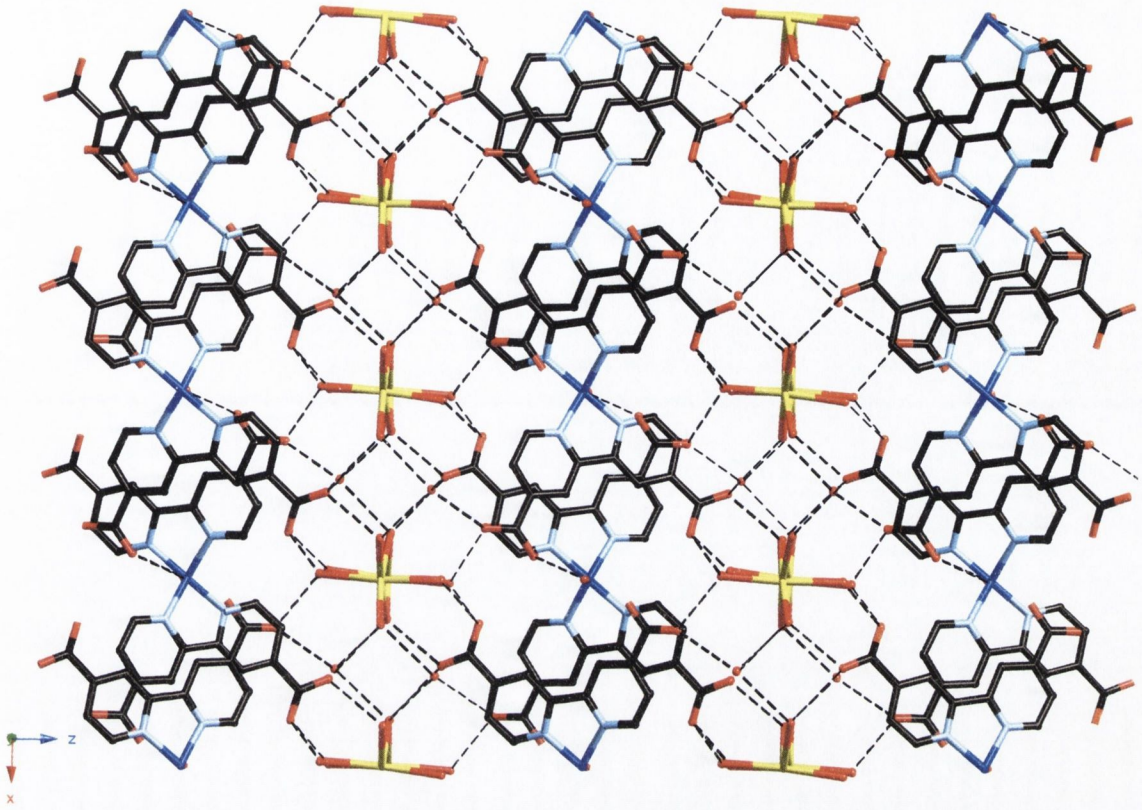

Figure 4.12 – Overall packing in **15**. The 2D sheets formed by the $[Cu(4,4'\text{-dcbp})_2(H_2O)]^{2-}$ units are linked into a 3D network *via* hydrogen bonding with the lattice water molecules. The 1D chains formed by the sodium cations and lattice water molecules are running into the page. (Hydrogen atoms omitted for clarity. Hydrogen bonds shown as dashed bonds)

4.3 Conclusions

Several new metal complexes of 4,4'-dcbp have been formed and assembled into 3D networks *via* hydrogen bonding interactions. Discrete metal complexes of 4,4'-dcbp can be synthesized using conventional methods (reflux, stirring, etc.), by adjusting the pH of the reactions. **12** and **15** were synthesized in this manner by performing the reaction under basic conditions, thus deprotonating the ligand and consequently making it soluble in water. However, by the use of hydrothermal techniques **13** could be isolated, which wasn't possible using conventional techniques. Additionally, the harsh conditions created in the bomb hydrolyzed DMF to produce the dimethylammonium cations present in **13** and **14**. In **12**, **14** and **15** the 4,4'-dcbp ligand is fully deprotonated. Thus, direct hydrogen bonding between the metal complexes only occurs through interactions between the coordinated water molecules and the carboxylate groups. In **14**, the 4,4'-dcbp ligand is partially protonated, i.e. 5/6 of a proton *per* ligand, however these are disordered and thus no direct interactions between the carboxylate groups are observed. As has been seen for other bipyridine complexes, **12**,

13, **14** and **15** form layered arrangements, in which the metal complexes are π-stacked to form 2D sheets, in between which lie the solvent molecules and counterions.

The neutral, mono-4,4'-dcbp Co(II) complex, **12**, forms 2D layers by hydrogen bonding and π-stacking, linked by the lattice water molecules into a 3D network. The tris-4,4'-dcbp Co(II) complex (**13**), however, forms 2D sheets, held solely by π-stacking interactions, which are then linked into a 3D network *via* hydrogen bonding with the lattice water molecules and the dimethylammonium counterions.

The networks in **14** and **15** are very similar and consist of layers of $[Cu(4,4'\text{-dcbp})_2(H_2O)]^{2-}$ units hydrogen bonded into a 3D network. While in different amounts, both **14** and **15** have water molecules in the voids between the metal complex layers, however in **14** dimethylammonium cations are also present while in **15** it is sodium ions that occupy this space. Additionally in **15**, a 1D array of hexaaquocoordinated sodium cations is formed. Thus **14** and **15** differ in the number of hydrogen bond connections, but effectively have the same overall packing pattern of alternate layers of $[Cu(4,4'\text{-dcbp})_2(H_2O)]$ units and lattice molecules, with the metal complex layers separated by *a*/2 in **14** and *c*/2 in **15**.

As mentioned in Chapter 1, one of the advantages of using carboxylic acid ligands, such as 4,4'-H_2dcbp, for the formation of hydrogen bonded arrays of metal complexes is the potential formation of the strong carboxylic acid-carboxylate pair. In the complexes synthesized above the ligand is fully deprotonated and thus such an interaction cannot take place. However, by controlling the pH of the reactions the degree of protonation can be fine-tuned. For example if in **14** and **15** only half of the ligand was to be deprotonated, a neutral complex would be formed, thus avoiding the need of counterions, and allowing for the direct interaction of the carboxy functionalities. However, this brings back the problem of solubility of the 4,4'-H_2dcbp ligand, and thus an equilibrium would need to be found for an optimum reaction.

Chapter Five

Synthesis and Characterization of 4,4'-substituted-2,2'-bipyridines and some of their Derivatives.

5.1 Synthesis, crystallization and characterization of 4,4'-dicarboxy-2,2'-bipyridine and some of its salts.

Preamble

The initial aim of this thesis was the formation of transition metal complexes of 4,4'-H_2dcbp and the study of their properties. The most significant results have just been described in previous chapters. However, as part of some of the reactions carried out with this purpose in mind, a series of organic 4,4'-H_2dcbp derivatives were also obtained. The crystallization of some of these had been deliberately attempted before, without any successful results. This reflects how serendipity also plays a part in crystal engineering. While most of the following organic solids were obtained as by-products of sometimes completely unrelated reactions, their structures are all part of the same family (4,4'-H_2dcbp) and will all be presented in this chapter.

5.1.1 Synthesis and crystallization of 4,4'-H_2dcbp.

4,4'-H_2dcbp was prepared by dichromate oxidation of 4,4'-dimethyl-2,2'-bipyridine according to a previously reported method.[227] The insolubility of 4,4'-H_2dcbp in common organic solvents prevented its recrystallization from traditional methods. In an attempt to prepare [Fe(4,4'-H_2dcbp)$_3$]Cl_2, $FeCl_2$ and 4,4'-H_2dcbp (1:3) were reacted hydrothermally in a H_2O/HCl mixture (2:1) to 200°C for 3½ hrs, following the previously reported synthetic route to [Ru(4,4'-H_2dcbp)$_3$]Cl_2.[174] This produced long, colourless needles. An X-ray diffraction study revealed these to be the 'free' ligand with no iron complex being formed. Bernardelli and co-workers[228] reported that α-diimine complexes such as [Fe(diethyl-2,2'-bipyridine-5,5'-dicarboxylate)$_3$]$^{2+}$ and [Fe(phen)$_3$]$^{2+}$ were found to rapidly decompose under acidic conditions. Hence, it is perhaps not surprising that no Fe(II)-4,4'-H_2dcbp species were isolated.

In an effort to directly prepare the free ligand, hydrothermal reaction of 4,4'-H_2dcbp in H_2O/HCl mixture was performed and while crystals were produced, these were smaller and fewer than those obtained in the presence of iron salts. This may suggest that the iron salts, while not incorporated within the structure, aid the crystallisation of 4,4'-H_2dcbp.

*5.1.2 Crystal structure of 4,4'-H_2dcbp (**16**).*

Isonicotinic acid can be considered the 'progenitor' of 4,4'-H_2dcbp, and thus the solid-state structure of both would be expected to be related. The structure of the isonicotinic acid consists of head-to-tail (O-H···N) hydrogen bonded linear tapes. The adjacent hydrogen bonded chains participate in π-π interactions and are anti-parallel to

each other. The head-to-tail arrangement results because the best donor (carboxylic acid) and the best acceptor (pyridine nitrogen atom) form a short intermolecular hydrogen bond. A similar interaction is also found within the solid-state structure of nicotinic acid,[230] although in this instance a zig-zag tape results because of the *meta*-substitution (*cf. para*-substitution in isonicotinic acid). This association therefore may be considered predictable, and has been taken advantage of in the crystal engineering of designed solids. In addition to this, the solid-state structures of simple 2,2'-bipyridine and its derivatives are all in the *anti* conformation. Therefore, anticipated structures of 4,4'-H_2dcbp would consist of the 2,2'-bipyridine moiety in an *anti* conformation, accompanied by head-to-tail hydrogen bonding between adjacent carboxylic OH and bipyridyl nitrogen atoms.

4,4'-H_2dcbp crystallizes in the monoclinic *Cc* space group. Crystallographic data are shown in Table 5.2. The atomic numbering scheme and atom connectivity for **16** are shown in Figure 5.1. The two pyridyl rings within 4,4'-H_2dcbp are twisted with respect to each other at an angle of approximately 30° from the *anti* conformation, which confers a handedness upon the molecule. Additionally, the carboxylic acid group about C11 is essentially coplanar with the aromatic ring to which it is attached (*ca.* 3° torsion angle) whilst the other about C12 forms an angle of approximately 20°. This further distorts the symmetry of the molecule.

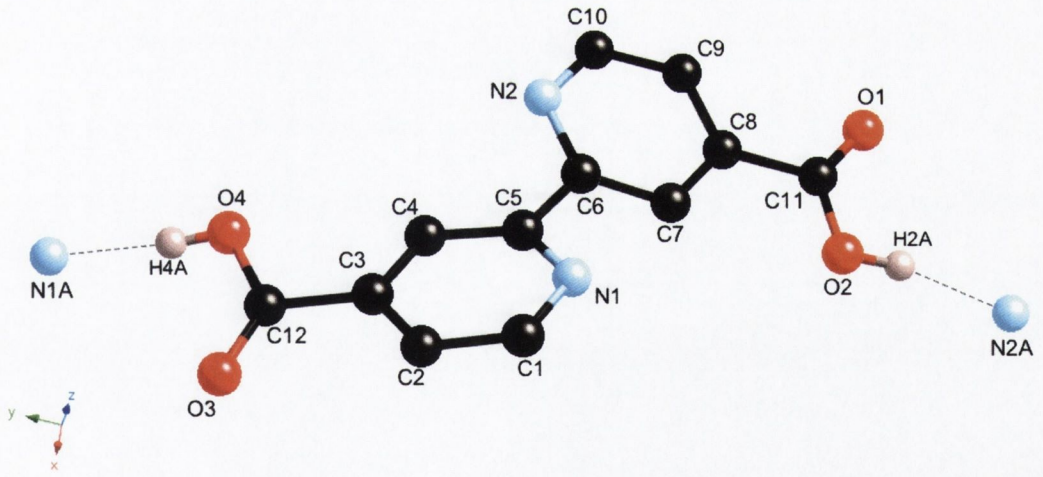

Figure 5.1 – Molecular structure and atomic numbering scheme for **16**. The dotted lines depict the unique conventional hydrogen bonds. (Bipyridyl hydrogen atoms omitted for clarity)

The overall structure of 4,4'-H_2dcbp consists of (4,4) 2D hydrogen bonded sheets as shown in Figure 5.2. Each molecule acts as a 4-connector with carboxylate OH groups forming hydrogen bonds to pyridyl nitrogens (O2···N2, O4···N1). All molecules within a single sheet have the same handedness. Equivalent isonicotinic acid sub-units, *i.e.* crystallographically equivalent halves of the 4,4'-H_2dcbp molecules,

reside on the same side of a sheet and hence participate in hydrogen bonding and face-to-face π-π interactions (closest contact of 3.404(4) Å) with like isonicotinic acid sub-units. Hence, each 2D sheet exists as a bilayer containing two sets of parallel hydrogen bonded chains, which are inclined to each other at an angle of 28°. This angle approximately corresponds with the twist in the 4,4'-H_2dcbp molecules from the *anti* conformation. Each pair of adjacent stacks of the 4,4'-H_2dcbp molecules also form hydrogen-bonded helices within each 2D layer that spiral down the crystallographic *a* axis.

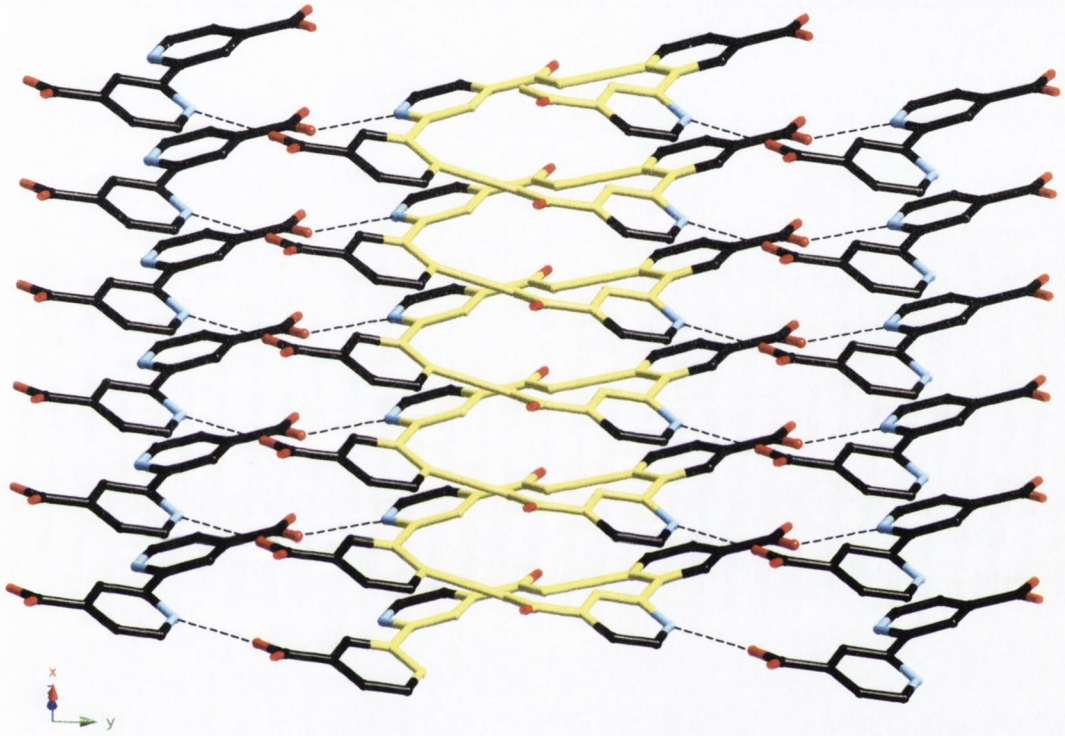

Figure 5.2 - A single (4,4) 2D hydrogen bonded sheet in **16**. A single helix is highlighted in yellow. Hydrogen bonding within the highlighted helix is represented by solid bonds. (Hydrogen atoms omitted for clarity)

Table 5.1 – Parameters of hydrogen bonding interactions for **16**.

D–H···A	D-H/Å	d(H···A)/Å	d(D···A)/Å	<(D–H···A)/°
O2-H2A···N2^{i}	0.88	1.79	2.646(3)	166
O4-H4A···N1^{ii}	0.86	1.81	2.669(3)	175
C2-H2···O1^{iii}	0.95	2.56	3.170(4)	122
C4-H4···O2^{iv}	0.95	2.43	3.153(3)	133
C7-H7···O4^{v}	0.95	2.57	3.106(4)	116
C9-H9···O3^{vi}	0.95	2.59	3.235(4)	126

Symmetry codes: i = 0.5+x, y-0.5, z; ii = 0.5+x, 0.5+y, z; iii = 0.5+x, 0.5-y, z-0.5; iv = x-0.5, 0.5+y, z; v = x-0.5, y-0.5, z; vi = x-1, 1-y, 0.5+z.

Table 5.2 - Crystallographic data for **16** and **17**.

Compound	**16**	**17**
Chemical Formula	$C_{12}H_8N_2O_4$	$C_{12}H_9N_2O_4Cl$
Formula weight	244.20	280.66
Crystal system	Monoclinic	Triclinic
Space group	*Cc*	*P*-1
μ (MoK_α)/ mm^{-1}	0.126	0.347
a/Å	3.625(1)	7.3104(5)
b/Å	14.644(5)	7.5438(5)
c/Å	18.649(7)	10.9411(7)
α/°	90	107.759(1)
β/°	91.199(5)	94.803(1)
γ/°	90	91.697(1)
V/$Å^3$	989.8(6)	571.64(7)
Z	4	2
D_{calc}/gcm^{-3}	1.639	1.631
T/K	173(2)	153(2)
Crystal size max/ mm	0.40	0.33
mid/ mm	0.15	0.13
min/ mm	0.10	0.05
$2\theta_{max}$/°	46.6	54.94
Min/Max trans. Factor	0.833/1.000	0.806/1.000
R_{int}	0.0380	0.0153
R_1, $wR_2[I>2\sigma(I)]$[a]	0.0329, 0.0718	0.0378, 0.0960
R_1, wR_2 (all data)	0.0370, 0.0745	0.0425, 0.0990
Reflections – collected:	4020	5534
unique:	1396	2614
observed:	1300	2373

[a] $R_1 = \Sigma||F_o| - |F_c||/\Sigma|F_o|$, $wR_2 = [\Sigma w(F_o^2 - F_c^2)^2/\Sigma w(F_o^2)^2]^{1/2}$

Since each 2D sheet contains molecules of the same chirality, all helices within a sheet likewise have the same chirality. Alternate layers within the structure contain helices of opposite chirality resulting in an AB type packing of the layers, Figure 5.3. The structure is nonetheless non-centrosymmetric since layers of alternate chirality are related by glide planes rather than inversion centres. Further intermolecular close contacts are observed between the aromatic protons and carboxylic oxygen atoms both within (C4-H4···O2 and C7-H7···O4) and between (C2-H2···O1 and C9-H9···O3) the 2D layers, the latter linking the sheets into the third dimension. Full details of all hydrogen bonding interactions are given in Table 5.1.

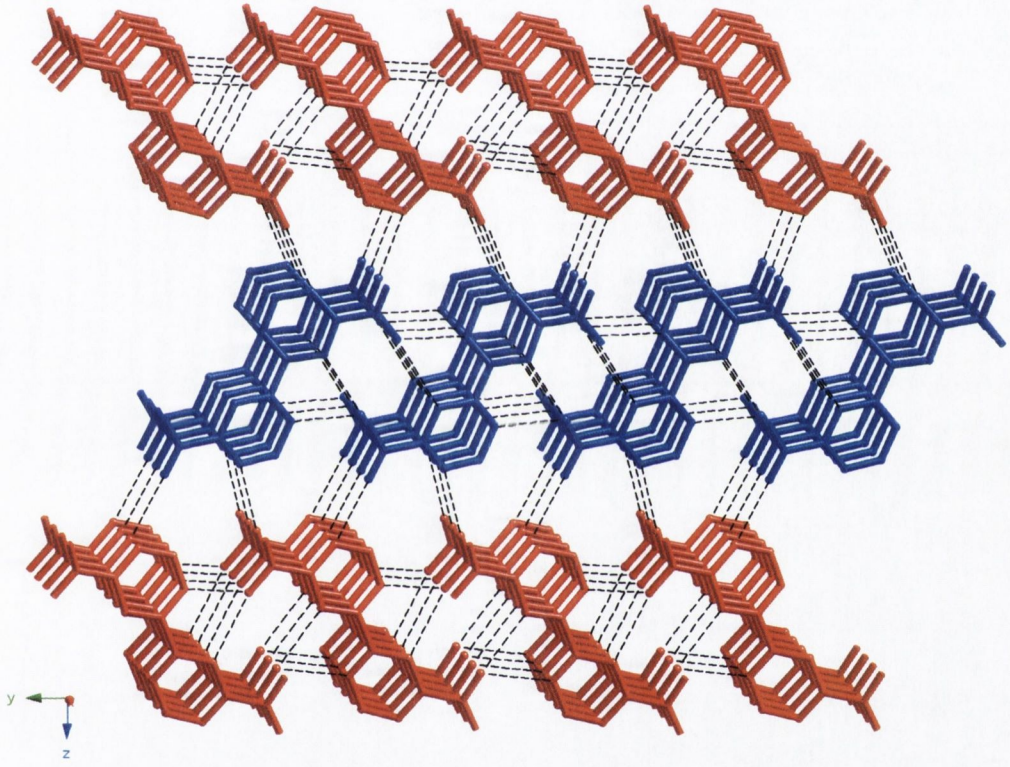

Figure 5.3 - The AB packing of the 2D sheets in **16**. Alternate layers are of opposite chirality (red layers contain right handed helices). Both weak and strong hydrogen bonds are shown as dashed bonds.

5.1.3 Synthesis and crystallization of (4,4'-H_3dcbp)(Cl).

On carrying out decarboxylation studies of 4,4'-H_2dcbp the ammonium salt of 4,4'-dcbp was reacted hydrothermally in a H_2O/HCl (1:2) mixture to 240 °C for 3hrs[231] directly yielding colorless needles. On visual inspection these looked like those of 4,4'-H_2dcbp, but an X-Ray diffraction study determined them to be (4,4'-H_3dcbp)(Cl). While hydrothermal reaction with H_2O/HCl (2:1) at 200°C yielded 4,4'-H_2dcbp, as just explained, in this case the higher concentration of acid protonated 4,4'-H_2dcbp to yield its chloride salt.

*5.1.4 Crystal structure of (4,4'-H_3dcbp)(Cl) (**17**).*

17 crystallizes in the triclinic *P*-1 space group. Crystallographic details are shown in Table 5.2. The 4,4'-H_2dcbp molecule is protonated at the N2 bipyridyl nitrogen atom yielding the 4,4'-H_3dcbp cation, with a chloride as the anion (Figure 5.4). In contrast to all the other structures containing 4,4'-(H_2)dcbp, the pyridyl rings are in the *syn* conformation. The structure of the related (6,6'-H_3dcbp)(Cl) has been previously reported and the 6,6'-H_3dcbp cation also adopts the *syn* conformation.[232] For 2,2'-bipyridine and its derivatives the *anti* conformation is more stable than the *syn* conformation as it avoids electronic repulsion between the nitrogen lone pairs. However, when one of the nitrogen atoms donates its electron pair to a hydrogen atom to produce 2,2'-bipyridinium cations, the *syn* conformation is now free of electronic repulsion. Moreover, it can be said that the *syn* conformation is further stabilized by N-H···N interactions. The 4,4'-H_3dcbp cation adopts an almost planar conformation with only a small torsion angle of 7° between the pyridyl rings and with the carboxylate groups nearly coplanar with the aromatic rings to which they are attached (twisted at approximately 2° about C11 and C12). As expected for carboxylic acid groups, C-O bond lengths differ for the hydroxyl (C11-O2 1.309(2) Å, C12-O4 1.320(2) Å) and carbonyl oxygen atoms (C11-O1 1.215(2) Å, C12-O3 1.201(2) Å).

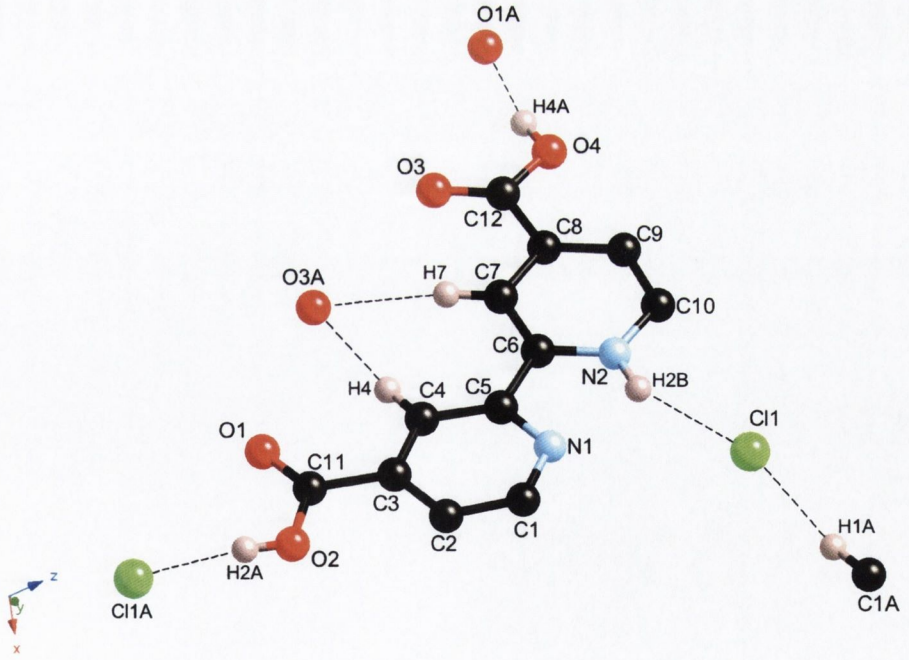

Figure 5.4 – Molecular structure and atomic labelling scheme in **17**. Hydrogen bonds are represented as dashed bonds. Note the *syn* conformation of the 4,4'-H_3dcbp cation. (Hydrogen atoms not participating in hydrogen bonding omitted for clarity)

Table 5.3 – Parameters of hydrogen bonding interactions in **17**.

D–H···A	D-H/Å	d(H···A)/Å	d(D···A)/Å	<(D–H···A)/°
O2-H2A···Cl1^{i}	0.84	2.05	2.880(1)	167
N2-H2B···Cl1	0.88	2.28	3.056(1)	147
O4-H4A···O1^{ii}	0.84	1.85	2.680(2)	168
C1-H1···Cl1^{iii}	0.95	2.66	3.597(2)	171
C4-H4···O3^{ii}	0.95	2.38	3.326(2)	174
C7-H7···O3^{ii}	0.95	2.34	3.278(2)	171

Symmetry codes: i = x, y+1, z+1; ii = 2-x, 1-y, 1-z; iii = -x, 1-y, -z.

There are six unique hydrogen bonds in the structure of **17**, shown in Figure 5.4. The protonated bipyridyl nitrogen atom, N2 donates a hydrogen bond to the chloride anion (Cl1) as does one of the carboxylate OH groups (O2). The other carboxylate OH group (O4) forms a hydrogen bond with the carbonyl oxygen of the other carboxylic group (O1). Weaker hydrogen bonds also exist. Aromatic carbon C1, donates a hydrogen bond to the chloride anion (Cl1). Two other aromatic carbons, C4 and C7, both donate a hydrogen bond each to an adjacent carbonyl oxygen atom, O3.

The three strongest hydrogen bonds link the 4,4'-H_3dcbp molecules to form a 1D ladder, as shown in Figure 5.5. The O4-H4A···O1 catemeric interaction gives rise to 4,4'-H_3dcbp hydrogen bonded 'dimers', forming a centrosymmetric $R_2^2(22)$ motif. Further C-H···O interactions between these 4,4'-H_3dcbp dimers give rise to other cyclic systems. The C4-H4···O3 interaction also forms centrosymmetric $R_2^2(10)$ rings; this interaction combined with the C7-H7···O3 interaction forms $R_2^1(7)$ rings; the latter interaction combined with the O4-H4···O1 interaction gives rise to $R_2^2(9)$ rings. These 4,4'-H_3dcbp dimers are then bridged by chloride anions to form a ladder. N2-H2B···Cl1 and the O2-H2A···Cl1 interactions produce a centrosymmetric $R_6^4(26)$ ring, which bridges the dimers. The graph sets are shown in Figure 5.5.

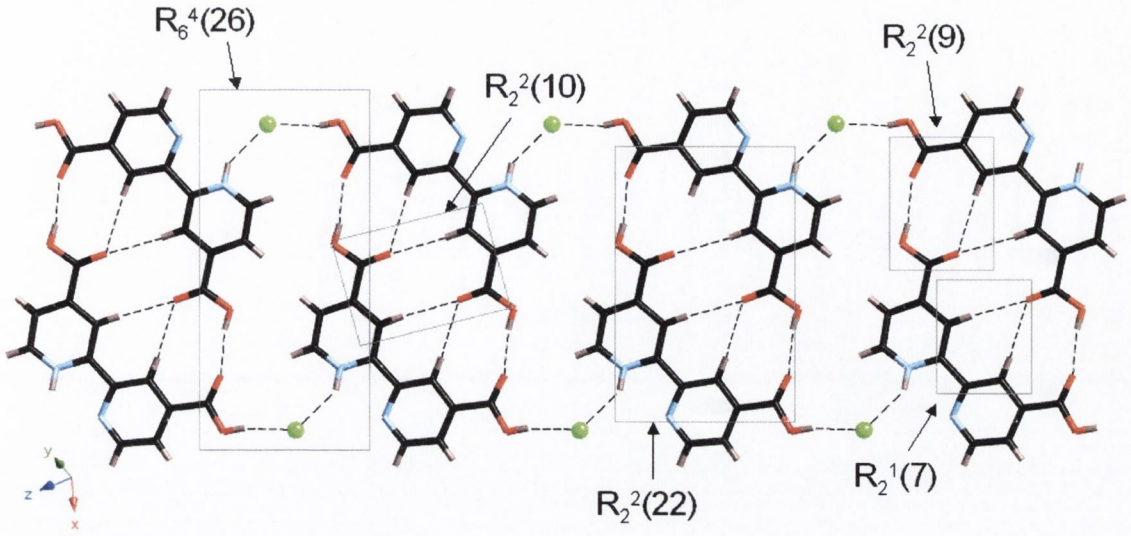

Figure 5.5 – Hydrogen bonded ladder formed in **17** showing some of the graph sets formed.

The 1D ladders are then hydrogen bonded into a 2D sheet through C-H···Cl interactions (Figure 5.6). This interaction gives rise to two hydrogen bonded rings between the ladders. The C1-H1···Cl1 interaction in combination with the N2-H2B···Cl1 interaction, and also with the O2-H2A···Cl1 interaction forms two centrosymmetric $R_4^2(16)$ rings. The combination of these with the 4,4'-H_3dcbp dimers can produce linear or zig-zag chains as shown in Figure 5.6. The 2D sheets are stacked in an offset manner through face-to-face π-π interactions between the 4,4'-H_3dcbp molecules, with the distance at closest contact being 3.250(2) Å.

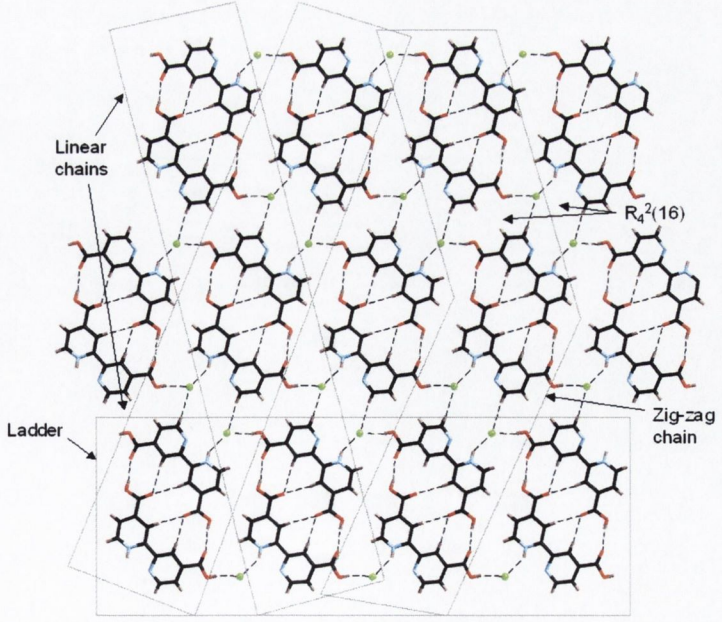

Figure 5.6 – Two-dimensional sheet formed in **17** by hydrogen bonding of the 1D ladders *via* $R_4^2(16)$ rings.

5.1.5 Synthesis of [(TBA)(4,4'-Hdcbp)]·4H_2O.

A second attempt to prepare crystals of the tris-4,4'-dcbp complex of Fe(II) was undertaken by following a previously reported method.[233] $(NH_4)_2Fe(SO_4)_2·6H_2O$ was reacted with the tetrabutylammonium salt of 4,4'-dcbp in a 2:1:1 methanol, acetone and water mixture yielding a deep red solution, which was left to evaporate. After several weeks, a handful of colorless crystals had grown. An X-ray diffraction study revealed the crystals to be the monotetrabutylammonium salt of 4,4'-Hdcbp.

*5.1.6 Crystal structure of [(TBA)(4,4'-Hdcbp)]·4H_2O (**18**).*

The structure of **18** was refined in the monoclinic *C*2/*c* space group. Crystallographic data are shown in Table 5.5. The molecular structure and atomic numbering scheme are shown in Figure 5.7. Overall only one of the carboxylic acid groups in 4,4'-H_2dcbp is deprotonated and the balanced charge is provided by a tetrabutyl ammonium cation. There are one and a half crystallographically unique 4,4'-Hdcbp molecules in the structure. The pyridyl rings in both are planar, however the carboxylate groups about C11 and C12 are twisted at *ca.* 8° and 4° from the aromatic rings, while no torsion angle exists in the carboxylate group about C18. The carboxy group about C11 is deprotonated while that about C18 is protonated. The carboxy group about C12 is protonated at half-occupancy. This is reflected in the C-O bond lengths (C11-O1 and C11-O2 1.249(6) Å; C12-O3 1.291(7) Å, C12-O4 1.211(7) Å; C18-O5 1.310(6) Å, C18-O6 1.225(6) Å). Conversely, one and a half unique tetrabutylammonium cations are present in the structure. The N4 containing cation is at full occupancy. *Trans* butyl groups exist in the same conformation, linear or L-shaped, but different to *cis* groups. One of the L-shaped arms is disordered over two positions thus facing *cis* or *trans* to the other L-shaped arm. The N5 containing tetrabutylammonium cation is at half occupancy and is disordered over two positions. The butyl arms adopt a similar conformation to that of the other cation. *Trans* butyl groups are in the same conformation: either linear or L-shaped. Both L-shaped arms are *cis* to each other.

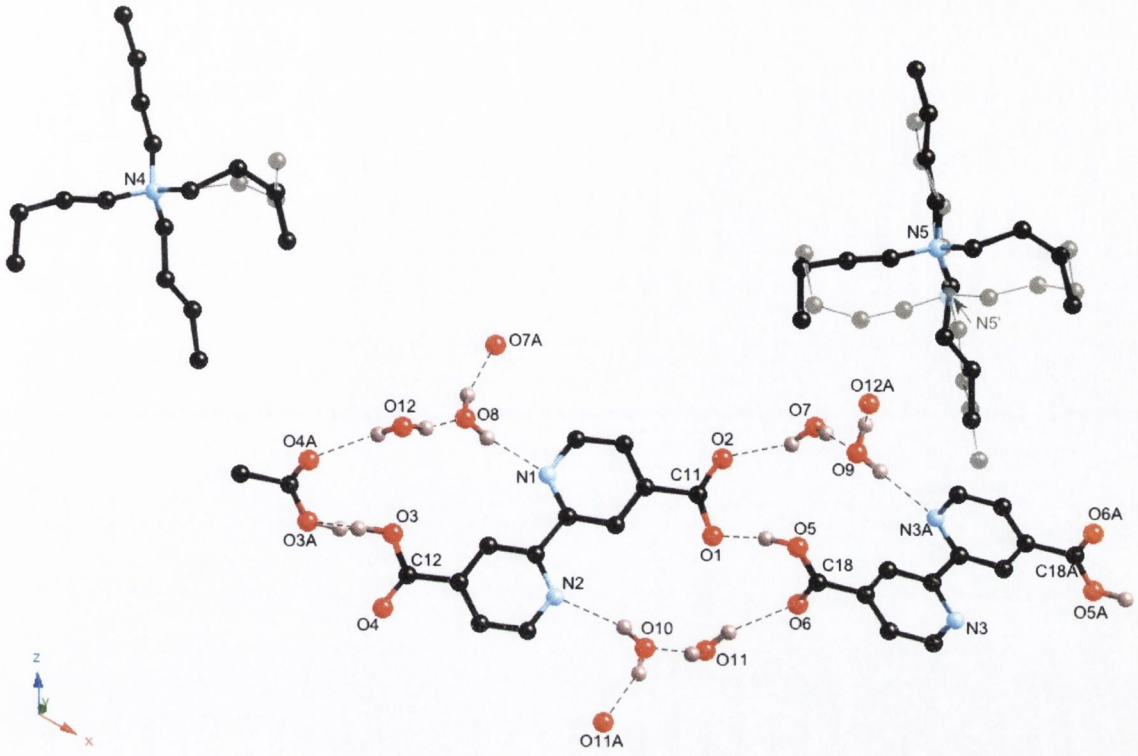

Figure 5.7 – Molecular structure and atomic labelling scheme in **18**. The fourteen unique hydrogen bonds are represented as dashed bonds. Translucent atoms represent disordered positions. (Bipyridyl and butyl hydrogen atoms omitted for clarity)

There are also six unique lattice water molecules in the structure. These are hydrogen bonding with each other as well as with the 4,4'-Hdcbp ions. In total there are fourteen unique hydrogen bonds in the structure of **18**, as shown in Figure 5.7. Bond lengths and angles for these are shown in Table 5.4. The 4,4'-Hdcbp molecules are hydrogen bonding *via* strong carboxylate-carboxylic acid interactions to form linear chains, as shown in Figure 5.8. Carboxylic acid oxygen O5, donates a hydrogen bond to carboxylate oxygen O1. The O3-H3···O3 interaction is disordered, i.e. the donor and acceptor groups switch their functions. This hydrogen bond disorder is most commonly observed in structures with strong hydrogen bonds, such as O-H··O$^-$, as is the case here.[7, 234]

All the water molecules are donating two hydrogen bonds and accepting one. O7 is a hydrogen bond donor to carboxylate oxygen O2 and to lattice water molecule O9. O8 donates a hydrogen bond to N1 bipyridyl nitrogen atom and to adjacent lattice water molecule O7. O9 also donates a hydrogen bond to a bipyridyl nitrogen atom, N3, and to lattice water molecule O12. O10 is a hydrogen bond donor to a third bipyridyl nitrogen atom, N2, as well as to lattice water molecule O11, which conversely donates a hydrogen bond to an adjacent O10 lattice water molecule as well as to carboxylate oxygen atom O6. O12 is a hydrogen bond donor to carboxylic acid oxygen atom O4 as well as to lattice water molecule O8.

Table 5.4 – Parameters of hydrogen bonding interactions in **18**.

D–H···A	D-H/Å	d(H···A)/Å	d(D···A)/Å	<(D–H···A)/°
O3-H3···O3^{i}	0.98	1.50	2.439(8)	157
O5-H5···O1	0.98	1.50	2.448(5)	161
O7-H7A···O2	0.84	2.03	2.825(6)	157
O7-H7B···O9^{ii}	0.84	1.92	2.762(7)	172
O8-H8A···N1	0.84	2.11	2.932(6)	166
O8-H8B···O7^{iii}	0.84	1.91	2.719(6)	161
O9-H9A···N3	0.84	2.10	2.938(6)	172
O9-H9B···O12^{iv}	0.84	2.44	2.683(7)	98
O10-H10A···O11^{v}	0.85	1.98	2.796(5)	162
O10-H10B···N2	0.85	2.14	2.956(6)	161
O11-H11A···O10	0.84	1.96	2.770(5)	162
O11-H11B···O6	0.84	2.13	2.945(6)	162
O12-H12A···O4	0.84	2.07	2.846(6)	153
O12-H12B···O8^{i}	0.85	1.96	2.764(6)	158

Symmetry codes: i = 1-x, y, 0.5-z; ii = -x, 1-y, -z; iii = 0.5-x, 1.5-y, -z; iv = 0.5-x, 0.5+y, 0.5-z; v = 0.5-x, y-0.5, 0.5-z.

The 4,4'-Hdcbp molecules in the hydrogen bonded chains are further bridged by water molecules (O2···O7···O9···N3, O6···O11···O10···N2, O4···O12···O8···N1) forming $R_4^4(16)$ graph sets.

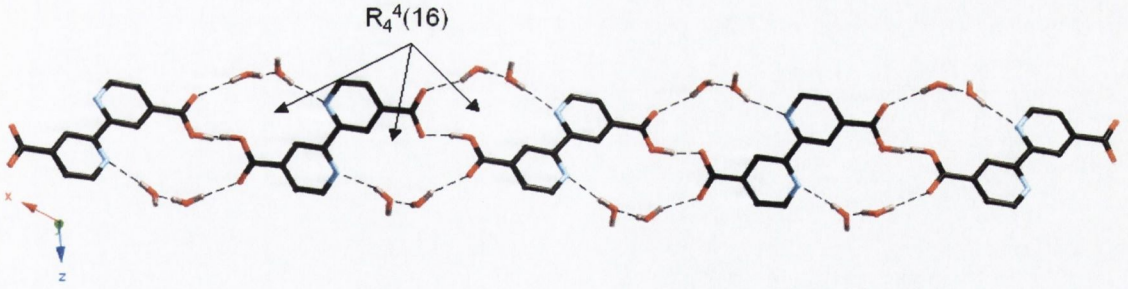

Figure 5.8 – Hydrogen bonded chain formed in **18** *via* hydrogen bonding of the 4,4'-Hdcbp molecules.

All the chains run parallel to each other along the *ac* plane. Adjacent chains are linked through hydrogen bonds with the lattice water molecules to form a 3D network as shown in Figure 5.9. Hydrogen bonding between the lattice water molecules gives rise to helical chains going down the *b* direction. Two crystallographically distinct helices exist: those formed by hydrogen bonding between O10 and O11 lattice water molecules and those formed by hydrogen bonding between the remaining lattice water molecules,

O7, O8, O9 and O12. In both cases equal amounts of right-handed and left-handed helices occur, rendering the overall structure achiral.

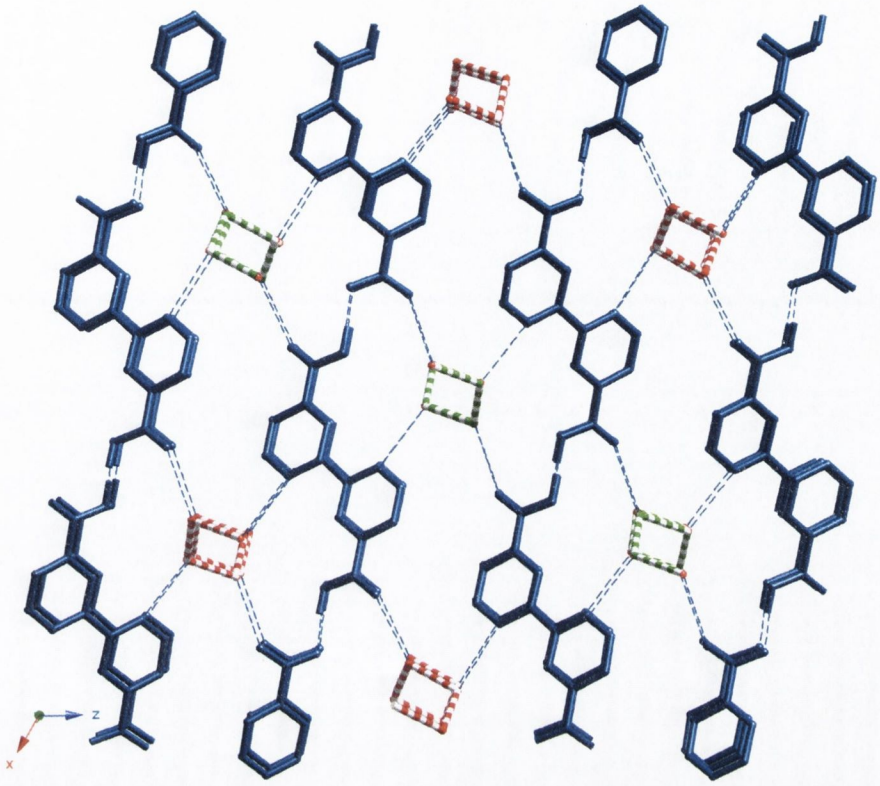

Figure 5.9 – Hydrogen bonding of the 4,4'-Hdcbp molecules in **18** into a 3D network. The 4,4'-Hdcbp chains (represented in blue) are linked through hydrogen bonding with the lattice water molecules. Hydrogen bonding between the lattice water molecules gives rise to left and right handed helices, in equal amounts, extending along the *b* direction. Left handed helices are represented by red and white dashed bonds, while right handed helices are represented as green and white dashed bonds. (Tetrabutylammonium cations, bipyridyl and lattice water hydrogen atoms omitted for clarity)

The tetrabutylammonium cations sit between the 4,4'-Hdcbp hydrogen bonded chains as shown in Figure 5.10. While no π-interactions between the aromatic rings are observed, weaker interactions between the butyl protons and the carboxy oxygen atoms reinforce the network.

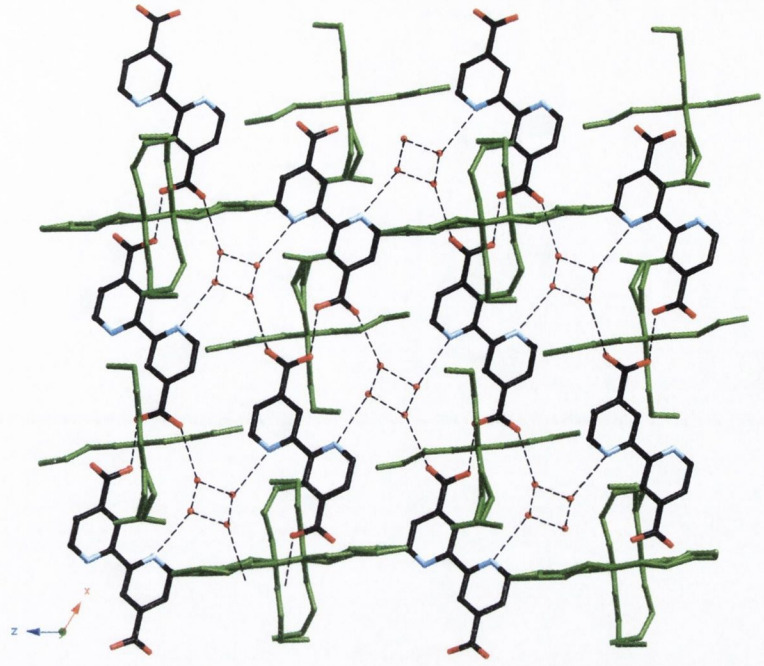

Figure 5.10 – Overall packing diagram for **18** viewed down (010). Tetrabutylammonium cations highlighted in green. (Hydrogen atoms omitted for clarity)

5.1.7 Synthesis of $(DEA)_2$(4,4'-dcbp).

Hydrothermal reaction of $MnCl_2$ and 4,4'-H_2dcbp (1:2) in diethylformamide (DEF) at 200 °C for 16 hrs yielded a mixture of yellow powders and crystals, as well as a small amount of colourless crystals. The structure of the yellow crystals has been described in Chapter 2. After performing an X-ray diffraction study on the colourless crystals, they were determined as the diethylammonium salt of 4,4'-dcbp. As in **13** and **14**, where DMF was hydrolysed to form dimethylammonim cations, diethylformamide has lost its formyl group to yield diethylammonium (DEA) cations under the harsh conditions of the reaction.

*5.1.8 Crystal structure of $(DEA)_2$(4,4'-dcbp) (**19**).*

19 crystallizes in the monoclinic $P2_1$ space group. Crystallographic details are shown in Table 5.5. The atomic numbering scheme and atom connectivity for $(DEA)_2$(4,4'-dcbp) are shown in Figure 5.11. The 4,4'-dcbp molecule exists in the *anti* conformation, and like in **18**, the pyridyl rings are coplanar in this structure. However distortion of the molecule arises from the twist of the carboxylate groups with the aromatic ring to which they are attached: that about C12 forms a small torsion angle of *ca.* 6°, whilst the other about C11 forms an angle of approximately 13°. The C-O bond lengths about C11 and C12 are typical for delocalised carboxylate groups, ranging from 1.246(3) to 1.257(3) Å.

Table 5.5 - Crystallographic data for **18** and **19**.

Compound	**18**	**19**
Chemical Formula	$C_{28}H_{51}N_3O_8$	$C_{10}H_{15}N_2O_2$
Formula weight	557.72	195.24
Crystal system	Monoclinic	Monoclinic
Space group	*C*2/*c*	$P2_1$
μ (MoK_α)/ mm^{-1}	0.086	0.086
a/Å	38.960(5)	8.9038(7)
b/Å	8.472(2)	11.1419(9)
c/Å	33.056(4)	10.8140(8)
α/°	90	90
β/°	120.646(2)	94.797(2)
γ/°	90	90
V/Å^3	9387(3)	1069.1(1)
Z	12	4
D_{calc}/gcm^{-3}	1.184	1.213
T/K	153(2)	153(2)
Crystal size max/ mm	0.18	0.28
mid/ mm	0.18	0.25
min/ mm	0.12	0.13
$2\theta_{max}$/°	50.00	59.94
Min/Max trans. Factor	0.920/1.000	0.325/1.000
R_{int}	0.0852	0.0220
R_1, $wR_2[I>2\sigma(I)]$[a]	0.0885, 0.1887	0.0649, 0.1516
R_1, wR_2 (all data)	0.1735, 0.2097	0.0809, 0.1622
Reflections– collected:	34516	8278
unique:	6122	5731
observed:	2772	4680

[a] $R_1 = \Sigma||F_o| - |F_c||/\Sigma|F_o|$, $wR_2 = [\Sigma w(F_o^2 - F_c^2)^2/\Sigma w(F_o^2)^2]^{1/2}$

Two crystallographically independent diethylammonium cations provide the charge balance in the structure. Each cation exists in a different conformation. The N3 containing cation is in a linear conformation, with the carbon and nitrogen atoms almost coplanar and only a small dihedral angle of *ca.* 8° between N3-C13-C15 and N3-C14-C16. In contrast, the N4-containing diethylammonium cation exists in an 'L-shaped' conformation with C20 pointing sideways (C19-C18-C20 105°) to the plane within which the other carbon and nitrogen atoms reside.

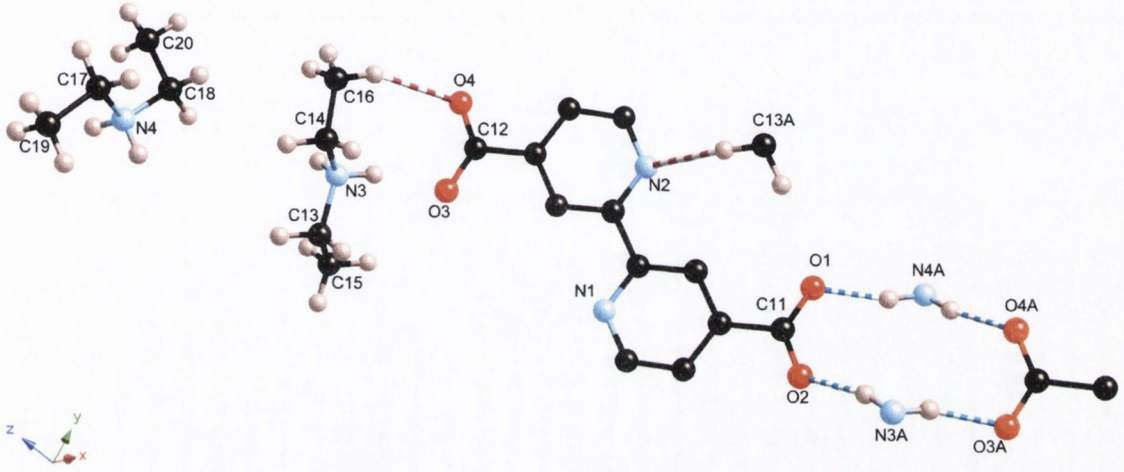

Figure 5.11 – Molecular structure and labelling scheme in **19**. The blue and white dashed bonds depict strong hydrogen bonds, while the red and white dashed bonds represent weaker C-H···O bonds. (Bipyridyl hydrogen atoms omitted for clarity)

Table 5.6 – Parameters of hydrogen bonding interactions for **19**.

D–H···A	D-H/Å	d(H···A)/Å	d(D···A)/Å	<(D–H···A)/°
N3-H3A···O2^{i}	0.92	1.80	2.692(2)	163
N3-H3B···O3	0.92	1.82	2.703(2)	160
N4-H4A···O4^{ii}	0.92	1.85	2.751(2)	168
N4-H4B···O1^{iii}	0.92	1.82	2.702(2)	159
C20-H20C···O4^{ii}	0.98	2.6	3.288(4)	130
C13-H13B···N2^{iii}	0.99	2.62	3.561(3)	159
C16-H16C···O4	0.98	2.53	3.438(3)	155

Symmetry codes: i = 1+x, y, z-1; ii = 1-x, y-0.5, 1-z; iii = -x, y-0.5, 2-z.

Hydrogen bonding between the carboxylate oxygen atoms and the diethylammonium protons propagates the 4,4'-dcbp anions into linear chains through the characteristic cyclic $R_4^4(12)$ motif formed in this type of interactions (Figure 5.12). Pairs of ammonium cations act as 'spacers' between pairs of carboxylate groups on the 4,4'-dcbp anions. Adjacent chains run in an anti-parallel fashion. The diethylammonium cations sit above and below the hydrogen bonded chains in an almost parallel fashion, and this allows for weaker intra-chain hydrogen bonding between ethyl protons and one of the carboxylate oxygen atoms (H16C···O4 2.53 Å, H20C···O4 2.57 Å). A detail of the interactions between two carboxylate groups and two diethylammonium cations is shown in Figure 5.13.

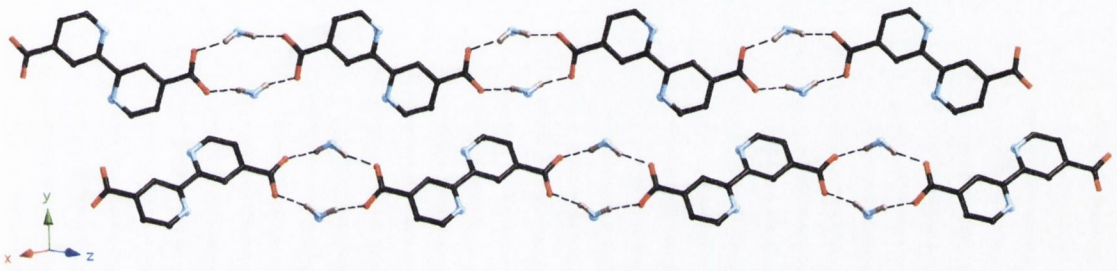

Figure 5.12 – Two antiparallel linear chains formed in **19** by hydrogen bonding of the carboxylates with diethylammonium cations forming an $R_4^4(12)$ motif. (Bipyridyl hydrogen atoms and ethyl groups on the ammonium cations omitted for clarity)

The hydrogen bonded chains pack such that adjacent ones are related by a two-fold screw axis and thus run anti-parallel to each other. Hydrogen bonding between one of the ethyl protons (H13B) and the bipyridyl N2 nitrogen atom links adjacent chains into a two-dimensional 'pleated' hydrogen bonded sheet as shown in Figure 5.14. While the hydrogen bond angle (C13-H13B···N2 159°) is well within the range for weak hydrogen bonds, the torsion angle at the acceptor atom is *ca.* 132° (C7-C6-N2-H13B), which might lead to questioning this interaction as a legitimate hydrogen bond. However, while an in-plane contact (*i.e.* in the pyridyl ring plane) is ideally preferred, interactions above and below the plane cannot be completely disregarded. Steiner carried out a study on the acceptor directionality of C=O groups according to the angle (H···O=C) and torsion angle (H···O=C-Y) of the interaction.[235] He found hydrogen bond interactions even with a torsion angle of 60°. While no similar studies have been carried out for nitrogen acceptors, we will take the C13-H13B··N2 interaction as a valid hydrogen bond.

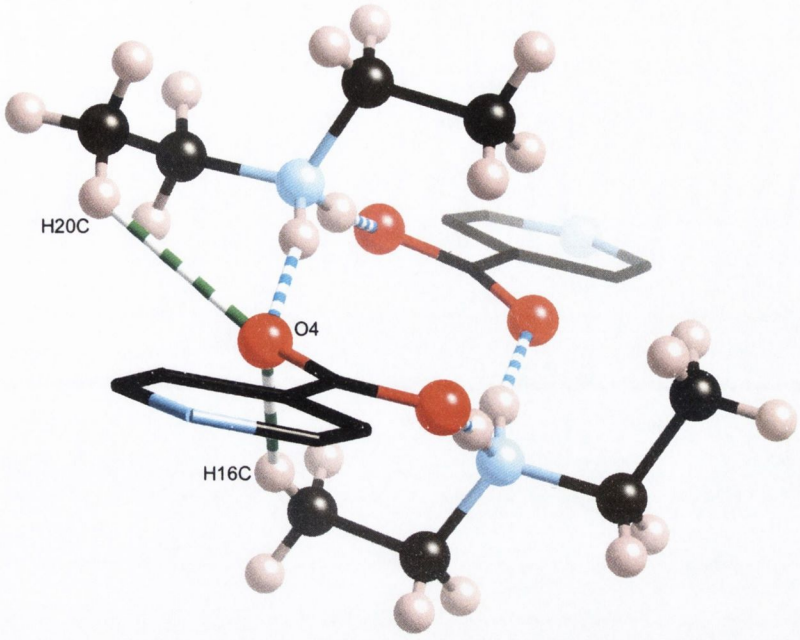

Figure 5.13 – Detail of the interactions between the carboxylate groups of 4,4'-dcbp and the diethylammonium cations in **19**. Blue and white dashed bonds represent hydrogen bonds between the DEA protons and the carboxylate oxygens, while green and white dashed bonds represent hydrogen bonds between the ethyl protons and one of the carboxylate oxygen atoms. Note the arrangement of the diethylammonium cations above and below the 4,4'-dcbp molecules. (Half of the 4,4'-dcbp anions and bipyridyl hydrogen atoms omitted for clarity.)

In contrast to the previous structures no π-π interactions between the 4,4'-dcbp anions are found in this structure. Weak C-H···π interactions between one of the 'end' methyl groups and one of the pyridyl rings is observed, with a closest contact of 3.320(3) Å (C15···C8).

Figure 5.14 – Packing of the $(DEA)_2$(4,4'-dcbp) chains into pleated sheets *via* hydrogen bonding. Adjacent chains within a sheet run anti-parallel to each other. (Bipyridyl and ethyl protons omitted for clarity)

5.2 Synthesis and structural characterization of ester derivatives of 4,4'-H_2dcbp.

5.2.1 Synthesis and crystallization of 4,4'-dimethylcarboxy-2,2'-bipyridine (4,4'-dmcbp), 4,4'-diethylcarboxy-2,2'-bipyridine (4,4'-decbp), 4,4'-diisopropylcarboxy-2,2'-bipyridine (4,4'-dpcbp), and 4,4'-dibutylcarboxy-2,2'-bipyridine (4,4'-dbcbp).

After looking at the packing of 4,4'-H_2dcbp and some of its salts, it was decided to look at the packing of ester derivatives of 4,4'-H_2dcbp. The carboxylic acid functionality is lost and with it the strong hydrogen bonding directionality these functional groups offer, thus the packing of the ester derivatives is expected to be dramatically different to those described in the previous section.

All the esters were synthesized from the reflux of 4,4'-H_2dcbp in the appropriate solvent (methanol, ethanol, *etc.*), and crystallized from ethyl acetate.[236]

*5.2.2 Crystal structure of 4,4'-dmcbp (**20**).*

The structure of 4,4'-dmcbp was refined in the monoclinic $P2_1/c$ space group and crystallographic details are shown in Table 5.7. The molecular structure and atomic labeling scheme for 4,4'-dmcbp are shown in Figure 5.15. One half of the 4,4'-dmcbp molecule is related to the other by an inversion centre midpoint of the C5-C5A bond. The pyridyl rings adopt the *anti* conformation. The 4,4'-dmcbp molecule is almost planar with only a small twist of the carboxy-ester groups with respect to the aromatic rings (*ca.* 4°).

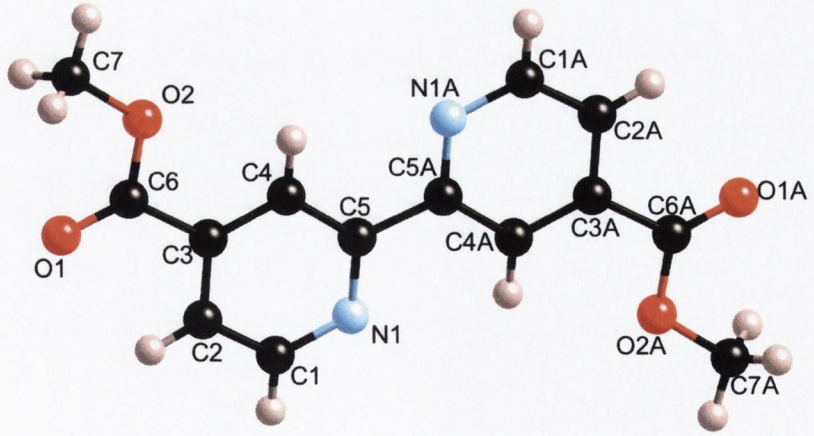

Figure 5.15 – Molecular structure and atomic labelling scheme for 4,4'-dmcbp.

Very weak hydrogen bonding interactions exist between the 4,4'-dmcbp molecules. C1 donates a hydrogen bond to N1 (H1···N1 2.68 Å, C1···N1 3.435(4) Å, <(C1-H1···N1) 137°) and this self-complementary edge-to-edge aryl C-H···N interaction

between adjacent 4,4'-dmcbp molecules propagates these into linear tapes through an $R_2^2(6)$ motif, as shown in Figure 5.16.

The H1 proton is approaching the nitrogen at approximately 13° to the plane of the bipyridyl ring and this results in a slight stepping of the chains. These tapes are stacked through offset face-to-face π-π interactions between the aromatic rings with a separation at closest contact of 3.309(4) Å. Adjacent stacked sheets are tilted at *ca.* 54° and are linked through weak hydrogen bonding between one of the methyl protons and the carboxy oxygen atom (C7···O1 3.580(4) Å, H7C···O1 2.65 Å, <(C7-H7C···O1) 159°).

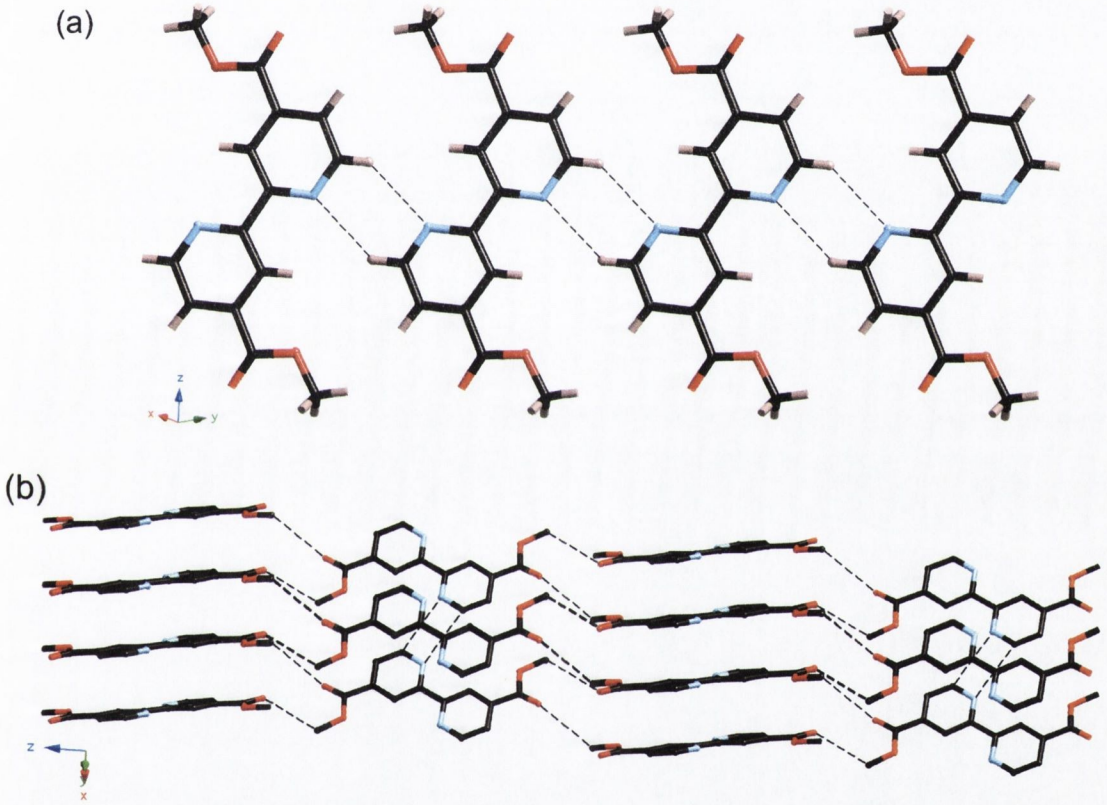

Figure 5.16 – (a) Linear tape formed in the structure of 4,4'-dmcbp *via* self-complementary hydrogen bonding of the pyridyl rings. While not shown here the tapes are slightly stepped. (b) Overall packing of 4,4'-dmcbp. Linear tapes are π-stacked to form 2D sheets, with adjacent sheets tilted at ca. 54° and linked *via* hydrogen bonding between the ester groups. (Hydrogen atoms omitted for clarity)

Table 5.7- Crystallographic data for **20** and **21**.

Compound	**20**	**21**
Chemical Formula	$C_{14}H_{12}N_2O_4$	$C_{16}H_{16}N_2O_4$
Formula weight	272.26	300.31
Crystal system	Monoclinic	Monoclinic
Space group	$P2_1/c$	$P2_1/c$
μ (MoK_α)/ mm^{-1}	0.110	0.100
a/Å	3.806(1)	3.9463(2)
b/Å	5.864(2)	13.7018(8)
c/Å	27.625(3)	13.5187(8)
α/°	90	90
β/°	93.704(6)	93.192(1)
γ/°	90	90
V/Å^3	615.3(3)	729.84(7)
Z	2	2
D_{calc}/gcm^{-3}	1.470	1.367
T/K	153(2)	153(2)
Crystal size max/ mm	0.25	0.28
mid/ mm	0.18	0.15
min/ mm	0.02	0.13
$2\theta_{max}$/°	50.06	49.98
Min/Max trans. Factor	0.678/1.000[†]	0.890/1.000
R_{int}	0.0373	0.0213
R_1, $wR_2[I>2\sigma(I)]$[a]	0.0721, 0.1807	0.0337, 0.0926
R_1, wR_2 (all data)	0.0939, 0.1873	0.0365, 0.0952
Reflections – collected:	3156	7560
unique:	1804	1290
observed:	1368	1191

[a] $R_1 = \Sigma||F_o| - |F_c||/\Sigma|F_o|$, $wR_2 = [\Sigma w(F_o^2 - F_c^2)^2/\Sigma w(F_o^2)^2]^{1/2}$

[†] Absorption correction performed with TWINABS

*5.2.3 Crystal structure of 4,4'-decbp (**21**).*

The structure of 4,4'-decbp was refined in the monoclinic $P2_1/c$ space group. Crystallographic details are shown in Table 5.7. The molecular structure and atom labelling scheme for 4,4'-decbp are shown in Figure 5.17. An inversion center exists in the middle of the C5-C5A bond and thus only one half of the 4,4'-decbp molecule is unique. Thus, the two pyridyl rings are in the *anti* conformation. The 4,4'-decbp molecule is virtually planar with only slight distortion arising from the small twist of the ester groups with respect to the aromatic rings (*ca.* 3°). The C-O bond lengths are typical for a carboxy-ester group, with C6-O2 1.333(2) Å and C6-O1 1.206(2) Å.

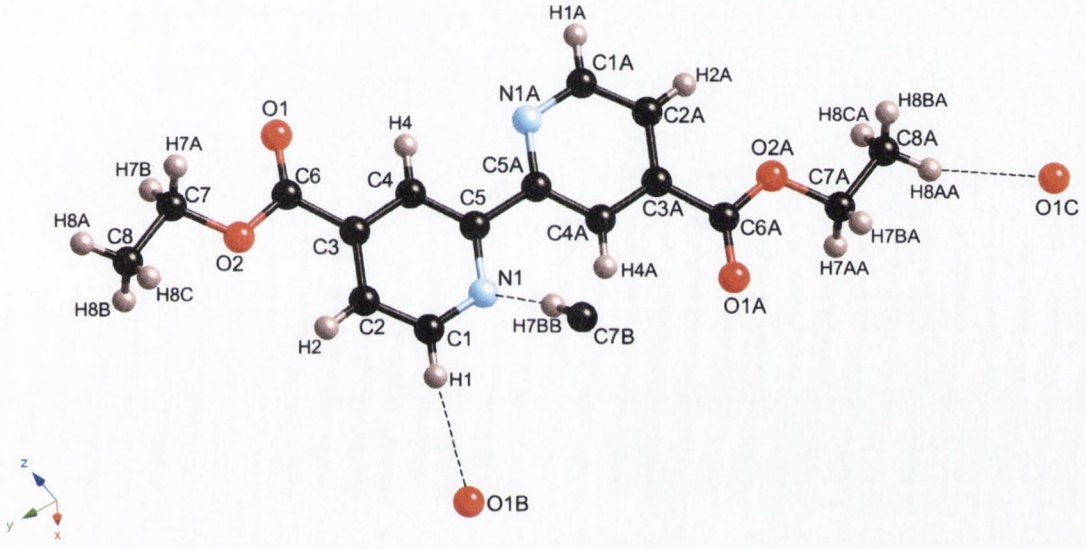

Figure 5.17 – Molecular structure and atomic labelling scheme for 4,4'-decbp.The three unique hydrogen bonds are depicted as dashed bonds.

As expected, there are no conventional hydrogen bonds within the structure of 4,4'-decbp, however three unique hydrogen bonds of the C-H···A type exist. Aromatic carbon C1 is a hydrogen bond donor to carbonyl oxygen O1, as is one of the ethyl carbons, C8. The other ethyl carbon, C7, donates a hydrogen bond to the bipyridyl nitrogen atom N1. Hydrogen bond distances and angles are shown in Table 5.8.

Table 5.8 – Parameters of hydrogen bonding interactions for 4,4'-decbp.

D–H···A	D-H/Å	d(H···A)/Å	d(D···A)/Å	<(D–H···A)/°
C1-H1···O1^{i}	0.95	2.51	3.441(2)	167
C8-H8A···O1^{ii}	0.98	2.53	3.470(2)	161
C7-H7B···N1^{iii}	0.99	2.61	3.586(2)	171

Symmetry codes: i =1+x, 1.5-y, z-0.5; ii = -x, 1.5-y, 0.5+z; iii = x, 1.5-y, 0.5+z.

The C1-H1···O1 and the C8-H8A···O1 interactions link the 4,4'-decbp molecules to produce a hydrogen bonded 2D sheet as shown in Figure 5.18(a). Both interactions produce C(6) motifs individually, but when combined produce two types of rings: a centrosymmetric $R_4^2(20)$ motif and a non-centrosymmetric $R_2^2(15)$ motif. The 2D sheets are hydrogen bonded through the C7-H7B···N1 interaction into a 3D network as shown in Figure 5.18(b). The hydrogen bond angle of this last interaction is almost linear (171°), but the proton is approaching at approximately 60° to the pyridyl ring plane. However, despite this, as explained earlier, the hydrogen bond may be considered valid. Offset face-to-face π-π interactions exist between the pyridyl rings of 4,4'-decbp with a separation at closest contact of 3.436(2) Å.

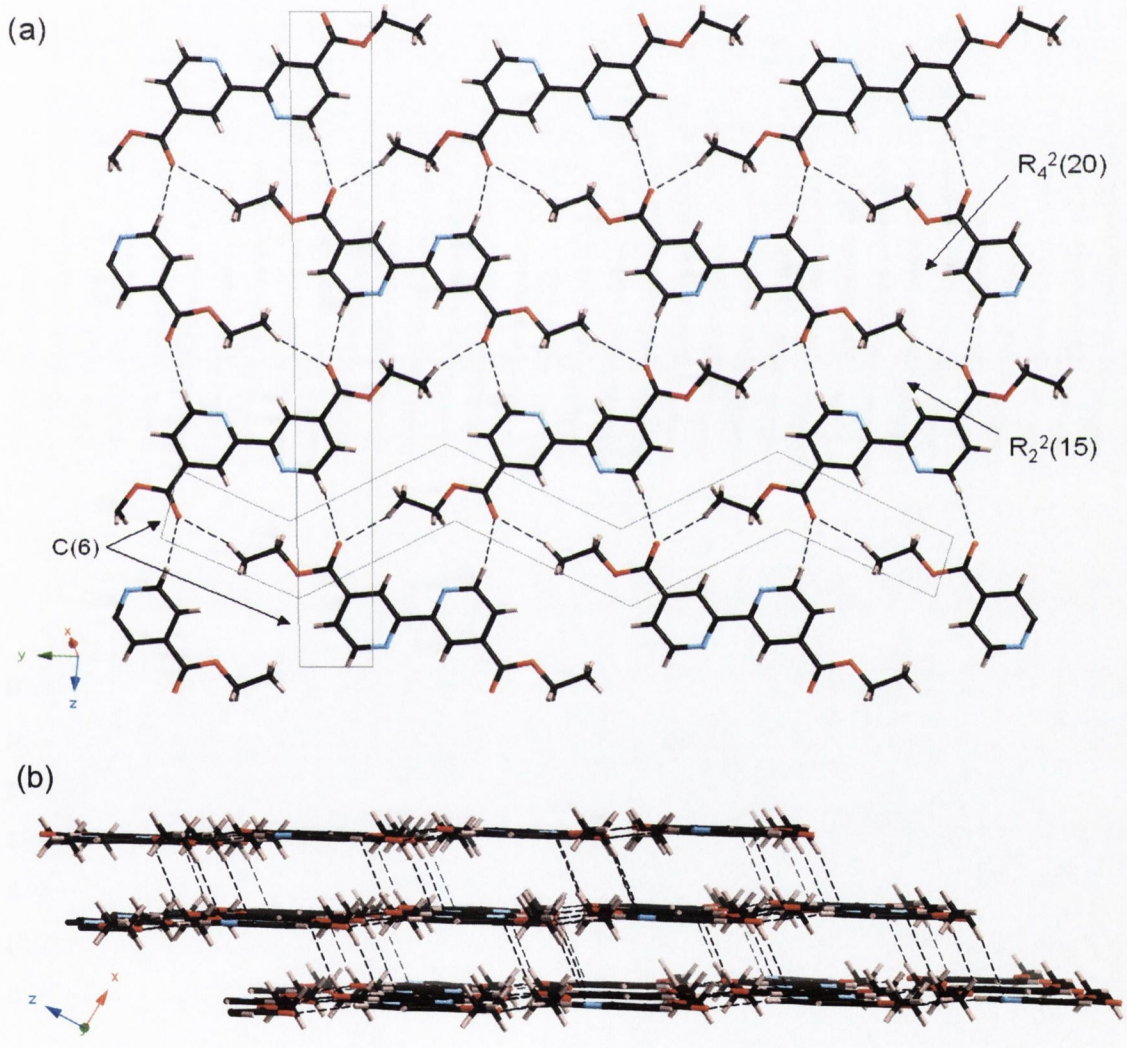

Figure 5.18 – (a) 2D sheet in the structure of 4,4'-decbp formed *via* hydrogen bonding. Two types of hydrogen bonds both give rise to a C(6) motif each, and to a centrosymmetric $R_4^2(20)$ ring and a non-centrosymmetric $R_2^2(15)$ ring when combined. (b) Packing of the 2D sheets in 4,4'-decbp *via* hydrogen bonding and π-π interactions. (Hydrogen bonds shown as dashed bonds)

*5.2.4 Crystal structure of 4,4'-dpcbp (**22**).*

The structure of 4,4'-dpcbp was refined in the triclinic P-1 space group and crystallographic details are shown in Table 5.9. The molecular structure and atomic connectivity for 4,4'-dpcbp are shown in Figure 5.19. Once again half of the molecule is related to the other half by inversion. The pyridyl rings are coplanar and are in the *anti* conformation. The carboxy-ester groups are slightly twisted with respect to the aromatic rings (*ca.* 3°). C-O bond lengths are typical for such groups (C6-O1 1.208(2) Å, C6-O2 1.337(2) Å).

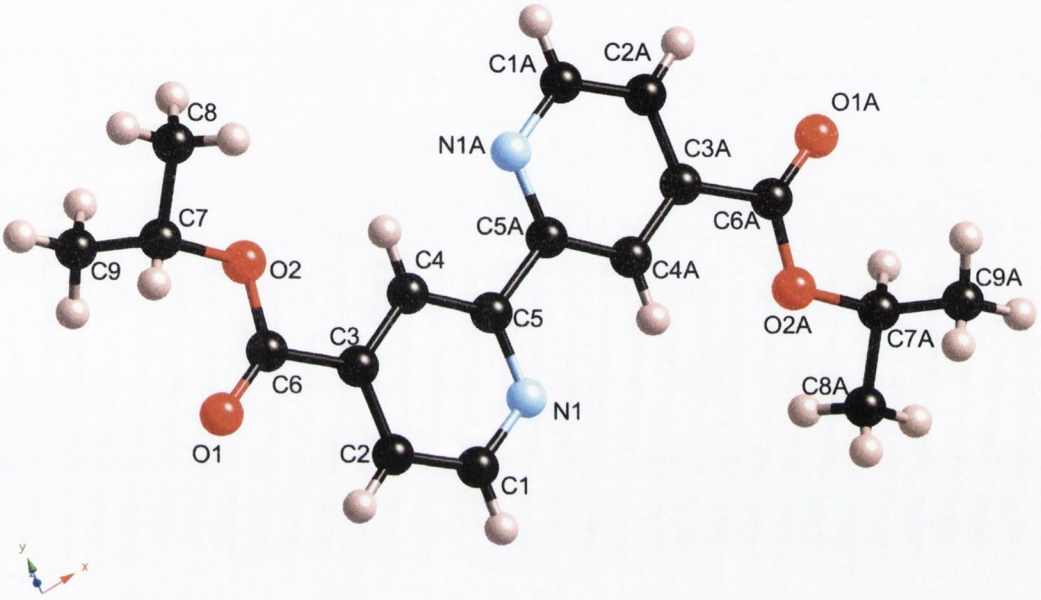

Figure 5.19 – Molecular structure and atomic labelling for 4,4'-dpcbp.

Like in 4,4'-dmcbp, a self-complementary C-H···N contact exists between the pyridyl rings (C1···N1 3.404(2) Å, H1···N1 2.73 Å, <(C1-H1···N1) 128°). In this case the proton approaches the nitrogen atom at 26° to the bipyridyl plane, considerably less planar than in 4,4'-dmcbp, but may still be considered an interaction. This results in similar tapes to those formed in 4,4'-dcmbp, however the step is more pronounced. The 4,4'-dpcbp tapes pack through offset face-to-face π-π interactions of the pyridyl rings (C2···C4 3.368(2) Å) to form stacked columns (Figure 5.20). No further interactions are observed between the rings.

Table 5.9 - Crystallographic data for **22** and **23**.

Compound		**22**	**23**
Chemical Formula		$C_{18}H_{20}N_2O_4$	$C_{20}H_{24}N_2O_4$
Formula weight		328.36	356.41
Crystal system		Triclinic	Monoclinic
Space group		*P*-1	$P2_1/c$
μ (MoK_α)/ mm^{-1}		0.095	0.091
a/Å		5.8683(7)	7.491(2)
b/Å		6.8410(8)	8.001(2)
c/Å		10.749(1)	15.233(3)
α/°		74.578(2)	90
β/°		81.482(2)	92.19(3)
γ/°		81.131(2)	90
V/$Å^3$		408.38(8)	912.3(3)
Z		1	2
D_{calc}/gcm^{-3}		1.335	1.297
T/K		153(2)	293(2)
Crystal size	max/ mm	0.40	0.40
	mid/ mm	0.09	0.25
	min/ mm	0.05	0.13
$2\theta_{max}$/°		50.00	55.72
Min/Max trans. Factor		0.900/1.000	n/a
R_{int}		0.0200	0.0553
R_1, $wR_2[I>2\sigma(I)]$[a]		0.0382, 0.0956	0.0471, 0.1378
R_1, wR_2 (all data)		0.0448, 0.0997	0.0877, 0.1885
Reflections–	collected:	3620	12461
	unique:	1430	2157
	observed:	1236	1475

[a] $R_1 = \Sigma||F_o| - |F_c||/\Sigma|F_o|$, $wR_2 = [\Sigma w(F_o^2 - F_c^2)^2/\Sigma w(F_o^2)^2]^{1/2}$

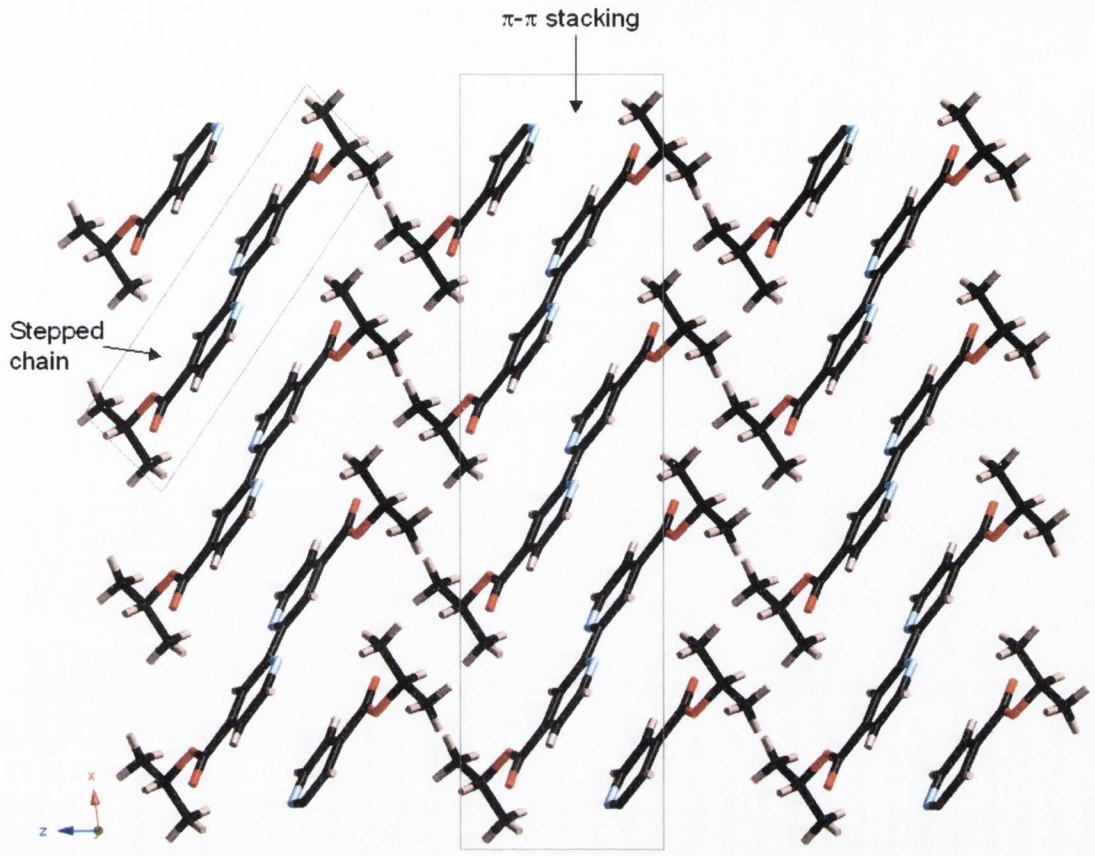

Figure 5.20 – Packing of 4,4'-dpcbp viewed along (010). The stepped hydrogen bonded chains are running into the paper and are stacked into columns through π-π interactions.

5.2.5 Crystal structure of 4,4'-dbcbp.

The structure of 4,4'-dbcbp was refined in the monoclinic $P2_1/c$ space group. Crystallographic details are shown in Table 5.9. The molecular structure and atom connectivity for 4,4'-dbcbp are shown in Figure 5.21. As in the structure of the other esters an inversion centre exist midpoint between C5 and C5A and thus half of the 4,4'-dbcbp molecule is related to the other by inversion. Likewise, the pyridyl rings are in the *anti* conformation. The 4,4'-dbcbp molecule is almost planar, with only a slight twist in the carboxylate groups of 4° with respect to the aromatic rings. C-O bond lengths are typical for a carboxyester group (C6-O1 1.210(2) Å, C6-O2 1.332(2) Å).

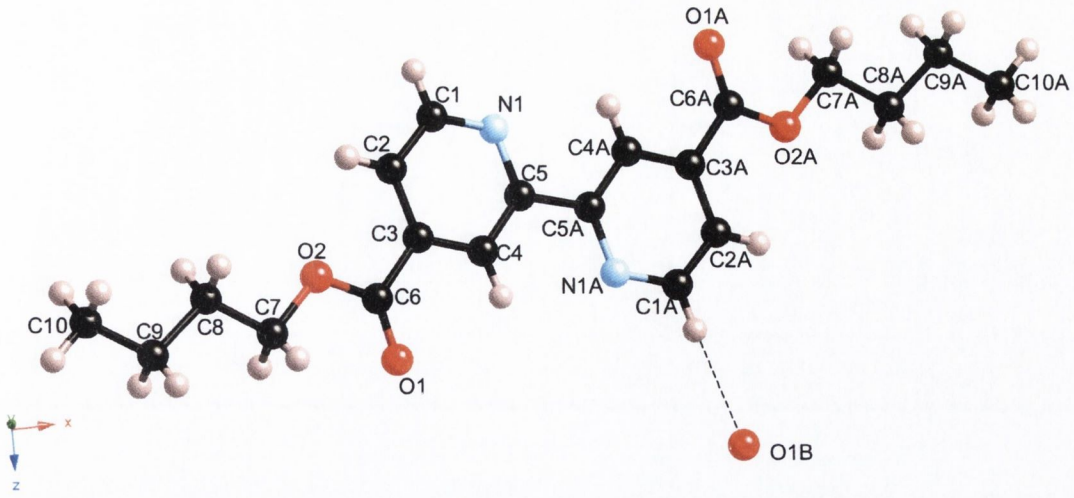

Figure 5.21 – Molecular structure and atomic labelling for 4,4'-dbcbp. The dashed line depicts the unique hydrogen bond.

Only one unique non-conventional hydrogen bond exists within the structure of 4,4'-dbcbp. One of the aromatic carbons, C1, is a hydrogen bond donor to carbonyl oxygen O1 (H1···O1 2.56 Å, C1···O1 3.448(2) Å, <(C1-H1···O1) 159°). This interaction links the 4,4'-dbcbp molecules into a 3D network. Adjacent hydrogen bonded 4,4'-dbcbp molecules lie at approximately 54° to each other as shown in Figure 5.22.

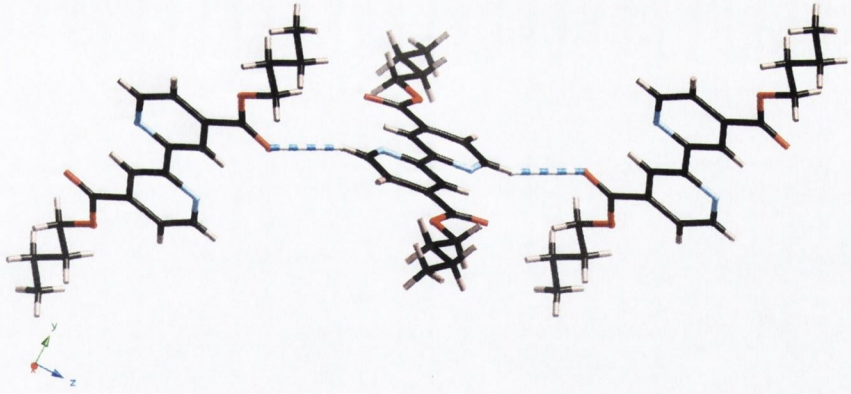

Figure 5.22 – Detail of the hydrogen bonding between 4,4'-dbcbp molecules. Note adjacent molecules are tilted by approximately 54°.

Since half of the 4,4'-dbcbp molecule is related to the other by inversion, each 4,4'-dbcbp molecule participates in four hydrogen bonds (two donors and two acceptors), and thus each molecule is connected to four others. Adjacent sheets are at 54° to each other (Figure 5.23). Offset face-to-face π-π interactions between the pyridyl rings occur within each sheet with the separation at closest contact of 3.369(2) Å. Additional weaker C-H···π contacts exist between the butyl protons and the pyridyl rings within a sheet (separation at closest contact 3.662 Å).

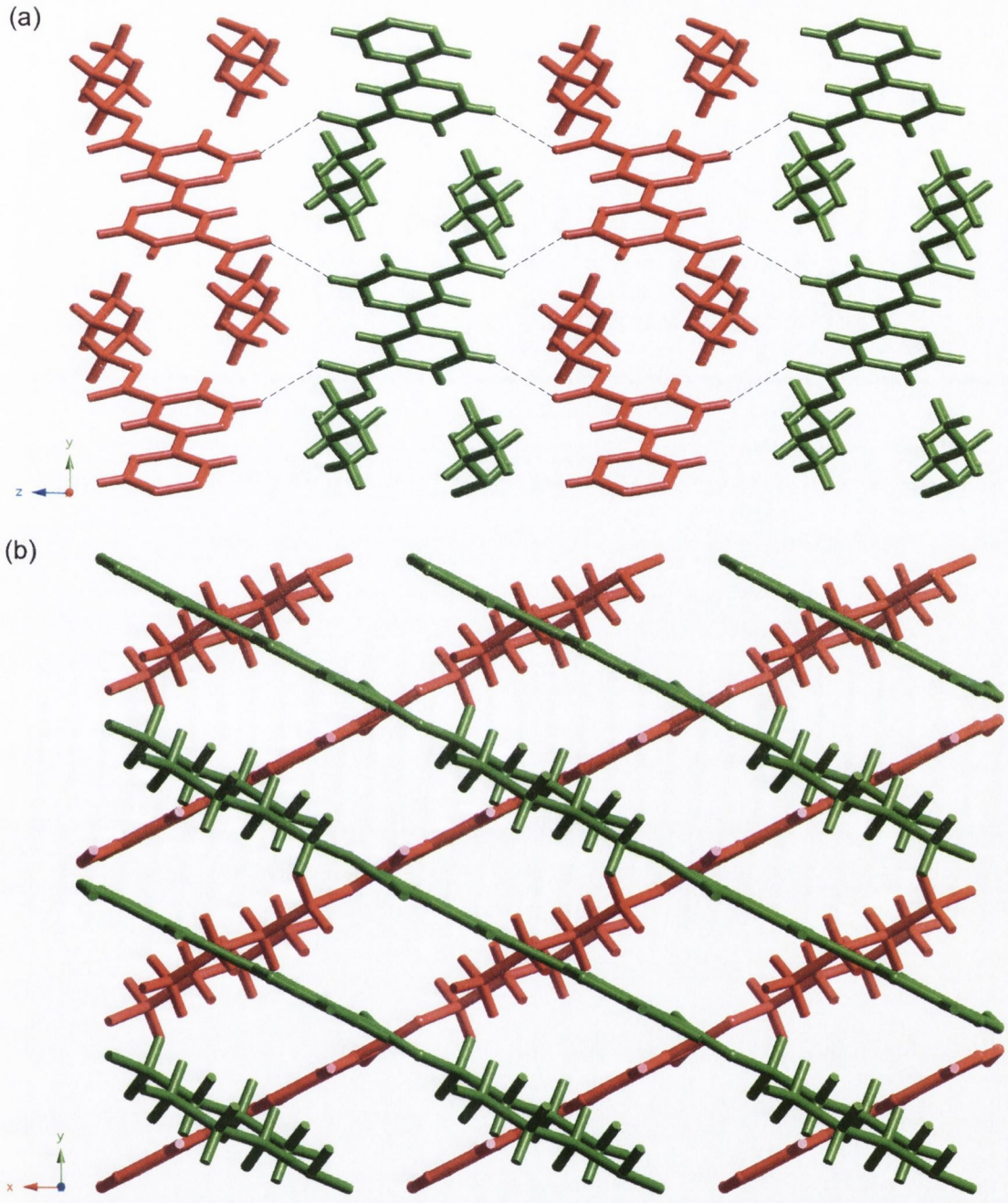

Figure 5.23 – Packing of the 4,4'-dbcbp molecules. Adjacent molecules of different colours are hydrogen bonded while adjacent ones of the same colour are π-π stacking. (a) view along (100) showing the hydrogen bond interactions. (b) view along (001) showing the π-π interactions.

5.3 Conclusions

The structure of 4,4'-H_2dcbp and various of its salts has been reported. The hydrothermal crystallization of 4,4'-H_2dcbp is dependent on both the temperature and amount of mineral acid in the reaction. A lower temperature and acid concentration lead to the crystallization of 4,4'-H_2dcbp, while a higher temperature and acid concentration produce the hydrochloride salt of 4,4'-H_2dcbp.

The structure of 4,4'-H_2dcbp proved to be more interesting than anticipated. While 'double' linear hydrogen bonded tapes would have been expected, a bilayer of inclined hydrogen bonded chains, giving rise to hydrogen bonded helices, is formed instead. In hindsight this arrangement could have been anticipated. The formation of simple 'double' linear tapes with each half of 4,4'-H_2dcbp running anti-parallel would result in unfavourable steric interactions between aromatic C-H and carboxylic OH groups. The twisting of the two halves of the 2,2'-bipyridine backbone by 30° from the true *anti* conformation avoids this problem while allowing the expected hydrogen bonding and π-π interactions to take place. This reflects the need to also consider weaker forces in the packing of molecules.

On formation of the hydrochloride salt of 4,4'-H_2dcbp, the hydrogen bonding capabilities, in terms of donors and acceptors within the structure are altered. Chloride anions are good acceptors, and can bind up to four donors. Protonation of one of the nitrogen atoms provides an additional hydrogen bond donor. The resulting hydrogen bonding gives rise to two-dimensional sheets in the structure of (4,4'-H_3dcbp)(Cl). Unlike in the structure of 4,4'-H_2dcbp the carboxylic acids do participate in self-complementary interactions through the catemer motif.

All the substituted ammonium salts were obtained as by-products of other reactions and thus were obtained in very small quantities. While this precluded the use of techniques other than X-ray diffraction for structural characterization, it produced good enough results for the interpretation of the structures. In [(TBA)(4,4'-Hdcbp)]·$4H_2O$ only one of the carboxylic acid groups in 4,4'-Hdcbp is deprotonated. This allows for the formation of the strong carboxylic acid-carboxylate synthon, between adjacent 4,4'-Hdcbp units. In $(DEA)_2$(4,4'-dcbp) both carboxylic acid groups are deprotonated and thus direct interaction between the carboxylate groups is not possible. Instead the salt forms the characteristic $R_4^4(12)$ ammonium-carboxylate interaction,[57] which linearly propagates the 4,4'-dcbp molecule.

In conclusion, for 4,4'-H_2dcbp and its salts the presence of good hydrogen bond donors and acceptors and consequently their interactions dictate the packing arrangement of these organic molecules, while the weaker hydrogen bonds are 'accommodated' within the overall framework.

When the carboxylic acid functionality is replaced with an ester, the hydrogen bonding capabilities of the molecule are drastically changed. Weaker C-H···O interactions occur and other forces, such as π-π stacking, play a more structure-determining role than in the carboxylic acid derivatives. In both 4,4'-dmcbp and 4,4'-dpcbp a self-complementary C-H···N interaction is observed between the pyridyl rings. A similar C-H···N dimer has been previously observed for quinoline derivatives, where the C-H aryl and nitrogen lone pairs are in a 1,3-*peri* arrangement (*c.f* 1,2-*peri* for

the 4,4'-dmcbp and 4,4'-dpcbp).[237] Bishop and co-workers found that the angle between the C···N vector of the intermolecular contact and the normal to the plane of the aryl group containing the C atom, peaked at 80° but ranged from 60° to 90° (exactly planar dimer). In 4,4'-dmcbp this angle is 77°, close to the peak, and in 4,4'-dpcbp it's 64°, which although low is within the range.

In 4,4'-decbp and 4,4'-dbcbp the alkyl groups are participating in hydrogen bonding. The ability of a C-H group to donate hydrogen bonds decreases with decreasing acidity, i.e. C(sp)-H > C(sp^2)-H > C(sp^3)-H. However, while the directionality of methyl groups is weakest, it is still that of a hydrogen bond and not a van der Waals interaction.[238]

In the same way the structure of isonicotinic acid and 4,4'-H_2dcbp have been compared, it would be interesting to compare the structure of the ester derivatives of both to try and rationalize the structures. However all the isonicotinic acid ester derivatives are liquids and the solid-state structures of these are not known.

Weak hydrogen bonding has been a controversial subject for years but it is now widely accepted that C-H groups can act as hydrogen bond donors.[239-241] The validity of the weak hydrogen bonding interactions in the esters may also be justified by the packing of the molecules which through offset face-to-face π-π interactions stack into sheets or columns rather than the herringbone manner which would be preferred if no other interactions were present.[239, 242] This may be exemplified by the structure of the related 4,4'-dimethyl-2,2'-bipyridine (4,4'-dmbp), in which there are no oxygen atoms, and indeed adopts the herringbone packing mode (see Appendix).

Chapter Six

Materials & Methods.

Experimental.

6.1 Materials and methods.

6.1.1 Reagents.

All chemicals and solvents were of reagent grade (unless stated) and purchased from Aldrich Chem. Co. Ltd., Fluka Chemika-Biochemica (U.K.), Lancaster Synthesis Ltd. or local solvent suppliers, and were used as received, unless otherwise stated. Water was deionised before use.

6.1.2 Elemental analysis.

Elemental Analysis was carried out at University College, Dublin by Ms. Ann Connelly using a Carlo Erba 1006 automatic analyser. Expected range C, N ± 0.3%, H ± 0.5%

6.1.3 Nuclear magnetic resonance spectroscopy.

^{1}H NMR spectra were recorded on a Bruker DPX 400 machine operating at 400.14 MHz. Samples were run in deuterated solvents and are listed for each spectrum. Standard abbreviations for spectra: s, singlet; d, doublet; t, triplet, m, multiplet; br, broad.

6.1.4 Infrared spectroscopy.

Infrared spectra were recorded in the range 4000 – 600 cm^{-1} on a Mattson Genesis II FTIR. Samples were run as 8 mm diameter potassium bromide pellets prepared under vacuum. The following abbreviations were used to describe the intensities: vs, very strong; s, strong; m, medium; w, weak; vw, very weak; sh, shoulder; br, broad; vbr, very broad.

6.1.5 Thermogravimetric analysis (TGA).

Thermogravimetric analysis were performed by Dr. Manuel Ruther (Trinity College, Dublin) on a Mettler TC 11 system using an open aluminium crucible. Sample weights were approximately 5mgs and the heating rate was 10° C per minute.

6.1.6 X-Ray crystal diffraction.

X-ray analysis for (**1**) was performed by Dr. Mark Nieuwenhuyzen (Queen's University of Belfast) with a Bruker SMART 1000 CCD diffractometer. Data collection for 4,4'-dibutylcarboxy-2,2'-bipyridine (4,4'-dbcbp) was performed by Dr. Paul Jensen at Monash University, Australia, with a Nonius Kappa CCD diffractometer. X-ray analyses for the remaining crystals were performed by Dr. Paul Jensen at Trinity College, Dublin, with a Bruker SMART APEX CCD diffractometer. The candidate was involved in all aspects of structure determination at Trinity College, Dublin. The final refinements were

performed by the candidate, with assistance provided by Dr. Paul Jensen where necessary.

All diffractometers utilised graphite-monochromated Mo-Kα radiation (λ = 0.71073 Å). With the Bruker diffractometers (Trinity College and Queen's University), the omega scan method was used to collect either a full sphere or hemisphere of data for each crystal with detector-to-crystal distance of either 5 or 6 cm at temperatures of 153, 173 or 343 K. Data were collected, processed, and corrected for Lorentz and polarisation effects using SMART and SAINT-NT software. [243, 244] Absorption corrections for single crystals were applied using SADABS.[245] With the Nonius diffractometer (Monash University), ϕ and ω rotations with 1° frames, and a detector-to-crystal distance of 29mm, were used to collect a full sphere of data. The data were collected, processed, and corrected for Lorentz and polarization effects using Nonius software.[246,247] Absorption corrections were not applied.

The structures were solved using either Patterson or direct methods and refined on HKLF4 data with the SHELXTL program package.[248] Data for non-merohedral twinned crystals were indexed using the GEMINI program[249] rather than the usual SMART routine. The twinned data were processed using the twin output option of SAINT (version 6.22)[250] and corrected for absorption using TWINABS.[251] The twinned structures were solved as for the single crystals using HKLF4 data for a single domain containing overlap but were successfully refined on HKLF5 data with the required number of BASF (twin component) parameters.

All non-hydrogen atoms were refined anisotropically. Hydrogen atoms (excluding water) were assigned to calculated positions using a riding model with appropriately fixed isotropic thermal parameters. Water hydrogen atoms, however, were located from difference maps and their positions refined with O-H distance restraints (DFIX, SAME, SADI) and isotropic thermal parameters fixed at 1.5 times that of the adjoining oxygen atom. The water hydrogen atoms in **15** were assigned to calculated positions and then restrained using FLAT, DFIX and SADI commands.

6.1.7 Solvo(hydro)thermal synthesis.

Solvothermal synthesis was carried out using a Parr Instrument Company Series 4760/4765 general-purpose digestion bomb employing two different Teflon® inserts (45ml and 23ml). Maximum loading of the insert was dependent on reagents but a typical volume of 5ml was used. The heating cycles are specified for each reaction and were performed in a Carbolite PF200 programmable oven with a Eurotherm 2408CP temperature controller.

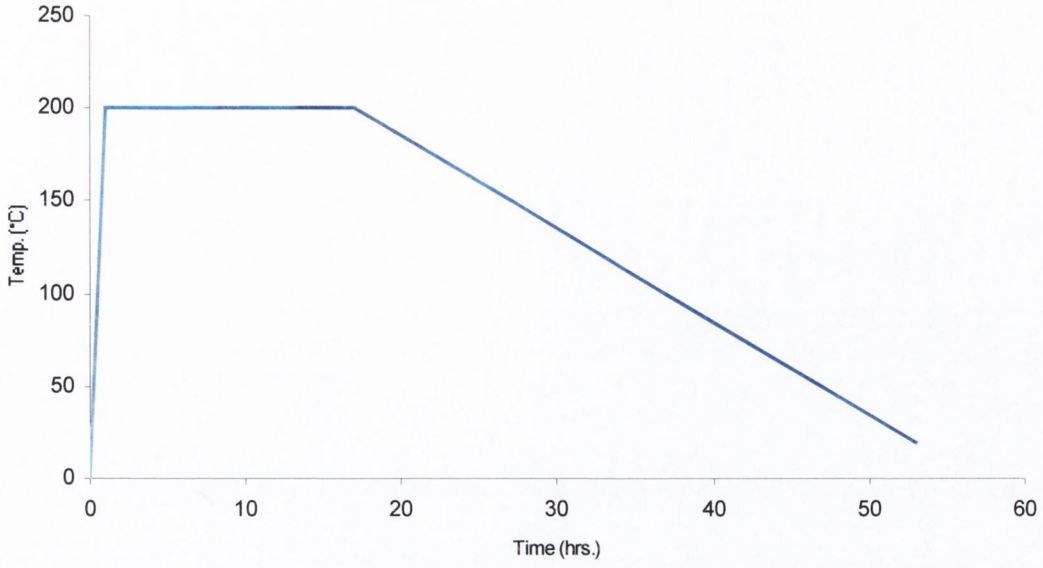

Figure 6.1 – Graphical representation of a heating cycle used in hydrothermal reactions.

Figure 6.2 - Photograph of a sealed Parr Instrument general-purpose acid digestion bomb.

6.1.8 Magnetic measurements.

Variable temperature magnetic measurements for **1** and **10** were performed by Professor Miguel Julve and Professor Francesc Lloret (Chemistry Department, University of Valencia, Spain) on a Quantum design SQUID susceptometer in the temperature range 4.2-300K with an applied magnetic field of H = 50 G unless otherwise stated. Crystalline samples (typically 40 mgs) were obtained directly from the reaction mixture, air-dried and powdered in a mortar. Samples were enclosed in gelatin capsules that were suspended at the middle of a plastic straw, which was rigidly fixed within the sample rod, and lowered into the instrument. The chamber was then Helium purged. The sample was centred between opposing faces of the magnet using computerized DC-centring.

Variable temperature magnetic measurements for the rest of the samples were performed by Dr. Boujemaa Moubaraki (Monash University, Australia) using a Quantum Design MPMS 5 SQUID magnetometer in the range 4-300 K with an applied magnetic field of 1 Tesla. The machine was calibrated by use of a standard palladium sample (Quantum Design) of accurately known magnetization or by use of magnetochemical calibrants such as $CuSO_4 \cdot 5H_2O$ and $[Ni(en)_3]S_2O_3$. Samples were contained in gelatine capsules held at the end of a plastic straw, which was fixed to the end of the sample rod. Prof. Keith Murray is thanked for his assistance with the interpretation of the magnetic data

6.2 Experimental.

6.2.1 Chapter 2.

Synthesis of $\{[Cu(4,4'\text{-dcbp})(H_2O)_2] \cdot 2H_2O\}_n$ ***(1)***.

4,4'-Na_2dcbp (120 mg, 0.4 mmol) was added to a stirred mixture of $Cu(NO_3)_2 \cdot 3H_2O$ (96 mg, 0.4 mmol) and $(NH_4)_2HPO_4$ (26 mg, 0.2 mmol) producing a blue precipitate. Adjustment of pH to 10 with dilute NaOH yielded a clear blue solution from which small blue crystals, suitable for a single crystal diffraction study, were obtained directly in 50% yield. The crystals were not sensitive to solvent loss.

IR (KBr): 3395(s, br), 3307(s, br), 1612(vs), 1556(s), 1482(w), 1428(m), 1380(vs), 1295(m), 1244(m), 1070(w), 1031(w), 919(w), 883(w), 786(m), 704(s), 628(m), 539(m), 470(w) cm^{-1}. Found Cu 16.84; C 37.99; H 3.45; N 7.29%. Required for $CuC_{12}H_{14}N_2O_8$ Cu 16.82; C 38.15; H 3.74; N 7.41%.

Synthesis of β-$[Co(4,4'\text{-dcbp})(H_2O)_2]_n$ ***(2)***.

$CoSO_4 \cdot 7H_2O$ (70 mg, 0.25 mmol) and 4,4'-H_2dcbp (61 mg, 0.25 mmol) were placed in a 23ml Teflon®-lined digestion bomb with 4ml H_2O and 1ml pyridine. After sealing the bomb, it was placed in an oven and heated to 185 °C for 3 days and then slowly cooled to room temperature (5 °C/hr). A mixture of orange prisms and pale pink prisms, suitable for a single crystal diffraction study, were obtained directly. The pale pink prisms were identified as β-$[Co(4,4'\text{-dcbp})(H_2O)_2]_n$.

IR (KBr): 3541(m), 3371(m), 2892(br,s), 1593(vs), 1550(vs), 1424(s), 1401(s), 1375(s), 1260(w), 1299(w), 1289(w), 1232(m), 1162(w), 1145(w), 1120(w), 1068(w), 993(w), 979(w), 895(m), 909(w), 874(m), 786(m), 759(m), 729(m), 695(m), 666(w), 459(w) cm^{-1}. Found C 43.86, H 2.70, N 8.50%. Required for $CoC_{12}H_{10}N_2O_6$ C 42.75; H 2.99; N 8.31%.

*Synthesis of {[Mn(4,4'-dcbp)]·½ DMF}$_n$ (**3**).*

$MnCl_2 \cdot 4H_2O$ (56 mg, 0.285 mmol) and 4,4'-H_2dcbp (140 mg, 0.57 mmol) were placed in a 23ml Teflon®-lined digestion bomb with 2ml H_2O and 2ml DMF. The bomb was sealed, placed in an oven and heated to 200 °C for 16 hrs and then very slowly cooled to room temperature (3 °C/hr). Yellow plates, suitable for a single crystal diffraction study, were obtained directly in 80% yield. The crystals are air-stable and insoluble in water and common organic solvents.

IR (KBr): 1673(s), 1600(vs), 1558(s), 1427(m), 1397(s, sh), 1380(vs), 1289(w), 1256(w), 1233(w), 1141(w), 1089(w), 1011(w), 925(w), 905(w), 883(w), 786(m), 687(s), 571(w), 538(w), 501(w) cm^{-1}. Found: C 48.24; H 2.64; N 10.29%. Required for $Mn_2C_{27}H_{19}N_5O_9$: C 48.59, H 2.87, N 10.49.

*Synthesis of {[Mn(4,4'-dcbp)]·½ DEF}$_n$ (**4**).*

$MnCl_2 \cdot 4H_2O$ (56 mg, 0.285 mmol) and 4,4'-H_2dcbp (140 mg, 0.57 mmol) were placed in a 23ml Teflon®-lined digestion bomb with 4ml diethylformamide. The bomb was sealed, placed in an oven and heated to 200 °C for 16 hrs and then very slowly cooled to room temperature (3 °C/hr). A yellow powder was obtained, within which a small amount of yellow plates suitable for a single crystal diffraction study were found.

*Synthesis of {[Mn(4,4'-dcbp)]·2H_2O}$_n$ (**5**).*

$MnCl_2 \cdot 4H_2O$ (56 mg, 0.285 mmol) and 4,4'-H_2dcbp (140 mg, 0.57 mmol) were placed in a 23ml Teflon®-lined digestion bomb with 4ml H_2O. The bomb was sealed, placed in an oven and heated to 200 °C for 16 hrs and then very slowly cooled to room temperature (3 °C/hr). Pale yellow needles were obtained in 74% yield. The yellow crystals are air stable and insoluble in common organic solvents.

IR (KBr): 3550(m, br), 3391 (w, br), 3230(w, br), 1600(vs), 1550(s), 1427(s, sh), 1408 (s, sh), 1383(vs), 1334(m, sh), 1296(w), 1228(w), 1151(w), 1113(w), 1010(w), 916(w), 863 (w), 791 (m), 690(vs), 597(w), 437(w) cm^{-1}. Found: C 42.94, H 1.68, N 8.27%. Required for $MnC_{12}H_{10}N_2O_6$: C 43.26, H 3.03, N 8.41%.

6.2.2 Chapter 3.

*Synthesis of {[Co(4,4'-dcbp)(py)(H_2O)$_2$]·½(4,4'-bipy)·2H_2O}$_n$ (**6**).*

$CoSO_4 \cdot 7H_2O$ (70 mg, 0.25 mmol), 4,4'-H_2dcbp (61 mg, 0.25 mmol) and 4,4'-bipy (39 mg, 0.25 mmol) were placed in a 23ml Teflon®-lined digestion bomb with 4ml water and 1ml pyridine. The bomb was sealed, placed in the oven, heated to 180 °C for 7 days and then cooled to room temperature at 5 °C/hr. Orange crystals were obtained directly in a 47% yield.

IR (KBr): 3288(m, br), 3118(m, br), 1614(s), 1548(s), 1417(m, sh), 1376(s), 1294(w), 1261(w), 1238(w), 1141(w), 1072(w), 1039(w), 1014(w), 917(w), 808(w), 777(m), 727(m), 700(s), 613(m), 551(w), 441(w), 420(w) cm^{-1}. Found C 48.03; H 4.10; N 11.15%. Required for $CoC_{22}H_{23}N_4O_9$ C 49.82; H 4.59; N 10.56%. (Microanalysis indicates that other species or impurities are present)

*Synthesis of [Cu(4,4'-dcbp)(4,4'-bipy)(H_2O)]·4½H_2O}$_n$ (**7**).*

$Cu(NO_3)_2 \cdot 3H_2O$ (120 mg, 0.5 mmol), 4,4'-H_2dcbp (122 mg, 0.5 mmol) and 4,4'-bipy (78 mg, 0.5 mmol) were placed in a 45ml Teflon®-lined digestion bomb with 8ml water and 1ml pyridine. The bomb was sealed and placed in a Carbolite oven where it was heated to 180 °C for 7 days, cooled to 100 °C and left for 10 hrs, and finally cooled to room temperature at 5 °C/hr. A blue powder had formed in a green solution. After filtering, the solution was left to evaporate and blue crystals formed within five days in 18% yield.

IR(KBr): 3386(vs, br), 3263(vs, br), 1629(vs), 1554(s), 1489(w), 1425(m, sh), 1402(s, sh), 1365(vs), 1292(m), 1241(m), 1221(w), 1141(w), 1122(w), 1101(w), 1072(w), 1024(w), 1003(w), 929(w), 858(w), 813(m), 782(s), 708(s), 630(m), 570(w), 512(w), 418(w) cm^{-1}. Found C 46.66; H 3.82; N 9.83%. Required for $Cu_2C_{44}H_{50}N_8O_{19}$ C 46.72; H5.26; N 9.91%.

*Synthesis of {[$Cu_2(OH)_2$(2,2'-bipy)$_2$(μ-4,4'-bipy)]$_2$·[[$Cu_2(OH)_2$(2,2-bipy)$_2$(4,4'-bipy)]$_2$-μ-(4,4'-bipy)]}·(NO_3)$_4$·xH_2O (**8**).*

Several repetitions of the above reaction produced the same result, except in one instance when a black powder was obtained, directly from the bomb, in a deep green solution. After filtering, the solution was left to stand and after a few hours had turned blue. Evaporation of this solution produced blue crystals within a week which were characterized by X-Ray diffraction.

IR (KBr): 3417(vs, br), 3060(m), 2396(w), 2034(w, br), 1763(w), 1600(vs), 1567(w), 1553(m), 1534(w), 1494(m), 1475(m), 1445(s, sh), 1378(vs), 1318(m), 1251(w), 1219(m), 1160(m), 1105(w), 1065(w), 1031(m), (1018(w), 1002(w), 940(w), 826(m), 800(s, sh), 779(s), 733(s), 659(w), 621(w), 492(m) cm^{-1}.

*Synthesis of [Cu(4,4'-H_2dcbp)Cl_2]$_2$·H_2O (**9**).*

$CuCl_2 \cdot 2H_2O$ (34 mg, 0.2 mmol) and 4,4'-H_2dcbp (97 mg, 0.4 mmol) were placed in a 45ml Teflon®-lined digestion bomb with 2ml water and 1ml conc. HCl. The bomb was sealed and placed in the oven where it was heated to 200 °C for 5 hours before slowly cooling to room temperature (3 °C/hr). Blue/green crystals were obtained directly in a 87% yield.

IR(KBr): 3619(w, br), 3428(w, br), 3183 (m), 3118 (m), 3085 (m), 3068 (m), 2518 (w, br), 1868 (w, br), 1729 (vs), 1700(s, sh), 1618(w), 1591(w), 1560(m), 1427 (m, sh), 1403(vs), 1376(m), 1290(s), 1238(m), 1211(vs), 1143(s), 1124(w), 1109(w), 1072(w), 1025(w), 971(w), 931(w), 866(w), 825(m), 769(m), 754(w), 713(w), 686(w), 659(s), 538(w) cm^{-1}. Found C 36.07; H 2.43; N 6.86; Cl 17.59%. Required for $CuC_{12}H_{10}N_2O_5Cl_2$ C 36.34; H 2.54; N 7.06; Cl 17.88%.

*Synthesis of {[Cu(4,4'-H_2dcbp)(SO_4)]·⅓H_2O}$_n$ (**10**).*

$CuSO_4 \cdot 5H_2O$ (99 mg, 0.4 mmol) and 4,4'-H_2dcbp (97 mg, 0.4 mmol) were placed in a 45ml Teflon®-lined digestion bomb with 2ml H_2O and 1ml conc. H_2SO_4. After sealing the bomb, it was placed in an oven where it was heated to 200 °C for 5 hrs and then slowly cooled to room temperature (3 °C/hr). Big, blue needles were obtained directly in a 70% yield.

IR (KBr): 2873(w, br), 2613(w), 1735(s), 1608(w), 1562(w), 1523(w), 1486(w), 1402(m), 1313(m), 1234(s), 1187(vs), 1122(vs), 1103(vs), 1025(s, sh), 991(vs), 767(w), 678(m), 655(w), 599(m), 453(w) cm^{-1}. Found C 34.58; H 1.87; N 6.60%. Required for $Cu_3C_{36}H_{26}N_6O_{25}S_3$ C 35.17; H 2.13; N 6.84%.

*Synthesis of [Cu(4,4'-H_2dcbp)(NO_3)$_2$(H_2O)] (**11**).*

$CuNO_3 \cdot 3H_2O$ (97 mg, 0.4 mmol) and 4,4'-H_2dcbp (97 mg, 0.4 mmol) were placed in a 45ml Teflon®-lined digestion bomb with 2ml H_2O and 1ml conc. HNO_3. After sealing the bomb, it was placed in an oven where it was heated to 200 °C for 5 hrs and then slowly cooled to room temperature (3 °C/hr). A blue solution was obtained from which blue crystals grew on evaporation over a period of three weeks in a 33% yield.

IR (KBr): 3627(w), 3471(w), 3196(br, m), 3079(br,m), 2644(br, m), 1732(s), 1594(w), 1560(m), 1391(vs), 1292(m), 1212(s), 1143(m), 1126(w), 1072(w), 1023(w), 931(w), 866(w), 826(m), 769(m), 753(w), 713(w), 659(m), 540(w), 475(w) cm^{-1}.

6.2.3 Chapter 4.

*Synthesis of [Co(4,4'-dcbp)(H_2O)$_4$]·4H_2O (**12**).*

Triethylamine (0.15 ml) was added to an aqueous suspension of 4,4'-H_2dcbp (50 mg, 0.2 mmol) and $CoSO_4 \cdot 7H_2O$ (18 mg, 0.064 mmol) and the mixture was heated to reflux until all the solid had dissolved. On slow evaporation of the yellow solution, needle-like yellow crystals suitable for a diffraction study were formed in approximately 30% yield. The crystals gradually lose solvent on exposure to air.

IR (KBr): 3237(vs, br), 1593(s), 1543(vs), 1422(m), 1380(s), 1292(w), 1262(w), 1234(m), 1152(w), 1120(w), 1082(w), 1043(w), 1016(w), 922(w), 787(m), 700(m), 659(w), 624(w), 579(w) cm^{-1}.

Synthesis of $[Me_2NH_2]_{1.5}[Co(4,4'\text{-}H_{5/6}dcbp)]\cdot 10\frac{1}{2}H_2O$ (**13**).

$CoCl_2\cdot 6H_2O$ (45 mg, 0.19 mmol) and 4,4'-H_2dcbp (140 mg, 0.57 mmol) were placed in a 45 ml Teflon® insert with 2ml H_2O and 2ml DMF. The bomb was sealed and placed in an oven where it was heated to 200°C for 36 hrs and cooled to room temperature at 3°C/hr. Orange needles were obtained directly in 25% yield. After filtering these the remaining brown solution was left to evaporate producing brown prisms after two weeks in ca. 20% yield. These are unstable out of solution.

IR (KBr): 3424(br, s), 3023(br, s), 2782(br, s), 2482(br, m), 1618(vs), 1553(vs), 1470(m), 1405(m), 1366(Vs), 1287(m), 1244(m), 1147(w), 1108(w), 1057(w), 1023(w), 912(w), 876(w), 850(w), 780(S), 706(m) cm^{-1}.

Synthesis of $[NH_2Me_2]_2[Cu(4,4'\text{-}dcbp)_2(H_2O)]$ (**14**).

$CuCl_2\cdot 2H_2O$ (48 mg, 0.28 mmol) and 4,4'-H_2dcbp (140 mg, 0.57 mmol) were placed in a 45 ml Teflon® insert together with 2ml H_2O and 2ml DMF. The bomb was sealed and placed in an oven where it was heated to 200°C for 36 hrs and cooled to room temperature at 3 °C/hr. A dark brown solution, containing some brown powder, was obtained. The powder was filtered and the remaining solution was left to evaporate, yielding blue/green crystals within a week in *ca.* 19% yield.

IR (KBr): 3842(w), 3620(w), 3433(m, br), 3059(m, br), 1616(vs), 1549(vs), 1487(m), 1400(s), 1363(vs), 1289(w), 1262(w), 1244(m), 1137(w), 1094(w), 1020(m), 922(w), 779(s), 719(m), 698(s), 422(w) cm^{-1}.

Synthesis of $[Na_2][Cu(4,4'\text{-}dcbp)_2(H_2O)]\cdot 10H_2O$ (**15**).

An aqueous solution of 4,4'-Na_2dcbp (230 mg, 0.82 mmol) was added to an aqueous mixture of $Cu(NO_3)_2\cdot 3H_2O$ (96 mg, 0.4 mmol) and $(NH_4)_2HPO_4$ (26 mg, 0.2 mmol) producing a blue solution. Blue prisms grew on evaporation of the blue solution after two weeks in 32 % yield.

IR (KBr): 3326(br, s), 2171(m), 1610(vs), 1557(vs), 1482(m), 1427(w), 1402(w), 1378(vs), 1297(s), 1246(s), 1139(w), 1071(w) 1033(w), 919(w), 8852(m), 786(s), 704(s) cm^{-1}. Found: C 34.57; H 2.61; N 7.30%. Calcd. for $CuC_{24}H_{34}N_4O_{19}Na_2$: C 36.39, H 7.07, N 4.33%. (Microanalysis indicates that other species or impurities are present)

6.2.4 Chapter 5.

4,4'-dicarboxy-2,2'-bipyridine was obtained by dichromate oxidation of 4,4'-dimethyl-2,2'-bipyridine according to the modified procedure of Oki and Morgan.[227]

*Crystallisation of 4,4'-dicarboxy-2,2'-bipyridine (**16**).*

$FeCl_2$ (37 mg, 0.19 mmol) and 4,4'-H_2dcbp (140 mg, 0.57 mmol) were placed in a 45ml Teflon®-lined digestion bomb together with 2ml H_2O and 1ml HCl. The bomb was sealed and placed in an oven where it was heated to 200 °C for 3½ hours and then slowly cooled to room temperature (3 °C/hr). Long, colorless needles were obtained directly in 80% yield.

IR (KBr): 3109(w), 2435(m, br), 1860(w, br), 1717(s), 1603(w), 1457(m), 1364(s), 1289(vs), 1267(s), 1241(s), 1137(m), 1065(m), 1010(m), 914(w), 864(w), 819(w), 764(s), 679(s) and 516(w) cm^{-1}. ^1H NMR (d_6-DMSO, 400MHz): δ 8.92 (d, 2H, J = 5Hz, H6), 8.85 (brs, 2H, H3), 7.92 (dd, 2H, J = 5Hz, J = 1.5Hz, H5). Found C 58.72; H 3.64; N 11.19%. Required for $C_{12}H_8N_2O_4$ C 59.02; H 3.30; N 11.47%. mp > 325 °C

*Crystallisation of (4,4'-H_3dcbp)(Cl) (**17**).*

$(NH_4)_2$(4,4'-dcbp) (73 mg, 0.26 mmol) was placed in a 45ml Teflon®-lined bomb with 1ml H_2O and 2ml HCl. After sealing the bomb, it was placed in an oven and heated to 240 °C for 3 hours and then cooled to room temperature at 0.3 °C/hr. Colorless needles were obtained in 82% yield.

IR: 3135(m), 3074(m), 2830(m, br), 2265(s, br), 1841(s), 1729(vs), 1666(s), 1596(s), 1561(m), 1511(w), 1487(w), 1450(m), 1427(s), 1399(m), 1367(w), 1334(w), 1241(s), 1213(vs), 1140(s), 1101(w), 1071(w), 1024(w), 1006(w), 994(w), 947(s), 884(w), 814(s), 772(m), 760(w), 74(m), 707(w), 671(w), 659(s), 538(m) cm^{-1}. Found: C 51.00; H 2.89; N 9.77%. Calcd. for $C_{12}H_9N_2O_4Cl$: C 51.35; H 3.23; N 9.98%.

*Crystallisation of [(TBA)(4,4'-Hdcbp)]·4H_2O (**18**).*

4,4'-H_2dcbp (71 mg, 0.30 mmol) was placed in 50ml MeOH, 25ml acetone and 580µl of tetrabutylammonium hydroxide (1M in MeOH) and heated until all the 4,4'-H_2dcbp had solubilised. $[(NH_4)_2Fe(SO_4)_2]\cdot 6H_2O$ (44 mg, 0.11 mmol) in 10ml H_2O was then added, immediately producing a red solution. A further 20ml H_2O were added and the MeOH and acetone were boiled off. The aqueous solution was then reduced on the rotary evaporator to a third its volume, obtaining a very concentrated red solution, from which a few colorless crystals formed on evaporation. The small amount of crystals produced did not allow for any further analysis other than single crystal X-Ray diffraction.

*Crystallisation of $(DEA)_2$(4,4'-dcbp) (**19**).*

$MnCl_2\cdot 2H_2O$ (56 mg, 0.285 mmol) and 4,4'-H_2dcbp (140 mg, 0.57 mmol) were placed in a Teflon®-lined 23ml digestion bomb with 4ml diethylformamide. The bomb was sealed and placed in an oven where it was heated to 200 °C for 16 hours before cooling to

room temperature (3 °C/hr). Within the yellow powder and crystals obtained, a few colorless crystals were found.

Synthesis of ester derivatives of 4,4'-H_2dcbp.

All the esters were synthesized by a modification of a previously reported method.[236] 4,4'-H_2dcbp was refluxed for 24 hrs in the appropriate alcoholic solvent with a catalytic amount of conc. H_2SO_4 to yield the corresponding ester.

4,4'-dimethylcarboxy-2,2'-biyridine (**20**): Yield 75%. Mp 211°C. ^{1}H NMR ($CDCl_3$): δ 8.99 (s, 2H, H3), 8.90 (d, 2H, *J* = 4.5 Hz, H6), 7.94 (d, 2H, *J* = 4 Hz, H5), 4.03 (s, 6H, OC**H**$_3$).
4,4'-diethylcarboxy-2,2'-biyridine (**21**): Yield 64%. Mp 165 °C. ^{1}H NMR ($CDCl_3$): δ 8.98 (s, 2H, H3), 8.89 (d, 2H, *J* = 4.5 Hz, H6), 7.93 (d, 2H, *J* = 4Hz, H5), 4.49 (q, 4H, *J* = 7 Hz, -OC**H**$_2$), 1.47 (t, 6H, *J* = 7 Hz, CH_2C**H**$_3$).
4,4'-diisopropylcarboxy-2,2'-biyridine (**22**): Yield 18%. Mp 143 °C. ^{1}H NMR ($CDCl_3$): δ 8.95 (s, 2H, H3), 8.88 (d, 2H, *J* = 5 Hz, H6), 7.93 (d, 2H, *J* = 5 Hz, H5), 5.35 (septuplet, 1H, *J* = 6.5 Hz, OC**H**), 1.44 (d, 6H, *J* = 6.5 Hz, OCH(C**H**$_3$)$_2$).
4,4'-dibutylcarboxy-2,2'-biyridine (**23**): Yield 44%. Mp 115°C. ^{1}H NMR ($CDCl_3$): δ 8.99 (s, 2H, H3), 8.89 (d, 2H, *J* = 5Hz, H6), 4.43 (t, 6H, *J* =6.5 Hz, OC**H**$_3$), 1.83 (quintet, 4H, *J* = 7 Hz, *J* = 7.5 Hz, CH_2C**H**$_2$$CH_2$), 1.52 (sextet, 4H, *J* = 8, *J* = 7.5, CH_2C**H**$_2$$CH_3$), 1.02 (t, 6H, *J* = 8, C**H**$_3$)

Appendix

Chapter 1

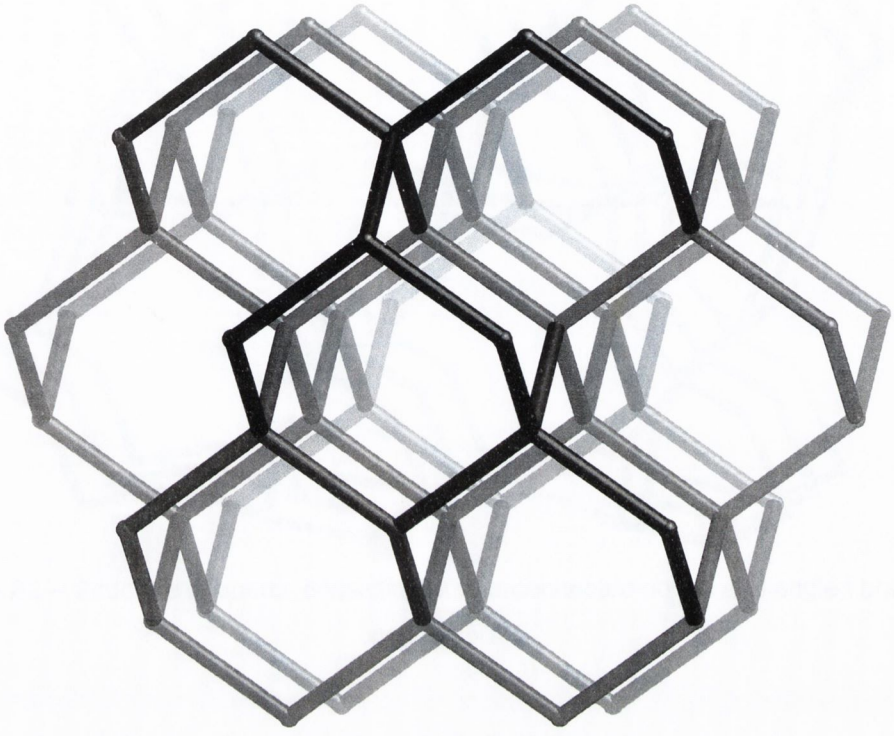

Figure A1 – Structure of diamond, consisting of four-connected nodes.

Figure A2 – Structure of lonsdaleite, consisting of four-connected nodes.

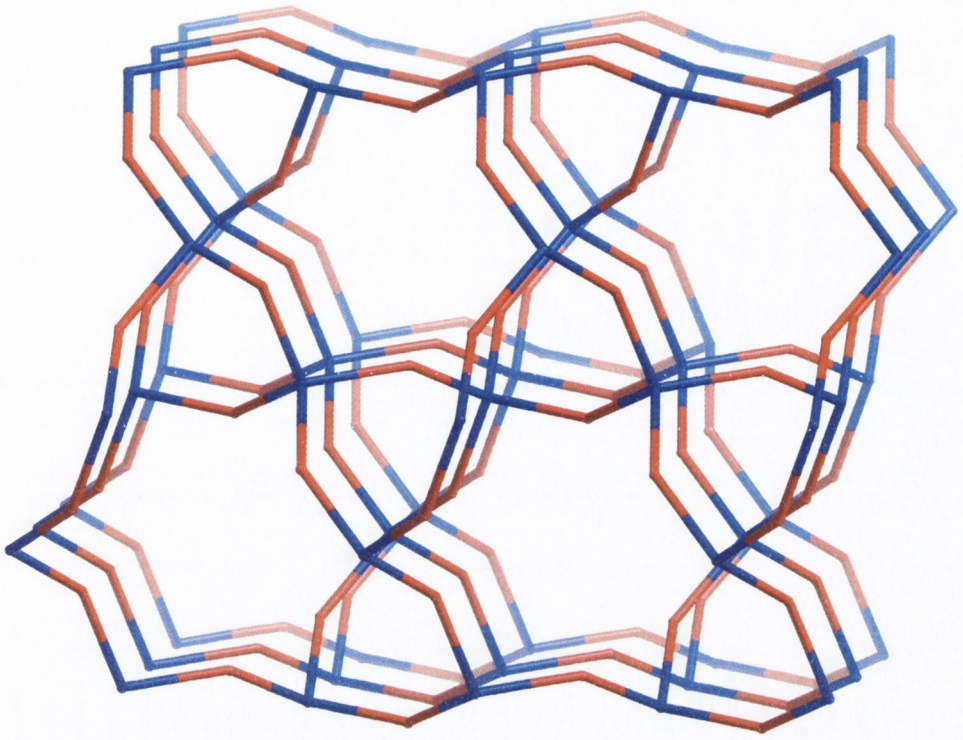

Figure A3 – Structure of quartz, consisting of four-connected nodes and angled bridging connectors.

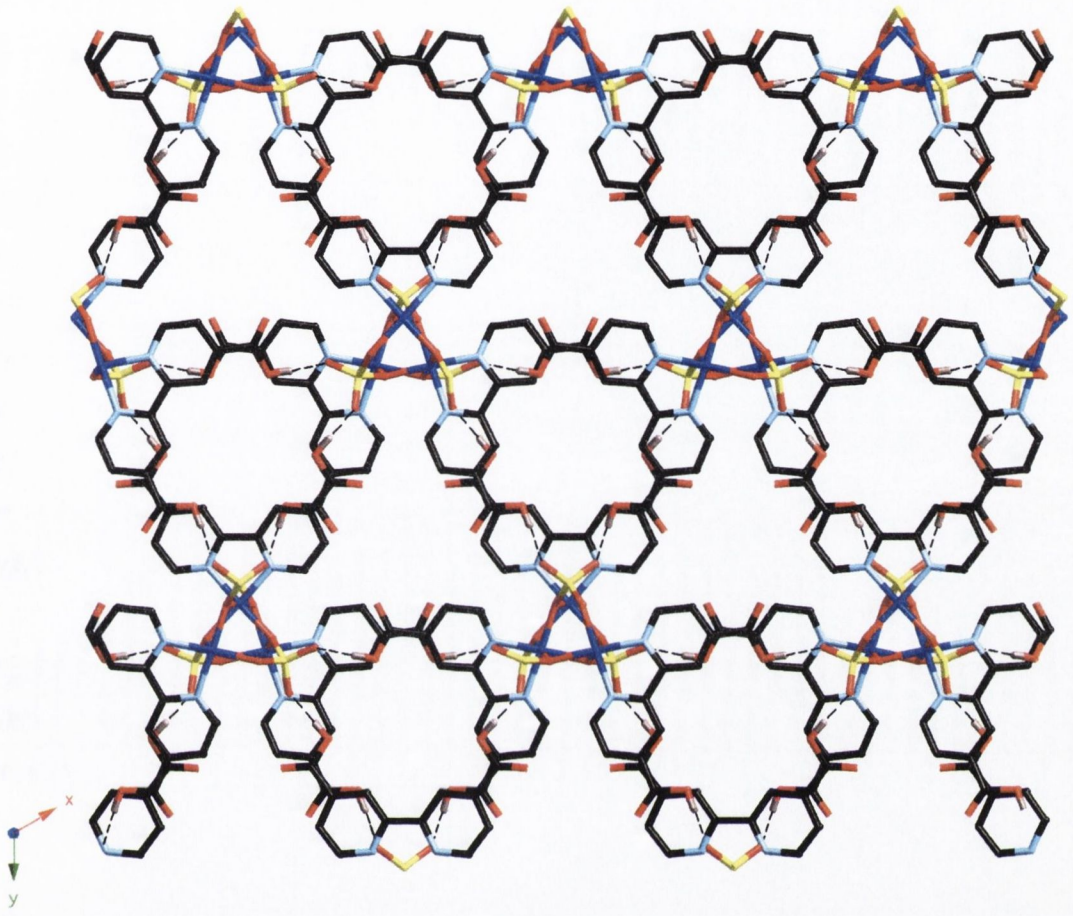

Figure A4 – Structure of **10a**, showing the empty channels. (Hydrogen bonds shown as dashed bonds. Bipyridyl hydrogen atoms omitted for clarity)

Table A1 – Crystallographic data for **10a**.

Compound		**10a**
Chemical Formula		$CuC_{12}H_8N_2O_8S$
Formula weight		403.8
Crystal system		Trigonal
Space group		*R*32
$\mu(MoK_\alpha)$/ mm^{-1}		1.698
a/Å		23.1081(9)
b/Å		23.1081(9)
c/Å		7.0541(3)
α/°		90
β/°		90
γ/°		120
V/$Å^3$		3262.1(2)
Z		9
D_{calc}/gcm^{-3}		1.850
T/K		153(2)
Crystal size	max /mm	0.33
	mid /mm	0.33
	min /mm	0.25
$2\theta_{max}$/°		60.06
Min/Max trans. Factor		0.836/1.000‡
R_{int}		0.0285
R_1, $wR_2[I>2\sigma(I)]$[a]		0.0278, 0.0721
R_1, wR_2 (all data)		0.0284, 0.0724
Largest diff. Peak		0.89 e.$Å^{-3}$
Reflections –	collected:	25246
	unique:	4389
	observed:	4301

[a] $R_1 = \Sigma||F_o| - |F_c||/\Sigma|F_o|$, $wR_2 = [\Sigma w(F_o^2 - F_c^2)^2/\Sigma w(F_o^2)^2]^{1/2}$

‡ Absorption correction performed with TWINABS

Figure A5 – Herringbone packing of 4,4'-dmbp. Nearest neighbours are non-parallel and C···H interactions (as opposed to C···C interactions) are maximized. (Hydrogen atoms omitted for clarity)

Attached CD-ROM

The CD-ROM attached to this thesis contains electronic versions of various files for the structures given in this thesis.

The CIF folder contains all the crystallographic information files (*.cif). The naming of each file corresponds to the structure as given in the thesis (e.g. Struct1 corresponds to Structure **1**. CIFs can be viewed in the Mercury program, which is a program available as a free download from the CCDC website (www.ccdc.cam.ac.uk))).

The PDF folder contains portable document format files (*.pdf). These files are complete listings of the crystallographic information (including bond lengths and angles tables) for all the structures presented herein. (PDF files can be viewed in the Adobe Acrobat Reader program, which is available as a free download from the Adobe website (www.adobe.com/products/acrobat/readermain.html)).

References

[1.] J.-M. Lehn, *Supramolecular Chemistry, Concepts and Perspectives,* VCH, Weinheim, 1995.

[2.] J.-M. Lehn, *Angew. Chem. Int. Ed.*, 1988, **27**, 89.

[3.] W. M. Latimer and W. H. Rodebush, *J. Am. Chem. Soc.*, 1920, **42**, 1419.

[4.] M. L. Huggins, *J. Phys. Chem.*, 1922, **26**, 601.

[5.] G. R. Desiraju and T. Steiner, *The Weak Hydrogen Bond In Structural Chemistry and Biology,* Oxford University Press, 1999.

[6.] G. A. Jeffrey and W. Saenger, *Hydrogen Bonding in Biological Structures,* Springer-Verlag, 1991.

[7.] G. A. Jeffrey, *An introduction to hydrogen bonding,* Oxford University Press, 1997.

[8.] T. Steiner, *Angew. Chem. Int. Ed.*, 2002, **41**, 49.

[9.] C. B. Aakeröy and K. R. Seddon, *Chem. Soc. Rev.*, 1993, 397.

[10.] L. Pauling, *The Nature of the Chemical Bond and the Structure of Molecules and Crystals - An introduction to Modern Structural Chemistry,* Oxford University Press, 1940.

[11.] G. C. Pimental and A. L. McClellan, *The Hydrogen Bond,* Freeman, 1960.

[12.] P. W. Atkins, *General Chemistry,* Scientific American Books, 1989.

[13.] M. Chaplin, http://www.lsbu.ac.uk/water/hbond.html

[14.] G. R. Desiraju, *Acc. Chem. Res.*, 2002, **35**, 565.

[15.] J.-M. Lehn, A. Rigault, J. Siegel, J. Harrowfield, B. Chevrier and D. Moras, *Proc. Natl. Acad. Sci. USA*, 1987, **84**, 2565.

[16.] K. O'Donaghue, *Towards Binuclear Metal Complexes as Probes for DNA: a Study of Bis-Phenanthroline ruthenium (II) Dipyrido[3,2-d:2',3'-f]quinoxaline and its derivatives*, University of Dublin, Dublin, 2002.

[17.] D. Philp and J. F. Stoddart, *Angew. Chem. Int. Ed.*, 1996, **35**, 1154.

[18.] G. Schmidt, *Pure Appl. Chem.*, 1971, **27**, 647.

[19.] D. Braga, *Chem. Commun.*, 2003, 2751.

[20.] J. D. Dunitz, *Perspectives in Supramolecular Chemistry*, G. R. Desiraju, Ed., John Wiley & Sons Ltd., 1996.

[21.] G. R. Desiraju, *J. Mol. Struct.*, 2003, **656**, 5.

[22.] M. D. Hollingsworth, *Science*, 2002, **295**, 2410.

[23.] D. N. Reinhoudt, *Supramolecular Materials and Technologies,* John Wiley & Sons Ltd., 1999.

[24.] O. Kahn, *Acc. Chem. Res.*, 2000, **33**, 647.

[25.] D. Y. Curtin and I. C. Paul, *Chem. Rev.*, 1981, **81**, 525.

[26.] J. Y. Ying, C. P. Mehnert and M. S. Wong, *Angew. Chem. Int. Ed.*, 1999, **38**, 56.

[27.] D. Braga and F. Grepioni, *Acc. Chem. Res.*, 2000, **33**, 601.

[28.] D. Braga and F. Grepioni, *Coord. Chem. Rev.*, 1999, **183**, 19.

[29.] G. R. Desiraju, *J. Chem. Soc., Dalton Trans.*, 2000, 3745.

[30.] A. J. Blake, N. R. Champness, P. Hubberstey, W.-S. Li, M. A. Withersby and M. Schröder, *Coord. Chem. Rev.*, 1999, **183**, 177.

[31.] S. R. Batten, *Curr. Opin. Solid State Mater. Sci.*, 2001, **5**, 107.

[32.] C. Janiak, *Dalton. Trans.*, 2003, 2781.

[33.] D. W. Bruce and D. O'Hare, *Inorganic materials,* John Wiley & Sons Ltd., 1996.

[34.] K. Biradha, *Cryst. Eng. Comm.*, 2003, **5**, 374.

[35.] R. Bishop, *Synlett*, 1999, **9**, 1351.

[36.] D. S. Reddy, B. S. Goud, K. Panneerselvam and G. R. Desiraju, *J. Chem. Soc., Chem. Commun.*, 1993, 663.

[37.] S. S. Kuduva, D. C. Craig, A. Nangia and G. R. Desiraju, *J. Am. Chem. Soc.*, 1999, **121**, 1936.

[38.] S.-F. Lai, C.-Y. Cheng and K.-J. Lin, *Chem. Commun.*, 2001, 1082.

[39.] K. S. Min and M. P. Suh, *Eur. J. Inorg. Chem.*, 2001, 449.

[40.] A. Gavezzotti, *Acc. Chem. Res.*, 1994, **27**, 309.

[41.] M. U. Schmidt and U. Englert, *J. Chem. Soc., Dalton Trans.*, 1996, 2077.

[42.] P. Ball, *Nature*, 1996, **381**, 648.

[43.] J. Hulliger, *Angew. Chem. Int. Ed.*, 1994, **33**, 143.

[44.] G. R. Desiraju, *Crystal Engineering: the Design of Organic Solids,* Elsevier, 1989.

[45.] M. C. Etter, *Acc. Chem. Res.*, 1990, **23**, 120.

[46.] J. Bernstein, R. E. Davis, L. Shimoni and N.-L. Chang, *Angew. Chem. Int. Ed.*, 1995, **34**, 1555.

[47.] G. R. Desiraju, *Angew. Chem. Int. Ed.*, 1995, **34**, 2311.

[48.] E. J. Corey, *Pure Appl. Chem.*, 1967, **14**, 19.

[49.] L. Leiserowitz, *Acta Crystallogr.*, 1977, **B33**, 2719.

[50.] B. Moulton and M. J. Zaworotko, *Chem. Rev.*, 2001, **101**, 1629.

[51.] C. B. Aakeröy, A. M. Beatty and B. A. Helfrich, *J. Am. Chem. Soc.*, 2002, **124**, 14425.

[52.] N. Shan, A. D. Bond and W. Jones, *Cryst. Eng.*, 2002, **5**, 9.

[53.] C. V. K. Sharma and M. J. Zaworotko, *Chem. Comm.*, 1996, 2655.

[54.] A. M. Beatty, K. E. Granger and A. E. Simpson, *Chem. Eur. J.*, 2002, **8**, 3254.

[55.] C. V. K. Sharma, C. B. Bauer, R. D. Rogers and M. J. Zaworotko, *Chem. Commun.*, 1997, 1559.

[56.] K. Biradha, D. Dennis, V. A. MacKinnon, C. V. K. Sharma and M. J. Zaworotko, *J. Am. Chem. Soc.*, 1998, **120**, 11894.

[57.] D. J. Plaut, K. M. Lund and M. D. Ward, *Chem. Commun.*, 2000, 769.

[58.] J. P. Sauvage, *Transition metals in supramolecular chemistry,* John Wiley & Sons Ltd., 1999.

[59.] B. Olenyuk, A. Fechtenkotter and P. J. Stang, *Dalton. Trans.*, 1998, 1707.

[60.] B. J. Holliday and C. A. Mirkin, *Angew. Chem. Int. Ed.*, 2001, **40**, 2023.

[61.] P. J. Stang and B. Olenyuk, *Acc. Chem. Res.*, 1997, **30**, 502.

[62.] S. Leininger, B. Olenyuk and P. J. Stang, *Chem. Rev.*, 2000, **100**, 853.

[63.] M. Albrecht, *Chem. Rev.*, 2001, **101**, 3457.

[64.] J. Keegan, P. E. Kruger, M. Nieuwenhuyzen, J. O'Brien and N. Martin, *Chem. Commun.*, 2001, 2192.

[65.] C. Piguet, G. Bernardinelli and G. Hopfgartner, *Chem. Rev.*, 1997, **97**, 2005.

[66.] M. Fujita, F. Ibukuro, H. Seki, O. Kamo, M. Imanari and K. Ogura, *J. Am. Chem. Soc.*, 1996, **118**, 899.

[67.] M. Fujita, *Acc. Chem. Res.*, 1999, **32**, 53.

[68.] G.-C. Guo, Q.-M. Wang and T. C. W. Mak, *Inorg. Chem. Comm.*, 2000, **3**, 313.

[69.] B. F. Abrahams, K. D. Lu, B. Moubaraki, K. S. Murray and R. Robson, *J. Chem. Soc., Dalton Trans.*, 2000, 1793.

[70.] M. Maekawa, K. Sugimoto, T. Kuroda-Sowa, Y. Suenaga and M. Munakata, *J. Chem. Soc., Dalton. Trans*, 1999, 4357.

[71.] A. J. Blake, N. R. Champness, A. Khlobystov, K. A. Lemenovskii, W.-S. Li and M. Schröder, *Chem. Commun.*, 1997, 2027.

[72.] M. Fujita, O. Sasaki, K.-Y. Watanabe, K. Ogura and K. Yamaguchi, *New J. Chem*, 1998, 189.

[73.] L. Carlucci, G. Ciani and D. M. Proserpio, *J. Chem. Soc., Dalton Trans.*, 1999, 1799.

[74.] V. Balzani, A. Credi, F. M. Raymo and J. F. Stoddart, *Angew. Chem. Int. Ed.*, 2000, **39**, 3349.

[75.] F. Vögtle, J. F. Stoddart and M. Shibasaki, *Stimulating Concepts in Chemistry,* Wiley-VCH, 2000.

[76.] B. Conerney, *Aspects of Supramolecular Chemistry. Molecular Helicates and Coordination Polymers*, Trinity College, Dublin, 2003.

[77.] C. J. Matthews, S. T. Onions, G. Morata, L. J. Davis, S. L. Heath and D. J. Price, *Angew. Chem. Int. Ed.*, 2003, 3166.

[78.] B. F. Abrahams, B. F. Hoskins and R. Robson, *J. Chem. Soc., Chem. Commun.*, 1990, 60.

[79.] B. F. Hoskins and R. Robson, *J. Am. Chem. Soc.*, 1990, **112**, 1546.

[80.] R. W. Gable, B. F. Hoskins and R. Robson, *J. Chem. Soc., Chem. Commun.*, 1990, 1677.

[81.] R. W. Gable, B. F. Hoskins and R. Robson, *J. Chem. Soc., Chem. Commun.*, 1990, 762.

[82.] S. R. Batten, Bernard F. Hoskins and R. Robson, *J. Chem. Soc., Chem. Commun.*, 1991, 445.

[83.] B. F. Abrahams, R. Robson and B. F. Hoskins, *J. Am. Chem. Soc.*, 1991, **113**, 3606.

[84.] A. F. Wells, *Models in Strucutral Inorganic Chemistry,* Oxford University Press, 1970.

[85.] A. F. Wells, *Three-Dimensional Nets and Polyhedra,* John Wiley & Sons, 1977.

[86.] X. Xu, M. Nieuwenhuyzen and S. L. James, *Angew. Chem. Int. Ed.*, 2002, **41**, 764.

[87.] E. Lozano, M. Nieuwenhuyzen and S. L. James, *Chem. Eur. J.*, 2003, **7**, 2644.

[88.] S. I. Noro, R. Kitaura, M. Kondo, S. Kitagawa, T. Ishii, J. Matsuzaka and M. Yamashita, *J. Am. Chem. Soc.*, 2002, **124**, 2568.

[89.] O. M. Yaghi and G. Li., *Angew. Chem. Int. Ed.*, 1995, **34**, 207.

[90.] S. R. Batten, J. C. Jeffery and M. D. Ward, *Inorg. Chim. Acta*, 1999, **292**, 231.

[91.] F. Robinson and M. J. Zaworotko, *J. Chem. Soc., Chem. Commun.*, 1995, 2413.

[92.] O. M. Yaghi and H. Li, *J. Am. Chem. Soc.*, 1996, **118**, 295.

[93.] K. Biradha, A. Mondal, B. Moulton and M. J. Zaworotko, *J. Chem. Soc., Dalton Trans.*, 2000, 3837.

[94.] K. Biradha, K. V. Domasevitch, B. Moulton, C. Seward and M. J. Zaworotko, *Chem. Commun.*, 1999, 1327.

[95.] B. Moulton, E. B. Rather and M. J. Zaworotko, *Cryst. Eng.*, 2001, **4**, 309.

[96.] K. Biradha and M. Fujita, *Chem. Commun.*, 2001, 15.

[97.] A. Nangia and G. R. Desiraju, *Chem. Commun.*, 1999, 605.

[98.] S. R. Batten and R. Robson, *Angew. Chem. Int. Ed.*, 1998, **37**, 1461.

[99.] B. F. Abrahams, P. A. Jackson and R. Robson, *Angew. Chem. Int. Ed.*, 1998, **37**, 2656.

[100.] J. Kepert and M. J. Rosseinsky, *Chem. Commun.*, 1998, 31.

[101.] C. J. Kepert, T. J. Prior and M. J. Rosseinsky, *J. Am. Chem. Soc.*, 2000, **122**, 5158.

[102.] S. Decurtins, H. W. Schmalle, P. Schneuwly and H. R. Oswald, *Inorg. Chem.*, 1993, **32**, 1888.

[103.] L. Carlucci, G. Ciani, D. M. Proserpio and A. Sironi, *J. Am. Chem. Soc.*, 1995, **117**, 12861.

[104.] S. Decurtins, H. W. Schmalle, P. Schnewusly, J. Ensling and P. Gütlich, *J. Am. Chem. Soc.*, 1994, **116**, 9521.

[105.] S. Decurtins, H. W. Schmalle, R. Pellaux, P. Schneusly and A. Hauser, *Inorg. Chem.*, 1996, **35**, 1451.

[106.] L. Carlucci, G. Ciani, D. M. Proserpio and A. Sironi, *Chem. Commun.*, 1996, 1393.

[107.] B. F. Abrahams, S. Batten, H. Hamit, B. F. Hoskins and R. Robson, *J. Chem. Soc., Chem. Commun.*, 1996, 1313.

[108.] O. M. Yaghi, C. E. Davis, G. Li and H. Li, *J. Am. Chem. Soc.*, 1997, **119**, 2861.

[109.] B. F. Abrahams, S. R. Batten, M. J. Grannas, H. Hamit, B. F. Hoskins, R. Robson, *Angew. Chem. Int. Ed.*, 1999, **38**, 1475.

[110.] M. M. Turnbull and C. P. Landee, *Science*, 2002, **298**, 1723.

[111.] M. J. Zaworotko, *Nature*, 1999, **402**, 242.

[112.] N. L. Rosi, M. Eddaoudi, J. Kim, M. O'Keefe and O. M. Yaghi, *Cryst. Eng. Comm.*, 2002, **4**, 401.

[113.] S. L. James, *Chem. Soc. Rev.*, 2003, **32**, 276.

[114.] O. M. Yaghi, H. Li, C. Davis, D. Richardson and T. L. Groy, *Acc. Chem. Res.*, 1998, **31**, 474.

[115.] A. Dyer, *An Introduction to Zeolite Molecular Sieves,* John Wiley & Sons Ltd., 1988.

[116.] M. Eddaoudi, D. B. Moler, H. Li, B. Chen, T. M. Reineke, M. O'Keeffe and O. M. Yaghi, *Acc. Chem. Res.*, 2001, **34**, 319.

[117.] N. L. Rosi, M. Eddaoudi, J. Kim, M. O'Keeffe and O. M. Yaghi, *Angew. Chem. Int. Ed.*, 2002, **41**, 284.

[118.] M. Eddaoudi, J. Kim, J. B. Wachter, H. K. Chae, M. O'Keeffe and O. M. Yaghi, *J. Am. Chem. Soc.*, 2001, **123**, 4368.

[119.] B. Chen, M. Eddaoudi, S. T. Hyde, M. O'Keeffe and O. M. Yaghi, *Science*, 2001, **291**, 1021.

[120.] H. Li, M. Eddaoudi, M. O'Keeffe and O. M. Yaghi, *Nature*, 1999, **402**, 276.

[121.] R. C. Mehrotra and R. Bohra, *Metal Carboxylate,* Academic Press Inc., 1983.

[122.] O. M. Yaghi, M. O'Keefe, N. W. Ockwit, H. K. Chae, M. Eddaoudi and J. Kim, *Nature*, 2003, **423**, 705.

[123.] M. Eddaoudi, J. Kim, N. Rosi, D. Vodak, J. Wachter, M. O'Keefe and O. M. Yaghi, *Science*, 2002, **295**, 469.

[124.] *Chem. Br.*, 2003, **39**, 17.

[125.] B. McEnaney, *Chem. Br.*, 2003, **39**, 24.

[126.] N. L. Rosi, J. Eckert, M. Eddaoudi, D. T. Vodak, J. Kim, M. O'Keefe and O. M. Yaghi, *Science*, 2003, **300**, 1127.

[127.] S.-I. Noro, S. Kitagawa, M. Kondo and K. Seki, *Angew. Chem. Int. Ed.*, 2000, **39**, 2082.

[128.] R. Kitaura, S. Kitagawa, Y. Kubota, T. C. Kobayashi, K. Kindo, Y. Mita, A. Matsuo, M. Kobayashi, H.-C. Chang, T. C. Ozawa, M. Suzuki, M. Sakata and M. Sakata, *Science*, 2002, **298**, 2358.

[129.] R. Kitaura, K. Seki, G. Akiyama and S. Kitagawa, *Angew. Chem. Int. Ed.*, 2003, **42**, 428.

[130.] J. S. Seo, D. Whang, H. Lee, S. I. Jun, J. Oh, Y. J. Jeon and K. Kim, *Nature*, 2000, **404**, 982.

[131.] G. J. Halder, C. J. Kepert, B. Moubaraki, K. S. Murray and J. D. Cashion, *Science*, 2002, **298**, 1762.

[132.] S. Subramanian and M. J. Zaworotko, *Angew. Chem. Int. Ed.*, 1995, **34**, 2127.

[133.] S. Chui, S. Lo, J. P. H. Charmant, A. G. Orpen and I. D. Williams, *Science*, 1999, **283**, 1148.

[134.] A. J. Fletcher, E. J. Cussen, T. J. Prior, M. J. Rosseinsky, C. J. Kepert and K. M. Thomas, *J. Am. Chem. Soc.*, 2001, **123**, 10001.

[135.] E. J. Cussen, T. J. Prior, M. J. Rosseinsky and C. J. Kepert, *J. Am. Chem. Soc.*, 2002, **124**, 9574.

[136.] A. M. Beatty, *Cryst. Eng. Comm.*, 2001, **51**, 1.

[137.] L. Brammer, M. D. Burgard, M. D. Eddleston, C. S. Rodger, N. P. Rath and H. Adams, *Cryst. Eng. Comm.*, 2002, **4**, 239.

[138.] U. Ziener, E. Breuning, J.-M. Lehn, E. Wegelius, K. Rissanen, G. Baum, D. Fenske and G. Vaughan, *Chem. Eur. J.*, 2000, **6**, 4132.

[139.] X. Xu, S. L. James, D. M. P. Mingos, A. J. P. White and D. J. Williams, *J. Chem. Soc., Dalton Trans.*, 2000, 3783.

[140.] A. D. Burrows, C.-W. Chan, M. M. Chowdhry, J. E. McGrady and D. M. P. Mingos, *Chem. Soc. Rev.*, 1995, 329.

[141.] C. B. Aakeröy and A. M. Beatty, *Cryst. Eng.*, 1998, **1**, 39.

[142.] C. B. Aakeröy and A. M. Beatty, *Chem. Commun.*, 1998, 1067.

[143.] C. B. Aakeröy and A. M. Beatty, *J. Mol. Struct.*, 1999, **474**, 91.

[144.] C. B. Aakeröy, A. M. Beatty and D. S. Leinen, *Angew. Chem. Int. Ed.*, 1999, **38**, 1815.

[145.] M. Munakata, L. P. Wu, M. Yamamoto, T. Kudora-Sowa and M. Maekawa, *J. Am. Chem. Soc.*, 1996, **118**, 3117.

[146.] C. B. Aakeröy, A. M. Beatty and B. A. Helfrich, *J. Chem. Soc., Dalton Trans.*, 1998, 1943.

[147.] M. Tadokoro, K. Nakasuji, K. Isobe, H. Uekusa, Y. Ohashi, J. Toyoda and K. Tashiro, *Angew. Chem. Int. Ed.*, 1999, **38**, 95.

[148.] D. G. Kurth, K. M. Fromm and J.-M. Lehn, *Eur. J. Inorg. Chem.*, 2001, 1523.

[149.] S. Decurtins, R. Pellaux, G. Antorrena and F. Palacio, *Coord. Chem. Rev.*, 1999, **190-192**, 841.

[150.] A. L. Gillon, G. R. Lewis, A. G. Orpen, S. Rotter, J. Starbuck, X.-M. Wang, Y. R. Martin and C. Ruiz-Perez, *J. Chem. Soc., Dalton Trans.*, 2000, 3897.

[151.] A. Angeloni and A. G. Orpen, *Chem. Commun.*, 2001, 343.

[152.] J. C. Mareque Rivas and L. Brammer, *Inorg. Chem.*, 1998, **37**, 4756.

[153.] C.-Y. Su, B.-S. Kang, H.-Q. Liu, Q.-G. Wang and T. C. W. Mak, *Chem. Commun.*, 1998, 1551.

[154.] D. A. Beauchamp and S. J. Loeb, *Chem. Eur. J.*, 2002, **8**, 5084.

[155.] C. L. Schauer, E. Matwey, F. W. Fowler and J. W. Lauher, *J. Am. Chem. Soc.*, 1997, **119**, 10245.

[156.] A. D. Burrows, R. W. Harrington, M. F. Mahon and C. E. Price, *J. Chem. Soc., Dalton Trans.*, 2000, 3845.

[157.] C. B. Aakeröy, A. M. Beatty, D. S. Leinen and K. R. Lorimer, *Chem. Commun.*, 2000, 935.

[158.] F. A. Cotton and G. Wilkinson, *Advanced Inorganic Chemistry,* John Wiley & Sons Ltd., 1988.

[159.] C. B. Aakeröy, A. M. Beatty and K. R. Lorimer, *J. Chem. Soc., Dalton Trans.*, 2000, 3869.

[160.] J.-H. Yu, J.-Q. Xu, L. Ye, H. Ding, W.-J. Jing, T.-G. Wang, J.-N. Xu, H.-B. Jia, Z.-C. Mu and G.-D. Yang, *Inorg. Chem. Comm.*, 2002, **5**, 572.

[161.] R. Sekiya and S.-I. Nishikiori, *Chem. Eur. J.*, 2002, **8**, 4803.

[162.] G. Demazeau, *J. Mater. Chem.*, 1999, **9**, 15.

[163.] S. Feng and R. Xu, *Acc. Chem. Res.*, 2001, **34**, 239.

[164.] R. M. Barrer, *Hydrothermal Chemistry of Zeolites,* Academic Press, 1982.

[165.] Ocean_Explorer, 2003, http://oceanexplorer.noaa.gov/explorations/02fire/background/vent_chem/media/chemistry.html.

[166.] W. Lin, O. R. Evans and G. T. Yee, *J. Solid State Chem.*, 2000, **152**, 152.

[167.] O. R. Evans and W. Lin, *Acc. Chem. Res.*, 2002, **35**, 511.

[168.] J. Y. Lu and A. M. Babb, *Chem. Commun.*, 2001, 821.

[169.] O. R. Evans, R.-G. Xiong, Z. Wang, G. K. Wong and W. Lin, *Angew. Chem. Int. Ed.*, 1999, **38**, 536.

[170.] T. Whitfield, L.-M. Zheng, X. Wang and A. J. Jacobson, *Solid State Sciences*, 2001, **3**, 829.

[171.] M. K. Nazeeruddin, S. M. Zakeeruddin, R. Humphry-Baker, M. Jirousek, P. Liska, N. Vlachopoulos, V. Shklover, C.-H. Fischer and M. Gratzel, *Inorg. Chem.*, 1999, **38**, 6298.

[172.] S. Ferrere, *Chem. Mater.*, 2000, **2000**, 1083.

[173.] A. C. Lees, C. J. Kleverlaan, C. A. Bignozzi and J. G. Vos, *Inorg. Chem.*, 2001, **40**, 5343.

[174.] E. Eskelinen, S. Luukkanen, M. Haukka, M. Ahlgren and T. A. Pakkanen, *J. Chem. Soc., Dalton Trans.*, 2000, 2745.

[175.] T. Schareina, C. Schick, B. F. Abrahams and R. Kempe, *Z. Anorg. Allg. Chemie*, 2001, **627**, 1711.

[176.] T. Schareina, C. Schick and R. Kempe, *Z. Anorg. Allg. Chemie*, 2001, **627**, 131.

[177.] Y.-H. Liu, Y.-L. Lu, H.-C. Wu, J.-C. Wang and K.-L. Lu, *Inorg. Chem.*, 2002, **41**, 2592.

[178.] D. Min and S. W. Lee, *Bull. Korean Chem. Soc.*, 2002, **23**, 948.

[179.] R. C. Finn and J. Zubieta, *Solid State Sciences*, 2002, **4**, 83.

[180.] D. Min, S. W. Lee and S. S. Yoon, *Inorg. Chem. Comm.*, 2002, **5**, 143.

[181.] R. C. Finn and J. Zubieta, *Inorg. Chem. Comm.*, 2000, **3**, 520.

[182.] C. Kaes, A. Katz and M. W. Hosseini, *Chem. Rev.*, 2000, **100**, 3553.

[183.] B. Bleaney and K. D. Bowers, *Proc. R. Soc. London, Ser. A*, 1952, **214**, 451.

[184.] F. E. Mabbs and D. J. Machin, *Magnetism and Transition Metal Complexes,* Chapman and Hall, 1973.

[185.] P. M. van der Werff, S. R. Batten, P. Jensen, B. Moubaraki, K. S. Murray and E. H.-K. Tan, *Polyhedron*, 2001, **20**, 1129.

[186.] M.-L. Tong, J. Ru, Y.-M. Wu, X.-M. Chen, H.-C. Chang, K. Mochizuki and S. Kitagawa, *New J. Chem*, 2003, 779.

[187.] A. L. Spek, PLATON- A Multipurpose Crystallographic Tool, Utrecht University, The Netherlands, 2000.

[188.] A. L. Spek, *Acta Cryst.*, 1990, **A46**, C34.

[189.] L. J. Farrugia, Platon for Windows Taskbar, Ver. 1.07, 2003.

[190.] T. M. Reineke, M. Eddaoudi, M. O'Keeffe and O. M. Yaghi, *Angew. Chem. Int. Ed.*, 1999, **38**, 2590.

[191.] T. M. Reineke, M. Eddaoudi, M. Fehr, D. Kelley and O. M. Yaghi, *J. Am. Chem. Soc.*, 1999, **121**, 1651.

[192.] J. L. Manson, C. D. Incarvito, A. L. Rheingold and J. S. Miller, *J. Chem. Soc., Dalton Trans.*, 1998, 3705.

[193.] G. S. Rushbrooke and P. J. Wood, *Mol. Phys.*, 1963, **6**, 409.

[194.] B. Rather and M. J. Zaworotko, *Chem. Commun.*, 2003, 830.

[195.] C. J. Kepert and M. J. Rosseinsky, *Chem. Commun.*, 1999, 375.

[196.] R. Batten, J. C. Jeffery and M. D. Ward, *Inorg. Chim. Acta*, 1999, **292**, 231.

[197.] F. Robinson and M. J. Zaworotko, *J. Am. Chem. Soc.*, 1995, **118**, 295.

[198.] S. M.-F. Lo, S. S.-Y. Chui, L.-Y. Shek, Z. Lin, X. X. Zhang, G.-H. Wen and I. D. Williams, *J. Am. Chem. Soc.*, 2000, **122**, 6293.

[199.] K.-B. Shiu, H.-C. Lee, G.-H. Lee, B.-T. Ko, Y. Wang and C.-C. Lin, *Angew. Chem. Int. Ed.*, 2003, **42**, 2999.

[200.] J. Tao, M.-L. Tong and X.-M. Chen, *J. Chem. Soc., Dalton Trans.*, 2000, 3669.

[201.] C.-D. Wu, C.-Z. Lu, D.-M. Wu, H.-H. Zhuang and J.-S. Huang, *Inorg. Chem. Comm.*, 2001, **4**, 561.

[202.] L.-M. Zheng, X. Fang, K.-H. Lii, H.-H. Song, X.-Q. Xin, H.-K. Fun, K. Chinnakali and I. A. Razak, *J. Chem. Soc., Dalton Trans.*, 1999, 2311.

[203.] P. Lightfoot and A. Snedden, *J. Chem. Soc., Dalton Trans.*, 1999, 3549.

[204.] T. J. Prior, D. Bradshaw, S. J. Teat and M. J. Rosseinsky, *Chem. Commun.*, 2003, 500.

[205.] J. A. Real, G. De Munno, M. C. Munoz and M. Julve, *Inorg. Chem.*, 1991, **30**, 2701.

[206.] J. Darriet, M. S. Haddad, E. N. Duesler and D. N. Hendrickson, *Inorg. Chem.*, 1979, **18**, 2679.

[207.] B.-Q. Ma, S. Gao, T. Yi and G.-X. Xu, *Polyhedron*, 2001, **20**, 1255.

[208.] N. H. Cantwell and E. V. Brown, *J. Am. Chem. Soc.*, 1953, **75**, 4466.

[209.] N. H. Cantwell and E. V. Brown, *J. Am. Chem. Soc.*, 1952, **74**, 5967.

[210.] M. R. F. Ashworth, R. P. Daffern and D. L. Hammick, *J. Chem. Soc.*, 1939, 809.

[211.] B. R. Brown and D. L. Hammick, *J. Chem. Soc.*, 1949, 173.

[213.] B. R. Brown and D. L. Hammick, *J. Chem. Soc.*, 1949, 659.

[214.] I. Castro, J. Faus, M. Julve, C. Bois, J. A. Real and F. Lloret, *J. Chem. Soc., Dalton Trans.*, 1992, 47.

[215.] A. T. Casey, B. F. Hoskins and F. D. Whillans, *J. Chem. Soc., Chem. Commun.*, 1970, 904.

[216.] J. Sletten, A. Sorense, M. Julve and Y. Journaux, *Inorg. Chem.*, 1990, **29**, 5054.

[217.] V. H. Crawford, H. W. Richardson, J. R. Wasson, D. J. Hodgson and W. E. Hatfield, *Inorg. Chem.*, 1976, **15**, 2107.

[218.] E. Ruiz, P. Alemany, S. Alvarez and J. Cano, *Inorg. Chem.*, 1997, **36**, 3683.

[219.] R. J. Majeste and E. E. Meyers, *J. Phys. Chem.*, 1970, **74**, 1970.

[220.] B. F. Hoskins and F. D. Whillans, *J. Chem. Soc., Dalton Trans.*, 1975, 1267.

[221.] P. J. Hagrman, D. Hagrman and J. Zubieta, *Angew. Chem. Int. Ed.*, 1999, **38**, 2638.

[222.] L. Pan, T. Frydel, M. B. Sander, X. Huang and J. Li, *Inorg. Chem.*, 2001, **40**, 1271.

[223.] N. N. Greenwood and A. Earnshaw, *Chemistry of the Elements,* Butterworth-Heinemann Ltd, 1984.

[224.] T. Steiner, *Acta Cryst.*, 2001, **B57**, 103.

[225.] P. Brunet, M. Simard and J. D. Wuest, *J. Am. Chem. Soc.*, 1997, **119**, 2737.

[226.] A. W. Addison, T. Nageswara Rao, J. Reedjik, J. van Rijn and G. C. Verschoor, *J. Chem. Soc., Dalton Trans.*, 1984, 1349.

[227.] A. R. Oki and R. J. Morgan, *Synthetic Communications*, 1995, **25**, 4093.

[228.] S. G. Telfer, G. Bernardinelli and A. F. Williams, *Chem. Commun.*, 2001, 1498.

[229.] F. Takusagawa and A. Shimada, *Acta Crystallogr., Sect. B*, 1976, **32**, 1925.

[230.] M. P. Gupta and P. Kumar, *Cryst. Struct. Commun.*, 1975, **4**, 365.

[231.] F. Krohnke, *Synthesis*, 1976, **1**, 1.

[232.] P. Homanen, M. Haukka, M. Ahlgren and T. A. Pakkanen, *Inorg. Chem.*, 1997, **36**, 3794.

[233.] S. Ferrere, *Inorg. Chim. Acta*, 2002, **329**, 79.

[234.] J. Emsley, *Chem. Soc. Rev.*, 1980, **9**, 91.

[235.] T. Steiner, *Chem. Commun.*, 1997, 727.

[236.] L. D. Ciana, W. J. Dressick and A. von Zelewsky, *J. Heterocyclic. Chem.*, 1990, **27**, 163.

[237.] C. E. Marjo, M. L. Scudder, D. C. Craig and R. Bishop, *J. Chem. Soc., Perkin Trans.*, 1997, **2**, 2099.

[238.] T. Steiner and G. R. Desiraju, *Chem. Commun.*, 1998, 891.

[239.] G. R. Desiraju, *Acc. Chem. Res.*, 1991, **24**, 290.

[240.] R. Taylor and O. Kennard, *J. Am. Chem. Soc.*, 1982, **104**, 5063.

[241.] R. Bishop, *Synlett*, 1999, **9**, 1351.

[242.] G. R. Desiraju and J. A. R. P. Sarma, *J. Chem. Soc., Perkin Trans. 2*, 1987, 1195.

[243.] Bruker SMART, Version 5.625, 1997-2001, Bruker-AXS Inc.

[244.] Bruker SAINT-NT, Version 6.02a,1997-2001, Bruker-AXS Inc.

[245.] SADABS, Version 2.03, 1999, Bruker-AXS Inc.

[246.] R. Hooft, COLLECT Software, Nonius BV: Delft, The Netherlands, 1998.

[247.] Z. Otwinowski and W. Minor, *Methods in Enzymology*, C. W. Carter and R. M. Sweet, Ed., Academic Press, 1996.

[248.] G. M. Sheldrick, SHELXTL, Version 5.1, 1998, Bruker AXS-Inc.

[249.] GEMINI, Autoindexing Program for Twinned Crystals, Version 1.02 Release 5/2000, 1999, Bruker-AXS Inc.

[250.] Bruker SAINT-NT, Version 6.22, 2003, Bruker-AXS Inc.

[251.] TWINABS, Version Beta Test, 2003, Bruker-AXS Inc.

Publications

"Coordination and Hydrogen bonded Networks featuring 4,4'-dicarboxy-2,2'-bipyridine (H_2dcbp): Structural characterization of H_2dcbp, [Co(dcbp)($H_2O)_4$]·$4H_2O$, and {[Cu(dcbp)($H_2O)_2$]·$2H_2O$}$_n$", Eithne Tynan, Paul Jensen, Paul E. Kruger, Anthea C. Lees and Mark Nieuwenhuyzen, *Dalton Trans.*, 2003, 1223.

"*Solvent templated synthesis of metal-organic frameworks: structural characterization and properties of the 3D network isomers {[Mn(dcbp)]·½DMF}$_n$ and {[Mn(dcbp)]·$2H_2O$}$_n$"*, Eithne Tynan, Paul Jensen, Paul E. Kruger and Anthea C. Lees, *Chem. Commun.*, 2004, 776.